Relating moisture ingress to component strength and stiffness for carbon-fibre composites.

Ryan, Joanne Maureen

A thesis submitted for the degree of Doctor of Philosophy in the School of Engineering

Swansea University

2011

Joanne Maureen Ryan, BEng (Hons), MRes

RELATING MOISTURE INGRESS TO COMPONENT STRENGTH AND STIFFNESS FOR CARBON-FIBRE COMPOSITES.

Swansea University
Prifysgol Abertawe

ProQuest LLC.
789 East Eisenhower Parkway
P.O. Box 1346
Ann Arbor, MI 48106 – 1346

Abstract

Moisture diffusion studies were performed using unidirectional (UD) tape and quasi-isotropic (QI) woven 5-harness satin fabric, carbon fibre reinforced (CFR) epoxy composite materials. Firstly the moisture constants, (i.e. diffusion coefficient, D_x, and equilibrium moisture content, M_{max}) were experimentally derived at 70°C and 85% relative humidity (%RH), for the two CFR materials. To investigate moisture absorption as a function of %RH test coupons were conditioned to differing equilibrium moisture levels viz., 70°C/60%RH, 70°C/75%RH, 70°C/85%RH, and 70°C/95%RH. Also oven dry (OD) and as-received (AR) tests were performed for baseline comparison.

The effect of moisture absorption on the mechanical behaviour was investigated; lamina properties were studied by measuring tension, compression, shear (inter/intralaminar) strength and stiffness of the UD material. This comprehensive set of testing provided quantitative relationships between moisture content and mechanical properties. The quasi-isotropic lay-up was then utilised to investigate multi-directional laminate lay-ups using open hole tension and compression testing.

The experimental data showed that the uptake of moisture in both the materials studied was described well by Fick's Second Law and the properties most affected by moisture ingress were matrix-dominated properties. More specifically, the transverse tensile strength, F_2^t was most affected by the ingress of moisture, with a near 50% reduction in strength when conditioned to equilibrium moisture content at 70°C/95%RH. Such information is a necessary prerequisite if improved design procedures are going to be developed in the future.

The initial phase of testing produced mechanical property/moisture relationships that were employed to predict the strength and stiffness of the material containing specific moisture gradients through-the-thickness (TTT). To be able to predict mechanical properties with different moisture distribution, firstly moisture distribution TTT of the material was modelled using an analytical solution to Fick's Second Law. Then moisture content was considered on a ply-by-ply basis TTT of the laminate; reductions were applied to each individual ply property dependent on the moisture content using the experimentally derived relationships, essentially applying environmental knock-down factors (K_{EKDF}'s) to each individual ply. Classical Laminate Analysis (CLA) was then performed using the Max Stress failure criteria in order to predict the overall laminate failure. A second phase of mechanical testing was then performed to validate these predictions. The mechanical property predictions compared well to the experimental data showing similar reductions in strength for a given profile of moisture in the laminate. The predicted strengths also fell within the measured standard deviation of the experimental data in a significant proportion of the results.

Declarations and Statements

DECLARATION

This work has not previously been accepted in substance for any degree and is not being concurrently submitted in candidature for any degree.

Signed .... (Candidate)

Date ..... 25/2/11 .....

STATEMENT 1

This thesis is the result of my own investigations, except where otherwise stated. Other sources are acknowledged by footnotes giving explicit references. A bibliography is appended.

Signed .... (Candidate)

Date ..... 25/2/11 .....

STATEMENT 2

I hereby give consent for my thesis, if accepted, to be available for photocopying and for inter-library loan, and for the title and summary to be made available to outside organisations.

Signed .... (Candidate)

Date ..... 25/2/11 .....

Table of Contents

Acknowledgements

I would like to thank my academic supervisor Professor S.G. Brown whose help in during my studies was invaluable and also the staff at the Materials Research Centre, at Swansea University.

I would also like to thank my industrial supervisor Dr Richard Adams (Airbus UK) for providing me with guidance and continued support throughout this programme of work.

Swansea University provided access to a pool of knowledge via their library and I thank them and the Materials Research Centre for access to its resources and facilities.

Also my family and friends have provided encouragement and support for this I am forever thankful.

This work was funded as part of the European Union Project 'ALCAS' (Project Reference no. 516092 in the 6th Framework Programme), for which I am very grateful. I would also like to thank Airbus for the support to this programme.

List of Figures

List of Tables

NOMENCLATURE

A	initial cross-sectional area of the coupon
AR	as-received condition
CFRP	carbon fibre reinforced plastics
CLA	classical laminate analysis
cpt	cure ply thickness
CV	coefficient of variation
b	coupon width
D	diffusion coefficient
D_x	diffusion coefficient through-the-thickness direction
ε_x	strain in the loading direction
DC	dry-core
ε_y	strain transverse to the loading direction
γ_{12}	shear strain
E_1	Young's modulus of elasticity, in the 0° fibre direction
E_2	Young's modulus of elasticity, in the 90° fibre direction
F	force
FAW	fibre areal weight
FPF	first ply failure
F_1^t	tensile strength, in the 0° fibre direction
F_2^t	tensile strength, in the 90° fibre direction
F_1^c	compressive strength, in the 0° fibre direction
F_2^c	compressive strength, in the 90° fibre direction
F_{12}	shear strength
Fxx^{oht}	open hole tensile strength
Fxx^{ohc}	open hole compressive strength
G_{12}	in-plane shear Modulus
h	thickness
ILS	Interlaminar shear
IPS	In-plane shear
K_{EKDF}	environmental knock-down factors
OD	oven dried
M	moisture content at any point mass of moisture, M in the laminate
M_{max}	equilibrium/saturated moisture content, wt%
M_0	is the initial/as-received percentage of moisture content, wt%

M_r	moisture uptake of the matrix, wt%
M_c	moisture uptake of the composite, wt%
OHC	open hole compression
OHT	open hole tension
QI	quasi-isotropic
RH	relative humidity, %
RT	room temperature, 23°C
σ_1^t	tensile stress, in the 0° fibre direction
σ_2^t	tensile stress, in the 90° fibre direction
σ_2^c	compression stress, in the 90° fibre direction
σ_{ILS}	interlaminar shear stress,
σ_{oht}	open hole tensile stress
σ_{ohc}	open hole compressive stress
τ_{12}	in-plane shear stress
t	time
T_g	glass transition temperature
TTT	though-the-thickness
UD	unidirectional
UTS	ultimate tensile strength
V_f	fibre volume fraction
V_v	void volume fraction
V_m	matrix volume fraction
W_0	as received coupon mass
W_f	fibre weight as a percentage of initial mass
W_d	oven-dry coupon mass
W_r	resin weight as a percentage of initial mass
wt%	weight percent

Subscripts

c	composite
m	matrix
f	fibre
r	resin
1,2,3	ply co-ordinate system (1 = fibre direction, 2 = normal to fibre direction)

1 Introduction

This programme of work was focused on the effects absorbed moisture has on the strength and stiffness of composite materials used in aircraft primary structures. The work was fully supported by Airbus in the UK. The experimental phase included acquiring detailed information on how composite matrix and ply properties evolve in the presence of moisture conditions and the role this evolution plays in the strength and stiffness behaviour of the composite material. Experimental procedures and mechanical testing methods and results can be found in chapters 3, 4 and 5 respectively. The mechanical properties focused on were resin dominated failure modes, which included tension[1,2,3,4,5], compression[6] and shear[7,8]. The tests were performed in accordance to British and European test standards and were also aligned with Airbus Industry Test Methods[9,10] (AITM's) so that the data could be utilized for material qualification purposes.

The Airbus standard philosophy at present is to design aircraft components made from CFRP using 'HOT/WET' (70°C/85%RH) material properties[11]. This assumes that the part is fully saturated with moisture and operating at elevated temperature. This represents the worst-case environmental condition for a component, as the ingress of moisture combined with a high operating temperature significantly weakens the material's mechanical properties. In the past this approach could be considered to be satisfactory as previous composite components have been relatively thin (<8mm)[11]. Airbus considers anything less than 8mm will become saturated during the aircraft lifecycle[11]. However, thick components typically found on primary wing-box structures (i.e. wing skins, spars, pylon fitting and landing gear attachments), which having thicknesses up to 70mm, will most likely never reach saturation over the 20-30 year lifecycle. Therefore the 'HOT/WET' knockdown design criteria may be considered too conservative[11]. As future Airbus aircraft move towards primary loaded CFRP materials it is important that the use of 'HOT/WET' design allowables are investigated in order that weight savings can be optimised. This is a new requirement, since with thin structures that will probably reach saturation the worse case 'HOT/WET' condition can be considered acceptable.

The first objective of the work was to generate a material property database for different levels of equilibrium moisture content that could be used by design and

stress engineers at Airbus. At present no such data exists within Airbus or the composites community as a whole. Currently Airbus produce lamina data for laminate design and typically only produce design values at -55°C/AR (as-received), RT/AR and 90°C/wet. So essentially they only have two points on the curve for predicting saturated strength/stiffness.

The second major objective was to develop and demonstrate an innovative and novel methodology to reduce the *knockdowns* associated with the HOT/WET environment. As stated earlier, Airbus does not typically produce stiffness/strength performance profiles over a range of different levels of saturation. However, the generation of stiffness/strength performance profiles over a range of different saturation levels is fundamentally required to understand the effect on material performance, as well as providing mechanical data that can be used to model/predict the mechanical properties of a laminate. The experimental work produced curves for each lamina property in order to give relationships between the material property and the moisture content. Once the equilibrium-saturated data set was generated and the relationships were derived, laminate properties could be predicted from the moisture degraded properties of each ply, the results of which can be found in chapter 6. Further validation studies were performed by investigating quasi-isotropic lay-ups for element level testing (i.e. open hole tension/compression). The data produced also provided validation to a modelling activity that is being carried out by Airbus and Swansea University to provide engineers with an analysis tool to evaluate the mechanical properties of composite materials degraded by moisture[12].

An analytical solution of Fick's second Law[13] was used to produce moisture distribution curves through-the-thickness of the coupons. From calculating individual plies' moisture content, the associated strength and stiffness predictions were performed using the derived relationships. A Classical Laminate Analysis (CLA) approach was then used to predict the first ply failure and ultimate failure of the materials, employing a Maximum Stress Criterion. Airbus applies environmental "HOT/WET" knock-downs to mechanical properties, e.g. 70°C/85%RH to saturation. If the approach suggested here (i.e. using less conservative and more realistic/accurate properties, which simulate the environmental profile seen in service) was employed for designing the aircraft components, there may potentially be advantages in strength and related weight savings.

2 Literature Review

There have been a number of reviews and publications on environmental effects on composite materials. These are addressed throughout this literature review and serve as a good basis for understanding environmental effects on composite materials [14,15,16,17,18,19,20,21].

2.1 Composites in Aerospace Applications

Carbon fibre reinforced polymeric composites are used in the aeronautical industry to manufacture several components such as flaps, aileron, landing-gear doors and others. Epoxy resins are the most used in these structural components because of their thermal, chemical, mechanical and corrosion resistance[22,23]. Compared to metals, polymeric composites have many advantages such as higher fatigue strength, higher corrosion resistance and lower weight[24]. These properties have led to a steady growth in the use of composites in all fields of aerospace applications due to the aerospace industry's goal to continually improve the performance of commercial and military aircraft, which drives the development and improvement of high performance and structural materials[25]. However, aircraft components fabricated from polymeric composites must satisfy tight requirements since they can suffer mechanical damage during service[18,22].

Composite materials are now playing a significant role in current and future aerospace components with one of the main reasons for their introduction into aerospace applications being weight reduction, which has the potential to reduce aircraft fuel consumption[23]. Although it is difficult to give precise figures, it can be estimated that the value of light weighting is around €100 to €1,000 (for specific applications) per kilogram of weight saved[25]. Figure 2-1 illustrates the growth of composites in civil aircraft structures over the last 30 years[25].

Fibrous composite materials were originally used in small quantities in military aircraft in the 1960s when boron-reinforced epoxy composite was used for the skins of the empennage (aircraft tail assembly – horizontal and vertical stabilizers, elevators, and rudder) of the US F14 fighters. Introduction within civil aviation took place from the 1970s. By the 1980s, composites were being used by civil aircraft

manufacturers for a variety of secondary wing and tail components such as rudder and wing trailing edge panels. However, it is with the advent of the latest generation of airliners, such as the Airbus A380, the world's largest passenger aircraft, that these materials have been deployed extensively in primary load carrying structure such as wings and fuselages has increased to the point where it is not uncommon to see a 50 percent by weight inclusion of composite material in an airframe[23,26].

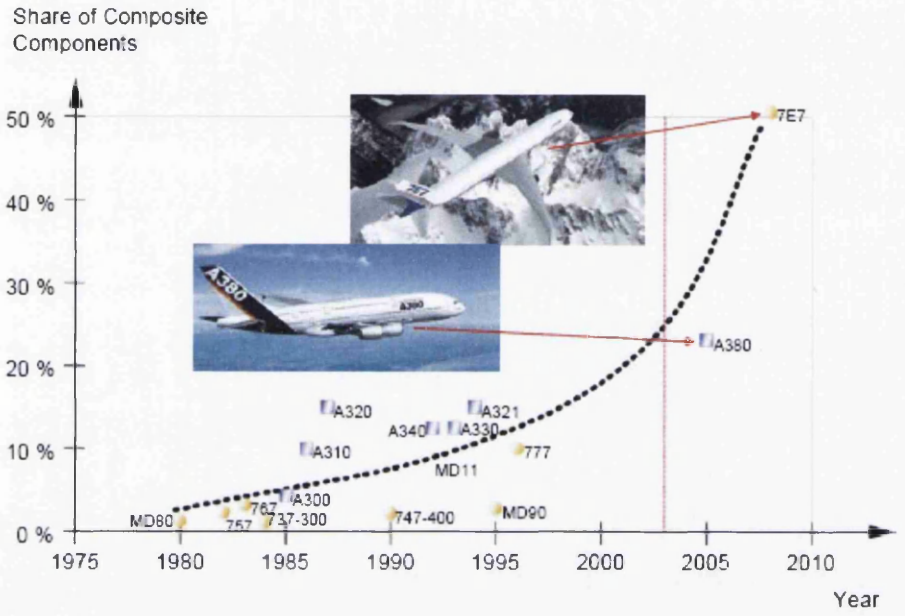

Figure 2-1: Development of composites in aerospace applications in the past 30 years [25].

So called 'conventional' metallic materials continue to be developed and improved upon and offer ever increasing performance. There is no doubt they will always play a fundamental role in aerospace structures but at the same time there is little doubt over the considerable benefits being offered by composite materials and these materials have yet to be fully understood and exploited.

As composite technologies develop so does their usage in aerospace applications, for example, in the new Boeing 787 Dreamliner aircraft where composite materials will account for half of the aircraft's structural weight. The 787's all-composite fuselage makes it the first composite airliner in production. While the Boeing 777 contains 50% aluminium and 12% composites, the 787 contains 15% aluminium, 50% composite (mostly CFRP) and 12% titanium. Each fuselage barrel will be manufactured in one piece and the barrel sections joined end to end to form the fuselage. This will eliminate the need for approximately 50,000 fasteners used in conventional airplane building. According to the manufacturer the composite is also

more durable, allowing a higher cabin pressure during flight compared to aluminium. Figure 2-2 shows that nearly all the exterior surfaces of the 787 Dreamliner are composites (blue), excepting the leading edges of the wings, the stabilizers and the engine pylons[26,27].

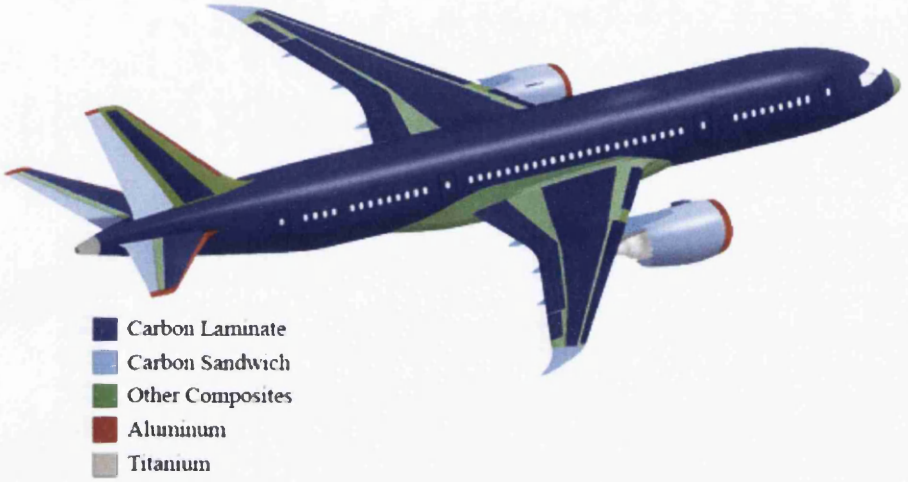

Figure 2-2: Material usage on the exterior surfaces of the Boeing 787 Dreamliner[27].

More recently the Airbus A350 has been publicised, due in full production by 2012. Airbus claims that 52% of the aircraft will be made out of composites[28] (as shown in figure 2-3, with a mostly composite fuselage and new all-composite wings[29].

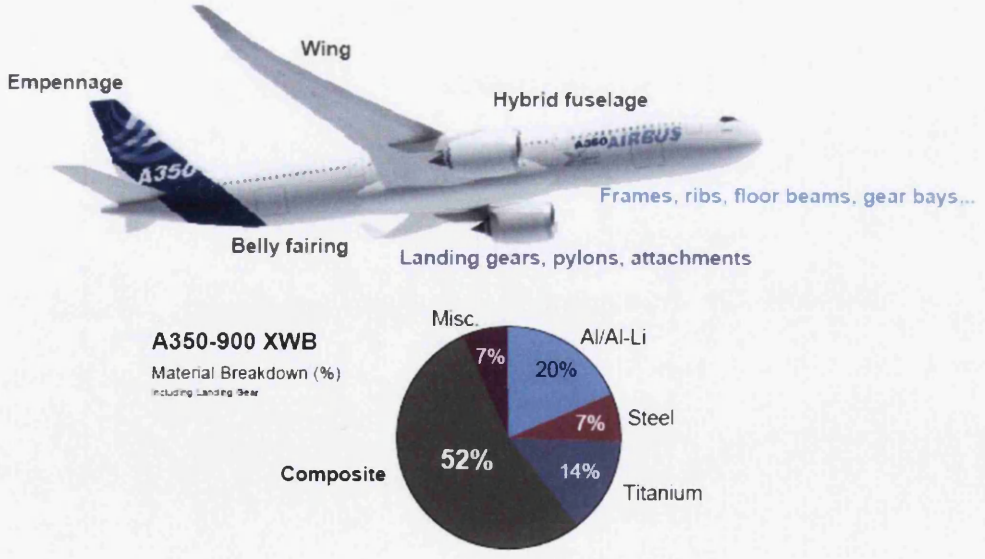

Figure 2-3: Material breakdown in the A350-900XWB, courtesy of Airbus.

2.2 Composite Materials

The word "composite" means, "consisting of two or more distinct parts." Composites are generally considered to be materials consisting of two or more constituents on a macro scale, having a distinct interface separating them[30].

There are two categories of constituent materials: "matrix" and "reinforcement". At least one portion of each type is required. The matrix material surrounds and supports the reinforcement materials by maintaining their relative positions. The reinforcements impart their special mechanical and physical properties to enhance the matrix properties. The reinforcement, added primarily to increase the strength and stiffness of the matrix, is usually in fibre form[31].

2.2.1 Advantages of Composite Materials

The main advantages of most composite materials are in the weight savings that can be achieved over "conventional" (i.e. metallic) materials. Composites main advantages are:

- High strength and stiffness.
- Low density (figure 2-4) - giving benefit of weight saving.
- Good fatigue performance.
- Excellent corrosion resistance (polymeric composites).

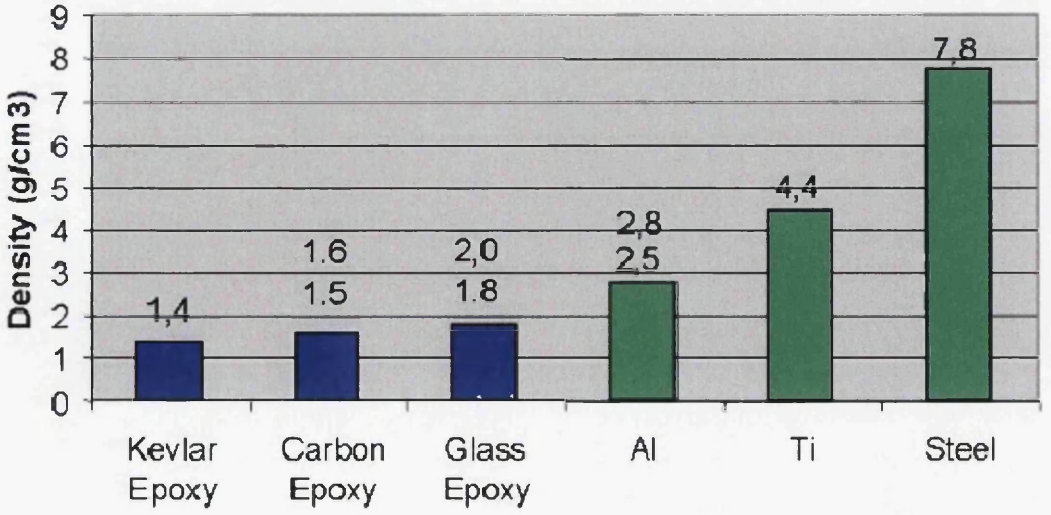

Figure 2-4: Comparison of aerospace materials densities[32].

The main factor that drives the use of composites in aerospace (and other high performance) applications is the potential for weight reductions, along with corrosion resistance and part count reduction. Other advantages that motivate some applications include wear resistance, good fatigue performance, and low thermal expansion. Weight reduction is usually the more important motivations in the aerospace industry. Composites are lightweight because both the fibres and the polymeric matrices have low densities. More significantly the fibres have higher values of strength-weight and stiffness-weight ratios than most materials[30].

Carbon reinforced epoxy structures can be designed to be typically 45% lighter than equivalent aluminium based structures designed to fulfil the same requirements. For example 7075 series aerospace aluminium alloy has a density of 2800 kg/m^3 and S4/8552 carbon fibre UD tape has a density of 1600 kg/m^3[32].

2.3 Matrix Materials

Today the most common man-made composites can be divided into three main groups, generally classified by their matrix type[31]:

Polymer Matrix Composites (PMC's) - (These are the most common and will the main area of discussion in this chapter). Also known as FRP - Fibre Reinforced Polymers (or Plastics) - these materials use a polymer-based resin as the matrix and a variety of fibres such as glass, carbon and Aramid as the reinforcement.

Metal Matrix Composites (MMC's) - Increasingly found in the automotive industry, these materials use a metal such as aluminium as the matrix and reinforce it with fibres such as silicon carbide.

Ceramic Matrix Composites (CMC's) - Used in very high temperature environments, these materials use a ceramic as the matrix and reinforce it with short fibres, or whiskers such as those made from silicon carbide and boron nitride.

2.3.1 Functions of the Matrix

Fibres, since they cannot transmit loads from one to another, have limited use in engineering applications. When they are embedded in a matrix material to form a composite, the matrix serves to bind the fibres together, transfer loads to the fibres and protect them against environmental attack and damage due to handling. The matrix has a strong influence on many of the mechanical properties of the composite, such as transverse modulus and strength, shear properties and the properties in compression[31].

The matrix isolates the fibres so they can act as separate entities. The matrix protects the fibres from mechanical damage. A ductile matrix will provide a means of slowing down or arresting cracks that may have originated at broken fibres. Conversely, a brittle matrix may depend on the fibres to act as matrix crack arresters[31]. Through the quality of the interfacial bond strength, the matrix can be an important means of increasing the toughness of a composite. By comparison to the reinforcing fibres the polymer matrix material is weak and ductile[31].

2.3.2 Polymer Matrix Composites (PMC's)

Polymers are the most widely use matrix materials in the aerospace industry. Their primary advantage is their low cost, easy processability, and low specific gravity[34]. On the other hand, low strength and modulus along with low operating temperature limit their use somewhat.

Most polymers are made from long molecules with a covalently bonded backbone of carbon; these long molecules are bonded together by weak Van-der-Waal or hydrogen bonds[34].

A polymeric matrix composite material typically consists of relatively strong, stiff fibres in a tough resin matrix, commonly referred to as fibre reinforced polymeric composites (FRP)[33]. Composite materials commonly used in the aerospace industry are carbon and glass-fibre-reinforced plastic (CFRP and GFRP respectively), which consist of brittle, yet stiff and strong fibres (for their density) in a matrix which is relatively ductile, but neither particularly stiff nor strong. Essentially, by combining materials with complementary properties in this way, a composite material with most or all of the benefits (high strength, stiffness, toughness and low density) is obtained with few or none of the weaknesses of the individual component materials, as can be seen in figure 2-5.

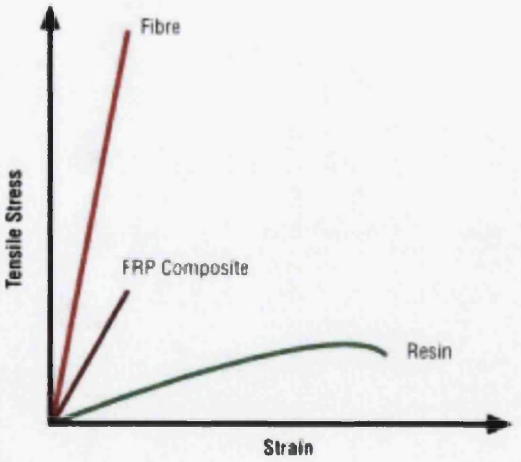

Figure 2-5: Properties of a composite compared to its constituent components[31].

All polymers exhibit an important common property in that they are composed of long chain-like molecules consisting of many simple repeating units. Polymers can

be classified under two types, 'thermoplastic' and 'thermosetting', according to the effect of heat on their properties[34]. Thermoplastics, like metals, soften with heating and eventually melt, hardening again with cooling[34]. Thermosets once heated past a certain temperature, start to degrade but due to their range of properties and ease of processability are more widely used as matrix material for composites in the aerospace industry.

2.3.2.1 Thermoset Matrices

Thermosetting materials, or 'thermosets', are formed from a chemical reaction where the resin and hardener/catalyst are mixed and then undergo a non-reversible chemical reaction to form a hard, infusible product. Once cured, thermosets will not become liquid again if heated, although above a certain temperature their mechanical properties will change[34]. This temperature is known as the Glass Transition Temperature (T_g), above which, the molecular structure of the thermoset changes from that of a rigid cross-linked polymer to a more flexible, rubbery polymer (see figure 2-6). Above the T_g properties such as resin modulus (stiffness) drop sharply, and as a result the compressive and shear strength of the composite does too.

T_g is expressed as the temperature at which the Gibbs free energy, ΔG, is such that the activation energy of the movement of the elements in the polymer is exceeded – this allows molecular chains to slide past each other when force is applied. The T_g of a resin can also be altered by adding plasticizers[36].

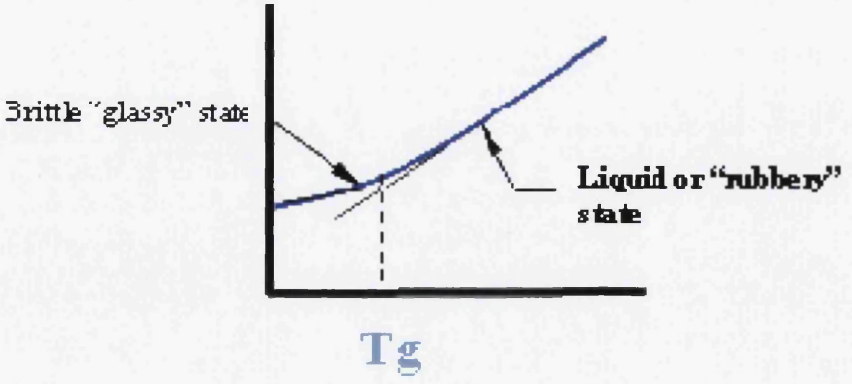

Figure 2-6: Effect of T_g on matrix material (x axis- temperature, y axis- specific volume)[32].

Thermoset matrices are the most commonly used resins at this time because of their high strength (due to cross-linked rigid 3D bonds) and relatively high operating

temperatures (due to large molecular weight). Low viscosity allows for excellent impregnation of the fibre reinforcement and high processing speeds[30]. Thermosets are easily processed and are low cost. The most common thermoset resins are polyesters, vinyl ester and epoxy.

Epoxy resins are considered to be high performance, as their strength is superior to that of other thermosets and also due to their resistance to environmental degradation, which leads to their extensive use in aircraft structural components[31].

2.3.3 Epoxy Matrices

The term "epoxy" refers to a chemical group consisting of an oxygen atom bonded to two carbon atoms that are already bonded in some way[34]. The simplest epoxy is a three-member ring structure known by the term 'alpha-epoxy' or '1,2-epoxy'. The idealised chemical structure is shown in figure 2-7 and is the most easily identified characteristic of any more complex epoxy molecule.

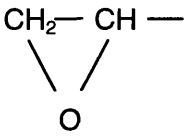

Figure 2-7: Schematic of 1,2-Epoxy Group[34].

Epoxy resins are formed from long chain molecular structures with reactive sites at either end (epoxy groups), which give good water resistance compared to other polymers. They also contain two ring-groups at its centre, which are able to absorb mechanical and thermal stresses better than linear groups, giving epoxies good stiffness, toughness and heat resistant properties[34]. The figure below shows the idealised chemical structure of a typical epoxy.

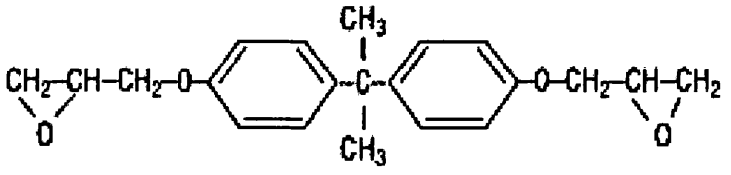

Figure 2-8: Idealised chemical structure of a typical epoxy [34].

Epoxies are made by mixing a resin and a hardener. The hardener (often amine) cures the epoxy by an addition reaction i.e. two epoxy sites bonding to each amine

giving a 3D complex structure. On addition of the hardener the epoxy becomes viscous until unable to flow (the gel point) and the epoxy continues to harden after it has gelled. The reaction is often accompanied by exothermic heat which in turn accelerates the reaction[34].

Epoxies are heavily cross-linked (by covalent bonds) and are made from polyfunctional monomers that contain three or more active bonds which form 3D network polymers. The structure is amorphous (cumbersome side-groups, atacticity, branching and cross-linking all hinder crystallisation). In the melt the thermal energy causes the molecules to rearrange continuously, this 'wriggling' of the molecules increases the free volume of the polymer. It is the free volume aided by thermal energy that allows molecules to move over each other giving viscous flow[36].

As temperature decreases free volume is lost but cross-linking prevents crystallization, the liquid structure is retained and not all the free volume is lost immediately, so flow can still occur but viscosity increases. As temperature decreases further the free volume becomes small to a point no movement/rearrangement occurs and all of the free volume is gone, this is called the glass transition T_g. Below T_g the polymer is a glass like structure as secondary bonds bind molecules into an amorphous solid. Epoxies are brittle at room temperature because they have a high T_g, typically around 150-200°C[36].

The T_g of a polymer reduces as a result of moisture absorption. The following empirical equation models data for some epoxy resins[30]:

$$T_{gw} = (1-0.1M+0.005M^2)T_{gd} \qquad 2\text{-}1$$

Where M is the moisture content and T_{gd} and T_{gw} are glass transition temperatures of the dry and wet polymeric matrix, respectively.

Typical mechanical properties of some epoxies are given in *table 2-1*, note that the higher T_g results in a more brittle matrix with lower elongation and decreased mechanical properties. This means there is always a trade off between high temperature application and mechanical properties when tailoring a resin system.

Table 2-1: Mechanical properties of epoxies[30]

Epoxy	Tensile Modulus [GPa]	Tensile Strength [MPa]	Tensile elongation [%]	T_g [°C]	Density [g/cm^3]
CYCOM 977-2 @23°C	3.52	81.4	3.0	212	1.31
9310/9360 @23°C	3.12	75.8	4.0	185	1.20
9310/9360 @150°C	1.40	26.2	5.2	185	1.20
9420/9470 (A) @23°C	2.66	57.2	3.1	195	1.162
9420/9470(B) @23°C	2.83	77.2	5.2	155	1.158

2.4 Reinforcing Fibres

The role of the reinforcement in a composite material is fundamentally one of improving the mechanical properties of the neat resin system[31]. The four main factors that govern the fibre's contribution are[31]:

- The basic mechanical properties of the fibre itself.
- The surface interaction of fibre and resin (the 'interface').
- The amount of fibre in the composite ('Fibre Volume Fraction').
- The orientation of the fibres in the composite.

The surface interaction of fibre and resin is controlled by the degree of bonding that exists between the two. The amount of fibre in the composite is largely governed by the manufacturing process used. However, reinforcing fabrics with closely packed fibres will give higher Fibre Volume Fractions (V_f) in a laminate than those fabrics which are made with coarser fibres, or which have large gaps between the fibre bundles. Fibre diameter is an important factor, with the more expensive smaller diameter fibres providing higher fibre surface areas, spreading the fibre/matrix interfacial loads. As a general rule, the stiffness and strength of a laminate will increase in proportion to the amount of fibre present. However, above about 60-70% V_f (depending on the way in which the fibres pack together), although tensile stiffness may continue to increase, the laminate's strength will reach a peak and then begin to decrease due to the lack of sufficient resin to hold the fibres together properly[31].

Finally, since reinforcing fibres are designed to be loaded along their length and not across their width, the orientation of the fibres creates highly 'direction-specific' properties in the composite. This 'anisotropic' feature of composites can be used to good advantage in designs, with the majority of fibres being placed along the orientation of the main load paths.

2.4.1 Carbon Fibres

Carbon fibres are lightweight and strong with excellent chemical resistance. Carbon fibre is produced by the controlled oxidation, carbonisation and graphitisation of carbon-rich organic precursors which are already in fibre form. The most common

precursor is polyacrylonitrile (PAN), because it gives the best carbon fibre properties, but fibres can also be made from pitch or cellulose. Variation of the graphitisation process temperature produces either high strength fibres (2,600°C) or high modulus fibres (3,000°C) with other types in between. Once formed, the carbon fibre has a surface treatment applied to improve matrix bonding and then chemical sizing which serves to protect it during handling[35].

When carbon fibre was first produced in the late 1960's the price for the basic high strength grade was about £200/kg. By 1996 the annual worldwide capacity had increased to about 7,000 tonnes and the price for the equivalent (high strength) grade was £15-40/kg. The filament diameter of most types is about 5-7μm. Carbon fibre has the highest specific stiffness of any commercially available fibre, very high strength in both tension and compression and a high resistance to corrosion, creep and fatigue.

2.4.1.1 Structure and properties

The atomic structure of carbon fibre is similar to that of graphite, consisting of sheets of carbon atoms (graphene sheets) arranged in a regular hexagonal pattern. The difference lies in the way these sheets interlock. Graphite is a crystalline material in which the sheets are stacked parallel to one another in regular fashion. The intermolecular forces between the sheets are relatively weak Van-der-Waals forces, giving graphite its soft and brittle characteristics. Carbon fibres have an aligned graphite hexagonal crystal structure with strong covalent bonds along the fibre length. Weak Van-der-Waals planes are intermingled across the fibre width. The degree of alignment of the structure provides a trade off for high strength or high stiffness, although strain to failure is relatively low in both cases, around 1%.

It is very difficult to get an accurate description of the atomic structure of carbon fibres because these materials are amorphous. Chemists have used similar techniques to x-ray crystallography and can provide a qualitative description of the structure of carbon fibres. A very tiny piece of a carbon fibre would look like graphite, but carbon fibres have less long-range ordering. Instead of the planar layers of carbon atoms which are found in graphite, carbon fibres consist of ribbons of carbon atoms aligned parallel to the axis of the fibres. Although the ribbons are essentially parallel on the surfaces of a carbon fibre, the fibre's inner layers fold in a "hairpin" fashion. This is a stark contrast to graphite in which the carbon sheets remain parallel on a long range scale. The layer planes along the axis of the carbon

fibre are interlinked in a complex way. It is believed that the great strength of carbon fibres is due to the interlocking and folding of ribbons (the sheets of carbon atoms cannot slide past each other as they do in graphite)[35].

Several thousand-carbon fibres are twisted together to form a yarn, which may be used by itself or woven into a fabric. The density of carbon fibre is 1800kg/m^3 making it ideal for applications requiring low weight. Carbon fibre use is widespread in high temperature applications, from the NASA space shuttle structure through to aircraft and formula one racing car brake discs. Carbon fibres are inert and can withstand extremely aggressive operating environments (corrosive environments, salt water and high atmospheric moisture conditions) at high temperature[32]. A classification system in terms of stiffness and strength is used for carbon fibre; referring to table 2-2, T300 and AS2 are considered high strength (HS), IM6 is intermediate modulus (IM) and HMS4 is high modulus (HM).

Table 2-2: Typical properties of carbon fibres[30]

Fibre	Modulus [GPa]	Tensile Strength [GPa]	Elongation [%]	Density [g/cm^3]
T300	230	3.53	1.5	1.75
AS2	227	2.75	1.3	1.8
IM6	276	5.10	1.7	1.7
HMS4	317	2.34	0.8	1.8

2.4.2 Fibre-Matrix Interface

The interfacial bond between the matrix and the fibres is an important factor influencing the mechanical properties and performance of the composite. The interface is responsible for transmitting the load from the matrix to the fibres, which contribute the greater portion of the composite strength[31]. The interface controls the mode of propagation of micro-cracks at the fibre ends[31]. When a strong bond exists between the fibres and the matrix, the cracks do not propagate along the lengths of the fibres. A strong bond is essential for higher transverse strengths and good environmental performance. Improved adhesion enhances water resistance of polymer matrix composites[31].

2.5 Unidirectional (UD) Composites

The physical properties of composite materials are generally not isotropic like metals, but rather are typically anisotropic[30]. An isotropic material under uni-axial tensile loading, as in figure 2-9, undergoes axial deformation (strain) ε_x in the loading direction, transverse deformation ε_y, but no shear deformation[31]. A general anisotropic material under uni-axial tension (figure 2-9) undergoes axial, transverse and shear deformations[31].

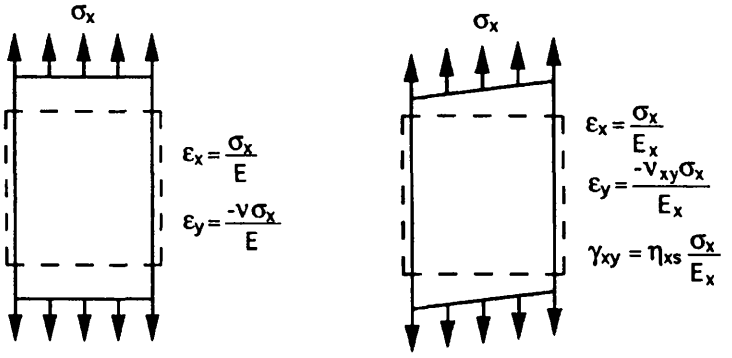

Figure 2-9: Isotropic deformation (metals) and anisotropic deformation (composites)[31].

A unidirectional (UD) composite consists of parallel fibres embedded in a matrix, see figure 2-10. UD composites are anisotropic; this anisotropy is overcome by stacking UD layers on top of one another with the fibres orientated at different angles to form a laminate, with each layer referred to as a ply or lamina[31]. Many properties such as stiffness, strength, Poisson's Ratio, thermal expansion, moisture expansion and thermal conductivity are associated with a direction or axis[31].

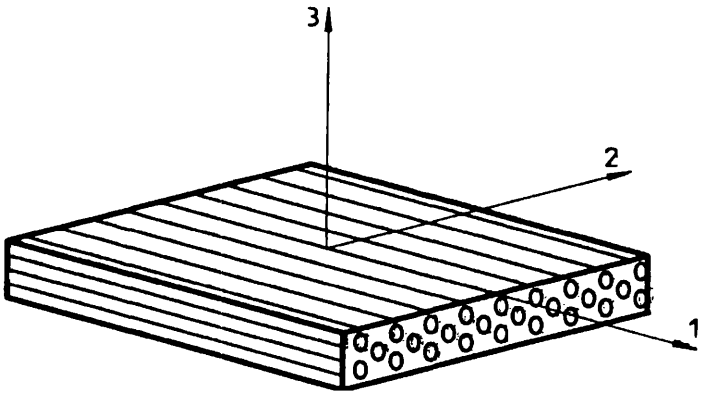

Figure 2-10: Schematic representation of a unidirectional composite[33]

2.6 Composite Preforms

To produce a composite component, individual plies which are often pre-impregnated ('pre-preg') with the resin matrix, are cut to their required size and then stacked in the specific sequence. The assembly is then subjected to a series of temperatures and pressures to 'cure' the laminate. The product is checked thoroughly for voids (small cavities in the resin) and delaminations (un-bonded areas between layers).

A composite fabric is defined as a manufactured assembly of long fibres, to produce a flat sheet of one or more layers of fibres. These layers are held together either by mechanical interlocking of the fibres themselves or with a secondary material to bind these fibres together and hold them in place, giving the assembly sufficient integrity to be handled.

Fabric types are categorised by the orientation of the fibres used and by the various construction methods used to hold the fibres together. The four main fibre orientation categories are: unidirectional, woven, multiaxial, and other/random. In this work UD and woven material was investigated, as these materials are commonly used in the aircraft industry. A unidirectional (UD) fabric is one in which the majority of fibres run in one direction only, usually the orientation of the primary load (i.e. 0° direction). Woven fabrics are produced by the interlacing of warp (0°) fibres and weft (90°) fibres in a regular pattern or weave style. The fabric's integrity is maintained by the mechanical interlocking of the fibres. Drape (the ability of a fabric to conform to a complex surface), surface smoothness and stability of a fabric are controlled primarily by the weave style (e.g. plain, twill, satin etc: see figure 2-11)[32].

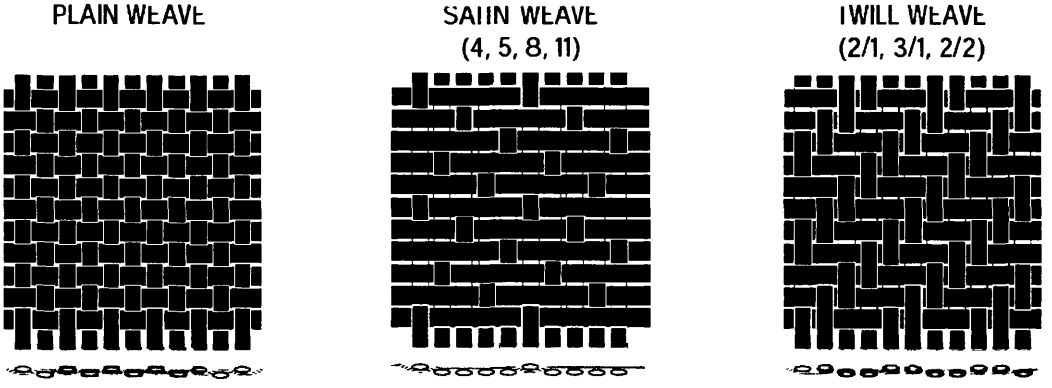

Figure 2-11: Types of composite fabric, plain, satin and twill weave[32].

2.7 Mechanical Characterisation of Composites

The mechanical properties of any material can be determined by loading the material and monitoring deformation or by deforming a material and monitoring the loads required. International/national/industry standards exist for methods to determine the properties of composite materials[3,4,5,6,12,37].

Composite materials and structures are designed to withstand different amounts and types of load, which testing will strive to emulate. There are four main direct loads that any material in a structure has to withstand: tension, compression, shear and flexure, see figure 2-12 to figure 2-15[32].

2.7.1 Tension

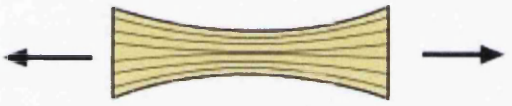

Figure 2-12: Tensile load applied to a UD composite[32].

Figure 2-12 shows a tensile load applied to UD composite. The response of a composite to tensile loads is dependent on the properties of the reinforcement fibres (when pulled in the fibre direction), since these are far higher than the resin system on its own.

2.7.2 Compression

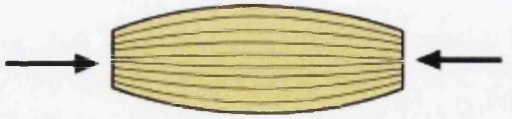

Figure 2-13: Compressive load applied to a UD composite[32].

Figure 2-13 illustrates a UD composite under a compressive load. Here, the adhesive and stiffness properties of the resin system are crucial, as it is the role of the resin to maintain the fibres as straight columns and to prevent them from buckling.

2.7.3 In-Plane Shear

Figure 2-14: Shear load applied to a UD composite[32].

Figure 2-14 demonstrates a composite experiencing a shear loading. This load is trying to slide adjacent layers of fibres over each other. Under shear loads the resin plays the major role, transferring the stresses across the composite. For the composite to perform well under shear loads the resin element must not only exhibit good mechanical properties but must also have high adhesion to the reinforcement fibre. The interlaminar shear strength (ILSS) of a composite is often used to indicate this property in a multi-layer composite ('laminate').

2.7.4 Flexure

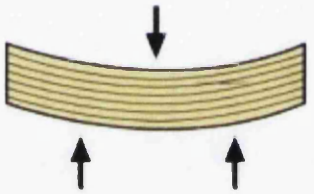

Figure 2-15 : Flexural load applied to a UD composite[32].

Flexural loads are really a combination of tensile, compression and shear loads[38]. When loaded as shown in figure 2-15, the upper face is put into compression, the lower face into tension and the central portion of the laminate experiences interlaminar shear.

2.7.5 Failure Modes in Composites

Failure of metals can be split into two distinct categories; brittle or ductile. Composites failure is much more complex and could be due to failure of matrix (tensile, compressive or shear), fibre (tensile, buckling or splitting) or the interface failure (de-bonding)[30].

In composites, internal material failure (microscopic) generally initiates long before any change in its macroscopic appearance or behaviour is observed. The internal material failure may occur in many forms, separately or jointly; such as (1) breaking

of fibres, (2) micro-cracking of the matrix, (3) separation of fibres from the matrix (debonding) and (4) separation of lamina from each other in a laminated composite (delamination) [39]. An example of a composite failure occurred when the carbon-fibre wing of the Space Shuttle Columbia fractured when it was impacted during take-off. It led to catastrophic break-up of the vehicle when it re-entered the earth's atmosphere on February 1st, 2003 [40].

It is important to observe the failure modes after testing as this can give clues to the major weaknesses in the combined materials. The principal forms of failure are matrix cracking, fibre/matrix debonding, inter-layer delamination, fibre fracture and fibre pull-out. Typical images of failures (fractographs) can be found in Bascom and Gweon [41].

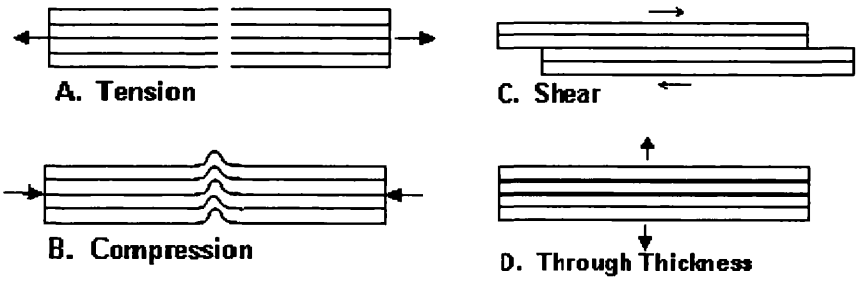

Figure 2-16: Failure modes of composites [41]

Laminate failure can occur in the fibres or in the resin. Figure 2-16 shows various failure modes for a laminate, modes A and B are fibre dominated while C and D are resin dominated.

2.7.5.1 Tension (Figure 2-16 A)

Tensile tests are usually performed using a coupon with parallel sides. It is usually necessary to add end tabs (often aluminium or glass-fibre) to prevent crushing in the grips of the testing machine and to introduce the load into the coupon [1,2,3,4,42,5].

2.7.5.2 Compression (Figure 2-16 B)

The compression test is essentially similar to the tension test except that the force is in the opposite direction (i.e. push instead of pull). An additional complication arises because of a further failure mode: for slender coupons, buckling may occur. Most standard test techniques employ some form of anti-buckling guide to suppress this type of failure[6,44,45,46].

2.7.5.3 In-plane shear properties (Figure 2-16 C)

In simple shear loading, two parallel faces move in opposite parallel directions. In pure shear, the plane is subjected to tensile forces and compressive forces of equal magnitude on the orthogonal axis. Many different techniques have been proposed for the determination of the in-plane and through-plane shear properties with variations appropriate to composite plates, rods and tubes[8,43].

2.7.5.4 Inter-laminar shear strength (Figure 2-16 D)

The inter-laminar shear strength (ILSS) test is a three-point bend test at very small span/depth ratio (typically 5/1). This parameter should not be used for design purposes as the coupon is not in a pure shear stress state due to the tensile and compressive stress states experienced on opposite faces of the test coupon[33]. The test is often used to monitor the quality of the laminate: it normally measures the strength of the fibre/resin interface or of the resin rich area between the lamina[7,37,42].

2.7.6 Effect of Stress Concentrations

Composites are elastic to failure. This means that local stress concentrations cannot be relieved by plastic deformation as with metals; therefore composites are subject to large stress concentration factors (SCF) at holes. The SCF at a hole reduces the static strength of composites, unlike metals where it affects the fatigue strength[9,10,39].

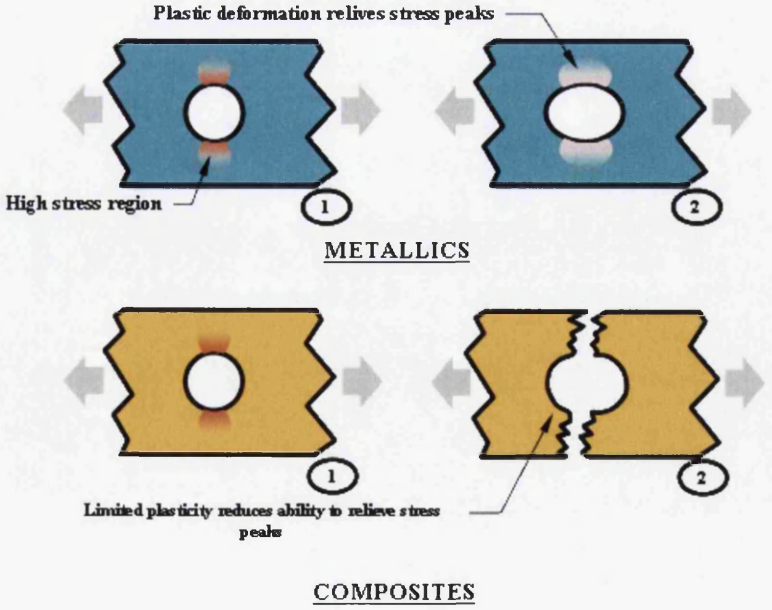

Figure 2-17: Plastic deformation in composites compared to metals[32].

2.8 Mechanical Testing

Composite testing is an extensive topic and many different standard methods exist for characterising mechanical properties[33]. A review of different composite test methods can be found in the Mil-handbook-17[47]. The methods chosen in this test programme were done so to be in line with validated test methods used at Airbus.

2.9 Moisture Absorption in Composite Materials

Composite applications will almost always entail contact with liquids or vapours, which can affect the immediate or the long-term performance of the material[48]. Immediately after manufacture the matrix material in a composite will begin to absorb moisture from humid air, the manner in which this occurs and to what extent is crucial in assessing the material's performance. Moisture can affect each of the three phases in a composite, that is, the fibre, the fibre/matrix interface and most importantly the polymer/resin matrix [49].

Moisture absorption can take place via the following mechanisms[15]:

1. fibre-matrix interface;
2. cracks and voids in the composite;
3. the resin.

The above is true for inorganic fibre composites such as boron, carbon and glass where the fibres do not seem to absorb significant amounts of moisture. Organic fibres however will absorb significant amounts of moisture. An important example is Aramid (or Kevlar™) composites which when saturated can hold up to 8wt% moisture, which is absorbed through an extensive internal defect structure consisting of a partially interconnected network of micro-voids and cracks[50,51].

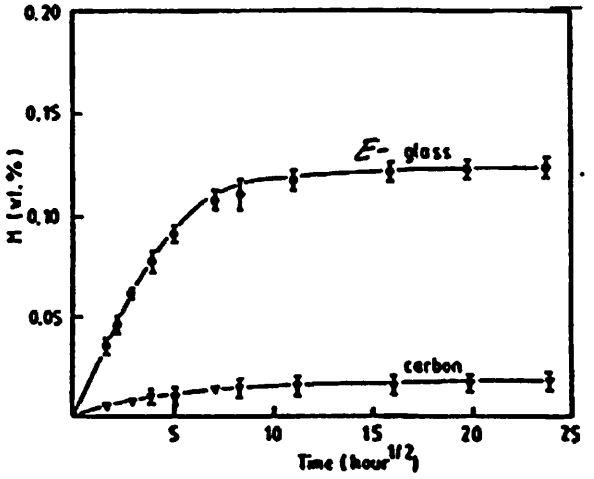

Figure 2-18: Water absorption of E-Glass and carbon fibres at 98%RH and 23°C [51].

It has been found that carbon fibre does not absorb moisture to any significant extent[51,52,53], as figure 2-18 illustrates (<0.01wt% moisture at equilibrium). This

makes it simpler to assess the diffusion properties of a composite material employing these fibres since the analysis only needs to consider the matrix material. Even though the fibre takes little moisture, it still plays a role in the effect moisture has on the composite material. As the matrix material absorbs water it can typically swell; the presence of the fibres tries to inhibit the matrix from swelling and thus induces internal stresses within the material[54]. As fibres are usually coated, or "sized" prior to being imbedded into the matrix resin to improve fibre/matrix adhesion, the sizing forms an integral part of the interface. Results from fibre pull out tests[62] have shown that the interface is especially sensitive to hygrothermal conditioning and may be the weak link in composite performance.

Table 2-3 lists some typical moisture weight gains of different polymer matrix materials. The corresponding moisture weight gain of the composite is typically about a third of the values noted in table 2-3. Polyether ether ketone (PEEK) is the most common thermoplastic matrix used in high performance applications; PEEK is a semicrystaline structure and has very low water absorption (0.5wt%) at room temperature.

Table 2-3: Equilibrium moisture contents for various polymers[51]

Material Supplier	Designation	Polymer Type	M_{max} (wt%)
Shell	9101	Epoxy	2.0
Hexcel	HX-1504	Epoxy	3.8
Hercules	2502	Epoxy	5.0
Union Carbide	4901	Epoxy	7.2
Hercules	220-3	Toughened Epoxy	4.0
Hexcel	F155	Rubber Toughened Epoxy	9.4
ICI	Victrex	PEEK thermoplastic	0.5
Armco	Torlon	Poly(amide-imide)	0.3

2.9.1 Polymer Permeability

Polymers are permeable to moisture, whilst ceramics, glasses and metals are impermeable. The fundamental reason for the permeability of polymers is the relatively high level of molecular motion, a factor that leads to high levels of creep in comparison to other materials[36]. Moisture absorption interrupts Van-der-Waals bonds between polymer chains and allows more freedom in their motion. This plasticization process increases strains and lowers T_g.

Transport processes in polymers depend on two major factors[52]:

- Polymer chain segmental mobility.
- Defect in the structure: i.e. voids/micro-cracks.

Moisture transport in polymers is related to the availability of molecular sized holes in the polymer structure and the polymer-water affinity. The availability of these holes depends on the polymer micro-structure, morphology and cross-link density.

The polymer-water affinity is related to the presence of hydrogen bonding sites along the polymer chain, which creates attractive forces between the polymer and water molecules[55]. Water molecules are free to move through holes/free volume and are referred to as unbound (i.e. fills unoccupied space/micro-voids, so no swelling of the material occurs).

Cured epoxy resin contains polar hydroxyl groups which because they retain a certain degree of steric freedom are able to hydrogen bond with similar groups, i.e. the polar water molecule. Diffusion of small molecules in polymers is influenced by "free volume" i.e. the space/volume in the material lattice/structure unoccupied by atoms. Epoxies have a significant amount of free volume, particularly at temperatures 50-150°C below T_g. Also the epoxy-water affinity is relatively strong due to polar hydroxyl groups created during curing.

There are two possible modes of absorption[56]:

- *Free volume of polymer* (depending on cross-linked density). This model assumes water diffuses in and resides in free volume. Bonding between water molecules and epoxy resin network is deemed insignificant.

- *Hydrogen bonding* of water molecules at hydrophilic sites present in the polymer network. This approach suggests water molecules are bonded to certain hydrophilic functional groups such as hydroxyl or amine.

In general, one would expect epoxy resins, which form low cross-link density systems, to absorb greater amounts of water than highly cross-linked systems. A study by Fleming and Rose[57] compared the relative amount of absorbed water for

various epoxy resin systems (figure 2-19). The term "hydrolytic stability", loosely implies the prolonged maintenance of structural properties in moist environments.

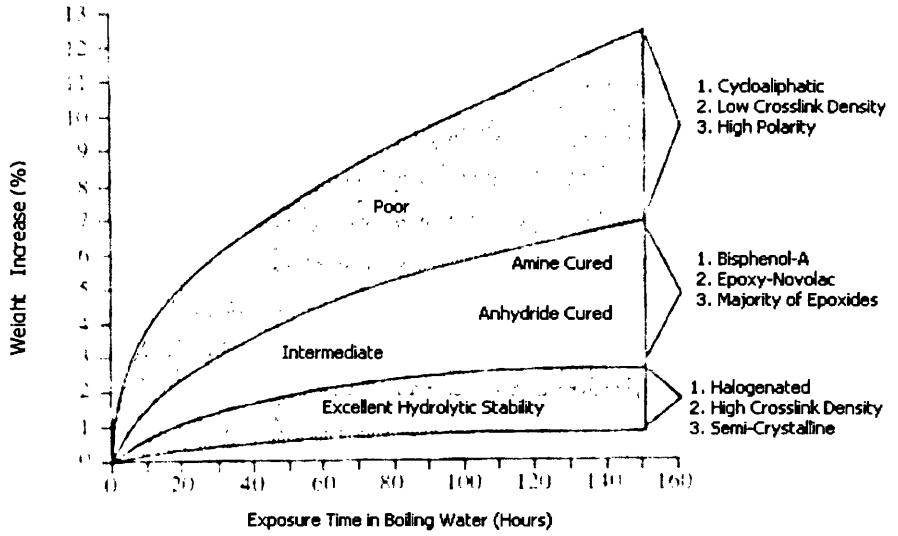

Figure 2-19: Relative stability of epoxy resin according to structure[57].

When measuring absorption and desorption of moisture from a CFRP material the curves will be similar in appearance but may not be super-imposable due to varied internal stress states. Desorption takes longer than absorption and non-postcured samples may never completely desorb due to bound sites for the H_2O. To remove all H_2O, it may be necessary to heat above T_g.

2.9.2 Effects of Moisture on the Polymer Matrix

Water molecules have a low molecular weight and can easily migrate into a polymeric material[36,58]. The chemical composition and microstructure are the two parameters that strongly influence water sorption mechanisms in polymers[58]. Effects of moisture in an epoxy matrix include:

- Plasticization
- Lowering glass transition temperature, T_g
- Diminishing mechanical properties.

Therefore, knowledge of the transport mechanisms of moisture in the epoxy structure is very important to the aircraft industry. The kinetics of absorption and distribution of water in a polymer matrix material has been widely investigated, but

still not fully understood. Epoxy resins typically absorb between 3.0 and 6.5wt% moisture at equilibrium and there is approximately a 20°C decrease in T_g for every 1.0wt% moisture absorbed[36]. Figure 2-20 shows a plot of T_g versus moisture content for neat epoxy 3501-5 resin, from work done by Browning et al[59].

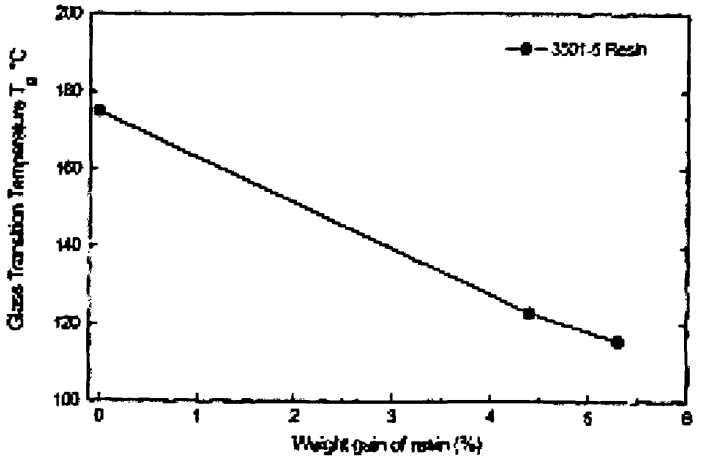

Figure 2-20: T_g versus wt% moisture for neat 3501-5 epoxy resin cured at 177°C[59].

Polymer based materials are often exposed to humid environments where water molecules (as well as other low-molecular weight substances) can easily migrate in the polymeric matrix, even at ambient temperatures, modifying their physical properties. The chemical composition and microstructure are two parameters that strongly influence water sorption mechanisms.

Epoxy resins are widely used as matrices for structural composite materials due to their good mechanical properties. However it is well known that epoxy resins will absorb moisture from their surroundings. Absorbed moisture acts as a plasticizer (it embeds in the chains of the polymer, spacing them apart, thus increasing the free volume and significantly lowering the T_g, making it softer), which diminishes mechanical properties. Therefore, mechanical properties of composites that are matrix or interface dominated, e.g. shear, flexural, compression and transverse tensile strength and stiffness, can be adversely affected by absorbed moisture. The amount of moisture absorbed mainly depends on the relative humidity (%RH), whereas the rate of diffusion depends mainly on the temperature[16].

2.9.3 Effects of Moisture on Fibre-Matrix Interface

The interface plays a key role in moisture absorption behaviour and strongly affects the composite response in a wet environment[60,61]. Results of fibre pull out tests have shown that the fibre/matrix interface is especially sensitive to hygrothermal conditioning and may be a 'weak link' in composite performance. It is perhaps important to consider that the glass transition temperature (T_g) and the diffusion properties of the interface may possibly be different to the bulk matrix.

The absorbed water at interfaces is considered to break the fibre/matrix bonding. Interface debonding by moisture absorption has been observed by many authors. Komai et al[62] noted that water absorption decreased the strength of the fibre-matrix interfaces of unidirectional reinforced carbon-epoxy composites. Jackson and Weitsman[63] showed that a cyclic moisture environment exposed to a laminate might cause debonding at the fibre/matrix interface.

2.10 Mechanisms of Moisture Diffusion

Water penetration into Polymer matrix composites (PMC) involves three mechanisms:

1. Direct diffusion of water molecules into matrix depending on the angle between penetration direction and fibres.

2. Flow of water molecules along interface (capillary action), followed by diffusion into bulk resin, which can result in de-bonding. This capillary flow, also known as water wicking, represents the second mechanism for conveying water to the interior of composites. It tends to occur preferentially along the interface if there is a failure of the bond between the fibre and the matrix.

3. Infiltration of water via micro cracks/pores already present in the material or generated by water attack[64].

Studies show diffusion into PMC follows a Fickian model, which corresponds to mechanism (1) above. Mechanism (2) and (3) deviate from ideal and are termed anomalous or non-Fickian diffusion.

Diffusion has great practical significance for composites. We need to know how much, how rapidly and to what extent a solvent diffuses into a composite material. The amount of liquid absorbed is a useful indication of the magnitude of change in mechanical properties.

2.11 Diffusion Theory

Diffusion is the movement of particles from an area of high concentration to an area of low concentration by random molecular motion. Initially, a concentration gradient will exist between the two regions. With time however, the gradient will become increasingly shallow until the concentrations are equal.

The diffusion equation provides a mathematical description of diffusion and is derived from Fick's Law (derived by Adolf Fick in 1855[65]). Fick summarised that diffusion occurs in solids in response to a concentration gradient. Fick suggested that wherever a concentration gradient occurred, diffusion should occur to reduce it. This produced 'flux': the rate of flow through a cross-sectional area. Once the concentration gradient is removed, the flux stops.

Fick's Law of diffusion is often referred to when describing the diffusion process and includes a diffusion coefficient, D. The diffusion coefficient depends on the diffusing species and the material through which diffusion occurs. Fick recognised that diffusion is a dynamic molecular process and he understood the difference between true equilibrium and a steady state. Transfer of heat by conduction is also due to random molecular motions and Fick recognised that there was an obvious analogy between the two processes, via a comparison with Fourier's work (in 1822) on heat conduction[13,66].

Fick's First Law is the fundamental law of diffusion for isotropic substances[13]. It states that the flux in the x-direction (F_x) is proportional to the concentration gradient ($\partial c/\partial x$):

$$F_x = -D\frac{\partial c}{\partial x} \qquad 2\text{-}2$$

where the flux is the amount of substance diffusing across a unit area in a unit time and D is the diffusion coefficient. Fick's First Law can only be directly applied in a steady state, that is where concentration, c, is not varying with time.

2.11.1 Fick's Second Law

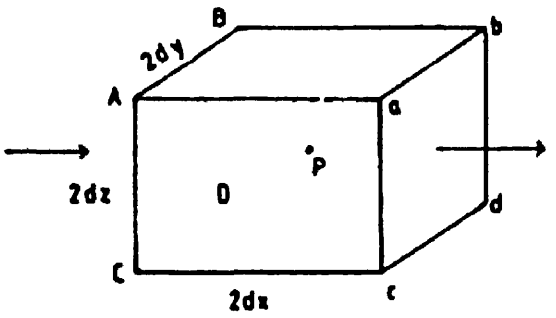

Figure 2-21: Volume element for the derivation of Fick's Second Law of diffusion[13].

The fundamental differential equation of diffusion in an isotropic medium is derived from equation *2-2*. Consider a box shaped element in Cartesian co-ordinates. A point "P" is at the centre of a volume element which has edges of length 2 dx, 2 dy and 2 dz (figure 2-21). If there is a flux gradient ∂F/∂x in the x-direction and the x-direction flux at "P" is F_x then the actual flux at the face ABCD is $(F_x - (\partial Fx/\partial x))dx$ and at the face abcd it is $(F_x + (\partial Fx/\partial x))dx$. So the material entering the face ABCD in a unit time is $4dy\ dz(F_x - (\partial Fx/\partial x))dx$ and leaving face abcd is $4dy\ dz(F_x + (\partial Fx/\partial x))dx$. Hence the material accumulating in the volume element due to diffusion in the x-direction is[13]:

$$R_x = -8dx\,dy\,dz(\partial F_x / \partial x) \qquad 2\text{-}3$$

And similarly equations can be derived for the y and z directions

$$R_y = -8dx\,dy\,dz(\partial F_y / \partial y) \quad \textit{and} \quad R_z = -8dx\,dy\,dz(\partial F_z / \partial z) \qquad 2\text{-}4$$

The concentration of diffusing substance is c, so the rate of concentration increase in the element is given by[13]:

$$\frac{\partial c}{\partial t} = \frac{R_x + R_y + R_z}{8dx\,dy\,dz} \qquad 2\text{-}5$$

So,

$$\frac{\partial c}{\partial t} = -\left(\frac{\partial F_x}{\partial x} + \frac{\partial F_y}{\partial y} + \frac{\partial F_z}{\partial z}\right) \qquad 2\text{-}6$$

The flux gradients are obtained by differentiating equation 2-2, for example $(\partial F_x/\partial x) = -D\partial^2 c/\partial x^2$, so that

$$\frac{\partial c}{\partial t} = D\left(\frac{\partial^2 c}{\partial x^2} + \frac{\partial^2 c}{\partial y^2} + \frac{\partial^2 c}{\partial z^2}\right) \qquad 2\text{-}7$$

reducing simply to[13];

$$\frac{\partial c}{\partial t} = D_x \frac{\partial^2 c}{\partial x^2} \qquad 2\text{-}8$$

if diffusion is one dimensional[13], D_x is the diffusivity of the material in the x-direction. Equation 2-8 is referred to as Fick's Second Law and is used in non-steady state diffusion, i.e. when the concentration within the diffusion volume changes with respect to time.

2.11.2 Diffusion in Composite Materials

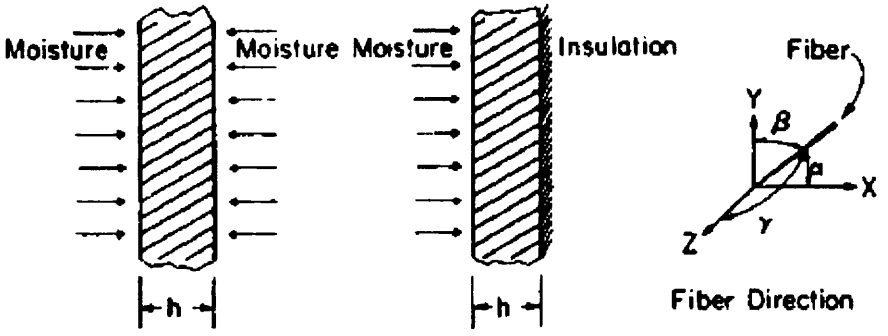

Figure 2-22: Composite plate exposed to hygro-thermal environment[22].

A plate of thickness h exposed on two sides to a humid environment (figure 2-22); it is assumed to be infinite in the y and z directions so that the moisture varies only in the x-direction (i.e. the problem is one dimensional). Initially (at time $t < 0$) the moisture concentration c_0 is uniform inside the plate. The plate is suddenly exposed to a humid environment in which the moisture concentration, c_∞ is constant. The aim is to calculate the moisture distribution c, and the total moisture content M_{max} of the material as a function of time. The moisture concentration can be described by Fick's Second Law (equation *2-8*).

The moisture concentration at the surface of the material M_{max} is related to the moisture content of the environment. The mass diffusivity D_x depends on the temperature and on the moisture concentration. The parameter D_x is a measure of the "speed" by which the moisture concentration changes inside the material.

Thermal diffusion coefficients are about 10^6 times faster than the moisture concentration[66]. For example, for a 12.5mm thick Graphite T-300 Fiberite 1034 composite exposed to 90%RH at 350K approaches temperature equilibrium across the plate in about 15 seconds while the moisture concentration reaches equilibrium in approximately 13 years[22]. Therefore, in most practical situations the temperature inside the material may be taken to be the same as the ambient temperature. It has also been observed that the moisture diffusivity changes very little with the moisture content.

2.11.3 Solutions to Fick's Second Law

General solutions of the diffusion equation can be obtained for a variety of initial and boundary conditions (such as those in equation 2-9) provided the diffusion coefficient is a constant. Solutions are either a series of error functions (suitable for numerical evaluations at small times) or in the form of a trigonometrical series which converges more satisfactorily at large times.

Consider the following boundary conditions (shown in figure 2-22):

$$\begin{array}{lll} c = c_0 & 0 < x < h & t = 0 \\ c = c_\infty & x = 0;\ x = h & t > 0 \end{array} \qquad \text{2-9}$$

where:

h is the plate thickness

c is concentration

c_0 is initial concentration

c_∞ is concentration at equilibrium

x is distance in the thickness direction

t is time

Given the previous boundary conditions, equation 2-8 has a variety of analytical and numerical solutions[13,67]. Using the "separation of variables" method for simple initial and boundary conditions (in equation 2-9), Jost[67] obtained the solution:

$$\frac{c-c_0}{c_\infty-c_0}=1-\frac{4}{\pi}\sum_{n=0}^{\infty}\frac{1}{(2n+1)}\sin\frac{(2n+1)\pi x}{h}\exp\left[-\frac{(2n+1)^2\pi^2 D_x t}{h^2}\right] \qquad 2\text{-}10$$

where n is an integer. This equation describes the transient concentration distribution in an infinite plate.

Another solution to equation *2-8*, which calculates concentration at a given depth and time[13] is given by:

$$c(x,t)=c_\infty erfc\left[\frac{x}{2\sqrt{D_x t}}\right] \qquad 2\text{-}11$$

In order to solve equation *2-11* values of "*erfc*", the complementary error function is required. The error function is related to the expression for a Gaussian distribution and has the form:

$$erfc(x)=1-erf(x) \qquad 2\text{-}12$$

where:

$$erf(x)=\frac{2}{\sqrt{\pi}}\int_0^x e^{-t^2}dt \qquad 2\text{-}13$$

Of the two solutions (eq. *2-10* and *2-11*) the version that contains the trigonometric functions converges rapidly for long times, while the solution employing the complementary error function converges rapidly for short times.

2.11.4 Experimental Identification of the Diffusion Parameters

If a material (either homogeneous or composite) is exposed to a moist environment, depending upon the environmental conditions and the condition of the material, the material either absorbs or loses moisture as manifested by weight gain or weight

loss. The percent moisture content, M (percent weight gain) of the material can be determined as a function of time, t.

The total amount of moisture, M in the laminate can be obtained by integrating equation *2-10* over the plate thickness, h.

$$M = \int_0^h c(x,t)\,dx \qquad 2\text{-}14$$

The result of this integration gives:

$$G = \frac{M - M_0}{M_{max} - M_0} = 1 - \frac{8}{\pi^2}\sum_{j=0}^{\infty} \frac{\exp\left[-(2j+1)^2 \pi \left(\frac{D_x t}{S^2}\right)\right]}{(2j+1)^2} \qquad 2\text{-}15$$

where G is a time dependent parameter, M is the moisture content at any time t, M_0 is the initial weight of moisture in the material (i.e. the weight prior to exposure to the environment) and M_{max} is equilibrium moisture content. For a material exposed on two sides to the same environment S is equal to the thickness ($S=h$). For a material insulated (i.e. impermeable to moisture) on one side, S is twice the thickness ($S=2h$).

In practice the percent moisture content, M, manifested as weight gain of the material *(wt%),* is the parameter of practical interest and is defined as:

$$M = \frac{Weight\ moist\ material - Weight\ dry\ material}{Weight\ dry\ material} \times 100 = \frac{W_i - W_d}{W_d} \qquad 2\text{-}16$$

Shen and Springer[19] found that when the following conditions were met:

a) The material is exposed to the environment on one side only, or on two sides with both sides being parallel (1D problem - figure 2-22).
b) Initially, the temperature and moisture distributions inside the material are uniform.
c) The moisture content and the temperature of the environment are constant.

Then equation *2-15* can be rearranged to calculate the moisture content, M, of a material during both absorption and desorption by:

$$M = G(M_{max} - M_0) + M_0 \qquad 2\text{-}17$$

M_0 is the initial moisture content of the material, M_{max} is the maximum moisture content, which can be attained under the given environmental conditions and G is a time dependent parameter.

An analytical approximation for G is given by[19]:

$$G = 1 - \exp\left[-7.3\left(\frac{Dt}{S^2}\right)^{0.75}\right] \qquad 2\text{-}18$$

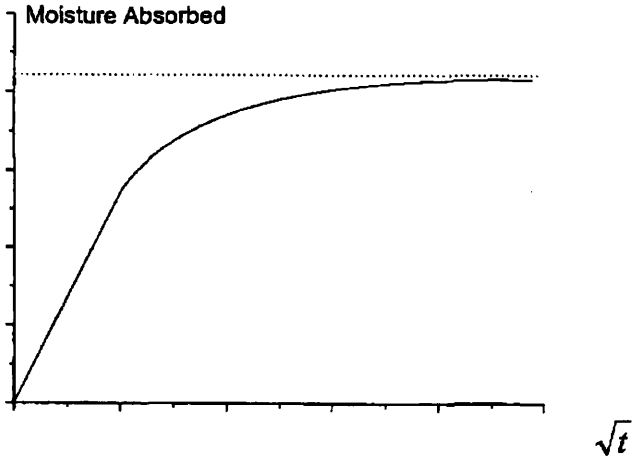

Figure 2-23: Moisture absorption vs.√t (constant RH and T).

Fickian diffusion is characterised experimentally by a moisture absorption curve that reaches an asymptotic value after a period of time. If the weight gain of a sample exposed to a constant humidity and temperature is plotted against the square root of time, there will be an initial linear region up to about 60% of the maximum moisture content (M_{max}) followed by a gradual approach towards the asymptotic value. This asymptotic value is the boundary condition and is defined as the concentration of moisture experienced at the surface layer of the material. A typical Fickian weight gain plot is shown in figure 2-23.

2.11.4.1 The Diffusion Coefficient, D_x

The presence of fibres means that the composite is anisotropic, and therefore has several diffusion coefficients. The reason why diffusion parallel to the fibre direction in unidirectional laminates is usually faster than in the other directions is probably a question of the simplicity of the diffusion path, although internal stresses and the presence of the interface cannot be entirely neglected[36]. For CFRP aircraft applications, moisture diffusion is through a large surface area with very few edges. As a result, diffusion through the thickness is of primary interest. For such a case, thin composite coupons are utilised for diffusion measurements with edges sealed with an impermeable coating or foil. For sufficiently small values of t, it can be shown that equation *2-15 is* closely approximated by[13]:

$$\frac{M}{M_{max}} = \left(\frac{4}{h}\right)\left(\frac{D_x t}{\pi}\right)^{\frac{1}{2}} \qquad 2\text{-}19$$

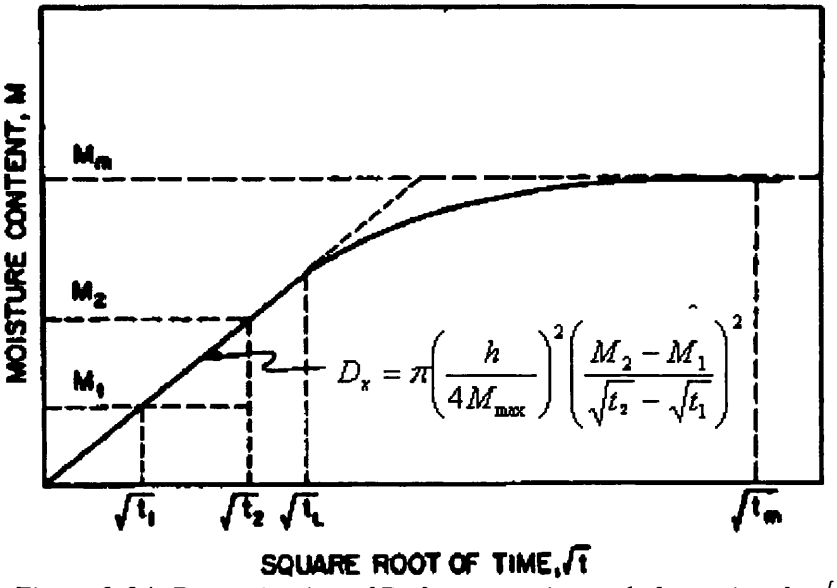

Figure 2-24: Determination of D_x from experimental absorption data[19].

Thus, in its initial stages, moisture absorption proceeds at a rate proportional to the square root of the time. For this reason, in graphical representation it is usual to plot moisture absorption against √t, as shown in figure 2-24. When this is done the initial part of the curve is a straight line and the diffusion coefficient D_x can be determined experimentally by the measurement of the slope of this line[19] using the following equation:

$$D_x = \pi\left(\frac{h}{4M_{max}}\right)^2\left(\frac{M_2 - M_1}{\sqrt{t_2} - \sqrt{t_1}}\right)^2 \qquad 2\text{-}20$$

where M_1 and M_2 are the percentage moisture at times t_1 and t_2 respectively, h is the laminate thickness and M_{max} is the equilibrium moisture level for the given relative humidity.

Two general features of moisture absorption in laminates are:

1. The higher the temperature the faster the moisture is absorbed, the diffusion coefficient being strongly dependent on temperature.
2. The thicker the laminate, the longer it takes for saturation to be achieved.

The slope, M/√t, is obtained from using the complete coupon (finite plate) and therefore includes moisture diffused through all six surfaces. This produces a greater slope than would have been obtained for an infinite sheet, as moisture has diffused through six sides instead of two. To get a better estimate of the true one-dimensional through thickness coefficient, D_x, a correction factor given by Shen and Springer[19] is used:

$$D_x = D\left(1 + \frac{h}{W} + \frac{h}{l}\right)^2 \qquad 2\text{-}21$$

where W and l are the coupon width and length, respectively. Shen and Springer[15] used this correction factor to account for edge effects when applying a 1-D solution to problems with finite laminated plates. Whitney[118] presented 3D solutions to Fick's equation. His trigonometric and Laplace solutions are both products of 1D solutions. He compared the solutions with experimental data and concluded for thin laminates a 1D solution can be used, while for moderately thick laminates a 1D solution with the edge factor correction gives good results.

2.12 Moisture Distributions

After manufacture, a composite material is essentially completely dry; this is time (t_0). Exposure to humid air allows moisture to begin to diffuse through the outer plies of the composite and through to the coupon centre after time (t_1). After a longer period of time under constant humidity conditions, an equilibrium moisture level is obtained and an even moisture distribution arises at time (t_∞); see figure 2-25. It is important to note that at stages other than the fully dry or fully saturated case, a profile of moisture concentration will exist in the matrix. Since moisture affects the mechanical properties of the matrix, this also implies that a profile of properties will also exist through the thickness[17].

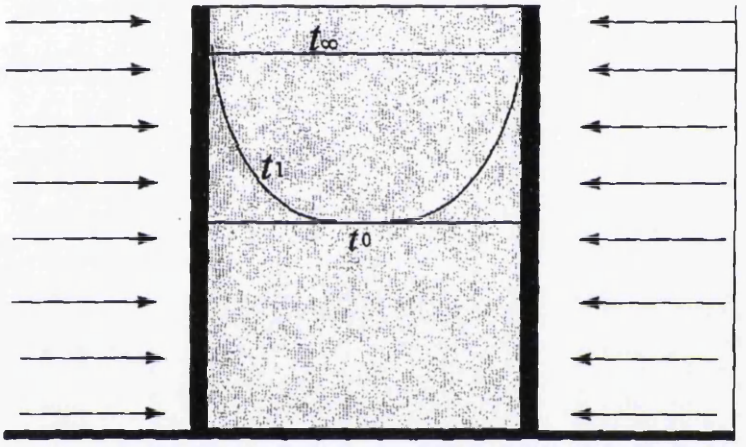

Figure 2-25: Diffusion of moisture into composite over time[17].

If the humidity conditions are transient (as occurs in normal weather patterns) a complex profile of moisture through the coupon may result. The moisture concentration profile that develops within the matrix is dependent on the boundary conditions, material type and exposure temperature[17]. Diffusion behaviour is material specific therefore experimental characterisation to define diffusion constants of each material is required. This is costly and time consuming but essential to fully understand environmental effects on composite materials.

Equations *2-10* and *2-11* are analytical solution to Fick's Second Law. Using the boundary conditions in equation *2-9*, they give the concentration of moisture at various depths in a laminate at various times. Figure 2-26 shows the theoretical plots of moisture distribution through the thickness, for a 1mm thick continuously aligned E-glass/F922 composite plate, following exposure to a hot/humid

environment (i.e. 70°C and 85%RH) for a period up to 1 year[68]. Moisture is absorbed by the surfaces and then slowly diffuses layer-wise towards the centre of the laminate. For sufficiently long durations, the moisture concentration attains a uniform (or equilibrium) saturation moisture level, M_{max}[78].

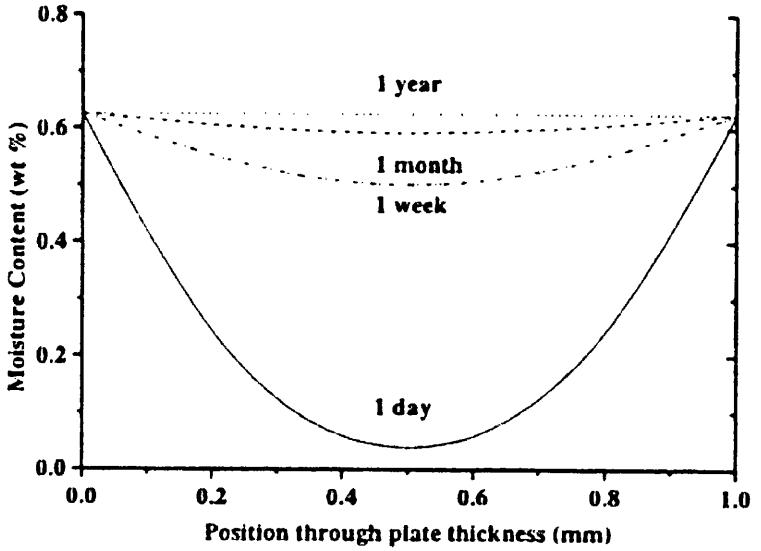

Figure 2-26: Moisture distribution in a 1mm thick E-glass/F922 plate following exposure at 70°C and 85%RH[68].

The profile of moisture concentration within a composite also reflects the profile of the properties through the thickness. Whilst weight gain data is one of the most commonly used means of detecting the ingress of moisture into composites, it tells us nothing about concentration profile[68,77]. From equations *2-10, 2-11* and *2-15* the moisture content and its distribution inside a laminate can be calculated, for any time at a given temperature and humidity, providing that the diffusion coefficient and moisture content at equilibrium are known. Weitsman[69] demonstrated a method to deduce the concentration of moisture within composites from weight gain data using numerical approximation. However very little data are available regarding moisture distributions within polymers or polymeric composites[70].

There are three main steps required to model diffusion of moisture in composites:

- Determine diffusion behaviour (e.g. Fickian/non-Fickian)
- Establish boundary conditions (surface concentration value, M_{max})
- Establish the diffusion constant, D.

Experimental techniques which have been used to directly measure the moisture profile content of polymeric composites are reviewed. The following techniques are not widely used and do not represent a routine moisture evaluation technique:

1. **Dielectric** - The change in dielectric response of polymer matrix materials with moisture has been demonstrated[71].The use of dielectric techniques on composites with conducting fibres is mostly unsuccessful due to the electric conductivity of the conducting fibres. A novel microwave dielectric technique developed by KDC Technology Corporation[72] has shown to be useful to profile Kevlar and glass fibre composites[73].

2. **Deuterium conditioning** - Delasi and Schulte[74] devised experimental method for evaluating localized moisture content, involving conditioning the coupon in D_2O, followed by measurement of the localized deuterium concentration by means of nuclear reaction. Both equilibrium moisture levels and profiles can be obtained this way. More recently Pilli et al[75] also used D_2O to condition CRFP and used NRA nuclear reaction analysis to measure moisture through-the-thickness.

3. **Sectioning** - Collings and Copley[76] reported a method by which a composite coupon 2mm to 3mm thickness is physically sectioned after exposure to a humid environment to allow the measurement of a profile. The method is attractive since the time required to extract both the diffusion coefficient and the moisture equilibrium level may be made in a relatively short time (30 days). Coupons are physically split through the thickness and then dried to measure moisture content by weight. The authors claim the method is accurate.

4. **Analytical techniques** - Mathematical solutions may be used to determine moisture profiles. Moisture profiles can be computed from the weight gain data[77] if the diffusion properties of the material are known.

Work performed by Revathi e al[78] on the moisture distribution profiles of nine different thickness (ranging from 0.25 to 2.25mm) glass/epoxy composites. They studied the comparative evolution of their moisture diffusion and distribution profiles across the thickness as a function of the exposure period; they used the solution shown in equation *2-10* to model the moisture distributions. Figure 2-27 shows the

moisture distribution times as a function of dimensionless exposure time t* for (a) a 0.25mm and (b) a 2.25mm thick laminate. It can be seen as exposure time increases the distribution becomes flatter, for the thicker laminate moisture distribution plots corresponding to larger exposure times become visible. Therefore it is concluded there is a thickness effect on the moisture distribution process, with larger exposure times. They also reported that the laminate thickness had a negligible effect on the diffusion coefficient, but did affect the absorption rates (slopes of the absorption curves) which decreased with increasing thickness.

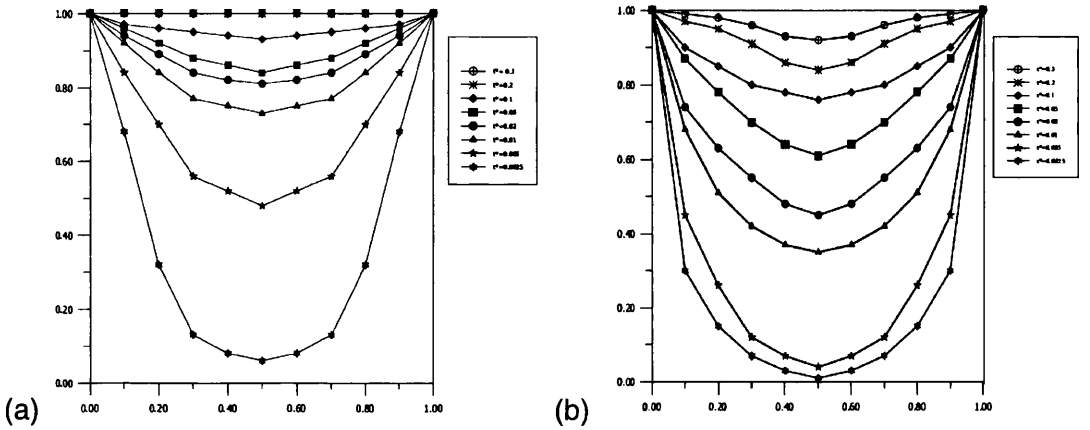

Figure 2-27: Moisture distribution as functions of exposure time (t) for (a) 0.25mm and (b) 2.25mm thick laminate specimens: x-axis: Position (x/h); y-axis: Moisture concentration*[78].

Profiles of water within graphite epoxy composites were recorded by radioactive D_2O conditioning at several times during the diffusion process by Whiteside et al[79]. Typical results of the later technique are shown in figure 2-28 where the recorded distributions (average recorded concentrations of heavy water (D_2O) after 2 months at 70%RH at 305K) are compared to Fickian diffusion predictions. In spite of the scatter in the results they tend to corroborate predictions.

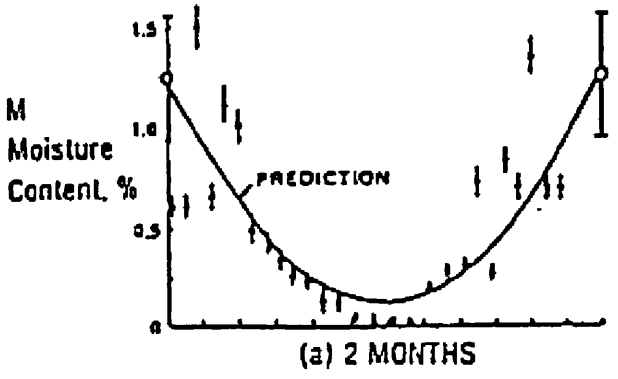

Figure 2-28: Measured concentration values with distribution predicted by Fick's Law[79].

2.13 Factors Affecting Moisture Concentrations

Two primary factors govern diffusion behaviour: (1) the rate at which the moisture is absorbed and (2) the final saturation level achieved. The rate at which the moisture absorption occurs is a function of the temperature to which the material is exposed. The saturation moisture absorption achieved after long exposure to the temperature and humidity condition, is usually governed by the moisture level or relative humidity to which the material is exposed. Thus the temperature and moisture level work together to determine the rate and ultimate quantity of moisture absorbed by the material[80]. Other influencing factors on the rate, amount and distribution of moisture in a structure include: voids/defects, thickness effects, stacking sequence and fibre content. These factors will be discussed in the following sections.

2.13.1 Relative Humidity, %RH

Rainfall and humidity are sources of moisture that composites in an aerospace application will often encounter. The higher the moisture concentration at the composite surface, the greater the quantity of moisture absorbed by the material. The limiting conditions are dry air (zero humidity) and immersed in water (100% humidity). Figure 2-29 illustrates the effects of increasing the humidity levels on the profile of a weight-gain versus time plot, under constant temperature.

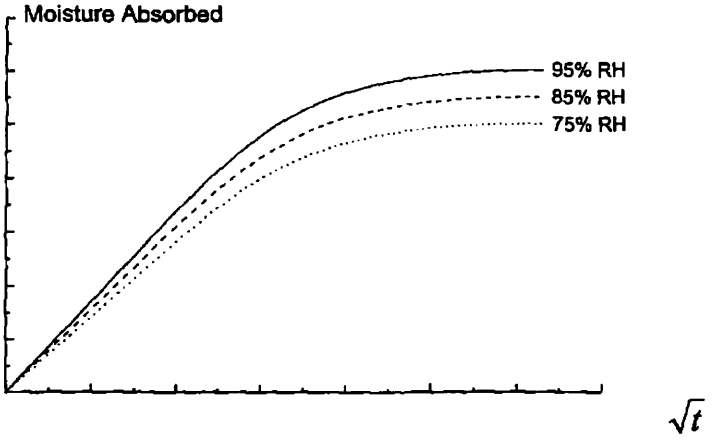

Figure 2-29: Effect of %RH on absorbed moisture with time[17].

Broughton et al[68] immersed UD T300/924 carbon epoxy for 216 days in de-ionised water (figure 2-30). He showed that Fick's Law applies for a temperature range of 25°C-60°C, with M_{max} being a constant with temperature. Table 2-4 lists equilibrium

moisture contents at varying *%RH* for a UD T300/924 (which is a typical aerospace CFRP), showing increasing M_{max} with increasing %RH.

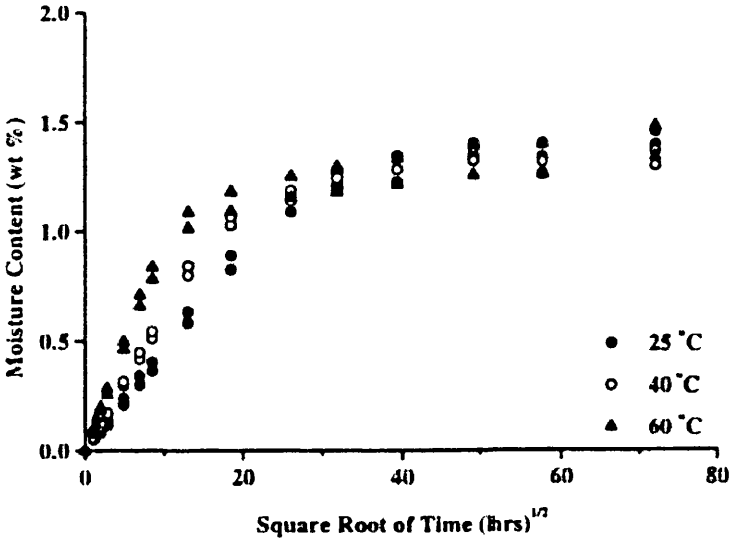

Figure 2-30: Moisture absorption in continuous aligned T300/924[68].

Table 2-4: M_{max} for T300/924 with varying %RH[17].

Material	Relative Humidity (%RH)	Temperature (°C)	Moisture Content M_{max}(wt%)
T300/924 Carbon epoxy (V_f=68%)	50	23	0.35
	75	23	0.78
	100	23	1.4
	fully immersed in water	23	1.8

For material immersed in water, the equilibrium moisture content is a constant. If the material is exposed to humid air, M_{max} increases with increasing relative humidity of the surrounding air with the following relationship[81]:

$$M_{\max} = k.(\%RH)^n \qquad 2\text{-}22$$

where *%RH* is the relative humidity, k, n are constants that depend on the type of polymer and the exponent n has a value between 1 and 2. Constants k and n are derived from a linear regression fit to the data (by plotting M_{max} as a function of *%RH*). Figure 2-31 shows experimental results produced by R. Vodicka[17] on a Boron/Epoxy composite system and fitted to this relationship. The value of n here

deviates from unity but the value of k is typical for many epoxy based systems. The deviation from linear behaviour at humidities greater than 75% could be due to a two-step non-Fickian diffusion process.

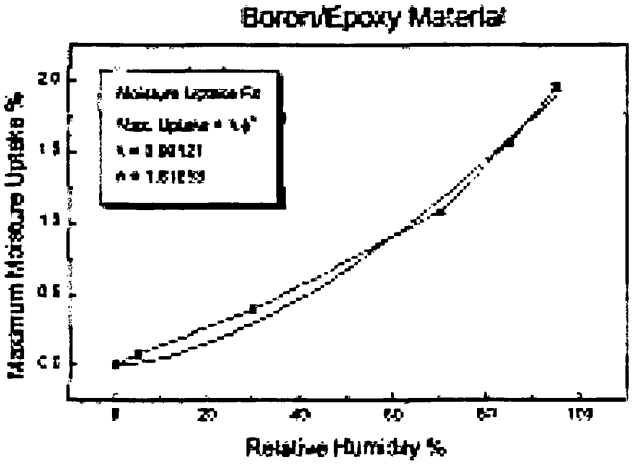

Figure 2-31: Maximum moisture uptake Boron/Epoxy material[17]

Shen and Springer showed equation *2-22* is independent of temperature for a number of graphite/epoxy systems[15].

2.13.2 Temperature Effects

Moisture diffusion into a polymer is an energy-activated process and the diffusion coefficient, D_x depends strongly on temperature[82]. In general the temperature dependence can be described by an Arrhenius-type equation:

$$D_x = D_o \exp\left(-\frac{E}{RT}\right) \qquad 2\text{-}23$$

where D_o is a constant, E is the activation energy of diffusion and R is the universal gas constant. D_o and E/R are determined from a linear regression fit to log D versus $1/T$ graph. Broughton[68] and co-workers determined the values of D_o and E/R for continuous aligned T300/924 laminates, immersed in de-ionised water at temperatures ranging from 25°C to 60°C. The diffusivity of the material increased by a factor of 5 for the temperature range shown in figure 2-32.

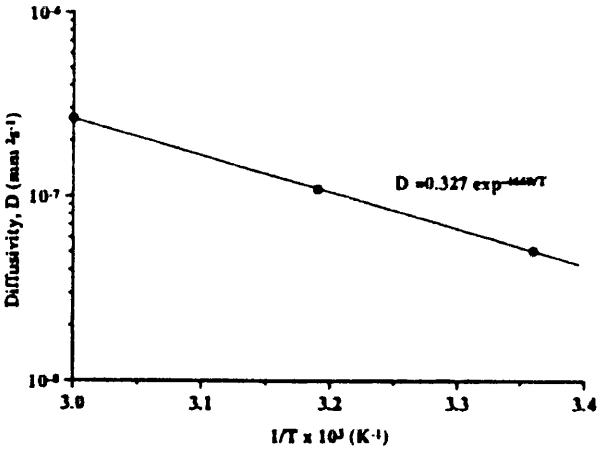

Figure 2-32: Transverse diffusivity vs. temperature for T300/924[68].

An investigation carried out by Papanicolaou[83] into the effect of temperature on water absorption kinetics found that the rate of water absorption increased with temperature. He argued that an increase in temperature results in an increase in the mobility of the molecules and in turn, results in an increase in the volume occupied by the molecules due to their thermally dependent vibrational movement and consequently, the overall volume occupied by the actual mass of the molecules. Thus, the density of the material decreases and the diffusion of the water molecules increases, therefore moisture saturation is reached more rapidly at higher temperatures and this is known to be the principal method of accelerating moisture testing.

While raising the temperature causes an increase in the rate of absorption, the maximum moisture concentration (M_{max}) should not be affected, since it is not a thermodynamic property.

2.13.3 Void Content

If there are microcracks in a structure, the moisture concentration in a laminate may exceed the equilibrium moisture concentration[77]. Moisture absorption is accelerated due to capillary action at the micro-cracks as well as exposed fibre matrix interfaces at the laminate edges. On the other hand, there may be an apparent reduction in moisture concentration if there is a loss of material from leaching or cracking.

Harper et al[84] investigated the effect of voids on the equilibrium moisture content of composites. They found laminates with low void content (about 1%) had equilibrium

moisture content of 1% whilst higher void contents (about 5%) lead to increased equilibrium moisture content of over 1.4%.

2.13.4 Lay-up Configuration

Choi et al[49] investigated the effect of thickness and fibre orientation on the water absorption behaviour in the through-the-thickness direction in a carbon/epoxy laminate (figure 2-33a). They concluded that the diffusion coefficient i.e. water absorption rate, is almost independent of the thickness of the coupons, with all other conditions unchanged.

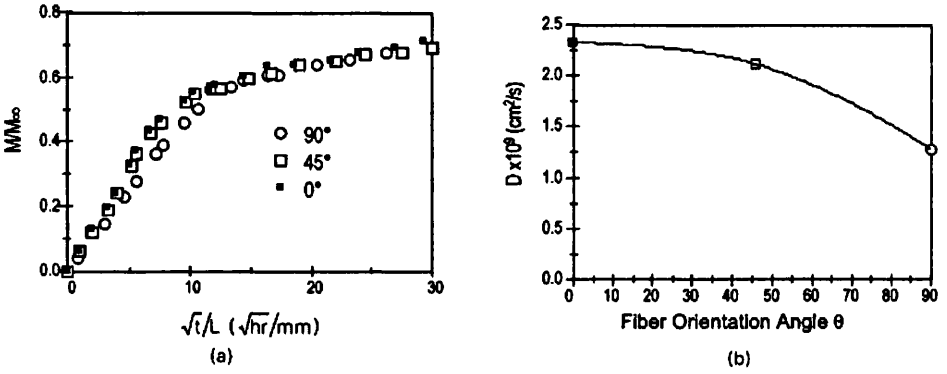

Figure 2-33: (a) Moisture absorption curves, (b) diffusion coefficients for unidirectional laminates with various fibre angles[49].

Choi et al[49] also investigated the effects of fibre orientation on diffusivity using 0°, 45°, and 90° coupons. Figure 2-33b shows that coupons of 0° fibre angle (corresponding to water diffusion in the axial direction) have the highest measured diffusion rate and coupons with a 90° fibre angle show the lowest, seemingly because the 90° fibres make the water molecules move around the fibre surfaces (figure 2-34).

From these studies it is apparent that with different fibre orientation in composite materials, moisture can penetrate at different rates into the polymeric matrix. Botelho et al[85] observed that when conditioning high strength CFR epoxy at 80°C and 90 %RH, cross-ply composites had a slower rate of moisture diffusion compared to UD reinforced composites, but UD material had a higher M_{max} of 1.8wt% compared to 1.4wt% for the cross ply composite.

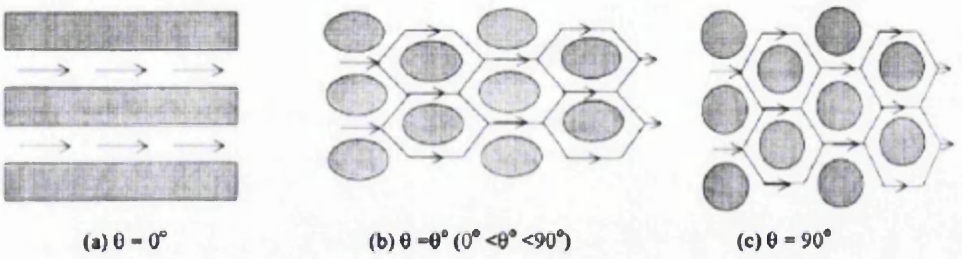

Figure 2-34: Diffusion path of moisture into composite in the thickness direction[49].

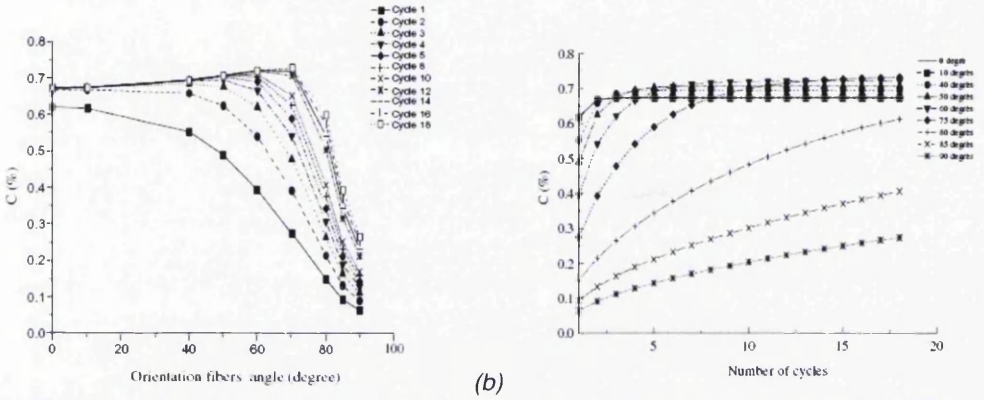

Figure 2-35: (a) Variation of moisture concentration vs. fibre orientation and (b) Variation of moisture concentration vs. fibre angle, with time[86].

Boukhoulda et al[86] also examined the effect of the fibre orientation angle of a composite material (T300/5208) on the diffusion of moisture. They agreed that the orientation of fibre material influences diffusion in the plate. The values of moisture concentration were calculated at different angles. The results obtained are presented in figure 2-35a. This figure shows the variation of moisture concentration versus the fibre (T300) orientation angle for different environmental cycles. The lowest values of moisture concentration calculated through the thickness of the plate correspond to the angle 90° (figure 2-35a). Boukhoulda et al[86] concluded that the disposition of the fibres under this manner formed a barrier to diffusion. For the angle 0°, the values of concentration are distinctly larger. Based on the above findings and the results reported in figure 2-35b, they concluded that the diffusion of moisture with lower angles is much easier than with higher angles. Figure 2-35b presents the variation of moisture concentration during 18 different environmental cycles for different fibre orientation angles (from 0° to 90°). For the angle 0°, the values of the concentration are distinctly larger than those of 90°.

Moisture absorption by composites has been the subject of considerable investigation, where moisture diffusion under normal environmental conditions is approximated as a Fickian process. In homogeneous materials, the kinetics of

moisture diffusion is governed by the maximum moisture content and the diffusivity. As was explained before, in the case of composites, the diffusion process is more complex. It depends on the diffusivities of the individual constituents, their relative volume fractions, constituent arrangement and morphology.

Traditionally, diffusivity has been used to predict the amount of moisture content. The effective diffusivity can be estimated either using a rule of mixtures approach or numerical analysis. Zhen and Morgan[87] developed equation *2-24* to determine the moisture content at equilibrium, using carbon fibre volume fraction and assuming water take up of the fibre is negligible:

$$M_{\max,c} = M_{\max,m} \frac{V_m \rho_m}{V_m \rho_m + V_f \rho_f} \qquad 2\text{-}24$$

Where M_{max} is the percentage of moisture content at equilibrium, V is the volume fraction and ρ is the density; the subscripts c, m and f refer to the composite, matrix and fibre respectively.

For fibre reinforced composites the diffusion coefficient D_x can also be calculated from the diffusivities of the fibres and matrix (D_r, D_f), the volume fraction of the fibre, V_f and the orientation of the fibres with respect to the exposed surface (figure 2-22). The relationship between D_x and D_r, D_f, V_f, and the fibre orientation can be established by noting the similarities between heat conduction and moisture diffusion. Springer and Tsai[88] gave approximations for the thermal conductivities parallel and normal to the fibres (V_f < 0.785). And the following analogies were drawn by Shen and Springer[19] taking into account that the diffusion of the fibre is small compared to that of the matrix:

$$D_{11} = D_r\left(1 - V_f\right) \qquad 2\text{-}25$$

$$D_{22} = D_r\left(1 - 2\sqrt{\frac{V_f}{\pi}}\right) \qquad 2\text{-}26$$

$$D_x = D_{11}\cos^2\alpha + D_{22}\sin^2\alpha \qquad 2\text{-}27$$

2.14 Non-Fickian Diffusion

The concentration-dependent Fickian process cannot describe water absorption behaviour in many glassy polymers. This phenomenon, which is usually applicable to the initial stages of diffusion, sometimes fails to describe the whole process, especially when the penetrant causes extensive swelling of the polymer. When this occurs, diffusion is described as 'anomalous' or 'non-Fickian' behaviour[55]. Diffusion behaviour in rubbery polymers on the other hand is almost always Fickian. The essential difference is that polymers in the rubbery state respond rapidly to changes in their condition. For example a change in temperature causes an immediate change in equilibrium volume, whereas glassy polymer properties tend to be time-dependent, deviations from Fickian behaviour are considered to be associated with the rates at which a polymer structure may change in response to the sorption/desorption of the penetrant molecules.

The spectrum of relaxation times associated with polymers varies greatly with structural changes. One constant is that with increasing temperature or penetrant concentration, relaxation time will decrease and hence motions of the polymer segments are enhanced. At a given concentration the transformation from glassy to rubbery will take place at the T_g. A sorption process will be influenced by the segmental motions, which occur at the same rate or slower than the diffusion process. In rubbery polymers well above T_g, chains move so quickly that they have no effect on the presence of penetrant and thus do not cause diffusion anomalies[77].

In general, diffusion behaviour in glassy polymers can be classified according to the relative rates of mobility of the penetrant and polymer segments. As such, three basic categories can be defined[77] as follows:

i. Case I (or Fickian) diffusion in which the rate of diffusion is much less than that of the polymer segmental mobility
ii. Case II diffusion, the other extreme where the rate of diffusion and penetrant mobility are greater compared with other relaxation processes
iii. Non-Fickian (or anomalous) diffusion, which occurs when the penetrant mobility and polymer segment relaxation rates are similar.

2.14.1 Characteristic Features of Absorption Curves

Figure 2-36 shows a curve illustrating different diffusion behaviour that may occur from different polymers and polymer composites. Curve LF in figure 2-36 shows typical Fickian behaviour while curves A, B, C and D illustrate various non-Fickian types of diffusion behaviours. The ratio $M(t^*)/M(\infty)$ refers to values of moisture content that have been normalised to maximum moisture content[36].

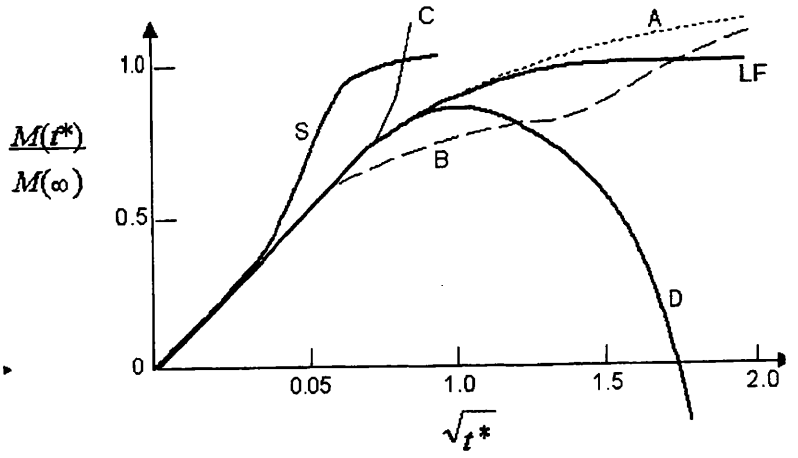

Figure 2-36: Curves illustrating different diffusion behaviours[17].

- Curve A shows a Pseudo-Fickian uptake: the curve shows a short initial linear portion.
- Curve S shows sigmoid behaviour: the curve is sigmoid in shape with a single inflection point at around 50% equilibrium.
- Curve B depicts Two-stage absorption behaviour: the initial uptake is rapid and a linear function of $t^{1/2}$. The sorption approaches a quasi-equilibrium followed by a slow approach to a final true equilibrium.
- Curve C shows continuously increasing moisture content, which could be due to damage to the structure caused by void/microcracks.
- Curve D shows weight loss suggesting material is being leeched from the polymer matrix, which may be due to chemical reactions such as hydrolysis. This typically happens when material is immersed in water especially at high temperatures[55].

Deviation from the ideal Fickian diffusion may arise for a number of composite materials. In many cases the use of Fickian diffusion mathematics will suffice. In cases where greater deviations are measured, alternative solution may be required

and modifications to the boundary conditions will be necessary. The inclusion of a time dependant component has been found to be useful when describing non-Fickian behaviour in many composite systems[17].

Zhou and Lucas[89] studied water absorption in T300/934 graphite/epoxy material, showing it exhibited both Fickian and non-Fickian diffusion behaviour. Data showed that time for onset of non-Fickian behaviour was inversely related to exposure temperature. Figure 2-37 shows the weight change of T300/934 carbon/epoxy composite immersed in distilled water at different temperatures. The solid line represents theoretical Fickian diffusion and the symbols are experimental data at different exposure temperatures. They proposed a crack/loss model to explain the behaviour of composite materials during the water absorption process.

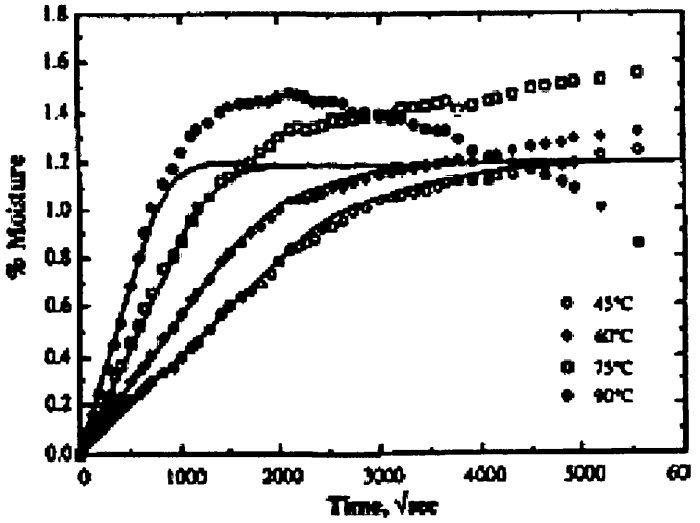

Figure 2-37: Moisture absorption rate with varying temperatures for T300/934(immersed in distilled water)[89].

2.15 Effect of Moisture on Structural Performance

Several investigations in the open literature verify that moisture influences the mechanical performance of reinforced polymers[14,15,16,19]. Absorbed moisture can reduce carbon/epoxy composite strength and stiffness by plasticising the matrix and weakening the fibre/matrix interface. Failure surfaces showing bare fibre surfaces are cited as evidence for weakened fibre/matrix interfaces. Decreased elastic moduli and lowered glass transition temperatures are evidence of matrix plasticization. The effects of moisture and temperature on mechanical performance are reviewed.

The tensile properties of carbon/polymer composite laminates, particularly those with orientations other than 90°, are generally considered to be insensitive to moisture. However, at moisture contents above 1wt%, 0° and 45° degree laminates have shown up to a 20% decrease in tensile strength[90]. Laminates of orientation 90° have been reported to undergo significant tensile strength and modulus reductions[93]. Moreover, some interlaminar shear strength degradation has also been reported for carbon/epoxy systems[91].

Lucas and Zhou[89] have studied water absorption effect on diffusion behaviour, moisture induced expansion and fracture properties of thermoset (T330/934) and thermoplastic (IM6/PEEK) composites. They have reported that graphite epoxy (T300/934) exhibits both Fickian as well as non-Fickian behaviour. However, graphite thermoplastic (IM6/PEEK) composite showed Fickian behaviour only. In width and thickness directions, significant dimensional changes were observed, with no significant expansion along the fibre (longitudinal) direction. The fracture toughness of IM6/PEEK composites was insensitive to the moisture absorption; however they observed significant reduction in the fracture toughness of T300/934 composites with moisture absorption.

Kumar et al[92] studied moisture absorption behaviour and its effects on mechanical performance of CFR epoxy composite laminates made from 913C-HTA. They measured longitudinal tensile, transverse tensile and in-plane shear properties as a function of moisture absorption using $[0]_8$, $[90]_{10}$ and $[\pm 45]_{10}$ laminates. They immersed the samples in distilled water, a weight gain of 1.2wt% over a period of 168 days was observed. The results revealed that the rate and amount of swelling in through thickness was greater compared to longitudinal and transverse directions.

They reported longitudinal tensile strength of the aged composite was reduced by 28% after 28 days of immersion and remained constant after that. The transverse tensile strength showed a decrease of about 16% at the end of 168 days exposure period. The in-plane shear strength and modulus initially slightly increased (strength by 34% and modulus by 15%) after 56 days of exposure and later on reduced gradually. They concluded moisture may have contributed to the cross-linking of the epoxy matrix (till 56 days of exposure) and later on plasticised it.

Bradley and Grant[93] found that for a graphite/epoxy system, the reduction in transverse strength due to water saturation is similar to the observed change in interfacial shear strength (30%). The authors consequently hypothesized that for their graphite/epoxy material system, the degradation of the composite system was primarily interfacial in nature rather than in the matrix.

A study carried out by Selzer and Friedrich[94] examined the influence of water absorption on the mechanical properties and failure behaviour of CFRP's. Their investigation showed that absorbed moisture decreases those properties which were dominated by the matrix or the interface and the influence of the water on the fibre-dominated properties was not detectable. They ascribed the distinct fall of the matrix-and-interface-based values to the weakening of bonding between the fibre and matrix and softening of the matrix material.

The effects of temperature and moisture on the tensile strength and modulus of carbon fibre reinforced epoxy laminates have been investigated widely. Shen and Springer[14,90] have summarised the available literature and drew the following conclusions:

1. For 0° and $[0/\pm45/90]_s$ quasi-isotropic laminates, the temperature changes up to 107°C have negligible effect on tensile strength and elastic moduli, regardless of the moisture content of the material. Although the effect on modulus is negligible up to 177°C, there may be up to a 20% decrease in tensile strength between 107-177°C.

2. For 0° and $[0/\pm45/90]_s$ quasi-isotropic laminates, the tensile strength and moduli were not affected by moisture absorption below 1wt% moisture concentration. Although the modulus is not affected by even higher moisture

contents, the tensile strength may decrease by as much as 20% for contents above 1wt%.

3. For 90° laminates the elastic moduli and strength decrease considerably with increase in moisture content and temperature. Depending on moisture content and temperature, the reduction may be as high as 50 to 90% of the room temperature properties, under dry conditions.

The interlaminar shear strength of composites also reduces with increasing moisture absorption. Short beam shear tests of a UD carbon fibre epoxy show a nearly 10% reduction in ILSS at a moisture content of 1.3wt%, which was attained after 33 days exposure to humid air of 95%RH at 50°C. Immersion in boiling water reduced the ILSS by 35% for the same exposure time[119].

It is the compression properties of composite laminates that are most susceptible to moisture effects. Individual fibres can carry tensile loads but it is necessary that they be bonded as a structural entity with support against buckling to be able to carry compressive loads. It is the matrix that provides this support, so if it becomes impaired degradation of the compression properties are likely. Collins[95] studied CFRP with different volume fractions. His observations revealed that the fibre and matrix interfacial bonding mainly controlled transverse compressive failure. A study by Weinberger et al[96] of compression strength of a 48 ply quasi-isotropic lay-up graphite/epoxy material (AS/3501-6) reported a 33% drop in compressive strength with 0.6% moisture at 120°C compared to RT/dry data.

From the work performed and documented in the literature it is apparent that the combined effects of moisture and temperature have the most detrimental effect on composite materials.

2.16 Other Environmental Effects

The external surfaces of carbon/epoxy aircraft structures are generally painted to prevent any long-term degradation due to ultraviolet radiation[97,98]. The paint also acts to prevent otherwise high absorption of thermal (solar) radiation by a "black body". However the paint has no significant effect in reducing moisture absorption, although efforts are being made to develop moisture-impervious coatings[99,100].

2.17 Effect of Moisture in Aircraft Structures

The primary and secondary composite structures used in aircraft environments experience a repeated absorption/desorption of water in a wide humidity and temperature range. This type of non-mechanical fatigue is considered to be closely associated with the long-term durability of composite materials[81], especially when the water absorption is accompanied by high variations of temperature and pressure, as well as mechanical load variations during the service life of the aircraft. Accordingly, design of composites for use in high performance applications is required to satisfy HOT/WET conditions. Current design specifications are over conservative, often resulting in overly thick structures, thus reducing the weight advantage over current metallic structures[11].

The environmental conditioning of composite materials is an important aspect of their certification for use in aircraft structures. When analysing laminates forming part of an aircraft in service, it is important to replace simple boundary conditions (those as described in equations *2-9*) by ones that represent the real aircraft life-cycle variations in humidity. It is also necessary to allow for the effects temperature variation has on the diffusion coefficient. The most detrimental effect of moisture on structural performance is in combination with high temperatures, as occurs in high-speed flight. Composite components on a supersonic fighter aircraft will experience temperatures 50°C-125°C depending on speed and altitude. As moisture reduces T_g when a composite is in its "wet" condition, the T_g of the matrix can be reduce by around 40-50°C[100]. Under these conditions the maximum service temperature could approach the T_g, which is typically in the region 150-200°C for epoxy materials (listed in *table 2-1*).

An experimental program was conducted from November 1977 to December 1990 to evaluate the influence of aircraft-associated environments on the performance of three composite materials systems that are available commercially[100,101]. More than 7,000 specimens made from T300/5208, T300/5209, and T300/934 were exposed for as many as 10 years and then tested for residual strength. Sets of specimens were sent to three commercial airlines and deployed on Boeing model 737 aircraft flying in daily revenue service. After a 10-year period most coupons had absorbed between 0.7 and 1.0wt% moisture. No other significant degradation mechanism was identified in this study apart from a slight decrease in ILSS of about 5% for coupons,

which were coated with the standard F/A-18 paint scheme. This may be attributed to the solvents used in the application of the paint. However, the benefits of the paint protecting the composite surface from erosion and UV degradation far outweigh this structurally insignificant change in ILSS. Matrix dominated properties were reduced by 20% after a 10 year exposure period, compared to baseline testing data[102].

At Airbus, a criterion is used for components that are environmentally susceptible. This criterion states an 8mm thickness limit, meaning thick components have to be conditioned to a point where the moisture has reached a through-the-thickness depth of 8mm. This is justified by showing that during the whole life cycle of the aircraft, moisture diffusion is such that less than 8mm of the laminate is saturated[11].

There is significant interest in the behaviour of composite material's reaction to moisture ingress as their use becomes more widespread in aircraft structure. Coupon tests are a good way of understanding this behaviour and because the properties of a composite material can vary depending on the constituent form used, it is important to perform testing on any resin fibre combination being considered for use.

Considerable effort is now being devoted to the development of resin systems that are less susceptible to moisture absorption than epoxies; the most promising of these to date seems to be the PEEK (polyether-ether-ketone) systems[99,103].

2.18 Moisture Knockdown Factors

The "design allowable strength" is the value that some percentage of the material population (usually 95% or 99%) can be expected to exceed with 95% confidence. Manufacturers must perform a significant amount of testing in order to establish the allowable strength for each material and manufacturing process. Currently, the full capability of some materials cannot be utilised, due to process variability and knockdowns for environmental effects.

The use of environmental HOT/WET 'knockdown factors' for the design of composite aerospace structures is persuasive, due to the widely varying global environments where aircraft operate[122]. Knockdown factors are commonly used to estimate properties of composites at varying environmental conditions. To calculate an environmental knockdown factor (K_{EKDF}), first it is necessary to determine reduced HOT/WET material allowables for each of the lamina properties (laminate ultimate strengths, notched strengths, fatigue, flexure properties, bearing strengths, etc.) for each of the material forms used in the structure. The large variety of tests performed on a statistically sufficient number of replicates for the HOT/WET condition adds tremendous cost to the materials qualification and design allowables process. The HOT/WET lamina knockdown factors are used in designing all composite structures of the given constituents and material form on the aircraft, regardless of their application on the structure. In addition to the environmental knockdown factors, damage tolerance knockdown factors are also applied to the designs. The damage tolerance factors may be determined through damaging full-scale components and testing them for a predetermined number of life cycles in a HOT/WET environment.

In order to simulate the environmental condition of an aircraft structure at the end of its in-service life, during the development phase structural parts are conditioned to simulate a moisture level to that reached by an aircraft after 20 years at 20°C 85% RH, (this conditioning regime represents an average of Tropical and European climates and is considered to be the worst average climate condition[11,47]). This is simulated in test by accelerated conditioning of parts for 1000 hours at 70°C 85%RH. Not all the thickness will be saturated with this conditioning regime, thus to apply the HOT/WET knockdowns to all structures at the design phase could be considered over-conservative.

Simulations based on Fick's law have shown in the case of the worst climatic conditions after 20 years a maximum thickness of 8mm is saturated in both side exposure (4mm in one-side exposure). Figure 2-38 shows the time to saturation as a function of laminate thickness for different materials employed in the A380 and A400M aircraft. Assumptions are made that the theoretical absorption is conservative compared to the real absorption, considering the operating environment are not identical to the average of Tropical and European climates.

As an alternative to the uniformly applied HOT/WET knockdown factors, this work proposes using a moisture profile approach, grading properties in each ply to replicate the actual in-service environmental conditions. For this approach to be applied successfully a relationship is required to quantify the variation of any given property with increasing moisture content. Plies at the exposed surfaces will have higher moisture contents and hence lower strength and stiffness properties. The properties of the laminate will be different from those where the conventional assumption of a uniform moisture level across all plies has been assumed. Replacement of the potentially over-conservative HOT/WET design approach holds out the possibility of weight savings in aircraft design (and all the attendant benefits in terms of improved fuel-efficiency, lower environmentally harmful emissions etc.).

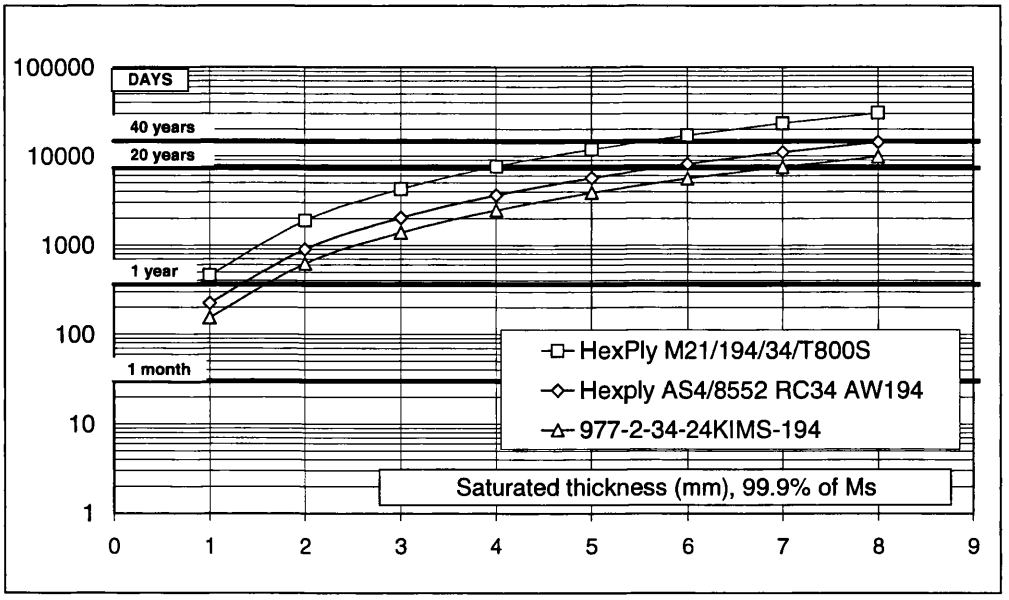

Figure 2-38: Saturation time with increasing thickness (A380 and A400M materials)[11].

2.19 Summary of Literature Review

- There have been many investigations that have defined the effect of moisture and temperature on composite materials materials[14,15,16,26], employing different theories that describe the water absorption kinetics on the materials. However, there are few publications that have analysed the influence of a moisture distribution through-the-thickness on the mechanical properties of high performance composite materials, which will form the basis of this programme of work.

- A critical aspect of using fibre-reinforced polymer matrix composites in aircraft applications is their performance in "HOT/WET" environments.

- Carbon fibres have been reported to be insensitive to moisture ingress[17,18], so material properties that are fibre dominated generally remain uneffected by the absorption of moisture in the structure.

- In composite systems such as carbon fibre reinforced epoxy materials, the moisture is mainly absorbed by the resin matrix[15,19]. The moisture lowers the temperature at which the matrix starts to soften and therefore matrix-dominated mechanical properties tend to degrade with increasing moisture content[118,16].

- The effect of moisture on the matrix of CFRP is to degrade the resin dominated mechanical properties, thus serious consideration must be given to the generation of moisture uptake data during design[76].

- The way in which composite materials absorb moisture depends upon many factors such as temperature, relative humidity, moisture equilibrium levels, area of exposed surfaces, resin content and diffusivity. All these factors must be taken into account before any prediction of the moisture content in a structure can be attempted.

- External surfaces in direct contact with the environment absorb or desorb moisture almost immediately, while moisture flow into or out of the laminate interior occurs relatively slowly[19].

- The moisture diffusion rate is many orders of magnitude slower than the heat flow associated with thermal diffusion, as the transfer of heat by conduction is due to random molecular motion, while diffusion is a process by which matter is transferred as a result of random molecular motion. This analogy was recognized by Fick who adopted the mathematical formulae of Fourier's law of Heat Conduction to diffusion. Fick's diffusion model has subsequently been applied to composite materials[20,66].

- The rate of moisture absorption is controlled by the material property called the moisture diffusion coefficient, D, which is primarily a function of temperature. The moisture content, M, in a laminate is a function of the relative humidity (%RH) to which it is exposed[19].

- Whilst the effects of moisture on composite properties and behaviour have been studied extensively, the studies involving investigations into the mechanical properties of materials with a distribution of moisture are not available in the current literature. Relevant experimental data is difficult to find and validated models robust enough to include combined environmental and mechanical effects are rare. The distribution of moisture within a composite is very important as it also reflects the distribution of properties through the thickness. While weight gain data is one of the most commonly used means of detecting the ingress of moisture into composites, it tells us nothing about concentration profile.

- The times to saturation increase with increasing laminate thickness and the rates of absorption show the reverse trend. However the diffusion coefficient seems to be unaffected by laminate thickness[78]. Experimental studies have shown that laminate thickness influences the moisture distribution process, with larger exposure times[78].

- For thick (>8mm) composite structures likely to undergo 20 to 30 years of in-service life on a typical commercial aircraft, it is accepted (and can be shown by both moisture uptake experimentation and numerical modelling[11]) that full saturation is unlikely to be achieved. Indeed it is quite likely that interior regions of thicker laminate composite structures will remain effectively dry throughout the entire lifetime of the aircraft. Therefore it is important that the

effect of a moisture profile on mechanical properties in composite materials is studied in depth.

- For CFR epoxy composites used in aerospace applications the matrix dominated properties will typically have HOT/WET environmental knockdown factors (K_{EKDF}) of 0.7[11], which can significantly reduce the material allowables used in stress analysis. Material designers at Airbus use HOT/WET material properties as a standard in design. This results in a substantial weight increase without a quantifiable increase in structural reliability.

2.20 Program Aims

- To examine the influence of moisture absorption on the mechanical properties and failure behaviour of carbon fibre-reinforced polymers.

- Determine quantitative relationships between absorbed moisture and mechanical property degradation.

- Using the derived relationships, perform predictions of mechanical properties of laminates with moisture gradients through-the-thickness.

- Validate predictions via a robust mechanical test campaign.

- This new approach suggests superseding the current Airbus homogeneous EKDF (Environmental Knock-down factors) method by using a moisture profile; which leads to an individual EKDF factor per ply based on a more realistic moisture profile.

- This study provides a well-rounded set of experimental data on a single material system that is not generally found in the literature, thus the experimental and analytical phases of this work provide original contributions to the literature.

3 Experimental Procedure

This chapter outlines the experimental procedures used during the programme of work, including the materials utilised along with the fabrication process for the composite panels and details of coupon manufacture. Also outlined are details of constituent determination, the environmental conditioning process and details of equilibrium saturation mechanical tests.

3.1 Materials and Panel Manufacture

The materials used in the test programme are all CFR epoxy composites that are presently in use by certified general aviation aircraft and will also be used on the new A400M aircraft. The materials used are outlined below and detailed specifications are given in table 3-1.

Material A: Unidirectional tape/180°C curing class, standard modulus fibre Cycom 977-2-34%-12KHTS-196. This material was used to determine basic UD ply properties.

Material B: Five harness satin woven fabric CFR epoxy prepreg, 977-2A-37%-3kHTA-5H-280, from Cytec was also used. This material was used to investigate multi-directional lay-ups.

For the second phase of testing a third material was utilised:

Material C: Unidirectional tape/180°C curing class, standard modulus fibre, Cycom 977-2-35/40-12KHTS-268. This material has the same resin and fibre type as material A. This material was used to manufacture thicker laminates using fewer plies and was utilised for 8mm thick moisture distribution validation testing.

Table 3-1: Material specifications for Cycom 977-2 epoxy resin composites.

Property	Material A	Material B	Material C
Fibre Type	Standard modulus fibre HTS 12000 filaments	Woven 5 Harness Satin	Standard modulus fibre HTS 12000 filaments
Resin	Cycom 977-2 180°C cure epoxy resin	Cycom 977-2 180°C cure epoxy resin	Cycom 977-2 180°C cure epoxy resin
Processing Conditions	Autoclave curing 180 – 210 min at 180±5°C 6 - 7 bar pressure	Autoclave curing 180 – 210 min at 180±5°C 6 - 7 bar pressure	Autoclave curing 180 – 210 min at 180±5°C 6 - 7 bar pressure
Laminate Cured Ply Thickness (mm)	0.184	0.280	0.250
Laminate Density (g/cm^3)	1.59	1.56	1.59
% Prepreg Resin Content (% weight)	35	37	35
Prepreg Areal Weight (g/m^2)	294	444	412
Fibre Areal Weight (g/m^2)	194	280	268

The composite panels were manufactured by the author, using a hand lay-up process. Appropriate lengths were cut from a reel of pre-preg tape/fabric and each layer oriented relative to each other in a pre-determined sequence, to make the panels from which the coupons were manufactured. It was essential that the layers were aligned as accurately as possible as even a few degrees misalignment can cause an effect on the mechanical properties. Following completion of the hand lay-up, the stack of pre-preg layers was vacuum bagged (the vacuum bag technique involves the placing and sealing of a flexible bag over the composite lay-up and evacuating all the air from under the bag, see figure 3-1), in order to better consolidate the part by extracting the gases and reducing porosity to give a better quality laminate. The laminates were then autoclave cured at Airbus. An autoclave is a pressure vessel, which provides the curing conditions for the composite where the application of vacuum, pressure, heat up rate and cure temperature are controlled.

The following cure cycle was applied:

1. Apply full vacuum to bag – atmospheric pressure (0.6-0.9bar).
2. Raise temperature to 135°C at 2°C per minute
3. Hold for 60 minutes
4. At same time, raise pressure to 7bar
5. Raise temperature up to 180°C at 2°C per minute
6. Hold for 180 minutes
7. Cool to 60°C at 2°C per minute

8. Release the pressure

A schematic of this cure cycle can be seen in Appendix A. New consumables were used for each panel to ensure a good quality laminate. The consumables for the vacuum bag processing (see figure 3-1) are:

- Peel ply - Allows free passage of volatiles and excess matrix during the cure. Is removed easily after cure to provide a bondable or paintable surface.
- Release agent - Allows release of the cured prepreg component from tool.
- Release film - prevents further flow of matrix, is slightly porous to allow the passage of air and volatiles into the breather layer above.
- Absorption fabric - glass fabric, absorbs any excess matrix.
- Breather fabric - Provides the means to apply the vacuum and assists removal of air and volatiles from the whole assembly.
- Vacuum bag/sealant tape - Provides a sealed bag to allow removal of air to form the vacuum bag.

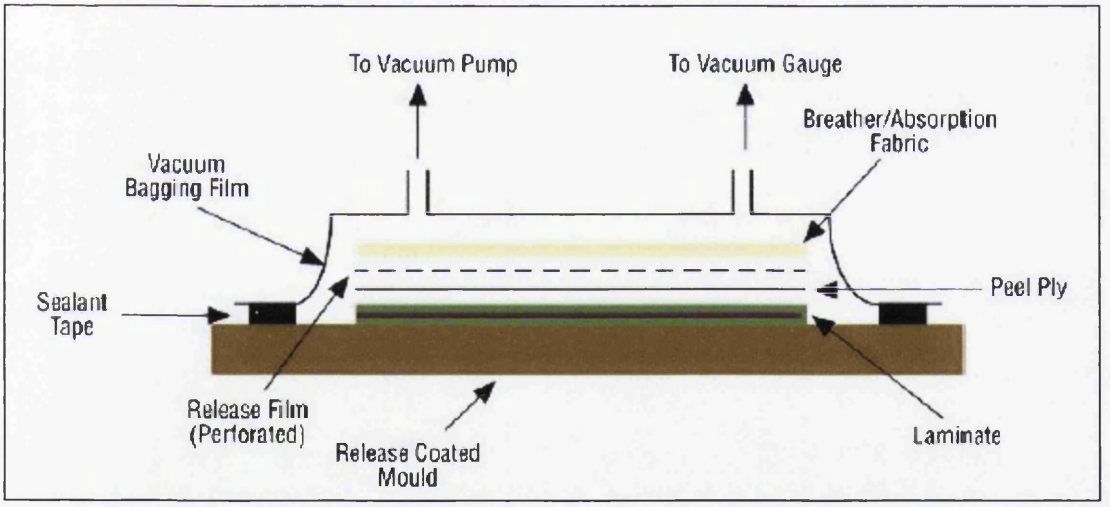

Figure 3-1: Vacuum-bagging schematic[33].

Table 3-2 shows the panel specifications for each test type and each panel was given a unique reference number for traceability.

Table 3-2: Panel specifications for each test type.

Panel Reference	Panel Test Method	Test Standard	No. of Plies	Material	Lay-up
CDC/05/5317	Moisture Coefficient Determination	EN 2564	11	A	$[0]_{11}$
CDC/05/5318			16	B	$[+45/0/-45/90]_{2S}$
CDC/05/5285	Tensile Strength and Modulus	BS EN ISO 527-5	6	A	$[0]_{6}$
CDC/05/5286	Tensile Strength and Modulus	BS EN 2597	11	A	$[90]_{11}$
CDC/05/9032	Tensile Strength and Modulus	BS EN 2597	32	C	$[90]_{32}$
CDC/05/5287	Compressive Strength	prEN 2851	11	A	$[90]_{11}$
CDC/05/5288	In plane Shear Strength and Modulus	BS EN ISO 14123	8	A	$[0/90]_{2S}$
CDC/05/5289					
CDC/05/5316	Interlaminar Shear Strength	BS EN ISO 14130	11	A	$[0]_{11}$
CDC/05/5293	Open Hole Tension	Airbus AITM 1-0007	16	B	$[+45/0/-45/90]_{2S}$
CDC/05/5295					
CDC/05/5294	Open Hole Compression	Airbus AITM 1-0008	16	B	$[+45/0/-45/90]_{2S}$

3.1.1 NDT - Ultrasonic Inspection

The manufacturing process, if not properly controlled can introduce defects into the laminate. Typical defects are voids (small cavities in the resin) and delaminations (unbonded areas between layers). All defects will degrade mechanical properties, particularly in compression, shear and flexure. Therefore, it is important that their presence is detected, so that faulty laminates can be discarded.

After lay-up and curing all laminates were inspected by ultrasonic testing at Airbus Filton. The NDT method used was Double Through Transmission (Glass Plate Reflection) C-Scanning, utilizing a 5MHz Unfocussed Immersion Probe. Ultrasonic tesing is a non-destructive test technique (NDT) used to find defects in a test part

without destroying it. High frequency sound waves are passed through the material; if the sound meets an interface (damage) the ultrasonic signal is bounced back. Typical defects are cracks, delaminations, porosity and foreign object inclusions.

The output from this technique is in the form of a C-scan, with copies of the scans carried out on the panels produced, along with comments on the panel quality located in Appendix B. All panels used here were considered to be good quality; free from defects and suitable quality for testing. To ensure quality, 50mm from each edge of the panel was cut and disguarded prior to coupon maufacture.

3.2 Coupon Extraction

Coupon extraction diagrams can be seen in Appendix C. The laminates were sent to an external contractor (*Polymeric Composites*[104]) for the machining of mechanical test coupons. All coupons were cut with a diamond tip saw, except for the coupons for partially saturated 90° tension tests, which were waterjet cut.

To avoid edge effects and resin starvation phenomena at the edges, 50mm was removed from all the edges of the manufactured laminates.

All coupons that required end tabs were tabbed with 2mm thick Tufnol®, 10G/40, which is an epoxy glass laminate with good mechanical strength and elastic modulus, along with excellent rigidity and dimensional stability. Technical specifications for Tufnol® are displayed in table 3-3.

Table 3-3: Technical specification for Tufnol®, 10G/40.

Property	Value
Compressive strength	415 MPa
Tensile Strength	355 MPa
Young's Modulus of elasticity	17.7 MPa
Maximum service Temperature	130°C
Relative Density	1.9
Water absorption	0.5 mg/cm^3

3.3 Constituent Content Determination

One of the most important factors determining the properties of a composite is the relative proportions of matrix and reinforcing materials. The fibre volume fraction, V_f, was determined by a matrix sulphuric acid digestion; Standard test method EN 2564 method A[105].

Before any evaluation of the consituents could be made, the density of the sample was measured following ISO 10119[106]. Coupon dimensions were 10x20x2mm (length x width x thickness). Firstly the oven dried sample was weighed (W_c) and each sample was weighed suspended in distilled water (W_w). Taking the density of water to be 0.997 g/cm³: The sample density ρ_c (g/cm³) was calculated as follows:

$$\rho_c = \frac{W_c}{W_c - W_w} \times 0.997 \qquad 3\text{-}1$$

Prior to any experimental work taking place the filter funnels were oven dried at 120°C for 45mins, and then weighed (*M5*) and left to cool in a desiccator.

The experiement was carried out in a fume cuboard, with the heating mantle set up as described in the standard, EN 2564[105]. The procedure for determining V_f required heating the coupon in 20 ml of sulphuric acid until the mixture reached 160 ±10°C, when it began to fume. Hydrogen peroxide was added slowly to the mixture until the solution remained clear. The solution was cooled to 80±5°C and added to a beaker containing 100ml of distilled water. The fibres were filtered through a sintered glass crucible and washed with acetone. After drying at 120°C for at least 45 minutes, the fibres were cooled in a desiccator and weighed to the nearest ±1 mg to give the mass of the resdulal fibres (*M6*), taking care to avoid the loss of any fibre.

3.3.1 Calculations

The density of the fibre, ρ_f, (g/cm³) and the density of the resin, ρ_r, (g/cm³) were obtained from the Airbus material specification documentation (values listed in table 3-4) and the specimen density, ρ_c, was calculated using equation *3-1*.

3.3.1.1 Fibre content by mass (W_f), %

$$W_f = 100 \times \frac{M6 - M5}{M_c} \qquad 3\text{-}2$$

W_f is the fibre content as a percentage of the initial mass

M_c is the initial mass of the specimen, in grams

$M5$ is the mass of the sintered glass crucible, in grams

$M6$ is the final total mass of the sintered glass crucible and the residue after acid digestion, in grams.

3.3.1.2 Fibre content by volume (V_f), %

$$V_f = W_f \times \frac{\rho_c}{\rho_f} \qquad 3\text{-}3$$

V_f is the fibre content as a percentage of the initial volume

ρ_c is the specimen density, in grams per cubic centimetre

ρ_f is the fibre density, in grams per cubic centimetre, given in table 3-4.

3.3.1.3 Resin content by mass (W_r), %

$$W_r = 100 - W_f \qquad 3\text{-}4$$

W_r is the resin content as a percentage of the initial mass.

3.3.1.4 Resin content by volume (V_m), %

$$V_m = 100 - W_f \times \frac{\rho_c}{\rho_m} \qquad 3\text{-}5$$

V_m is the resin content as a percentage of the initial volume.

ρ_m is the density of the cured resin, in grams per cubic centimetre given in table 3-4.

3.3.1.5 Void content by volume (V_v), %

$$V_v = 100 - V_f - \frac{100.\rho_c(W_c - W_f)}{W_c.\rho_r} \qquad 3\text{-}6$$

Table 3-4: Supplier's resin, fibre and laminate density.

Property	**Material A**	**Material B**	**Material C**
Resin density (g/cm^3)	1.31	1.31	1.31
Fibre density (g/cm^3)	1.77	1.76	1.77
Laminate density (g/cm^3)	1.59	1.56	1.59

3.4 Environmental Conditioning

Two Gallenkamp BR185H/C/WCC environmental chambers were utilised for all conditioning. The chambers were serviced and calibrated on a regular basis by JTS Environmental services[107]. The conditioning chambers were connected to a pump containing a reservoir filled with distilled water. The distilled water is pumped to the chamber, which then boils to steam to keep the chamber at the required relative humidity (%RH). Wet/dry bulb humidity measurements were used to control the humidity and temperature, while circulation fans maintained uniform conditions inside the chamber.

The conditioning temperatures were selected using EN ISO 291[108] as a guide and were well below the glass transition temperature, T_g of the resin (180°C) to avoid any damage such as micro-cracking as a result of high temperature exposure. They have an operating temperature range of 25-100°C and relative humidity range from 0-100%RH. The temperature and %RH was measured and logged every hour on a Gemini Tiny-tag Extra data logging system[109], used to ensure the chambers were accurately controlling the required environmental conditions. The data loggers were calibrated at 0 and 30°C and 20 to 80 % RH (at 25°C) by the suppliers when purchased and then at 12 month intervals for re-calibration. The temperature was kept within ±1°C and the humidity was kept within ±3%, as per ASTM standard D5229[110].

3.4.1 Determining Moisture Constants

The moisture diffusivity constant, D_x, is the property of a material that describes the rate at which the material absorbs or desorbs moisture. Before any mechanical test coupons were conditioned, or mechanical testing carried out, the moisture diffusion coefficients of the materials being used in this test programme were defined. The international standard ASTM D 5229[110] describes a procedure for determining the moisture absorption properties and diffusion coefficients in the "through-the-thickness" direction of flat and curved solid plastics. This standard method was followed in defining the diffusion coefficients of the composite laminates being used.

For these experiments UD and quasi-isotropic (QI) lay-up laminates were used; manufactured from Material A and Material B respectively. The laminates were cut

into square coupons of dimensions 100x100mm; the UD coupons were 2mm thick and the quasi-isotropic coupons 4mm thick. The coupons edges were coated with 3M aluminium tape to eliminate diffusion of moisture. The coupons were weighed before and after bonding of the tape in order to obtain mass increase due to the aluminium tape application. Measurements took place on a Fisher Scientific electronic balance, accurate to 0.1mg. Six of each material type were conditioned to get an average result, as required in the standard test method ASTM D 5229 section 8.1[110].

All test coupons were preconditioned by oven drying (in accordance with ASTM D 5229 Procedure D[110]) at 80°C. The coupons were weighed periodically and the percent mass change at each interval calculated using equation *3-7*.

$$M_0 = \frac{W_0 - W_d}{W_d} \times 100 \qquad 3\text{-}7$$

where;

M_0 = initial as-received moisture content, wt%

W_0 = initial as-received coupon mass, g

W_d = oven-dry coupon mass, g.

Desorption of moisture was monitored until a dry state was reached, as determined by equation *3-9*. After this preconditioning step, the thickness of the coupons was measured in three locations to the nearest 0.01mm and the plate dimensions measured. Following establishment of oven dry equilibrium, coupons were stored in a desiccator.

Following standard test method ASTM D 5229 Procedure A[110], the percentage moisture mass gain verses time is monitored for a coupon maintained in a steady state environment at a known temperature and moisture exposure level, until the material reaches effective moisture equilibrium.

The coupons were placed in the environmental chamber at 70°C and at 85%RH and were weighed periodically using an analytical balance with 0.1mg resolution to determine the percent weight change. Water uptake weight gains were recorded daily for one week and then on a weekly basis, until saturation levels were reached. Care was taken to shield the balance from air drafts and isolate it from vibrations

that could affect accuracy. Clean lint free gloves were used when handling the coupons.

From the data collated from the weighing, the moisture content, M (wt%), in the material, taken as the ratio of the mass of the moisture in the material to the mass of the oven dry material, was determined using equation *3-8*.

$$M = \frac{(W_i - W_d)}{W_d} \times 100 \qquad 3\text{-}8$$

where, W_i is the current coupon mass, in grams and W_d is the mass of the oven dry coupon, in grams.

Moisture equilibrium, M_{max} was reached when the average moisture content of the material changes by less than 0.01% between measurements. This was calculated by equation *3-9*.

$$|M_i - M_{i-1}| < 0.01\% \qquad 3\text{-}9$$

where:

M = coupon moisture content, %

i = value at current time

i-1 = value at previous time.

From the aforementioned absorption procedure, the % moisture content of the coupons was plotted against the square root of time to obtain the moisture absorption curves (shown schematically in figure 2-23). The diffusion coefficient, D_x was determined from the initial slope of the percentage moisture gain versus $\sqrt{t}$ curve and was calculated by equation *2-20*. The diffusion coefficient, D_x, can be regarded as a material constant for a composite at a given fibre fraction and exposure condition.

3.5 Equilibrium Saturation Testing

Mechanical testing was performed on test coupons that had been environmentally conditioned to different levels of %RH. Chapter 4 describes in detail the test methods and coupon types. Details of each test type are outlined in table 3-2, showing the standard method followed, material type, number of plies and coupon lay-up. Batches of six coupons were tested for each test type and condition. The equilibrium moisture content, M_{max}, the time to equilibrium saturation and fibre volume fraction (V_f) were experimentally measured for each material/conditioning regime, as described in sections 3.3 and 3.4.1.

Conditioning was performed, as described in section 3.4 and the level of absorbed moisture was measured as a percentage weight increase of the coupon. From conditioning at the different levels of %RH, curves similar to the schematic diagram in figure 3-2 were produced for each mechanical test coupon type. However these test coupons were not oven dried prior to conditioning, which in hindsight was an experimental error that will be discussed in some detail in Chapter 7.

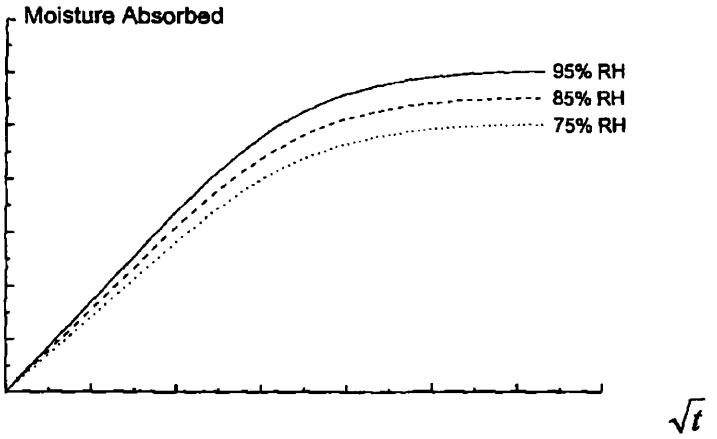

Figure 3-2: Effect of %RH on the amount of moisture absorbed with time[17].

Mechanical test coupons underwent accelerated environmental conditioning at a temperature of 70°C, at a RH of 60%, 75%, 85% and 95%. The test coupons were placed in environmental chambers and weighed at regular intervals until equilibrium saturation levels were reached. For test coupons that had end tabs, the mass of the end tab was subtracted at each weighing. Moisture equilibrium, M_{max}, was achieved when the average moisture content of the coupon changed by less than 0.01% for two consecutive readings, within a span of 7 ±0.5 days.

3.5.1 RT/AR Condition

Mechanical test coupons were also tested in the room temperature/as-received (RT/AR) condition. This means that the test coupon has been exposed to ambient room temperature and relative humidity (%RH) conditions from manufacture. Table 3-5 shows the wt% moisture in the RT/AR samples, where the range was between 0.1-0.27wt%. The different amount of moisture in each of the samples is attributed to the fact the coupons were exposed for different lengths of time to ambient environmental conditions prior to oven drying, due to different manufacturing timescales.

Table 3-5: Wt % moisture in the AR coupons prior to oven drying at 80°C.

Test Coupon	Moisture Content [wt%]
0° Tension	0.27 ±0.02
90° Tension	0.10 ±0.01
90° Compression	0.26 ±0.01
ILSS	0.27 ±0.02
IPS	0.25 ±0.01
OHT	0.14 ±0.01
OHC	0.10 ±0.01

3.5.2 Oven-Dry Conditioning

For the oven-dry (OD) condition, coupons were dried in electric ovens at 80°C until their weight loss had stabilised, which was verified using equation *3-9*. After drying, the test coupons were stored in a desiccator with silica gel until testing took place. The temperature was chosen as 80°C, as it needed to remain below the resin glass transition temperature, T_g of 180°C in order to avoid the onset of irreversible damage, which would permanently alter the absorption characteristics of the material.

3.5.3 Strain Gauging

Strain gauges were used for measuring local deformation during loading. The gauge measures strain in a single direction. To measure strain in multiple directions, tee-rosette gauges were used. As PMC's are quite poor thermal conductors, 350Ω

resistance gauges were used, as they are less likely to produce errors due to self-heating[111].

Gauges were purchased from the Vishay measurement group and Instruction Bulletin B-127-14[112] was followed in the application of the strain gauges to each of the mechanical test coupons. The author attended a strain gauging application course run by the Britsh Society for Strain Measurements (BSSM), in order to ensure the strain gauging was carried out to the standard. The gauges were applied after the conditioning, prior to testing, with the application taking approximately 10 minutes. Coupons were tested immediately after application and it was determined that moisture loss was negligible in this time. This was determined by leaving a specimen in air for a 10 minute period, followed by re-weighing and no moisture loss was measured. Table 3-6 lists the gauge types utilised for each of the coupons.

Table 3-6: Strain gauges used for each coupon type[113].

Coupon	Strain Gauge used	Type	Code	Resistance (Ohms, Ω)
Unidirectional Tension	Yes	UD	CEA-06-250UN-350	350
Transverse Tension	Yes	UD	CEA-06-250UN-350	350
Transverse Compression	Yes	UD	CEA-06-125UW-350	350
In-plane Shear	Yes	Tee-Rosette	CEA-06-125UT-350	350
Interlaminar Shear	No	-	-	-
Open Hole Tension	No	-	-	-
Open Hole Compression	No	-	-	-

3.5.4 Microscopy & Fractography

After failure, the coupons were "reassembled" to the greatest practical extent and photographed, to record the relative locations of failed regions. The failure surfaces were also visually examined with low-power optical microscopes, in order to record general observations of failure morphology. The failure regions were then prepared for scanning electron microscope (SEM) examination. Micrographs in this thesis were captured with a Philips FEI XL30 CP SEM, using a 20kV accelerating voltage.

4 Mechanical Testing Methods

Tension[1,2,3,4,5], compression[6], interlaminar[7] and intralaminar[8] shear tests were carried out on UD and QI woven CFRP coupons, using universal testing machines in accordance to the relevant standard method.

All tests were repeated six times to obtain an average result, as required in the standard test method descriptions. Test coupons were all measured before testing; width measurements were taken with a Vernier calliper and thickness measurements were taken with a flat-face micrometer. The measurements that were taken according to each test method were subsequently used to calculate the mechanical properties of the material, as specified in each test method.

The load displacement diagrams were monitored for all the test coupons through a PC linked to the testing machine. The strains were measured and recorded for each test type using strain gauges connected to a Vishay System 5000 digital strain meter[113].

All tests were performed on a servo-hydraulic Instron 100kN capacity universal testing machine with a constant cross-head rate, at ambient temperature. For tension tests, hydraulic wedge grips were fixed in such a way that neither bending nor torsion influenced the coupons. All machines and hydraulic equipment were calibrated to UKAS certification prior to any testing being performed.

4.1 Longditudinal (0°) Tension Testing

The tensile properties of composites were determined experimentally according to Standards: BS EN ISO 527-1[1] and BS EN ISO 527-5[3].

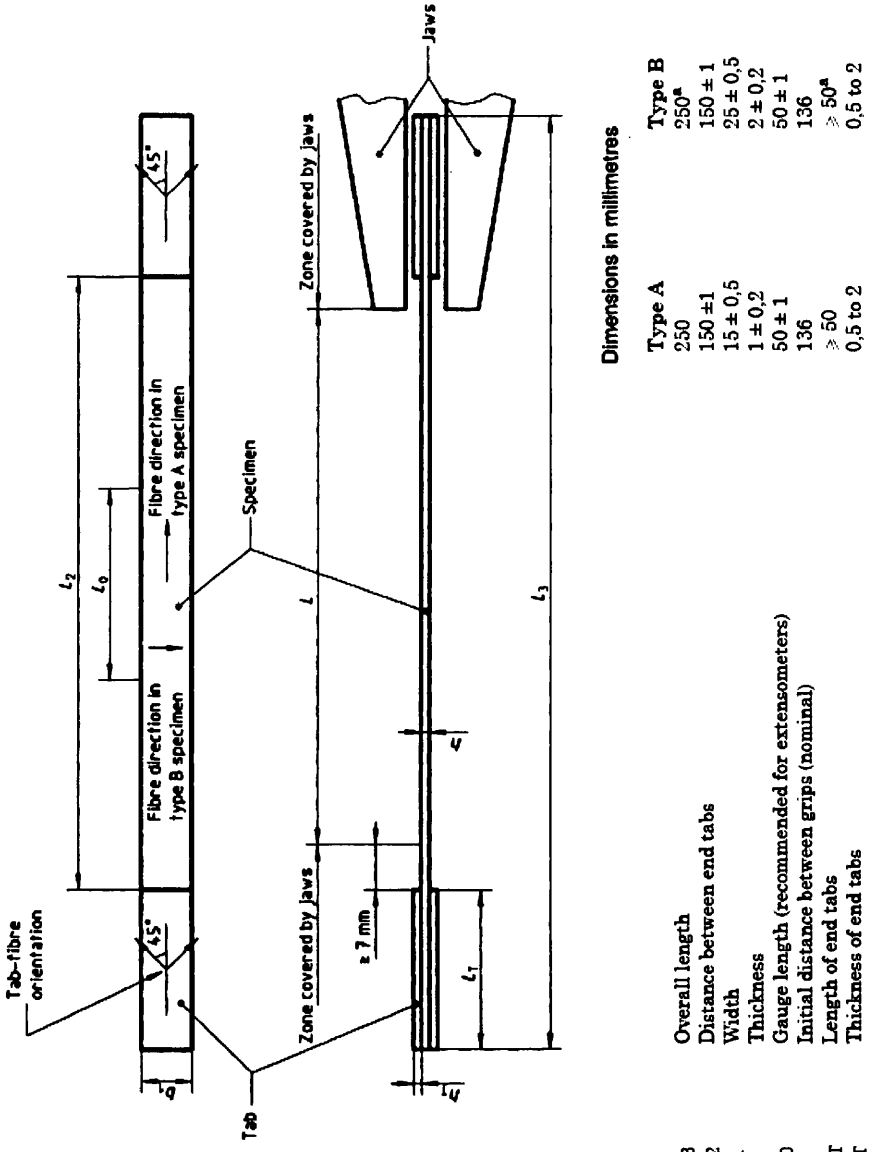

Figure 4-1: Schematic diagram of tensile test coupons. (For 0° tension test Type A was used and Type B for 90° tension)[1].

0° test coupon dimensions are as shown in figure 4-1 (coupon type A). End tab material specifications are listed in table 3-3. To measure Young's modulus strain gauges (as specified in table 3-6) were bonded to the centre of the gauge section, on both sides of the coupon. Each test was repeated six times per test condition, as recommended in the standard.

4.1.1 Tensile test Procedure

The cross sectional dimensions at five points on the test coupons were measured using a micrometer. Coupons were inserted into the grips of a properly aligned and calibrated test frame, with the crosshead rate is set to 2mm/min. Eye protection was worn at all times in the test area and a safety screen was positioned around the test area. Strain readings were recorded continuously and the coupons were monitored to failure.

4.1.2 Data Reduction

The longitudinal tensile stress, σ was calculated using equation 4-1, where, σ_1^t, is the longitudinal tensile stress value in MPa, F is the measured force in N, b is coupon width and h is coupon thickness in mm.

$$\sigma_1^{\ t} = \frac{F}{bh} \qquad 4\text{-}1$$

The longitudinal Young's modulus, E_1 is calculated on the basis of two specified strain values using the following equation:

$$E_1 = \frac{\sigma_2 - \sigma_1}{\varepsilon_2 - \varepsilon_1} \qquad 4\text{-}2$$

where:

E_1 is Young's modulus of elasticity, expressed in MPa.

σ_1 is the stress in MPa, measured at the strain value $\varepsilon_1 = 0.0005$.

σ_2 is the stress in MPa, measured at the strain value $\varepsilon_2 = 0.0025$.

4.2 Transverse (90°) Tension Testing

Standard method BS EN ISO 527-5[3] was followed for these tests. The 90° tension mechanical test coupon dimensions can be seen in figure 4-1, coupon type B is used. End tab material specifications are listed in table 3-3. To measure Young's modulus and strength, a longitudinal strain gauge as specified in table 3-6 is bonded to the centre of the gauge section, on both sides of the coupon. The test is repeated six times per test condition as recommended in the standard.

4.2.1 Tensile Test Procedure

The cross sectional dimensions at several points on the test coupon were measured using a micrometer. The coupon is then inserted into the grips of an aligned and calibrated test frame. The crosshead rate is set at 1mm/min. Strain readings are recorded continuously. The coupons were monitored to failure, which is defined as the maximum load attained during testing.

4.2.2 Data Reduction

The transverse (90°) tensile stress, σ_2^t and modulus E_2 were calculated as for 0° tensile tests (equations 4-1 and 4-2 respectively).

4.3 Transverse (90°) Compression Testing

Standard test procedure prEN 2850[116], method B was followed for these test types. This type of compression test, sometimes referred to as a modified ASTM D 695 compression test, features an end-loaded, face-supported coupon. When compression strength determination coupons are tabbed, the short gauge length between the tabs prevents the use of strain gauges for modulus determinations. Therefore, a second set of un-tabbed coupons was required for modulus determination. The un-tabbed coupons are not suited for compression strength determination, as the coupon ends typically crush before compression failure occurs in the gauge section. The test fixture used for both test methods, shown in figure 4-2, was purchased from Wyoming Test Fixtures, Inc.[117]. The fixture supports the face of the tabs on the tabbed coupon, but not the coupon gauge length itself. The coupon was end-loaded through hardened steel plates.

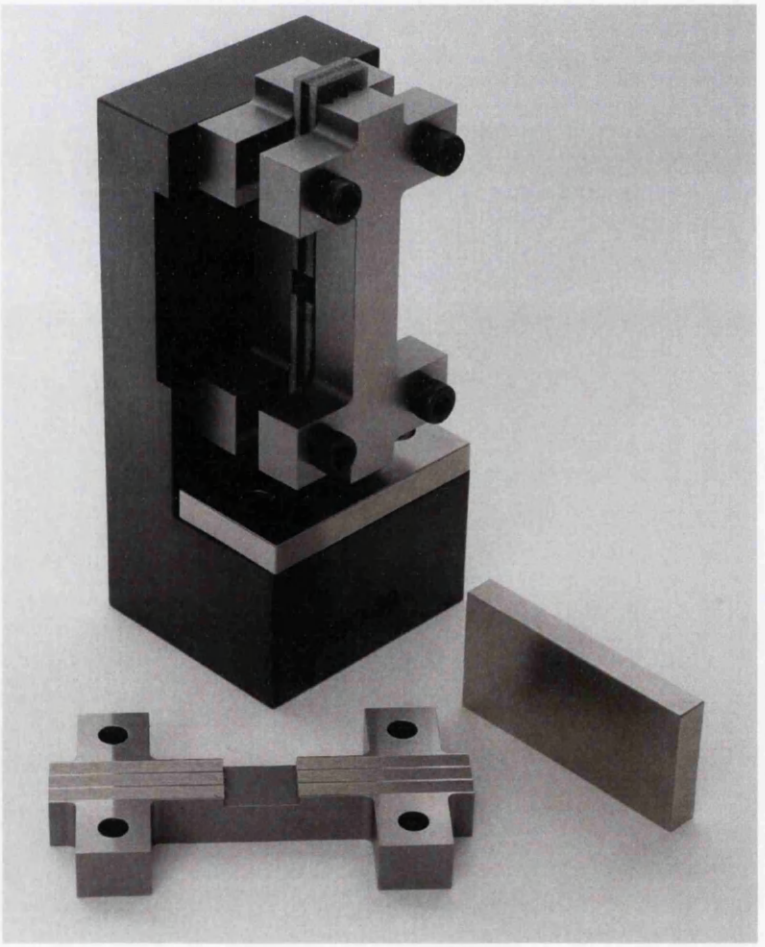

Figure 4-2: Modified ASTM D 695 compression test fixture, with strength measurement test coupon inserted.

A straight-sided coupon 12.5mm wide, 80mm long and 2mm thick is utilised for these tests. Coupons used to measure transverse compressive strength were tabbed on each end with Tufnol (see table 3-3). The coupons have a 5mm gauge length. Six of each coupon (tabbed and un-tabbed) were tested for each test condition. Schematic diagrams with dimensions and tolerances can be seen in figure 4-3.

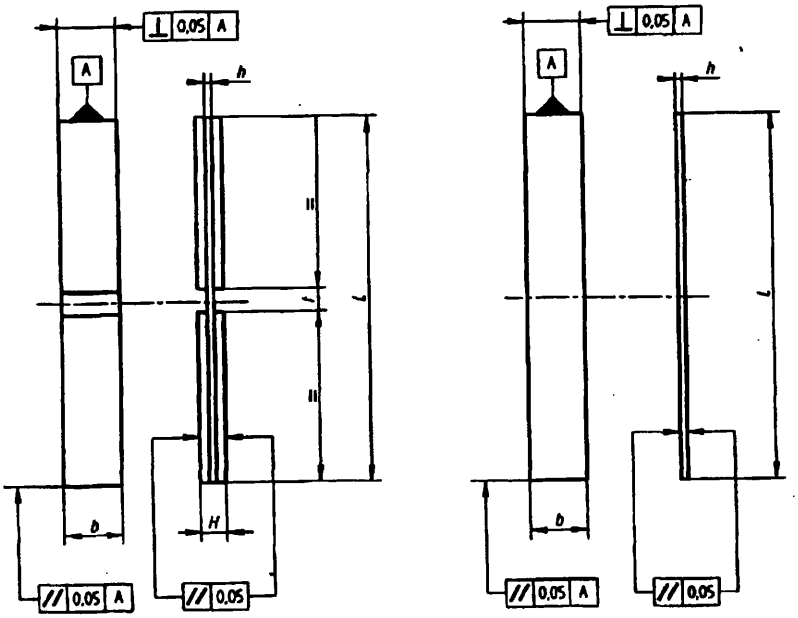

Dimensions in millimetres

Type of test piece	B_1	B_2
h	2 ± 0,2	2 ± 0,2
H	4,5 to 6	/
b	12,5 ± 0,2	12,5 ± 0,2
L	75 to 80	75 to 80
t	$5^{+0,5}_{0}$	/

Figure 4-3: 90° compression coupons dimensions [116].

The coupon was compressed at a constant speed of. 1mm/min. On the modulus test piece only ε_{11} needs to be recorded. High loads do not need to be applied when determining compressive modulus, thus minimising the problems of buckling. Back-to-back strain gauges are used only when buckling or bending is a concern.

4.3.1 Data Reduction

The transverse compression stress, σ_2^c of the coupons was calculated using the following equation:

$$\sigma_2^{\,c} = \frac{F}{bh} \qquad 4\text{-}3$$

where σ_2^c is the compression stress value in MPa, F is the load at failure in N, and b is coupon width and h is coupon thickness in mm.

The transverse compressive modulus was measured from the stress/strain recording, with the modulus taken from the gradient of the linear part of the curve.

$$E_2^{\,c} = \frac{\sigma_2 - \sigma_1}{\varepsilon_2 - \varepsilon_1} \qquad 4\text{-}4$$

E_2^c is transverse compressive modulus of elasticity (MPa)

σ_1 is the stress, in MPa measured at the strain value ε_1 = 0.0005.

σ_2 is the stress in MPa measured at the strain value ε_2= 0.0025.

4.4 In-Plane Shear Tests

Standard test method, BS EN ISO 141219[6] was followed, to carry out uni-axial tension testing of a ±45° lay-up laminate. It is a simple but accurate method for determining the shear properties of unidirectional composites and is widely used in industry.

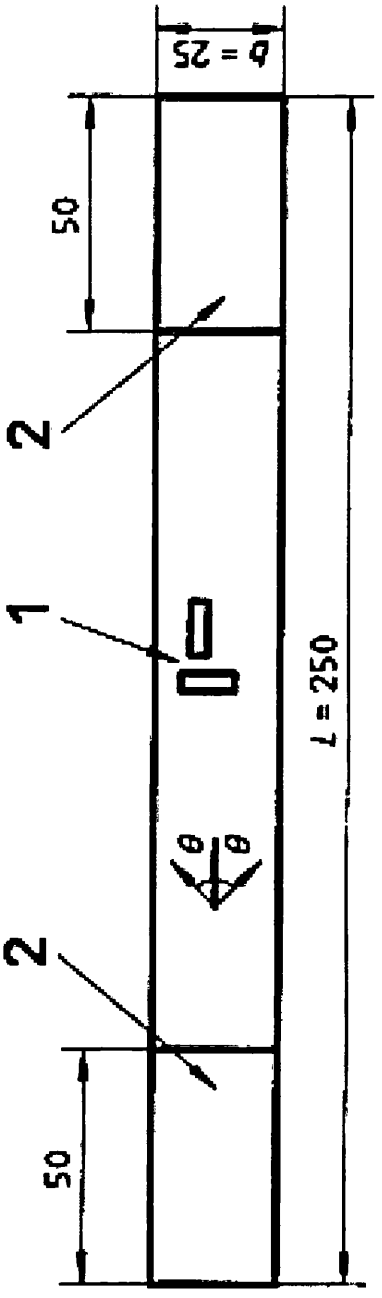

Figure 4-4: Schematic of an in-plane shear coupon, dimensions in mm[6].
***1** is strain gauge, **2** the tab and **θ** is the fibre angle (=45°), coupon thickness **h**=1.5mm.*

Straight sided coupons, dimensions of which can be seen in figure 4-4, with fibres oriented ±45° to the coupon axis, were end-tabbed with Tufnol and then loaded in tension. To determine the shear modulus, the strains parallel and perpendicular to the coupon axis were measured using a 90° tee rosette strain gauge (table 3-6), which were bonded to the back and front of the coupon. The test was performed at a speed of 2mm/min.

4.4.1 Data Reduction

The in-plane shear stress, τ_{12}, expressed in MPa was calculated using:

$$\tau_{12} = \frac{F}{2bh} \qquad 4\text{-}5$$

Where F is the load in N, and b and h are the width and thickness of the coupon in mm, respectively.

Shear strain, γ_{12} was calculated using equation 4-6.

$$\gamma_{12} = \varepsilon_x - \varepsilon_y \qquad 4\text{-}6$$

ε_x is the strain in the direction parallel to the coupon axis
ε_y is the strain in the direction perpendicular to the coupon axis

In-plane shear Modulus, G_{12} was calculated using equation 4-7.

$$G_{12} = \frac{\tau_{12}'' - \tau_{12}'}{\gamma_{12}'' - \gamma_{12}'} \qquad 4\text{-}7$$

τ_{12}' is the shear stress at a shear strain $\gamma_{12}' = 0.001$
τ_{12}'' is the shear stress at a shear strain $\gamma_{12}'' = 0.005$
G_{12} is the in-plane shear modulus (MPa).

4.5 Interlaminar Shear Tests

Standard BS EN ISO 14130[8] was followed to determine interlaminar shear strength (ILSS) of UD laminates using the Short Beam Shear test method.

Interlaminar shear strength is the maximum shear stress existing between layers of laminated material. It is applicable to all types of parallel fibre reinforced plastics and composites. As the name implies the Short Beam Shear test subjects a beam to bending, just as flexural testing methods do, but the beam is very short relative to its thickness. The objective is to minimise the flexural (tensile and compressive) stresses and to maximise the induced shear stress.

According to classical bending theory, the load has two major stress components. The normal σ has a maximum compressive stress on the top surface of the coupon, where it is being loaded and an equal maximum tensile stress on the bottom surface. The second component of stress is the longitudinal shear stress, which has a maximum value in the fibre direction along the mid section of the coupon. The failure mode depends on the span:depth ratio and shear failure occurring if the shear stress reaches a critical value before the normal tensile or compressive stresses. In CFRP this span:depth ratio is recommended to be 5:1.

Although the stress state in the short beam is not pure shear (which would be desirable in an ideal shear test method), there are some desirable features, as the short beam shear test produces values of shear strength. Because of the non-pure shear state, the results are not an absolute value and the term 'apparent' ILSS is used to define the quantity obtained. Therefore the short beam shear test is not suitable for design purposes. Despite this restriction, data generated from this test method is utilised for design allowables, primarily because of the lack of an alternative test method for measuring interlaminar shear strength[85].

4.5.1 Test Procedure

A bar of rectangular cross-section was loaded as a simple beam in flexure, so that interlaminar failure occurs. The bar rests on two supports and the load was applied by means of a loading member midway between supports. The fixture is shown schematically in figure 4-5 and a photograph of the test rig, which was purchased

from Wyoming Test Fixtures, Inc.[117], is shown in figure 4-6. Test coupons are small rectangular bars of uniform thickness of 2mm, with a length of 20mm and a width of 10mm.

The coupon was placed on a horizontal shear test fixture so that the fibres were parallel to the loading nose. The loading nose was then used to flex the coupon at a constant speed of 1mm/min until failure; each test/condition was repeated six times. The force and crosshead displacement was recorded continuously until failure.

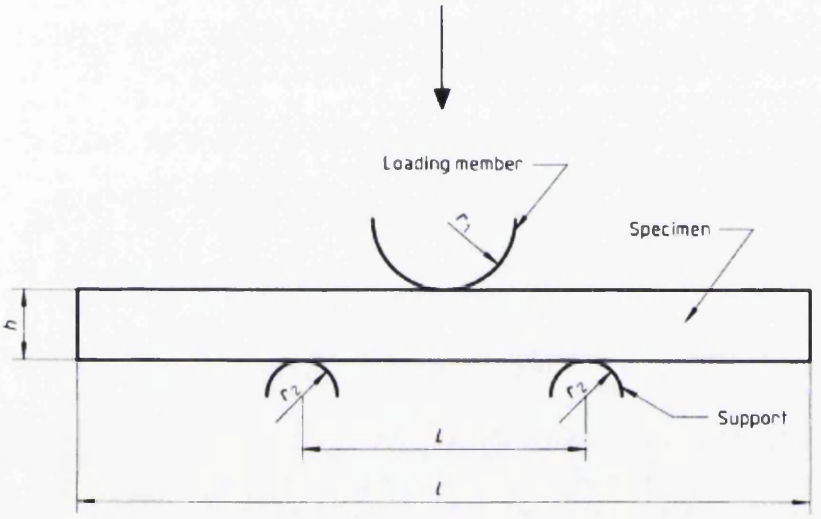

Figure 4-5: Loading configuration for SBS test[33]

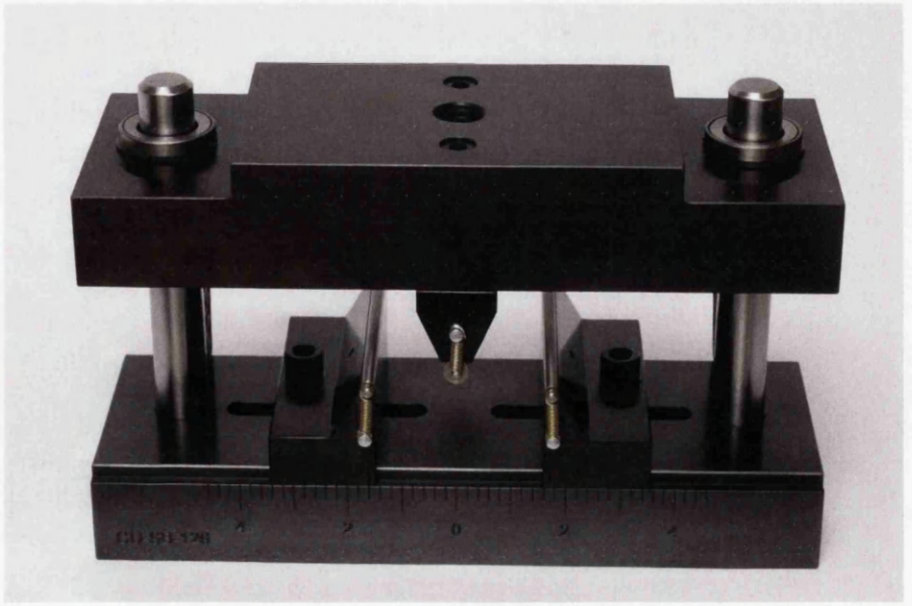

Figure 4-6: Short beam shear test fixture[117].

4.5.2 Data Reduction

The 'apparent' interlaminar shear strength, σ_{ILSS} was calculated using:

$$\sigma_{ILSS} = \frac{3}{4} \times \frac{F}{bh} \qquad 4\text{-}8$$

Figure 4-7 is a schematic diagram from the standard test method, showing the difference in load-extension curves for a single and multiple shear failure.

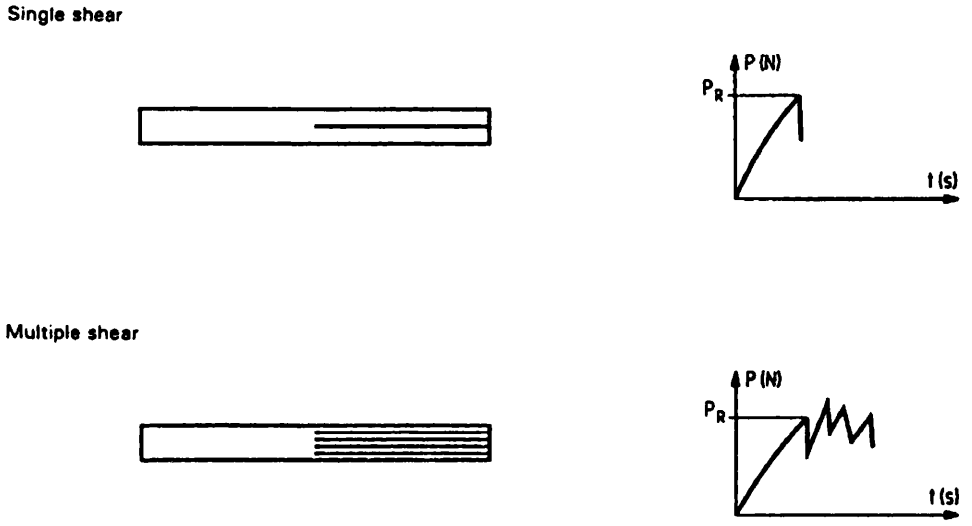

Figure 4-7: Schematic of shear failure[8].

4.5.3 Modes of Failure

The mode of failure was recorded using the following classifications[8]:

Acceptable failure modes:

- single shear, multiple shear (figure 4-8a)

Unacceptable interlaminar shear failure modes:

- mixed modes of failure (figure 4-8b): shear and tension, shear and compression
- non-shear modes of failure (figure 4-8c): tension , compression
- plastic shear (figure 4-8d).

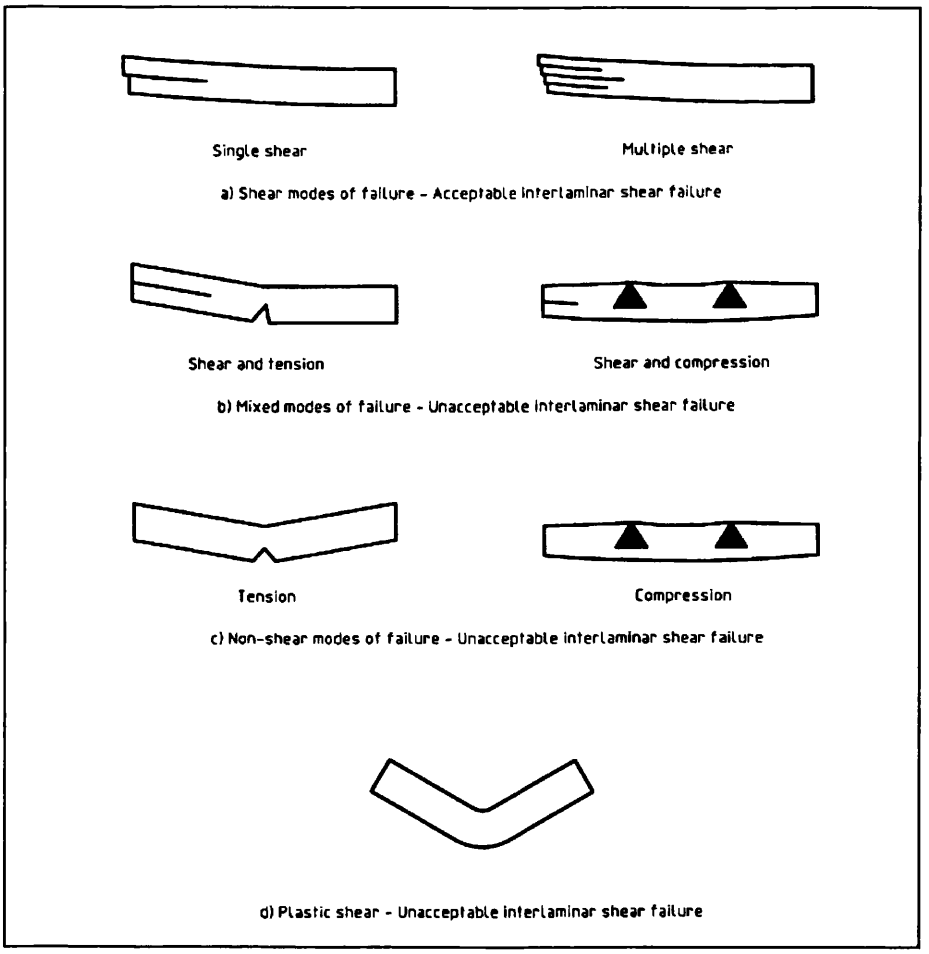

Figure 4-8: Modes of failure for short beam shear coupons[8].

4.6 Open Hole Testing

Mechanical fastening remains the primary means of joining composite components in modern aircraft structures, even though bolted joints are relatively inefficient. The stress concentration due to the hole causes a considerable reduction in both the notched tensile and compressive strength of a composite laminate. Experience with bolted joints in composite structures for aerospace applications has indicated a high level of complexity in joint design, due to the almost unlimited combinations of composite materials and fibre patterns and the fact that bolted joints in composites fail at loads that are not predicted by either perfectly elastic or perfectly plastic assumptions[39].

Experimental testing remains a significant part of the qualification process for new composite parts involving mechanical connections. Aircraft structural design follows a pyramidal structure of testing, ranging from coupon tests to full-scale structure tests. Open-hole tests are a part of the qualification process for composite parts that need to be joined to other parts, in aircraft structures.

The hole in the coupon creates a stress concentration with a small volume of material that is highly stressed. Testing was carried out following Airbus standard methods, AITM 1-0007[9] and AITM 1-0008[10] for the open hole tension and compression respectively.

4.6.1 Coupon Preparation

The open hole tension (OHT) coupon is a straight sided coupon 32mm wide, 300mm long and 4mm thick (16 plies). The open hole compression (OHC) coupon is also 32mm wide and 4mm thick, but is only 180mm in length. The diameter of the holes in each test coupon is 6mm. Schematics of the open hole tension and compression coupons can be seen in figure 4-9 and figure 4-10 respectively.

4.6.2 Test Procedure

The cross sectional dimensions at several points on the test coupon were measured using a micrometer. The coupon is then inserted into the grips of an aligned and calibrated test frame. The crosshead rate is set at 2mm/min for the tension tests and

1mm/min for the compression tests. The coupons were monitored to failure, which is defined as the maximum load attained during testing.

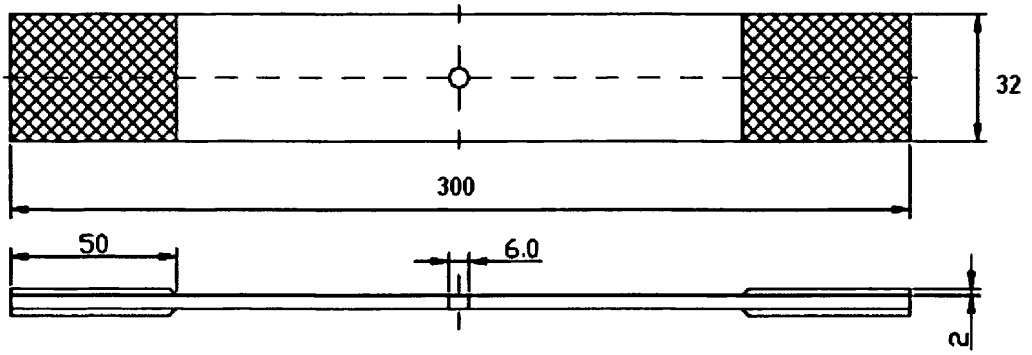

Figure 4-9: Dimension of coupon for open hole tensile test (mm)[9].

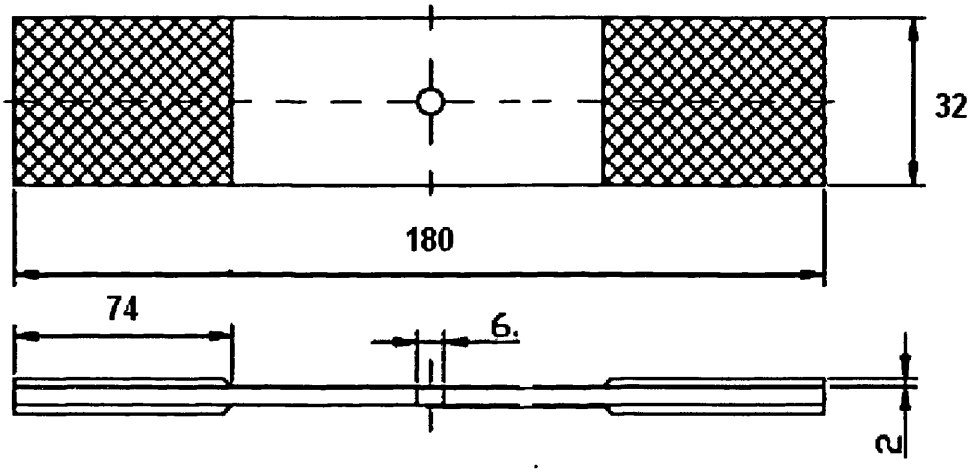

Figure 4-10: Dimension of coupon for open hole compression test (mm)[10].

4.6.3 Data Reduction

Tensile/compressive open hole strength (σ_{oht} and σ_{ohc}) can be calculated using equation *4-9*:

$$\sigma_{oht} = \frac{F}{bh} \qquad 4\text{-}9$$

where:

F is the maximum load (N)

b is the coupon width (mm)

h is the thickness (mm)

5 Experimental Results

Chapter 5 describes the experimental results for the initial phase of equilibrium saturation testing.

Firstly the constituent contents of the two materials were experimentally determined, with the results described here.

The results of the measured moisture and diffusion parameters (diffusion coefficient and maximum moisture content) of the materials are given. The diffusion of the resin is compared in relation to Fickian behaviour.

Results from the equilibrium saturation conditioning are stated and finally the mechanical test results from the equilibrium saturation tests (procedures described in Chapter 4) are presented.

5.1 Constituent Content Determination Results

Typical aerospace composite materials have a fibre volume, V_f, between 50 and 65%. Low V_f content results in lower lamina tensile strength and stiffness along the fibres, while higher V_f leads to reduction of strength under longitudinal compression and in-plane shear, due to poor bonding of the fibres[129,130]. As a necessity for data comparison, it is essential that the fibre volume fraction of each test coupon is known.

Table 5-1: Volume fraction and void content measured results.

Coupon type/panel ref.		Weight fibre W_f(g)	Coupon Weight in air W_c (g)	Coupon Weight in water W_w (g)	Specimen Density ρ_c (g/cm^3)	Fibre Volume V_f (%)	Void Volume V_v (%)
90° Tension	*Mean*	0.45	0.60	0.23	1.62	69.58	0.40
CDC/05/5286	*SD*	0.02	0.02	0.01	0.01	0.42	0.38
	CV					0.61	95.52
90° compression CDC/05/5287	*Mean*	0.42	0.57	0.21	1.60	67.42	1.23
	SD	0.01	0.04	0.01	0.03	3.95	0.59
	CV					5.85	48.18
IPS	*Mean*	0.32	0.43	0.16	1.59	66.27	1.57
CDC/05/5289	*SD*	0.00	0.00	0.00	0.00	0.60	0.41
	CV					0.91	26.00
ILSS	*Mean*	0.40	0.55	0.21	1.61	66.25	0.10
	SD	0.00	0.07	0.02	0.02	0.92	0.59
CDC/05/5316	*CV*					1.4	5.9
OHC	*Mean*	0.90	1.36	0.49	1.55	57.81	1.68
CDC/05/5293	*SD*	0.04	0.05	0.01	0.00	0.71	0.51
	CV					1.22	30.51
OHT	*Mean*	0.91	1.41	0.50	1.55	56.29	1.80
	SD	0.04	0.07	0.03	0.00	0.05	0.19
CDC/05/5293	*CV*					0.09	10.60

Table 5-1 lists the results of the measured constituent contents of the laminate panels produced, defined by the coupon test type they were used for. The measured fibre weight, coupon weight (in air and water) and specimen densities are shown. The calculated V_f and void volume, V_v, are also listed. All of the values were obtained by the experimental methods and calculations as described in section 3.3. The mean values and standard deviations are shown for each of the measured quantities. The mean values were determined from an average of three test coupons, as stipulated in the standard test method[105]. The coefficient of variation

(CV) was also calculated using equation A-1 in Appendix F for the calculated V_f and V_v.

The mean measured V_f values, varied between 56.29% (for the QI woven laminate) and 69.58 for the UD tape. The CV for the V_f values are within Airbus acceptable limits (5.8 % for properties where the fibres are predominant and 9.0% for properties where the resin behaviour is predominant). The void volume is below 2.0%, which is an acceptable limit for aerospace grade laminates[33].

However the CV for the V_v is between 10-95%. This is due to the property being very difficult to determine and the low number of samples used in the study (3 per panel).

5.2 Determining Diffusion Constants, (D_x, M_{max})

In order to predict the moisture content of a material, the maximum moisture content and the diffusion coefficient must be known. Section 3.4.1 describes the experimental procedure for determining the diffusion constants.

Prior to any conditioning, the test coupons were oven dried at 80°C. Figure 5-1 plots the desorbed moisture in wt%, against square root of time (√t) in days for Material A (UD tape) and Material B (woven fabric). These plots were produced from the coupon weighings, with each data point being an average of 5 coupons. Material A contained an initial moisture content of 0.310±0.005wt%, absorbed under ambient temperature and humidity conditions (approximately 23°C/50%RH) after manufacture, prior to drying. Material B contained 0.240±0.003wt% moisture. Table 5-2 shows the diffusion constants that were calculated from the drying data.

Table 5-2: Drying diffusion constants defined at 85%RH and 70°C.

Material	Lay-up	Thickness, mm	Moisture desorption, M_{max} (wt%)	Rate of Moisture desorption $x10^{-4}$ (wt%/s)	Diffusion Coefficient,D_x $x10^{-7}$ (mm^2/s)
Material A	$[0]_{11}$	2	0.310± 0.005	2.14	3.74
Material B	$[+45/0/-45/90]_{2S}$	4	0.240 ± 0.003	1.47	11.87

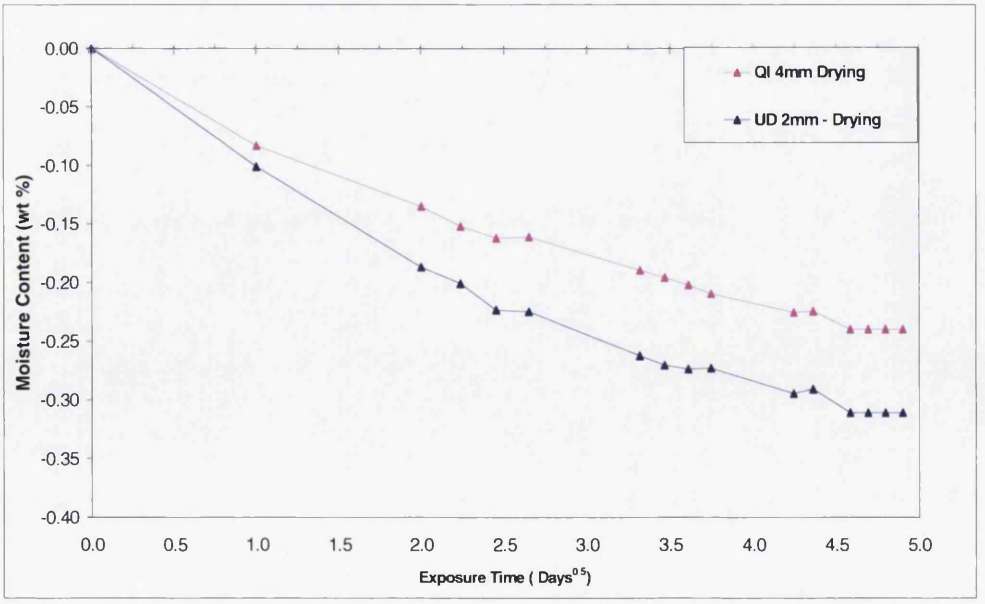

Figure 5-1: Average-drying curves for materials A and B.

Coupons were exposed to constant environmental conditions of 85%RH/70°C. Plots of absorbed moisture in wt% against square root of time (√t) in days, were produced from the data recorded during the coupon weighings. Figure 5-2 and figure 5-3 plots this data for Material A and B respectively. These plots were used to determine the moisture constants of both materials. The coupons were conditioned for 144 days in which time the coupons reached equilibrium moisture content and the values between weighings differed by less than 0.01wt%. Five coupons of each material type were tested and as can be seen, excellent repeatability was recorded.

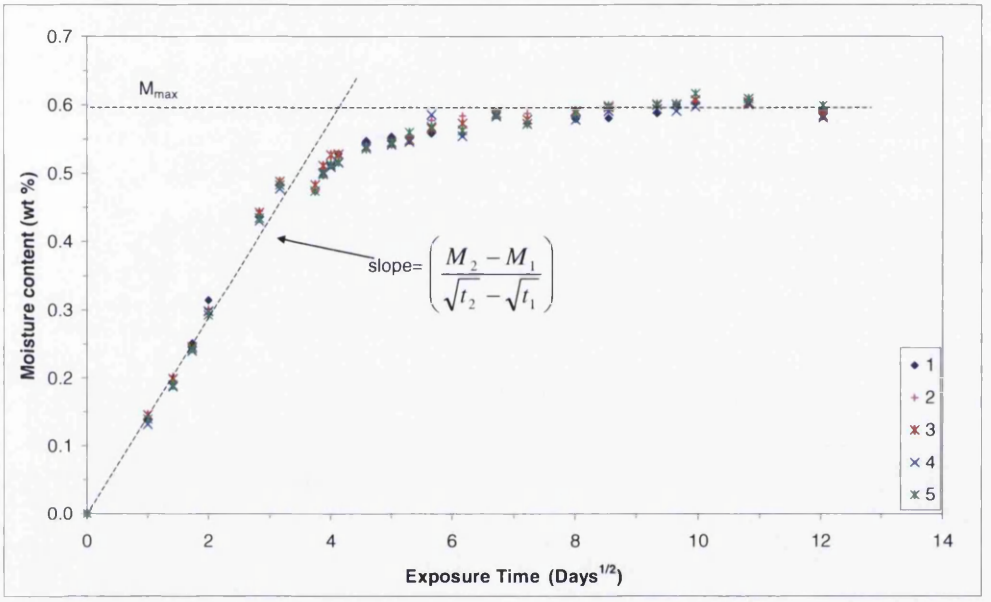

Figure 5-2: Moisture absorption curves for Material A, (70°C and 85%RH).

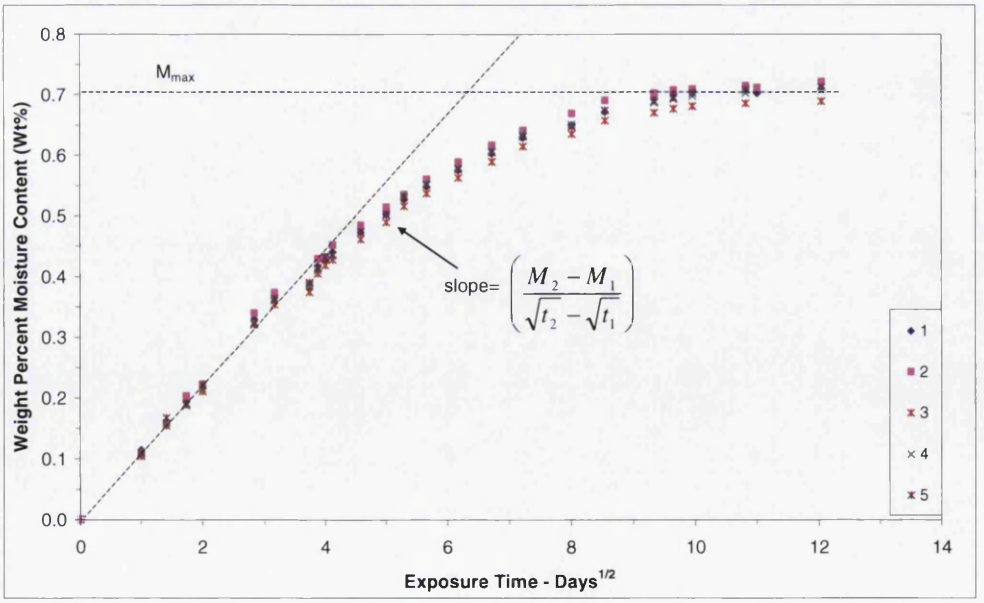

Figure 5-3: Moisture absorption curves for Material B (70°C and 85%RH).

From figure 5-2 it can be seen that the initial uptake of moisture in Material A was rapid, with almost 85% of total saturation weight being reached within 16 days. This was followed by a slow uptake, leading to equilibrium saturation. The equilibrium saturation weight, M_{max} was 0.607±0.007 wt%. At 16 days a kink in the curve is noticeable. This was due to a malfunction in the climatic chamber, which was resolved as quickly as possible. Figure 5-3 shows that the initial uptake of moisture in Material B was slower and more gradual; taking around 65 days to near full saturation, with equilibrium saturation reached in 144 days. Equilibrium moisture content, M_{max} was measured at 0.708±0.012 wt%. A comparison between the moisture uptake curves of Material A and Material B is shown in figure 5-4, each point on the curve is an average of 5 data points.

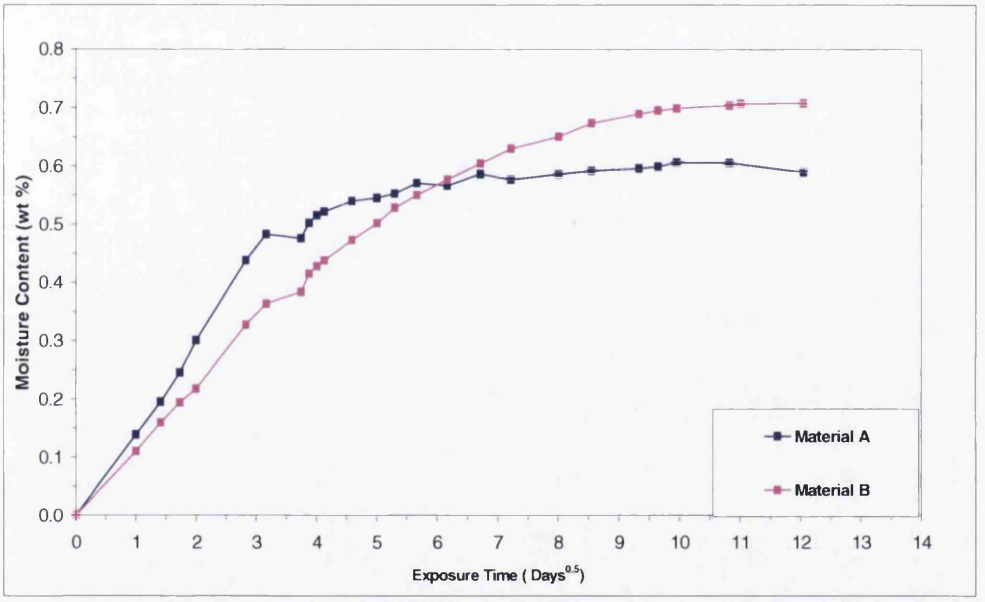

Figure 5-4: Comparison of moisture absorption curves for Material A and B.

The curves illustrate that the UD coupons (Material A) had a faster rate of absorption of moisture (i.e. a steeper initial gradient of uptake slope for the UD material) compared to the woven quasi-isotropic lay-up material (Material B) but the UD moisture uptake plateaus at a lower moisture equilibrium/saturation level than the woven material. The woven material has a lower V_f than the UD tape, thus has a greater percentage of resin and this may have attributed to the higher moisture content in the woven material.

The initial slope of the linear part of the uptake curves in figure 5-2 and figure 5-3 along with equation *2-20* was used in the calculation of the diffusion coefficient, D_x. The maximum moisture content was calculated using equation 3-8. The diffusion

constants are listed in table 5-3. Since the diffusion coefficient is not dependent on %RH but is temperature dependent, all further work done in this experimental programme was carried out at the same temperature (70°C), so the diffusion coefficients used in calculations will be assumed to be those stated in table 5-3. The equilibrium moisture content, M_{max} is not temperature dependent but is dependent on the %RH, thus being the variable in this work.

The rate of water absorption (measured from the initial slopes in figure 5-4) for the woven material B is lower than for the UD material A. This may be due to the nature of woven material making the diffusion path for the water molecules more complex than that of the UD tape and hence moisture traverses at a slower rate. Choi et al[49] showed that rate was fastest in laminates with 0° fibre angle. When comparing the calculated diffusion coefficients from table 5-3, the woven Material B (V_f ~0.58) has a greater calculated D_x. This is probably because of the greater amount of resin in this material than Material A (V_f ~0.68), thus giving a greater M_{max} level.

Table 5-3: Diffusion constants defined at 85%RH and 70°C.

Material	Lay-up	Thickness, mm	Moisture Content, M_{max} (wt%)	Rate of Moisture Absorption $x10^{-4}$ (wt%/s)	Diffusion Coefficient,D_x $x10^{-7}$ (mm^2/s)
Material A	$[0]_{11}$	2	0.607±0.007	5.53	6.67
Material B	$[+45/0/-45/90]_{2S}$	4	0.708±0.012	4.05	10.51

The Fickian numerical fits are plotted in figure 5-5 and figure 5-6; using the experimentally derived moisture constants in table 5-3 and the following relationship proposed by Shen and Springer[19] (discussed in section 2.11.4 of the literature review):

$$M = M_{\max}\left[1-\exp\left(-7.3\left(\frac{D_x.t}{h^2}\right)^{0.75}\right)\right] \qquad 5\text{-}1$$

where, M is the moisture content at any given point in time, t, M_{max} is the maximum moisture content, D_x is the diffusivity of the material through the thickness and h is the thickness of the coupon. Materials A and B appear to show a good correlation

with Fick's Second Law of diffusion, as can be seen in the numerical data in figure 5-5 and figure 5-6 respectively.

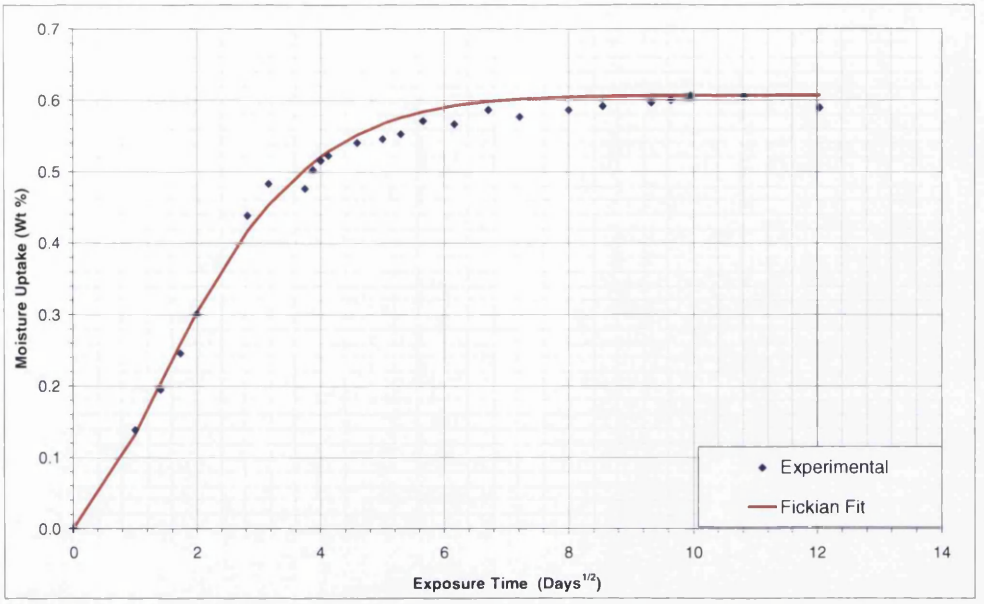

Figure 5-5: Comparison of mean experimental and predicted Fickian moisture uptake against root time for Material A, exposed to 85%RH and 70°C.

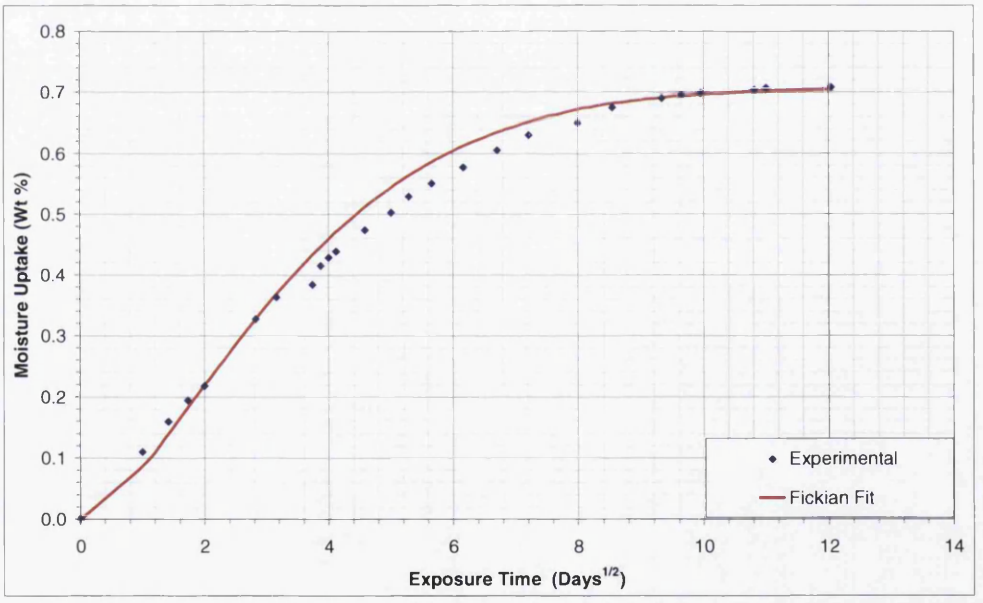

Figure 5-6: Comparison of experimental and predicted Fickian moisture uptake against root time for Material B, exposed to 85%RH and 70°C.

5.3 Equilibrium Saturation Conditioning Results

Chapter 3.5 describes the experimental procedure for carrying out the equilibrium saturation testing. These tests were performed by fixing the temperature and varying the humidity in the environmental chamber. Control in this way will allow a uniform level of moisture saturation through the thickness. The moisture absorption curves (i.e. average weight gain vs. time) for each of the test coupons were determined and are shown in Appendix D. The moisture uptake shows approximately Fickian behaviour and with increasing %RH the maximum moisture levels increased. Sudden drops in moisture uptakes on the curves can be explained from unavoidable malfunctions of the humidity chambers, which were rectified as soon as possible. Any deviations from Fickian behaviour were attributed to these malfunctions. As the diffusion coefficient D_x and the Fickian behaviour of the materials had already been established from the results in section 5.2, any deviations in behaviour were deemed acceptable.

Average values of equilibrium moisture content (M_{max}) of the composite test coupons conditioned at different relative humidity are listed in table 5-4. The measured value of M_{max} increased as a function of increasing %RH.

Table 5-4: M_{max} in each coupon type at different levels of %RH.

%RH	M_{max} in wt%					
	90° Tension	90° Compression	IPS	ILSS	OHT	OHC
0	0.00	0.00	0.00	0.00	0.00	0.00
60	0.22	0.40	0.40	-	-	-
75	0.36	0.57	0.56	0.50	0.40	0.38
85	0.44	0.67	0.64	0.70	-	-
95	0.57	0.77	0.86	0.86	0.65	0.61

From the literature review, Shen and Springer[19] showed that for many composite materials the maximum moisture uptake M_{max} is related to relative humidity by the following empirical formula:

$$M_{\max} = k.(\%RH)^n \qquad 2\text{-}22$$

Figure 5-7 shows the experimental relationship of equilibrium moisture content versus relative humidity for Material A. The trend-line shows the power law

relationship from equation *2-22*. From this, parameters k and n were determined, with the constants given in table 5-5. Studies have shown that an exponent n value of between 1.4 and 2.0 is typical of CFRP aerospace materials[19], which is in agreement with this work. M_{max} can be predicted for a composite at any %RH level, using the calculated constants, (k, n) and equation *2-22*. Table 5-5 shows the experimentally measured and predicted values of M_{max} at each %RH level. The ratio of experimental to predicted values shows that this relationship is within 10% accuracy of the average %wt moisture measured.

Table 5-5: Calculated constants a and b for materials A.

%RH	k	n	M_{max} experimental wt%	M_{max} theoretical wt%	Ratio M_{max} (experiment: theoretical)
60	0.0004	1.68	0.34	0.33	1.04
75			0.50	0.47	1.06
85			0.61	0.58	1.06
95			0.76	0.70	1.10

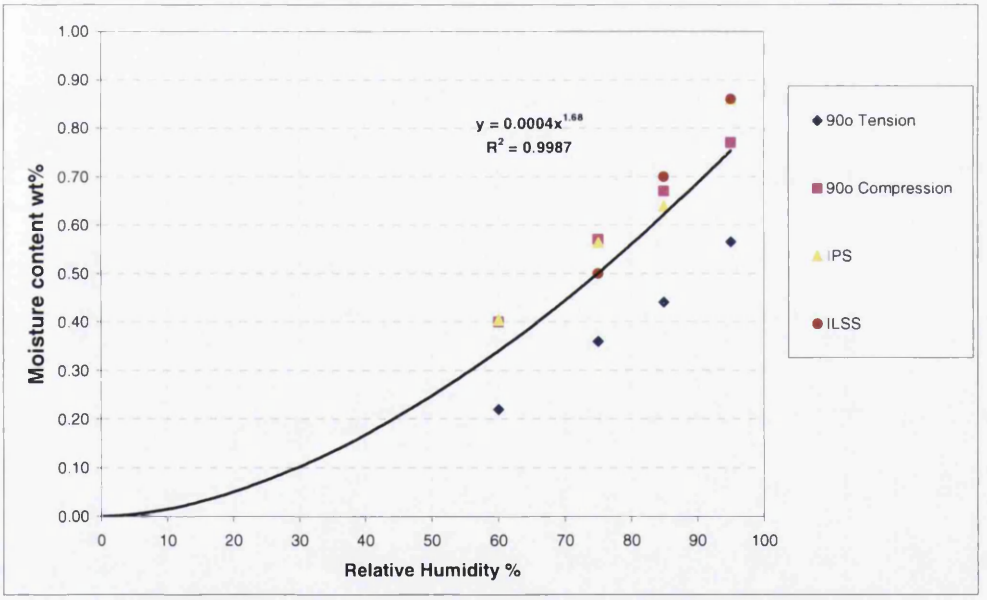

Figure 5-7: Moisture content as a function of %RH for Material A.

5.4 Equilibrium Saturation Mechanical Testing Results

The following sections 5.4.1 to 5.4.7 present and discuss the mechanical testing results for the coupons conditioned to equilibrium moisture content.

Table 5-6 shows a summary of the mechanical testing regime for the equilibrium saturated tests. Listed are the standard test procedures followed, the material type used, coupon tab and lay-up details and the test conditions used. All moisture uptake curves that were recorded for each individual coupon type can be seen in Appendix D. The raw experimental data can be found in Appendix E and details on the statistical analysis performed are in Appendix F.

The M_{max} values that were experimentally measured are listed in table 5-6.

Environmental knockdown factors, K_{EKDF} are calculated for each property/environmental exposure condition using the following approach:

$$K_{EKDF} = \frac{X_{mean-\%RH}}{X_{mean-OD}} \qquad 5\text{-}2$$

K_{EKDF} is the environmental knockdown factor, $X_{mean\text{-}\%RH}$ is the mean property at a particular %RH condition and $X_{mean\text{-}OD}$ is the mean property at the oven dry condition.

Table 5-6: Summary of mechanical testing regime.

Test	Standard Test Method	Coupon Type	End Tabs	Material	Orientation – Lay-up	Test Condition	M_{max} (wt%)
Tensile	BS EN ISO 527-5:1997	Type A	Yes	Material A	0 – UD	OD	0
						AR	0.26
						70°C / 75%RH	0.53
						70°C / 95%RH	0.73
					90 – UD	OD	0.00
						AR	0.10
						70°C / 60%RH	0.22
						70°C / 75%RH	0.36
						70°C / 85%RH	0.44
						70°C / 95%RH	0.57
Compression	prEN 2850	Type B	Yes	Material A	90 - UD	OD	0.00
						AR	0.26
						70°C / 60%RH	0.40
						70°C / 75%RH	0.57
						70°C / 85%RH	0.67
						70°C / 95%RH	0.77
IPS	DIN EN ISO 14129	See relevant specification	Yes	Material A	±45°	OD	0.00
						AR	0.25
						70°C / 60%RH	0.40
						70°C / 75%RH	0.56
						70°C / 85%RH	0.64
						70°C / 95%RH	0.86
ILSS	DIN EN ISO 14130	See relevant specification	No	Material A	See relevant specification – UD	OD	0.00
						AR	0.26
						70°C / 75%RH	0.50
						70°C / 85%RH	0.70
						70°C / 95%RH	0.86
Open Hole Tensile	AITM 1-0007	Type B	Yes	Material B	[90/±45/0]	OD	0.00
						AR	0.15
						70°C / 75%RH	0.40
						70°C / 95%RH	0.65
Open Hole Compression	AITM 1-0008	Type B	Yes	Material B	[90/±45/0]	OD	0.00
						AR	0.11
						70°C / 75%RH	0.38
						70°C / 95%RH	0.61

5.4.1 Longitudinal (0°) Tensile Testing Results

The test coupons were orientated with the fibres running along the major axis. The coupons were extended along the major axis at a constant speed until fracture occurred. Details of the test procedure can be found in section 4.1. Following mechanical testing, tensile stress was calculated from the load and coupon cross-sectional area using equation 4-1.

Table 5-7 summarises the 0° tensile test results, showing the variation of tensile strength with increasing equilibrium moisture content. The main observation was that there was no observed change in longitudinal tensile strength with moisture ingress, as the scatter was larger than any difference measured.

Table 5-7: : Summary of equilibrium saturated 0° tension tests.

Condition	Moisture Content, M_{max}, (wt%)	0° Tensile Strength, F_1^t (MPa)	0° Tensile Modulus, E1 (GPa)	Environmental Knockdown factor for F_1^t (K_{EKDF})	Environmental Knockdown factor for E_1 (K_{EKDF})
OD at 80°C	0	2357±143	152±2	-	-
RT/ AR	0.26 ±0.03	2396±79	144±3	1.0	0.948
75%RH/70°C	0.53 ±0.02	2395±80	145±3	1.0	0.936
95%RH/70°C	0.73 ±0.01	2349±123	142±4	0.996	0.955

Figure 5-8 shows the stress-strain response in regards to the varying environmental exposure conditions described earlier. Figure 5-9 shows the variation of unidirectional tensile strength with increasing moisture content. The error bars show ± one standard deviation for the data set.

The tensile stress-strain curve was linear up to the point of failure, (figure 5-8). These coupons failed by tensile rupture of fibres, followed by longitudinal splitting (de-bonding along the fibre-matrix interface) parallel to the fibres. Unidirectional laminates did not fail along a single plane but literally exploded into multiple fragments when tested in tension, thus making it impossible to identify the primary fracture plane and consequently no fracture pictures could be taken. This is typical behaviour for a high strength and high modulus carbon fibre composite with a fibre volume fraction of greater than 65%[33].

Young's Modulus values were calculated from the test data using equation 4-2. Figure 5-10 plots Young's modulus versus the amount of moisture absorbed in the test coupon. Table 5-7 lists the values. A reduction of 6% in stiffness is seen between oven dry (0wt%) and coupons conditioned to equilibrium at 70°C/95%RH.

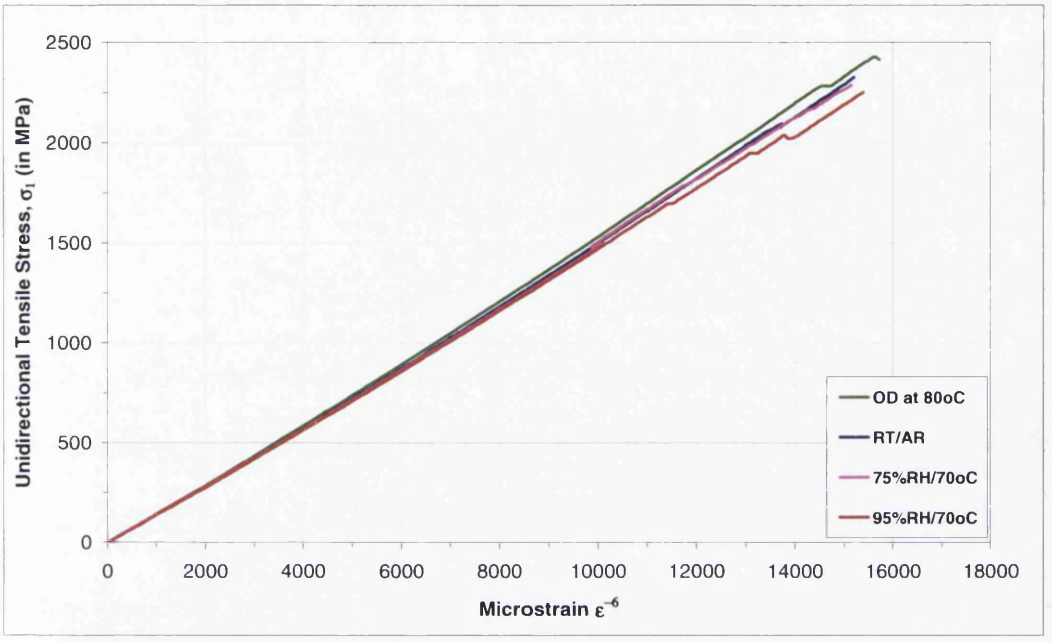

Figure 5-8: Stress-strain curves for 0° tension tests.

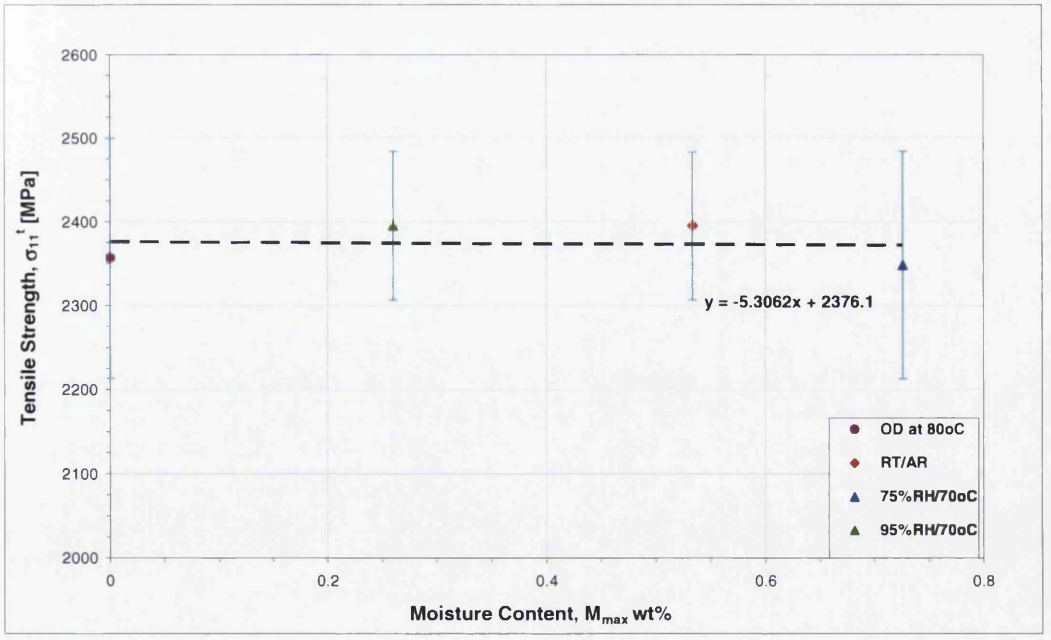

Figure 5-9: 0° tensile strength vs. moisture content.

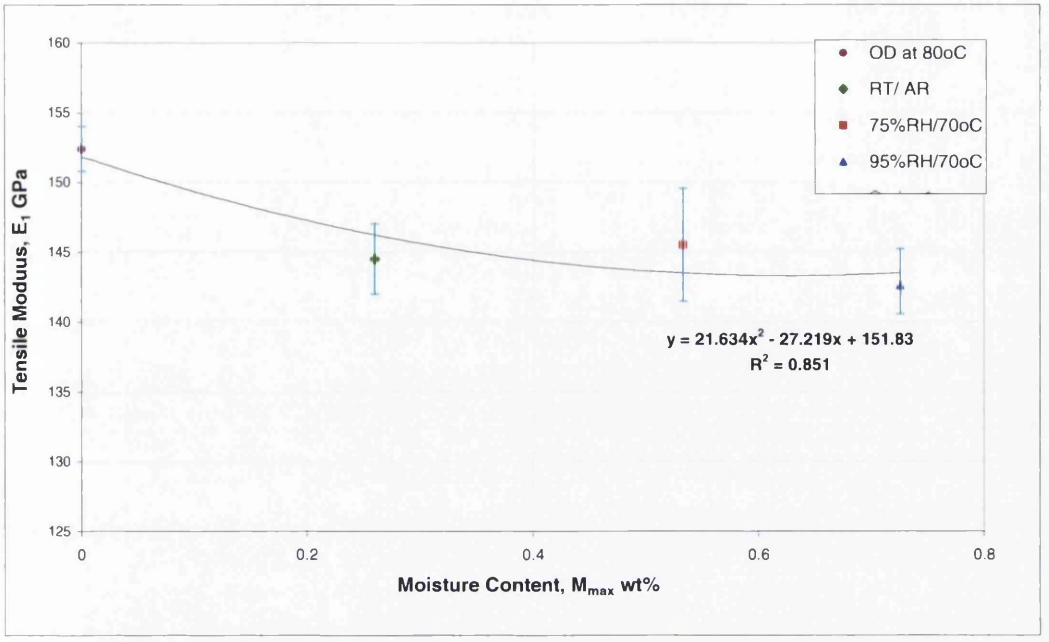

Figure 5-10: Young's Modulus E_1, vs. moisture content.

5.4.2 Transverse (90°) Tensile Testing Results

The test coupons were orientated with the fibres running perpendicular to the major axis. The coupons were extended along the major axis at a constant speed until fracture occurred. Details of the test procedure can be found in section 4.2. After the tests were performed the load and coupon cross-sectional area data were utilised to calculate the transverse tensile stress, using equation 4-1.

Table 5-8 summarises the 90° tensile test results, showing the mean strength and modulus results for the 90° tension tests the calculated K_{ENDF}'s are also listed.

Table 5-8: Summary of equilibrium saturated 90° tension tests.

Condition	Moisture content, $M_{max.}$ (wt%)	90° Tensile Strength, F_2^t (MPa)	90° Tensile Modulus, E_2 (GPa)	Environmental Knockdown factor for F_2^t (K_{EKDF})	Environmental Knockdown factor for E_2 (K_{EKDF})
OD at 80°C	0	55 ± 7	9.3 ± 0.1		
RT/AR	0.10± 0.01	54 ± 6	9.2 ± 0.1	0.982	0.989
60%RH/70°C	0.22± 0.01	51 ± 5	9.1 ± 0.1	0.927	0.978
75%RH/70°C	0.36± 0.01	41 ± 3	-	0.745	-
85%RH/70°C	0.44± 0.02	43 ± 3	9.0 ± 0.2	0.782	0.968
95%RH/70°C	0.57± 0.02	29 ± 5	8.9 ± 0.1	0.527	0.957

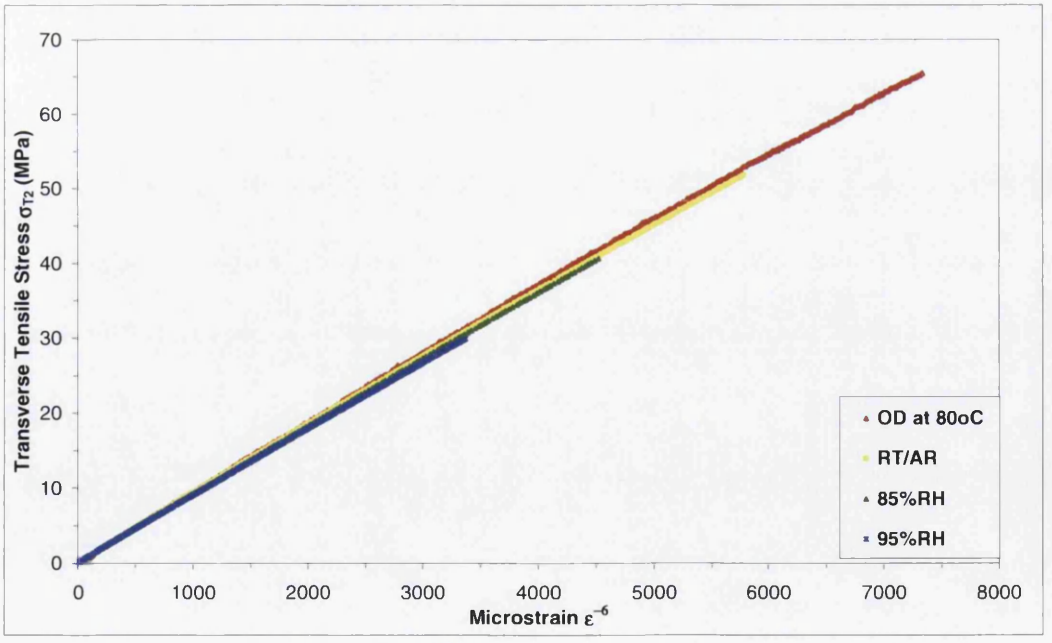

Figure 5-11: 90° tension stress-strain curves.

Figure 5-11 shows the stress-strain response for the transverse tension tests (i.e. θ=90°) with varying equilibrium moisture content. As expected the tensile stress-strain curves are linear up to the point of ultimate failure. Figure 5-12 plots tensile strength against equilibrium moisture content; the error bars show ±1 standard deviation of each data set (of 6 coupons). When conditioned to equilibrium at 70°C and 95%RH to give a M_{max} of 0.57wt%, there is a near 48% decrease in the UTS. E_2 is not greatly affected by moisture ingress.

Equation 4-2 was used to calculate the transverse tensile modulus. A 5% reduction in stiffness from oven dry to M_{max} of 0.57wt% moisture is measured. Figure 5-13 displays the transverse tensile modulus (E_2) versus weight percent moisture absorbed by the test coupon. This property is influenced by the increase of moisture in the material. The decrease in the transverse tensile modulus is a result of softening of the epoxy matrix due to the moisture absorption.

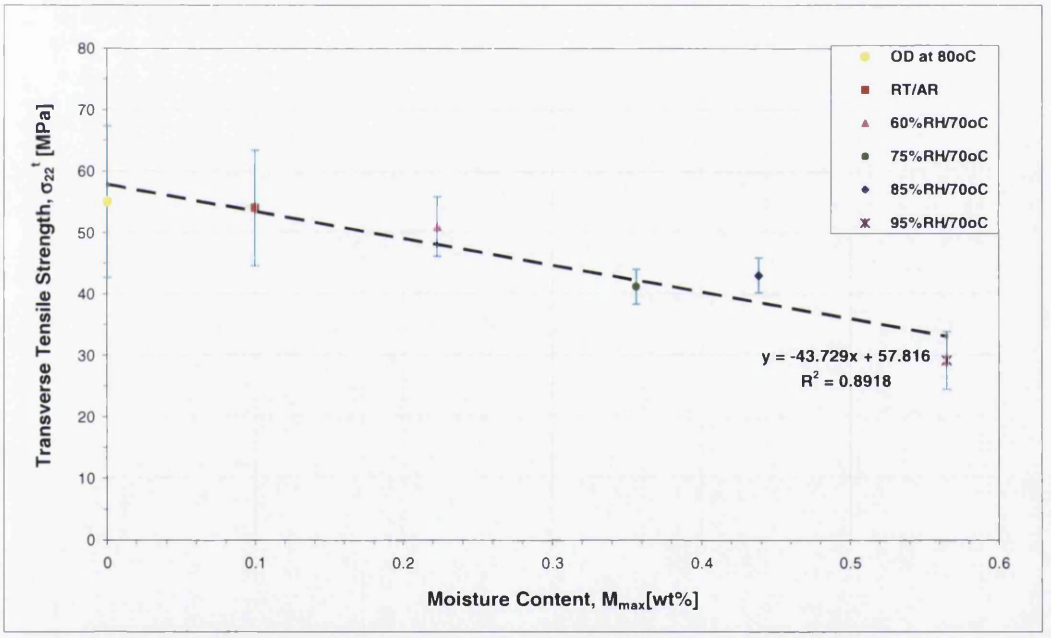

Figure 5-12: 90° tensile strength vs. moisture content.

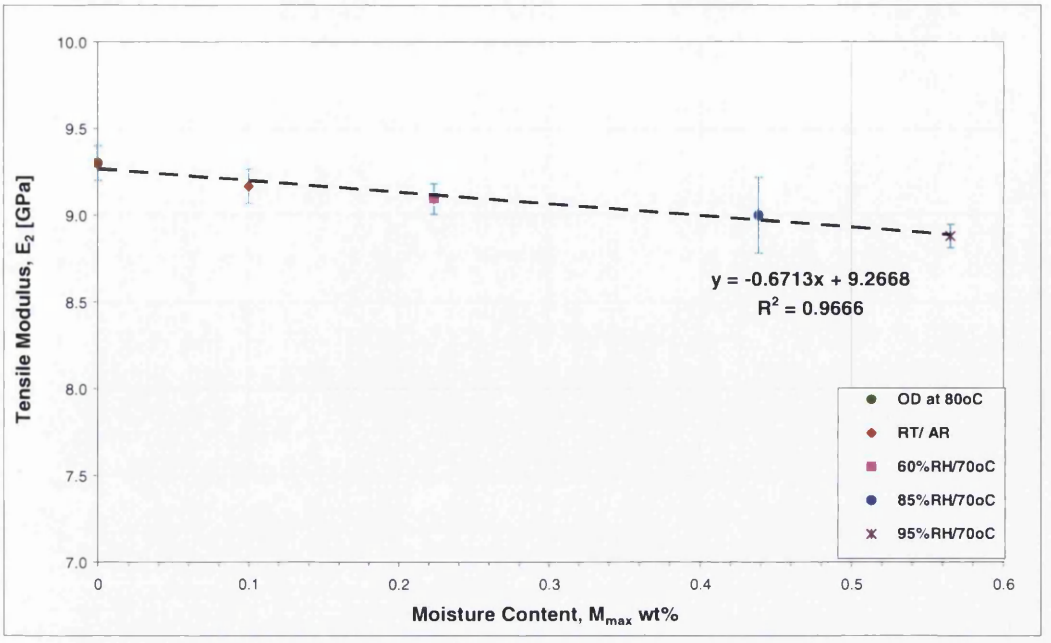

Figure 5-13: 90° tensile modulus vs. moisture content.

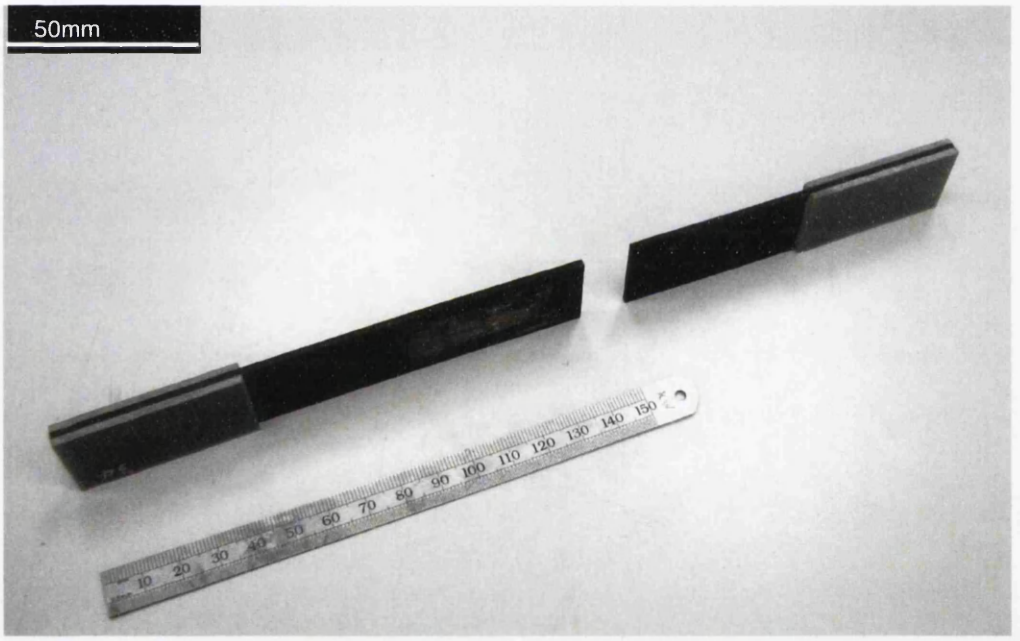

Figure 5-14: A tested transverse tension coupon.

Figure 5-14 depicts a tested 90° tension coupon, where failure has occurred in the gauge section. The failures observed did not seem to be affected by the amount of moisture present in the coupons. Fibres perpendicular to the loading direction act to produce a stress concentration at the interface and in the matrix. Therefore the 90° coupons failed because of tensile rupture of the matrix or fibre matrix interface. The composite failure mode under transverse tensile load can be described as (1) matrix tensile failure and (2) constituent de-bonding[39].

Figure 5-15 shows the details of the fracture surface for a typical 90° tension failure. The edge of the coupon shows where delamination between the plies has occurred, with an apparently clean fracture surface with no fibre pull out, indicating pure resin failure.

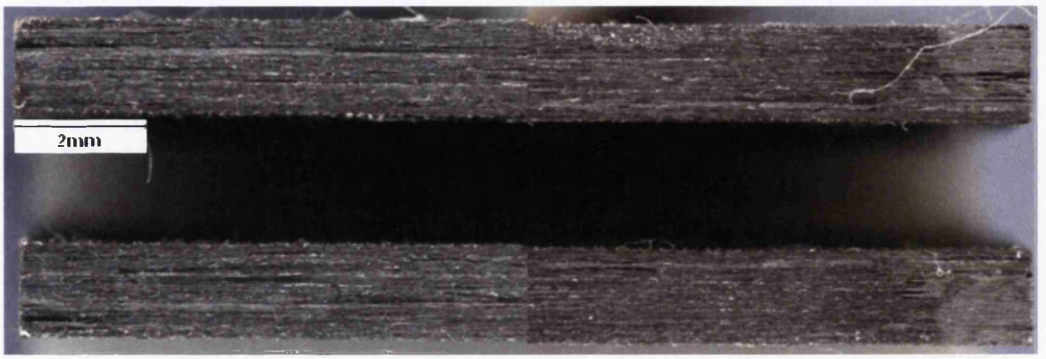

Figure 5-15: Detailed failure surface of 90° compression coupon.

5.4.3 90° Compression Testing Results

The test coupons were orientated with the fibres running perpendicular to the major axis. The coupons were compressed along the major axis at a constant speed until fracture occurred. Details of the test procedure and test rig can be found in section 4.3 of this report. The load data recorded from the test was used with equation 4-3 to calculate the transverse compression stresses produced.

Table 5-9 summarises all the test results obtained for the transverse compression tests. The main observation was that no reduction in transverse compressive strength was measured with increasing moisture content, as the scatter was larger than the variation in the mean values. Therefore a K_{EKDF} of 1.00 is applied across all the environments.

Table 5-9: Summary of equilibrium saturated 90° compression tests.

Condition	Moisture content, M_{max}, (wt%)	90° Tensile compression, F_2^c (MPa)	Environmental Knock-down factor for F_2^t (K_{EKDF})
OD at 80°C	0	232±5	-
RT/AR	0.26 ±0.01	240±15	1.00
60%RH/70°C	0.40 ±0.01	240±7	1.00
75%RH/70°C	0.57 ±0.01	247±13	1.00
85%RH/70°C	0.67 ±0.01	228±12	1.00
95%RH/70°C	0.77 ±0.01	245±14	1.00

Figure 5-16 shows representative transverse compression stress versus machine displacement curves for all the equilibrium conditioning parameters to which the coupons were exposed. The stress-extension curves were slightly non-linear, indicating that the material response was matrix dominated[39]. Figure 5-17 shows the effect of the moisture uptake on the value of transverse compression strength; the blue error bars show ±1 standard deviation for each data set.

Figure 5-18 shows a transverse compression coupon that has failed in the gauge section. This was a typical failure that was observed regardless of moisture content. Figure 5-19 illustrates the failure mode of a unidirectional composite subjected to transverse loads. The transverse compression fracture surface contains areas covered with debris of crushed fibres and the resin (see figure 5-20). This debris is a result of the damage caused during failure and cannot be removed by cleaning.

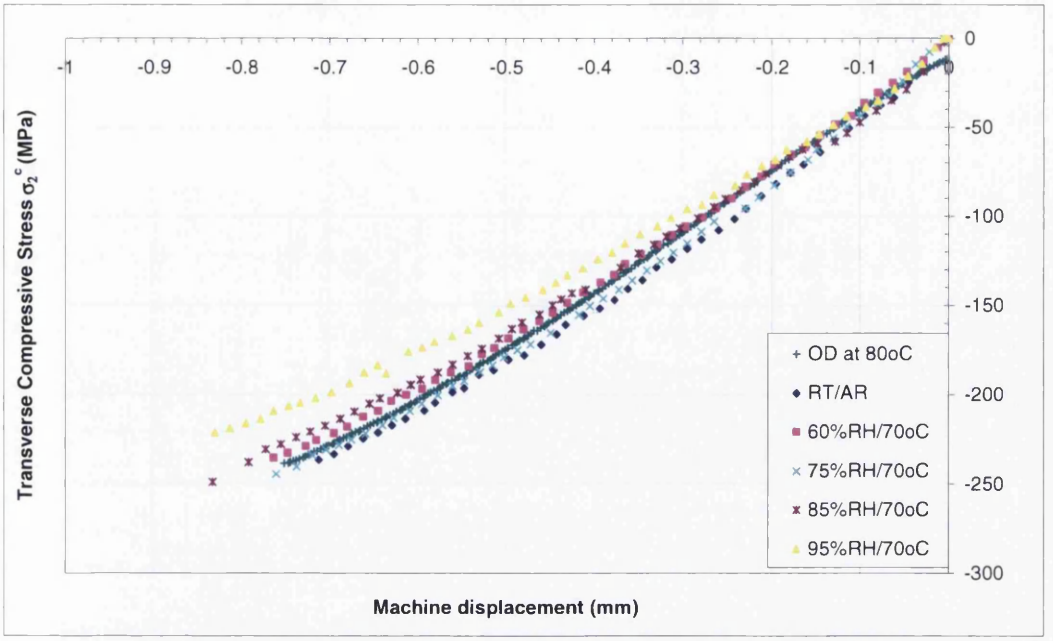

Figure 5-16: 90° compression strength-displacement curves.

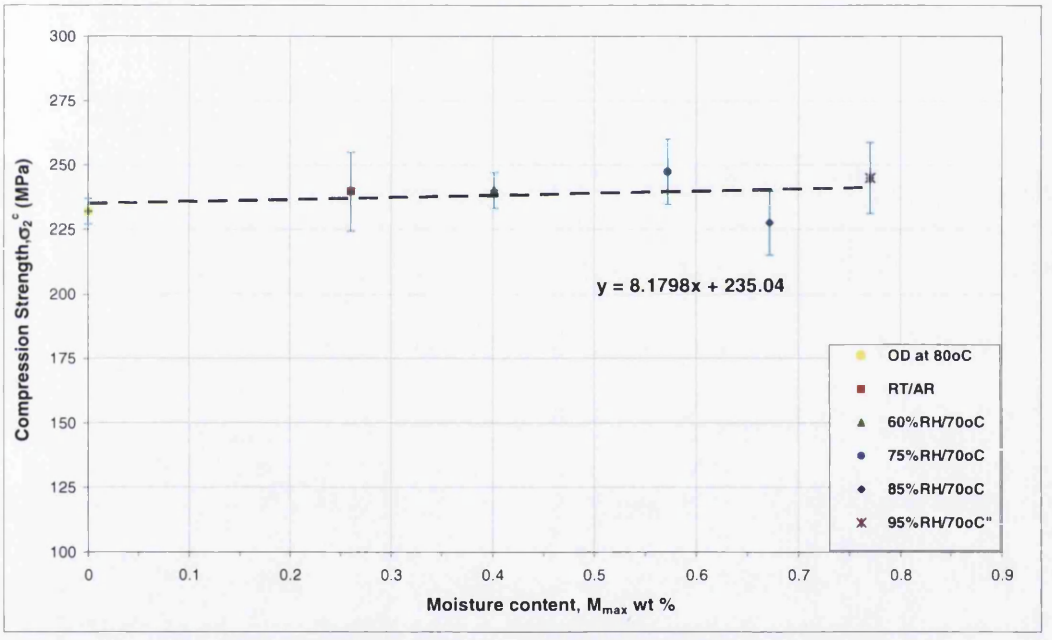

Figure 5-17: 90° compression strength vs. moisture content.

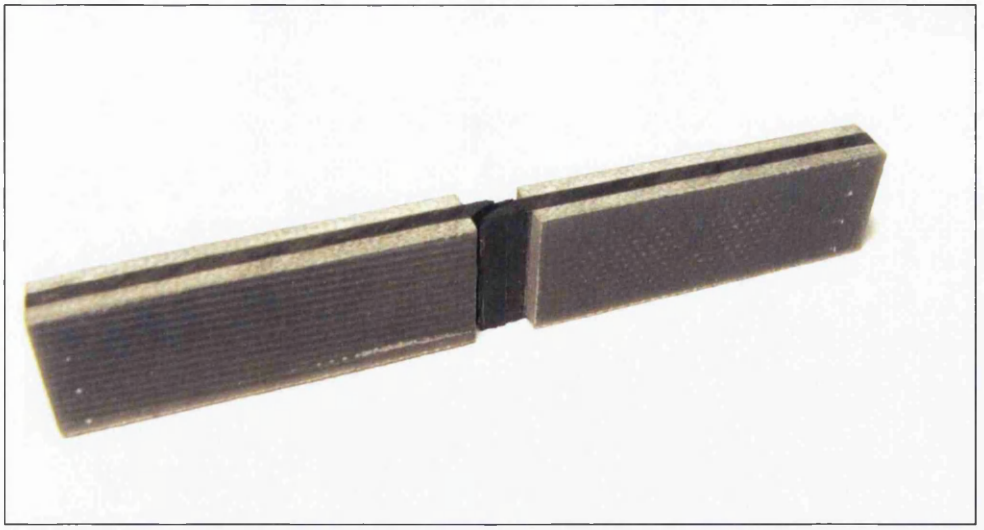

Figure 5-18: Failed transverse compression coupon.

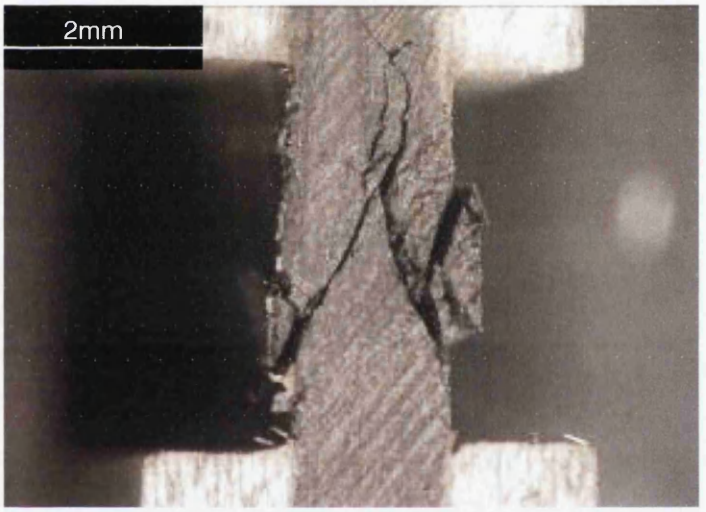

Figure 5-19: Typical failure of transverse compression failure.

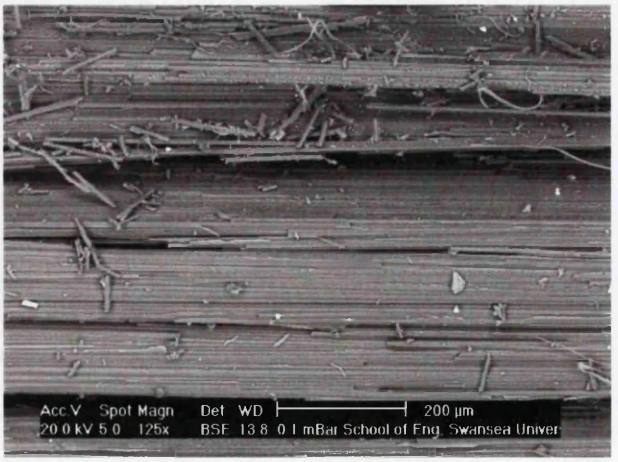

Figure 5-20: Transverse compression fracture surface showing debris and crushed fibres.

5.4.4 In-plane Shear Testing Results

In-plane shear (IPS) test coupons consisting of a rectangular cross-section with the fibres oriented ±45° to the coupon axis, were loaded in tension. To determine modulus values, strains parallel and perpendicular to the coupon axis were measured. Details of the test procedure and data reduction can be found in section 4.4.

Table 5-10 summarises the in-plane shear test data. Measured in-plane shear strength (taken at 5% strain) and modulus values are shown, along with the calculated K_{EKDF} for each environmental condition. The main observation from the test results is that both IPS strength and modulus decrease with increasing equilibrium levels of moisture.

Table 5-10: Summary of equilibrium saturated In-plane shear tests.

Condition	Moisture content, M_{max}, (wt%)	IPS Strength, F_{12} (MPa)	IPS Modulus, G_{12} (GPa)	Environmental Knockdown factor for F_{12} K_{EKDF}	Environmental Knockdown factor for G_{12} K_{EKDF}
OD at 80°C	0.0	85.3±1.1	5.2±0.1	-	-
RT/AR	0.25±0.01	73.6±2.7	4.9±0.1	0.87	0.9
60%RH/70°C	0.40±0.04	73.2±0.7	4.8±0.1	0.86	0.9
75%RH/70°C	0.56±0.04	73.5±1.1	4.7±0.1	0.86	0.9
85%RH/70°C	0.64±0.04	70.6±1.2	4.7±0.1	0.84	0.9
95%RH/70°C	0.86±0.01	66.8±0.8	4.6±0.1	0.79	0.9

Figure 5-21 shows the typical load versus machine displacement plots for dry and equilibrium saturated coupons. Significant plasticity can be seen in these curves. The curves show that the load increased rapidly up to around 2.5mm of cross-head displacement in all cases. Coupons continued to carry small amounts of load and continued to elongate until failure as figure 5-21 shows. This is a result of combined influence of the resin matrix and fibre-matrix interface of the ±45° laminate[92].

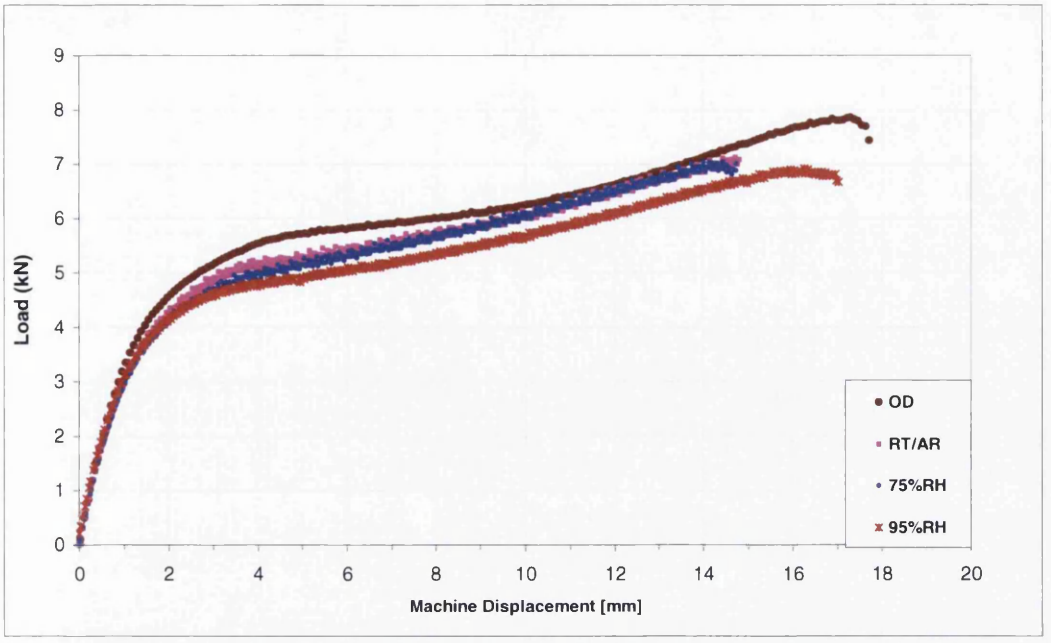

Figure 5-21: Load-displacement curves for IPS tests.

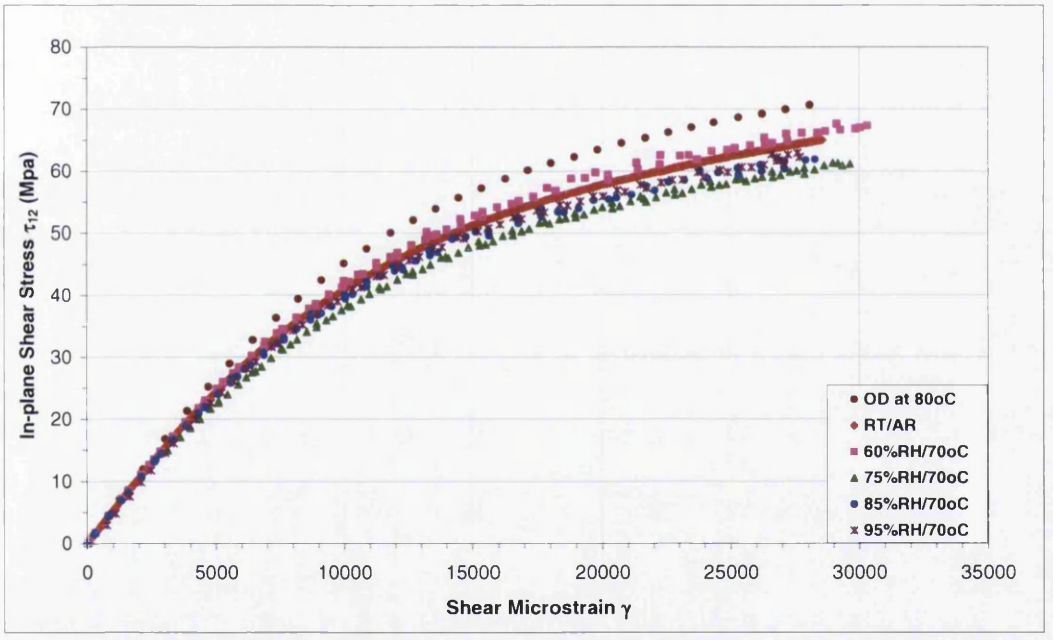

Figure 5-22: Stress-strain response for IPS tests.

The load-displacement data was used to calculate the in-plane shear properties using equations 4-5 and 4-6, representations of measured shear stress (τ) versus shear strain (γ) curves are plotted in figure 5-22. Back and front tee-rosette strain gauges were utilised on the coupons to check for bending. Because of the failure nature of these coupons, the large deformation caused the gauges to become un-bonded at around 30000 micro-strains, $\mu\varepsilon$.

Shear stress and strain was calculated using equation 4-5 and 4-6, the stress-strain response for these tests appear non-linear as they are dominated by the matrix and the fibre/matrix interface properties. The recorded curves for several coupons for each condition type almost overlapped each other, indicating excellent test repeatability.

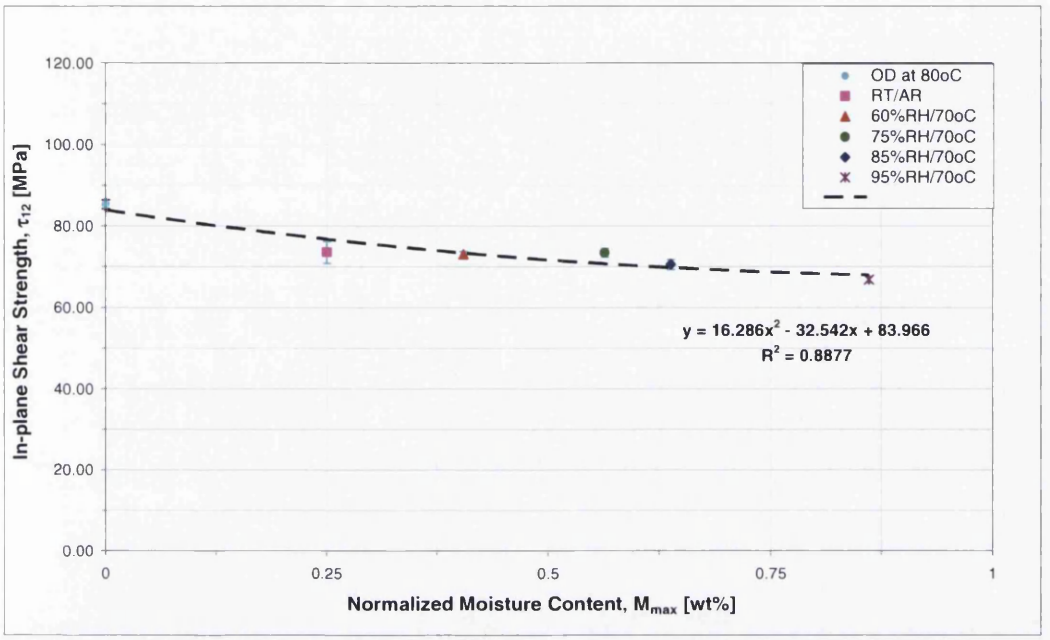

Figure 5-23: In-plane shear strength vs. moisture content.

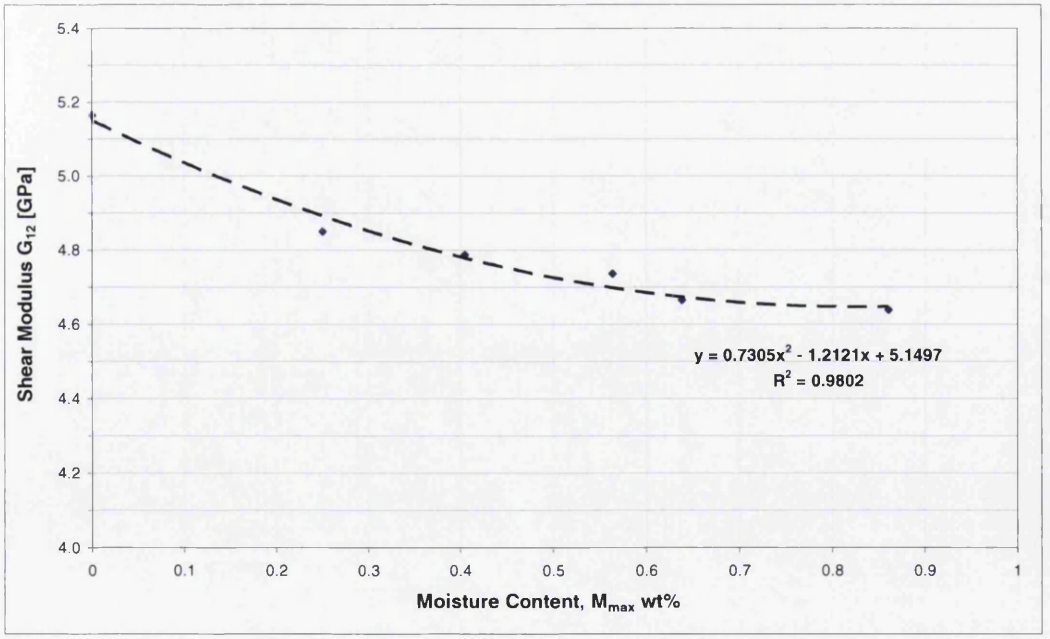

Figure 5-24: Shear modulus, G_{12} vs. moisture content.

Figure 5-23 shows the in-plane shear strength versus weight of water absorbed. The IPS modulus, G_{12} was calculated using equation *4-7*. G_{12} versus weight % moisture content plots are shown in figure 5-24. International standard ISO 14129[6] states that this test method is acceptable for modulus measurement, but there is concern over its use for the ultimate shear strength for high shear-elongation materials, due to the high strain at failure with only a small further increase in load, fibre rotation and associated temperature rise. Therefore, the stress at a maximum shear strain of 5 % or less is used as the failure criterion.

Figure 5-25 shows a typical gauge section failure in an in-plane shear coupon. Looking at the broken fibre ends it can be seen that under the tensile load the fibres have attempted to rotate/twist under load to align themselves in the 0° direction. This causes fibre twist, which increases the failure load. The fibre pull-out (rotation and delamination) can be seen clearly, with failures consistent regardless of moisture content.

Figure 5-25: Failure of OD ±45° In-plane shear coupon.

5.4.5 Interlaminar Shear Testing Results

Interlaminar shear (ILS) tests were performed according to BS EN ISO 14130[8], where a rectangular coupon was subjected to a three point bend loading until fracture occurred, the details of which can be found in section 4.5.

Equation 4-8 was used to calculate the interlaminar shear strength (ILSS) from the load data recorded during testing. Table 5-11 summarises the ILS test data, showing the moisture content, the mean ILSS and the associated K_{EKDF} at each level of equilibrium saturation.

Table 5-11: Summary of equilibrium saturated ILS tests.

Condition	Moisture content, $M_{max.}$ (wt%)	Interlaminar Shear Strength, σ_{ILSS} (MPa)	Environmental Knockdown factor, K_{EKDF}
OD	0.0	85±4	-
AR	0.26± 0.02	92±4	1.082
75%RH	0.50± 0.01	72±3	0.847
85%RH	0.70± 0.02	74±4	0.873
95%RH	0.86±0.01	65±4	0.765

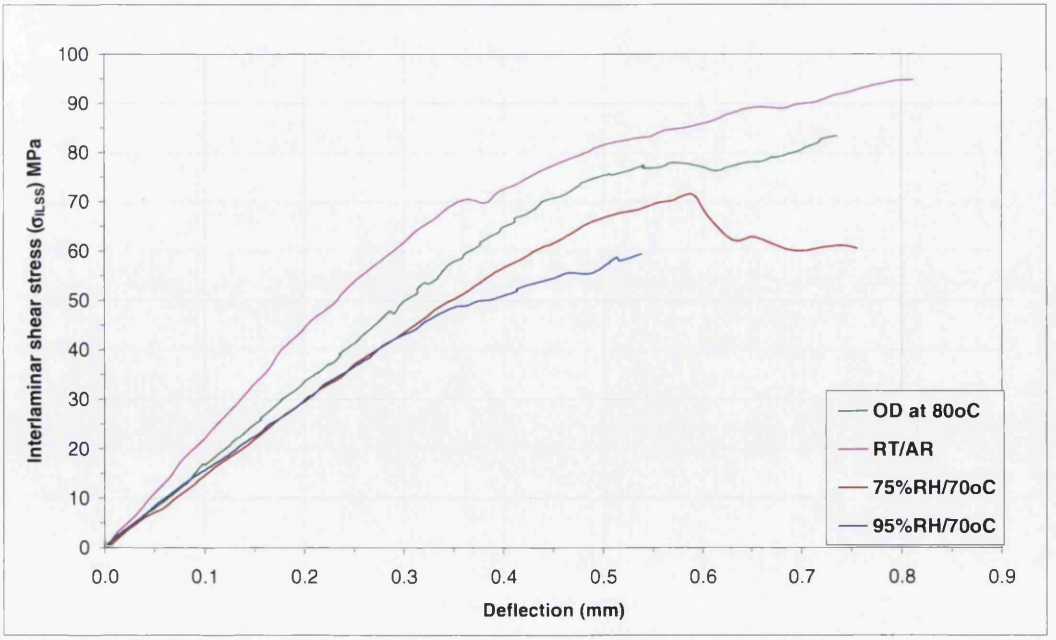

Figure 5-26: σ_{ILSS} vs. deflection curves.

Figure 5-26 presents the ILSS versus deflection curves for the carbon/epoxy composites exposed to varying hygro-thermal conditions, as well as oven-dry (OD) and as-received (AR) coupons. The curves have an initial linear section and then become non-linear as the ultimate ILSS is approached. Discontinuities in the curve indicate that localised crushing has occurred.

Figure 5-27 show the variation in ILSS with increasing moisture in the coupons, with the blue error bars displaying standard deviation in each group of test results. It is seen that the ILSS initially increases with a small amount of moisture present, then as equilibrium moisture content increases, the ILSS decreases.

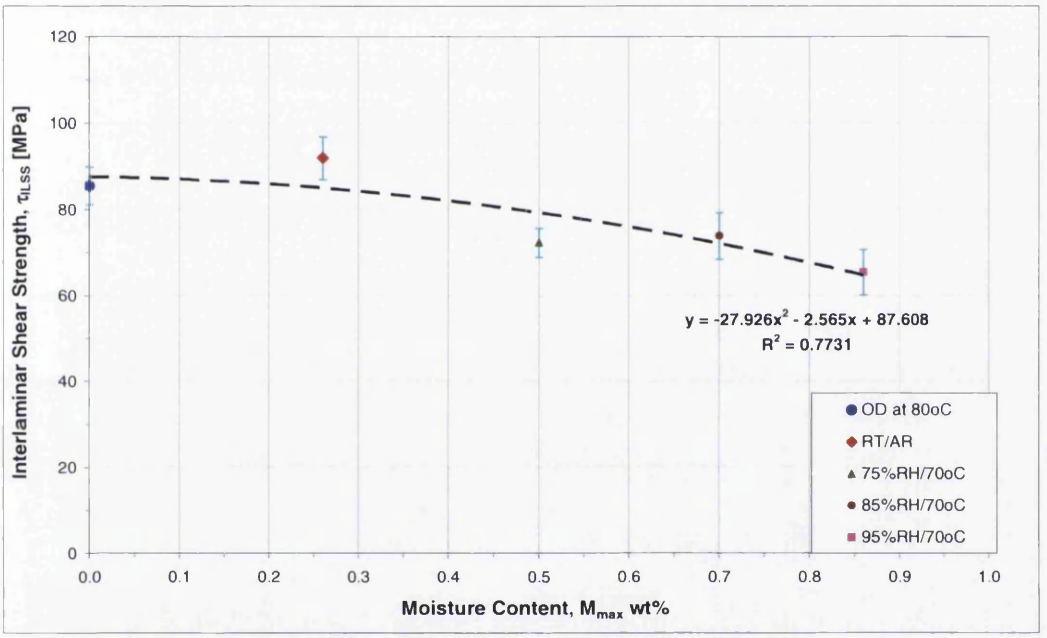

Figure 5-27: ILS strength vs. moisture content.

Figure 5-28: ILS coupon showing a single shear failure.

The failure in the ILS tests coupon was located opposite the central roller of the test rig. In ILS tests, failure occurs due to failure of fibre/matrix adhesion in combination with the stress concentration adjacent to the loading roller.

Failure analysis of the ILS coupons was performed, allowing the interlaminar cracks to be readily observed. Figure 5-28 shows a typical failure, the 0^{o} orientated laminates failed typically by interlaminar fracture between the layers with a single shear crack running between parallel planes[64]. Figure 5-29 shows a failure with multiple shear cracks running between the planes. Both of the failure types shown in figure 5-29 and figure 5-28 are acceptable interlaminar shear failures[8]. In most cases, a sharp cracking sound and a sudden drop in load indicated interlaminar failure. All the coupons either had a single crack, at or near the thickness middle plane of the beam, extending from the loading point to one end and crossing the entire width, or multiple cracks in similar positions. The cracks could be seen by looking at the side of the coupon as shown in figure 5-28 and 5-29. Most of the coupons also had a slight indentation at the touch points of the loading noses.

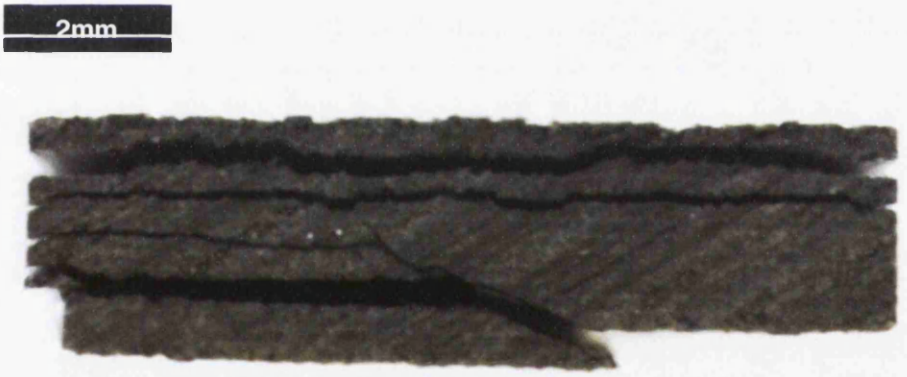

Figure 5-29: Short beam shear coupon showing multiple shear failures.

5.4.6 Open Hole Tension Results

Open hole tension (OHT) coupons were made out of a quasi-isotropic lay-up woven laminate, with a hole at the centre of the gauge section. The coupons were extended along the major axis at constant speed until fracture occurred. Details of the test procedure can be found in section 4.6.

Table 5-12 summarises the OHT test results, showing the M_{max} and measured mean stress. The main observation was that no measured decrease in OHT strength was seen, but an increase in open hole tension strength of nearly 10% was observed with moisture absorption. This may be attributed to stress relaxation effects, due to the presence of moisture at the stress concentration of the hole[33].

Table 5-12: Summary of equilibrium saturated OHT tests.

Condition	Moisture content, M_{max}, (wt%)	Open Hole Tension Strength, F_{xx}^{oht} (MPa)	Environmental Knock-down factor (K_{EKDF})
OD at 80°C	0	336±8	-
RT/AR	0.15±0.01	341±10	1.015
75%RH/70°C	0. 40±0.01	366±7	1.089
95%RH/70°C	0.65±0.02	359±21	1.068

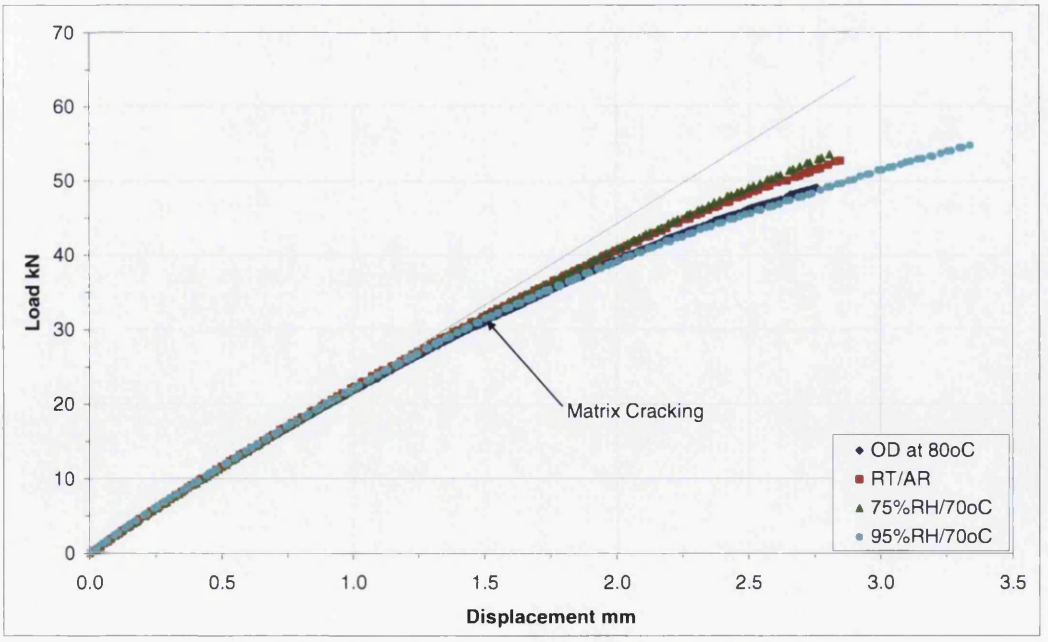

Figure 5-30: Open hole tension load-displacement curves.

Figure 5-30 shows the load versus machine displacement curves. From this data, open hole stresses were calculated using equation 4-9 and figure 5-31 plots the results of the calculations. The main characteristics of the curves are the nonlinearity of the load–displacement (figure 5-30) and stress–displacement diagrams (figure 5-31).

While testing tensile coupons with a hole, matrix cracking occurred at about 43% of maximum load (this was audible), see figure 5-30, where a "knee" in the curve can be seen (which is a characteristic of the weaker orientated plies failing), followed by catastrophic failure, due to the 0^{o} aligned fibres breaking. The slopes of the curves are all similar. A slight increase in ductility was observed for the test coupons conditioned at 95%RH and this may be attributed to the softening of the matrix material with increasing moisture content.

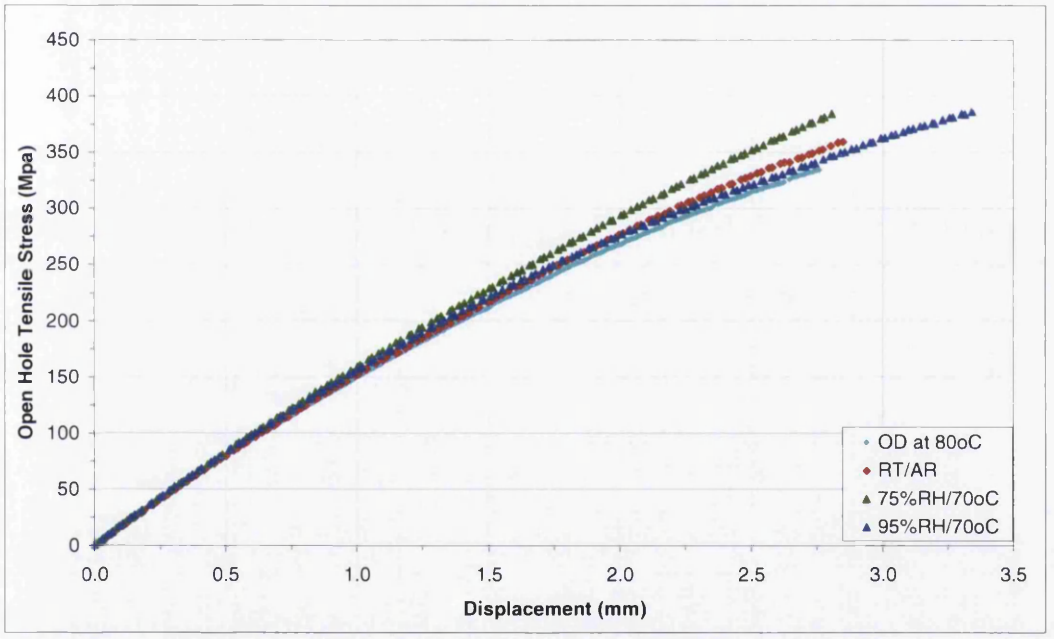

Figure 5-31: Open hole tension stress-displacement curves.

Figure 5-32 displays the open-hole tension strength versus equilibrium absorbed wt% moisture. As can be seen, no decrease in strength was observed with higher levels of equilibrium saturation, but as mentioned earlier a small increase was measured.

The quasi-isotropic open-hole tension coupons failed at the hole and exhibited multiple modes of failure in various sub-laminates, with a typical example of the type of failure observed shown in figure 5-33. Ultimate failure occurred in all coupons

almost instantaneously, with little warning given to the onset of failure, except for some audible "pings" (characteristic of fibre failure) and harsh tearing sounds (characteristic of large catastrophic laminate delamination), heard seconds before the ultimate failure. The open hole tensile strength was determined at the maximum tensile load (fracture).

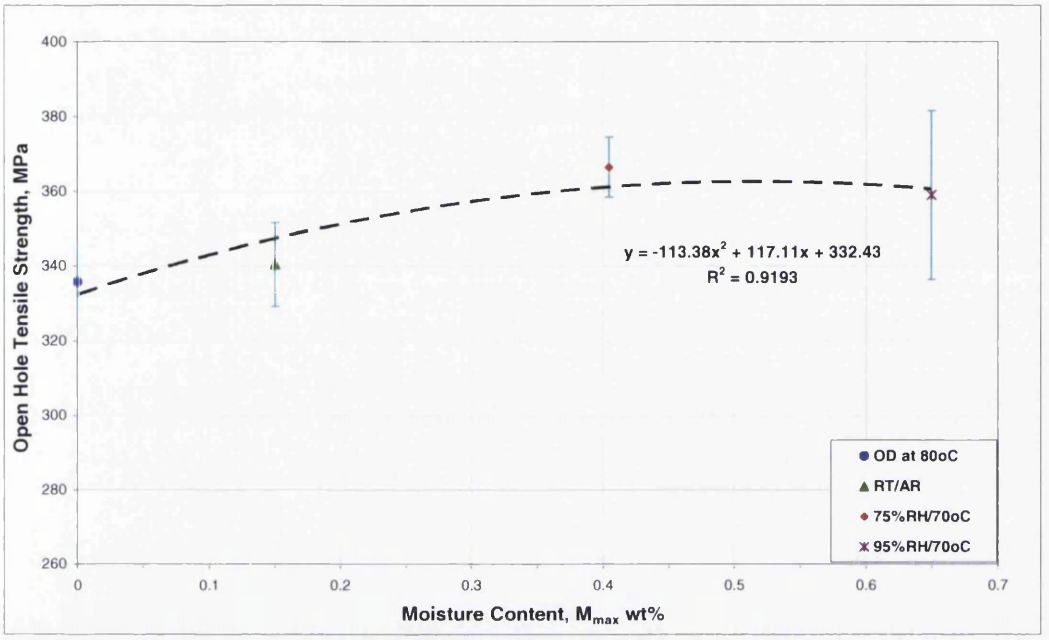

Figure 5-32: OHT strength vs. moisture content.

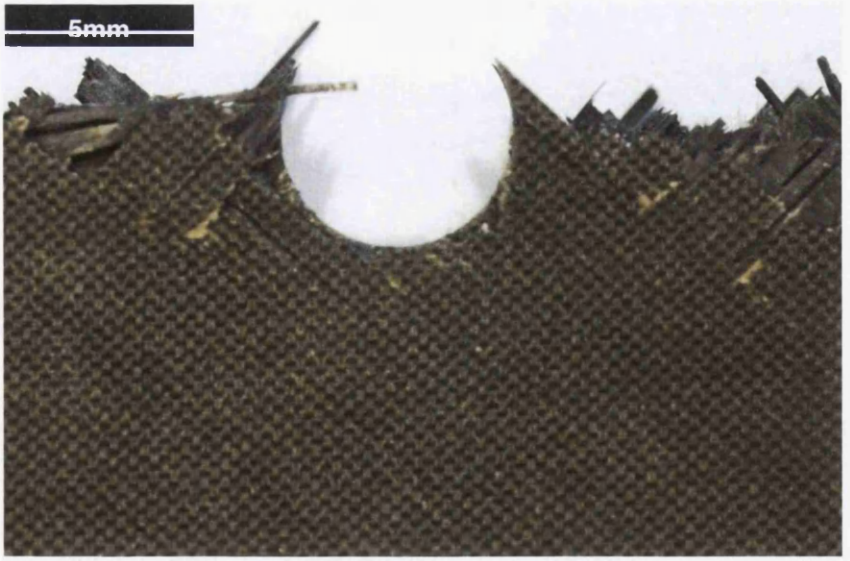

Figure 5-33: Open-hole tension failure.

5.4.7 Open Hole Compression Testing Results

Open hole compression (OHC) coupons were made out of a quasi-isotropic lay-up woven material, with a hole at the centre of the gauge section. The coupons were compressed along the major axis at a constant speed until fracture occurred. Details of the test procedure and coupon dimensions can be seen in section 4.6. OHC stresses were calculated from the load data and cross sectional area of the coupon using equation 4-9.

Table 5-13 summarises the OHC test results and lists the measured mean stress and M_{max} results, along with the calculated K_{ENDF} at each environment for the open hole compression tests. The main observation from these tests is that with increasing equilibrium moisture levels the OHC strength decreased.

Table 5-13: Summary of equilibrium saturated OHC tests.

Condition	Moisture content, M_{max}, (wt%)	Open Hole Compression Strength, F_{xx}^{ohc} (MPa)	Environmental Knock-down factor (K_{EKDF})
OD at 80°C	0	317±15	-
RT/AR	0.11 ± 0.01	299±15	0.943
75%RH/70°C	0. 38 ± 0.01	294±12	0.927
95%RH/70°C	0.61 ± 0.01	294±7	0.927

Figure 5-34 plots the open hole compressive stress versus displacement. The main characteristic of the curves was the slight nonlinearity, this behaviour being attributed to the quasi-isotropic lay-up of the laminate and the presence of ±45° plies. Figure 5-35 plots the open hole compressive strength versus the wt% moisture content in the coupon. The blue lines are error bars that show the standard deviation from the mean, for each data set. From figure 5-35 it can be seen that there is initial decrease in strength of around 7% with 0.11wt% equilibrium moisture content in the coupon. With further moisture ingress, the material does not see any further significant OHC strength deterioration.

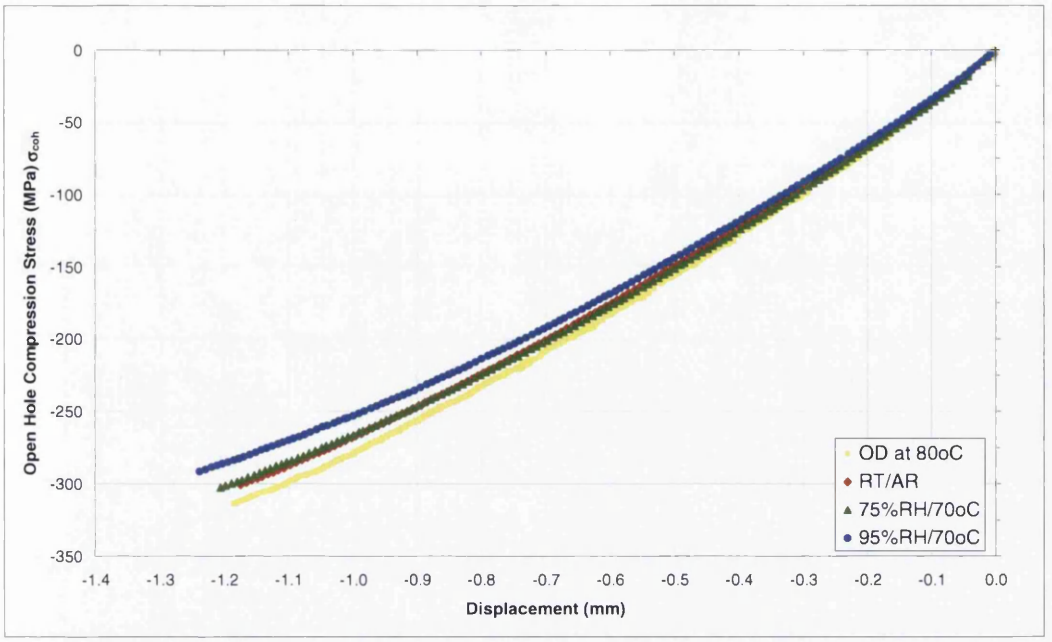

Figure 5-34: Open hole compression stress-displacement curves.

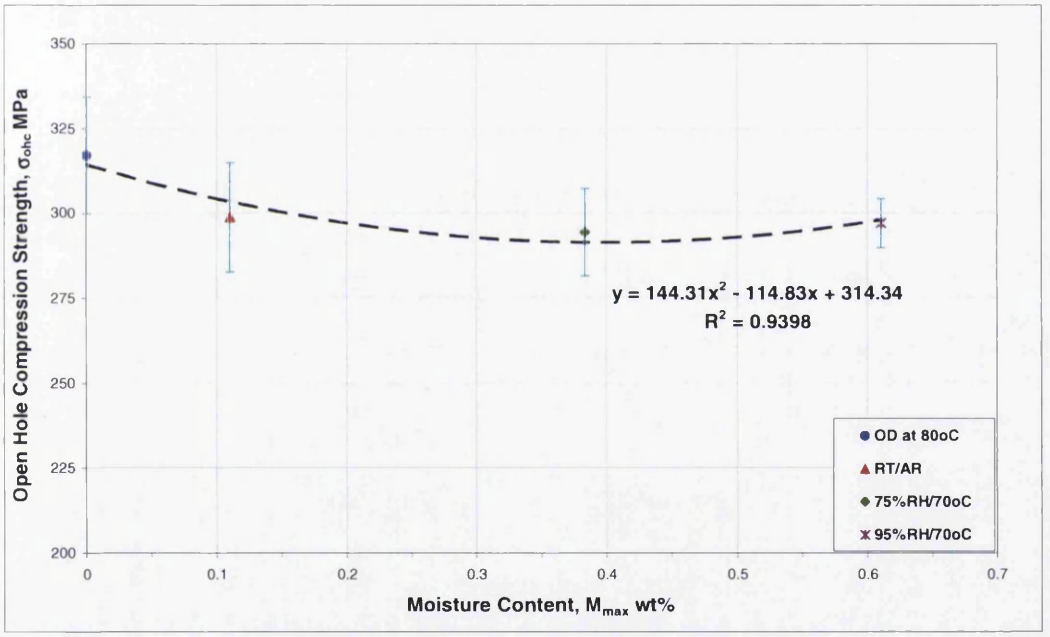

Figure 5-35: OHC strength vs. moisture content.

Figure 5-36 shows the open hole compression coupon failure. It was observed that failure of the coupons was initiated by buckling of the fibres in a small region of the test section, which was followed by the formation of kink zones[124] that propagated into the fracture. According to the literature [125], the failure mode in carbon-epoxy laminates under compression loading starts by shear, involving the fibre kinking. The kinked fibres disrupt the stability of the neighbouring fibres, which are then led

to fail in kinking mode. This damage propagation process continues until the complete failure of the composite.

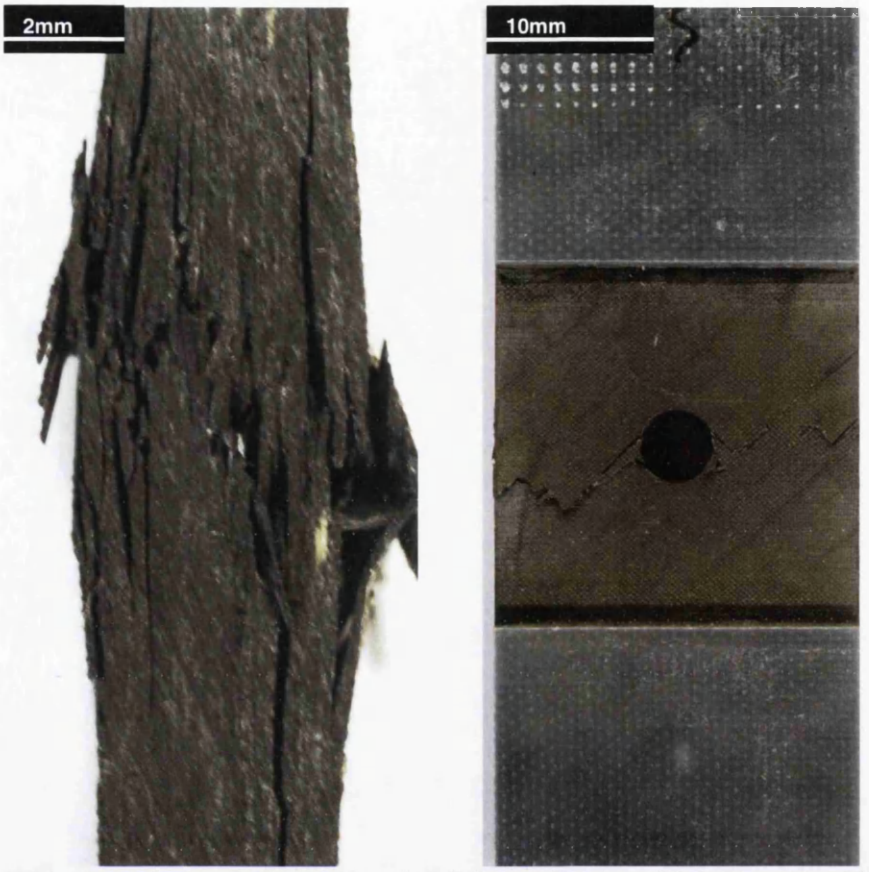

Figure 5-36: Typical open-hole compression failure, showing "kink zones" and fracture.

6 Mechanical Property Predictions

The current Airbus approach for design purposes is to apply a worst case, where the material is assumed to be fully saturated at the maximum temperature i.e. "HOT/WET". Material properties are derived by applying a knockdown factor, an approach that may be considered conservative, since typical in-service environments will not generate full saturation for thick structures[11] and as a result components may be over designed. In the case of composite components, this generally means adding further strengthening lamina, which consequently increases the overall weight of the component. With aircraft components, weight reduction is a high priority and the cumulative weight gain across many components can be significant.

To be able to predict mechanical properties with different moisture distribution, firstly the moisture distribution through-the-thickness (TTT) of the coupon needs to be modelled. As the resin diffusion properties can accurately be predicted using Fick's Second Law[13] (shown in section 5.2), the TTT moisture profiles were modelled here using an analytical solution to Fick's Second Law[13], which is discussed in the literature review. The modelled moisture distributions were then utilised to predict the mechanical properties of the CFRP test coupons with a distribution of moisture TTT. Mechanical property predictions were performed using the mathematical relationships derived from the equilibrium saturation, experimental test data and the predicted TTT moisture curves. To validate the property predictions, mechanical test coupons were conditioned for the predicted time, in order to produce the simulated distribution of moisture TTT prior to being tested.

6.1 Prediction of Moisture Distributions

The experimentally ascertained diffusion constants in table 5-3 were used to calculate moisture gradients through the thickness of the test coupons. Given the boundary condition (the concentration at the coupon/moisture interface, c_∞ is always fixed) and the initial condition (the concentration below the boundary is initially 0 everywhere), the solution to Fick's Second Law involves a fairly common mathematical function called the "complementary error function", that was discussed in the literature review (section 2.11.3), with the equation repeated here for convenience[13]:

$$c(x,t) = c_\infty erfc\left[\frac{x}{2\sqrt{D_x t}}\right] \qquad 2\text{-}11$$

The integral in the error function cannot be evaluated analytically, so values for *erfc* are computed via approximations and are available in table form. MS Excel spreadsheet has the function *erfc(x)* and this was used to perform the modelling of the moisture distributions using equation *2-11*.

In terms of weight savings, thick laminates will benefit most from this research, as the components will see relatively low levels of moisture, due to the time to saturation of a thick component. As a result, when performing moisture profile simulations it was important to leave the core of the coupon in a dry state, as to simulate the realistic aircraft condition. Thus, the moisture profiles modelled in the coupons had a section of material in the coupon core that was defined as "dry" (a dry-core was defined when there was less than 0.001wt% moisture content predicted in a single ply). When referring to %dry-core in this section, it corresponds to a percentage width of the test coupon about the mid-plane of the lay-up.

Figure 6-1 to figure 6-4 shows the theoretical moisture concentration plotted through a half thickness of the test coupons, illustrating the rapid moisture uptake near the surface together with the relatively slow uptake of moisture in the middle of the specimen. The moisture concentration was modelled using the complementary error function (equation *2-11*) and the diffusion constants, D_x and M_{max} experimentally derived in the initial phase of testing (table 5-3).

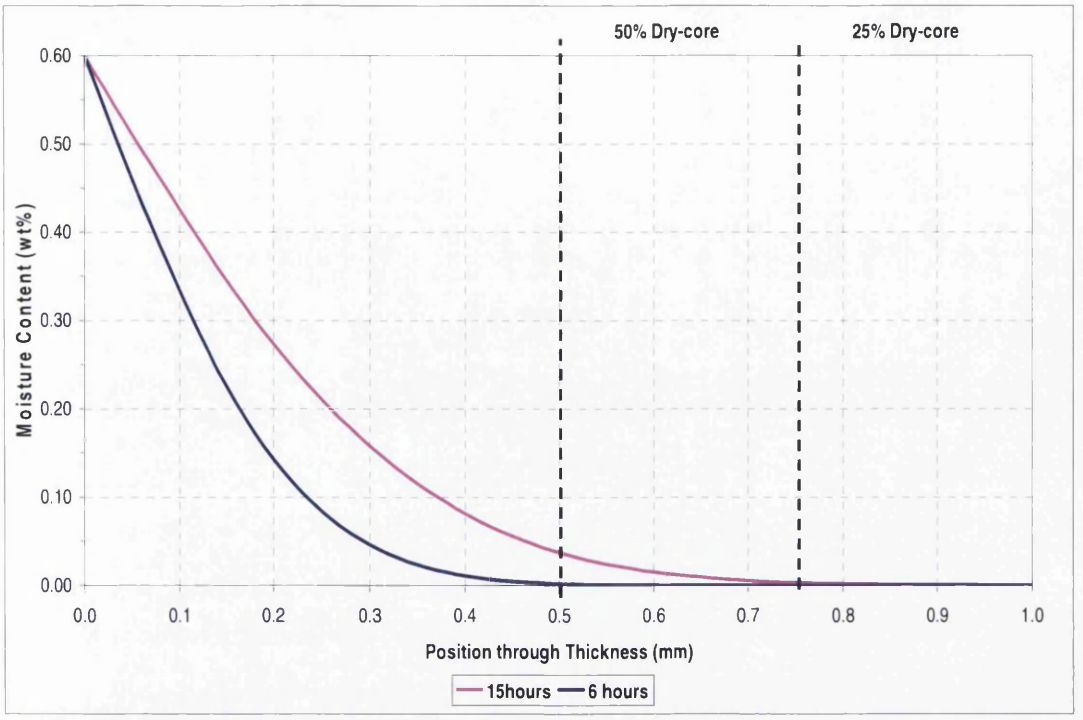

Figure 6-1: Moisture concentration-distance curve for 6 and 15 hours conditioning, UD coupon of thickness 2mm with uniform concentration at surface.

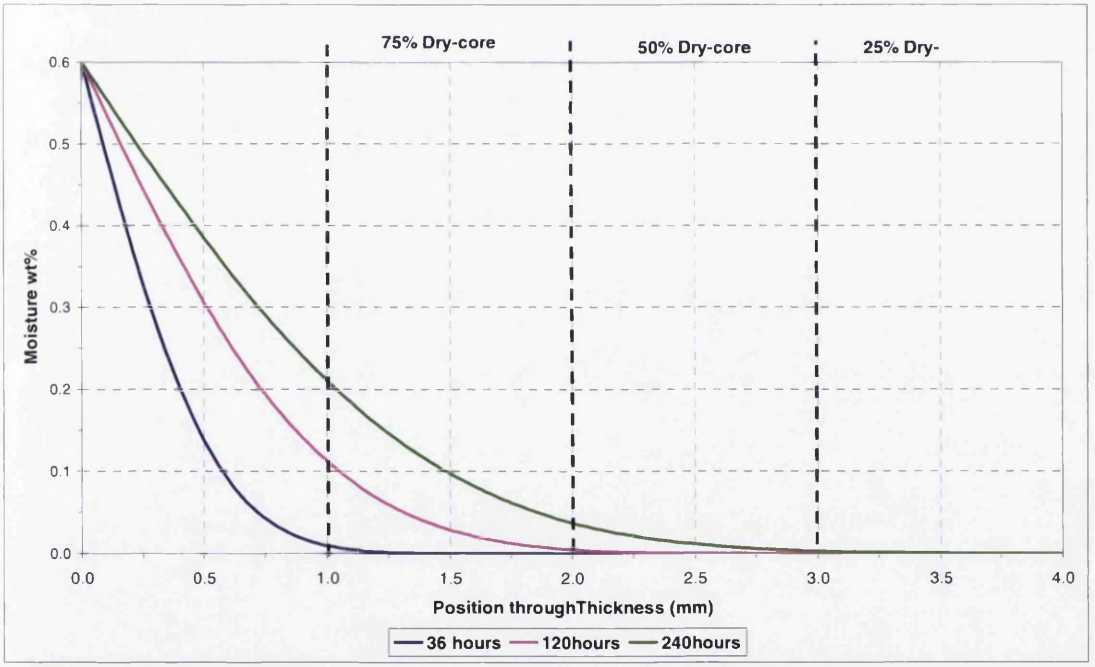

Figure 6-2: Moisture concentration-distance curve for 36, 120 and 240 hours conditioning, UD coupon of thickness 8mm with uniform concentration at surface.

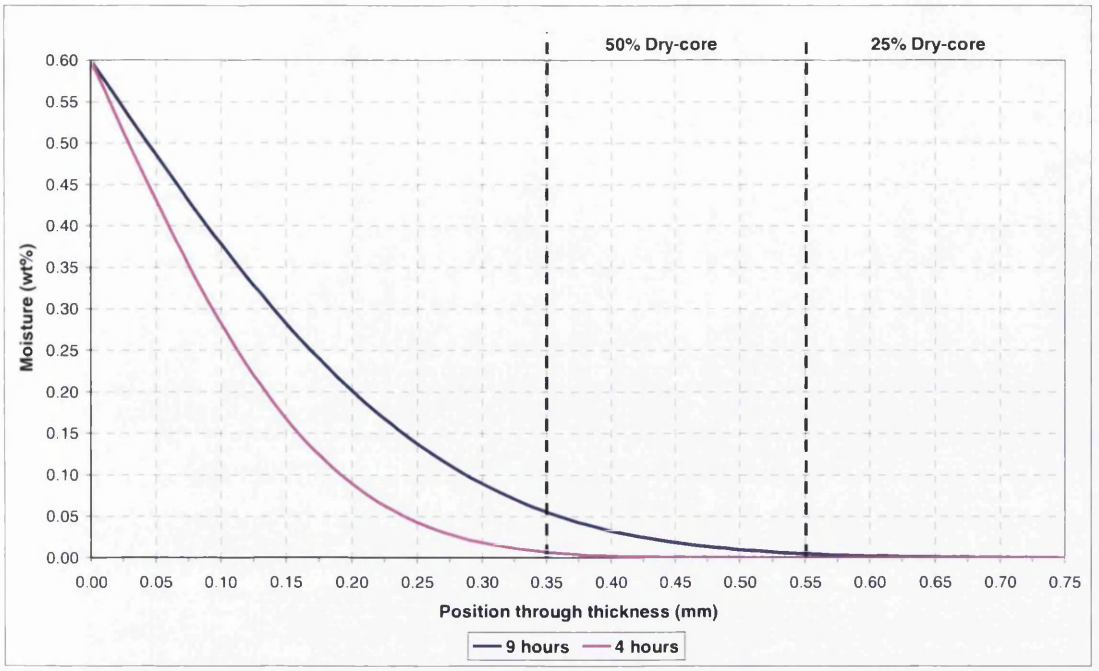

Figure 6-3: Moisture concentration-distance curve for 4 and 9 hours conditioning for UD coupon of thickness 1.5mm with uniform concentration at surface.

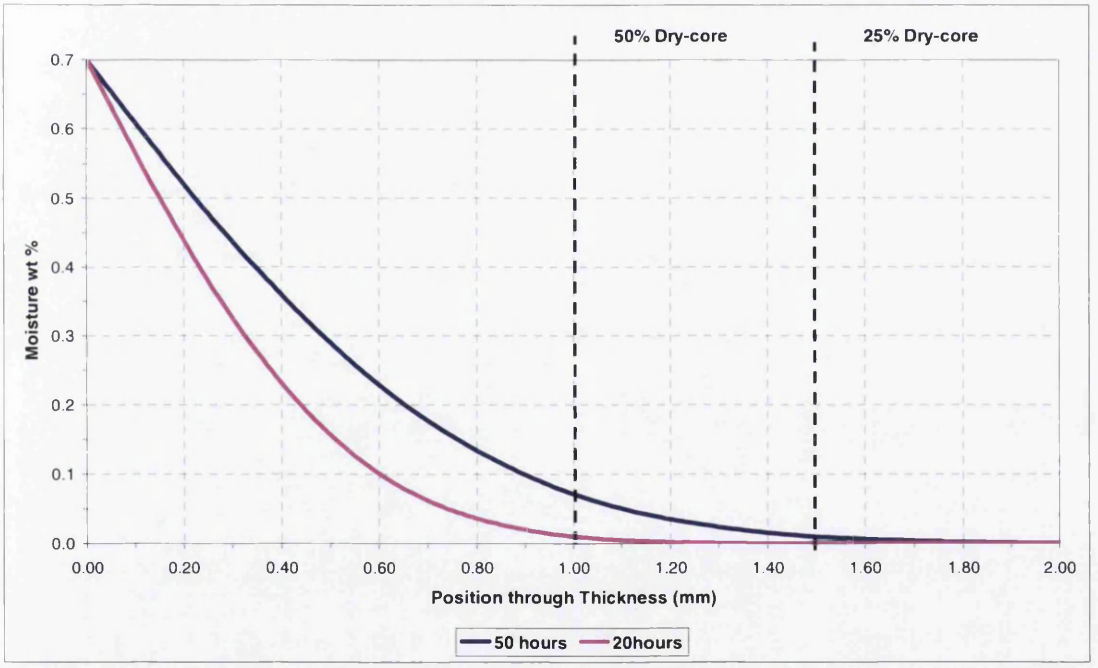

Figure 6-4: Moisture concentration-distance curve for 50 and 20 hours conditioning for woven coupon of thickness 4mm with a uniform concentration at surface.

Table 6-1: Predicted moisture content for coupons with moisture profile TTT.

Test Coupon Type	Material Type	Coupon Thickness (mm)	Conditioning Time (Hrs)	Predicted Moisture Content, M (wt%)
90° Tension	A	2	6	0.062
			15	0.117
	C	8	36	0.030
			120	0.072
			240	0.117
90° Compression	A	2	6	0.062
In-Plane Shear	A	1.5	4	0.046
			9	0.082
Open Hole Tension	B	4.4	50	0.144
			20	0.08
Open Hole Compression	B	4.4	50	0.144
			20	0.08

The amount of moisture absorbed, M, by each of the different validation test coupons (after being conditioned at 70°C and 85%RH for the time required to produce the moisture profiles TTT, as described in section 6.1) were predicted using equation *2-17* from the Literature Review (repeated here for convenience) and the diffusion constants calculated from table 5-3. Table 6-1 shows the results of the predictions for each test coupon, and the times used in the calculation.

$$M = G(M_{max} - M_0) + M_0 \qquad 2\text{-}17$$

where G is the time dependent parameter defined by:

$$G = 1 - \exp\left[-7.3\left(\frac{Dt}{S^2}\right)^{0.75}\right] \qquad 2\text{-}18$$

6.2 Laminate Property Prediction

Macro-mechanics is a method used to predict the strength and stiffness of composite structures, whereby the material is assumed to be homogeneous and the effects of the constituent materials are identified as averaged properties of the composite material[39].

From the equilibrium saturation tests performed (see section 5.4), a set of mathematical relationships for mechanical properties as functions of wt% moisture content, M, were derived. The relationships are listed in table 6-2 and were derived from a least squares fit to the data.

Table 6-2: Relationship between property and moisture, M is any given wt% moisture.

Property	Relationship
F_1^t	= -5.3062 x M + 2376.1
F_1^c	= -5.3062 x M + 2376.1
F_2^t	= -43.729 x M + 57.816
F_2^c	= 8.1798 x M + 235.04
F_{12}	= 16.286 x M^2 - 32.542 x M + 83.966
F_{xx}^{oht}	= -113.38 x M^2 + 117.11 x M + 332.43
F_{xx}^{ohc}	= 144.31 x M^2 - 114.83 x M + 314.34
E_1	= 21.634 x M^2 - 27.219 x M + 151.83
E_2	= -0.6713 x M + 9.2668
G_{12}	= 0.7305 x M^2 - 1.2121 x M + 5.1497

Here F_1^c is assumed equal to F_1^t; as issues with testing meant there was no available data for F_1^c. As compression in the longitudinal direction is a fibre dominated property, the assumption was made there would be no measurable effect with moisture ingress.

The relationships listed in table 6-2 were used to predict the mechanical properties of composite laminates on a macro-mechanical level by analysing on a ply-by-ply basis.

6.2.1 Macro-Mechanical Property Predictions

The macro-mechanical predictions are performed using the correlations obtained from the experimental data (table 6-2). The following steps were followed to perform macro-mechanical property predictions:

Step 1

The amount of moisture present in each ply for a specific moisture gradient TTT (figure 6-1 to figure 6-4) was calculated. This was done by discretizing the thickness of the laminate by the known cure-ply-thickness and then calculating the amount of moisture in each ply from the area under the curves using the Trapezoid Rule.

Step 2

The corresponding set of mechanical properties (i.e. strength/stiffness) of each ply was calculated using the derived relationships in table 6-2 and the calculated moisture content of each individual ply from Step 1.

Step 3

Finally, an average was computed across the number of plies in the laminate to predict each material property (i.e. strength/stiffness) of the laminate.

Figure 6-5 to figure 6-11 show charts displaying the calculated strengths and moduli of a laminate using the approach described above, with each bar representing a single ply with a moisture profile calculated from Step 1 and the related strength calculated from Step 2.

Figure 6-5 to figure 6-9 show the predictions for 90° tension strength, F_2^t and tensile modulus, E_2 within each ply using the relationships in table 6-2. The laminates have been subjected to different conditioning times, as shown in table 6-1. The 8mm laminates are shown only half thickness due to symmetry. The macro-mechanical predicted F_2^t and E_2 values for the laminates are listed in table 6-3.

Figure 6-10 and figure 6-11 show the predictions for IPS strength, F_{12} and shear modulus, G_{12} within each ply using the relationships in table 6-2. The laminates have been subjected to different conditioning times, as shown in table 6-1. The macro-mechanical predicted F_{12} and G_{12} values for the laminates can be found in table 6-3.

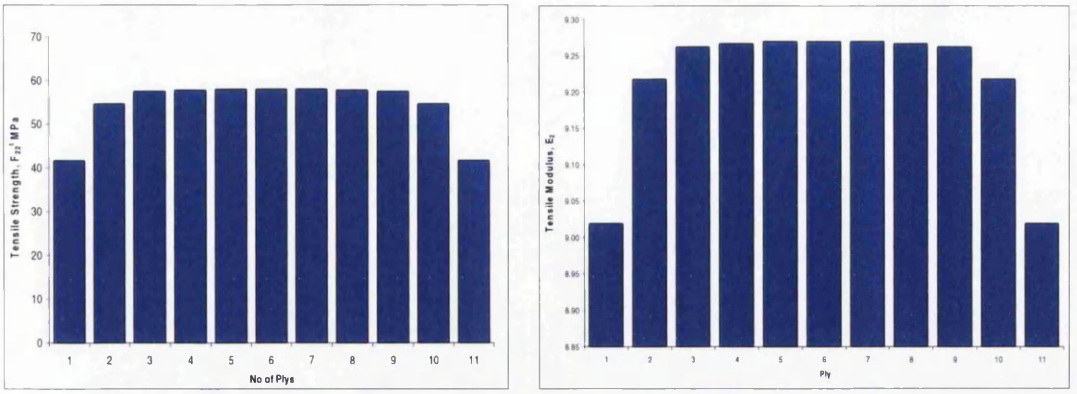

Figure 6-5: 90° tension 2mm thick – (6 hrs conditioning).

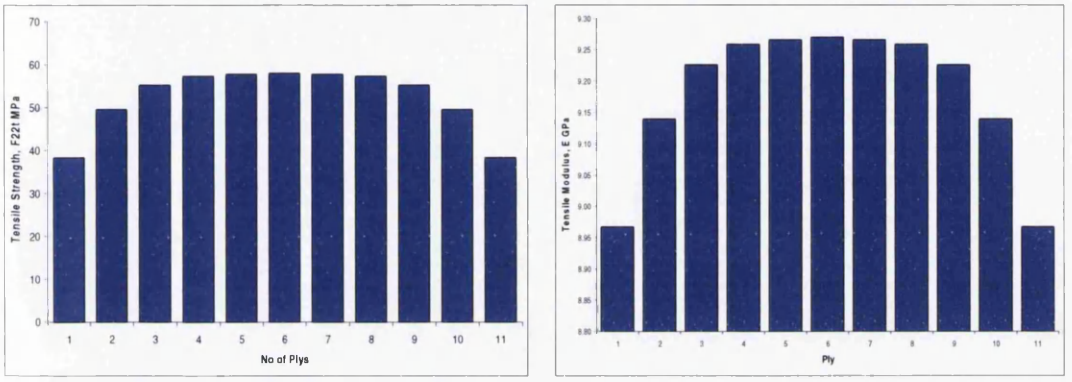

Figure 6-6: 90° tension 2mm – (conditioned for 15hrs)

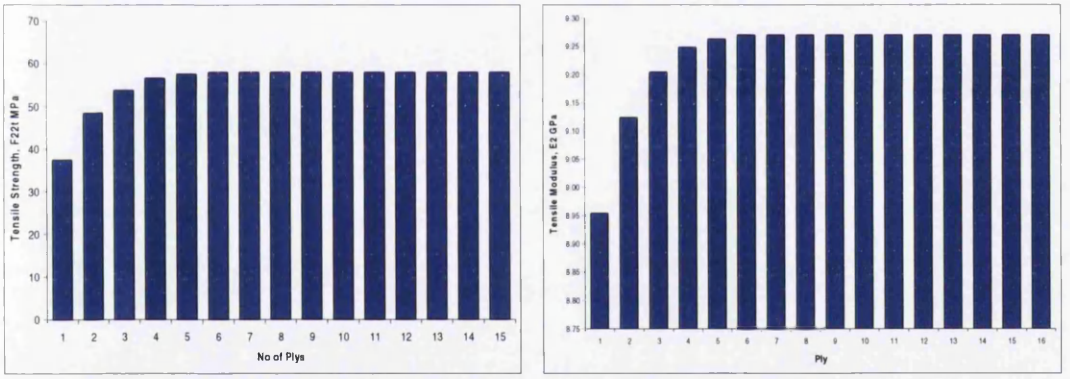

Figure 6-7: 90° tension 8mm (36 hours conditioning).

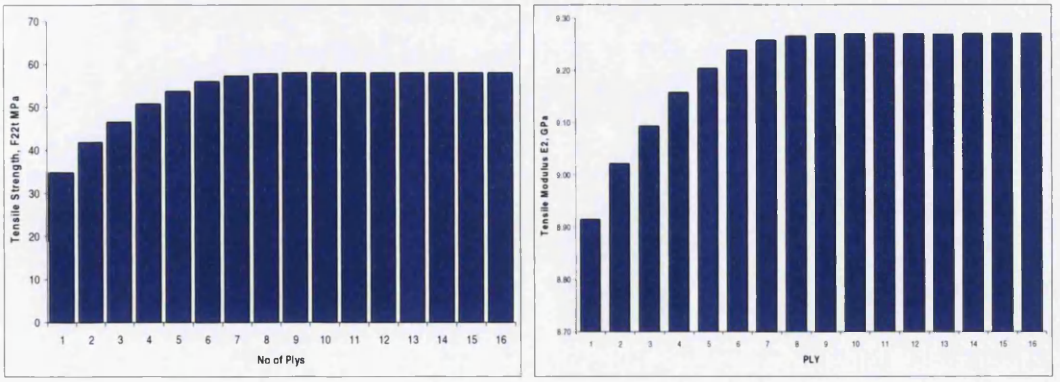

Figure 6-8: 90° tension 8mm (120 hours conditioning).

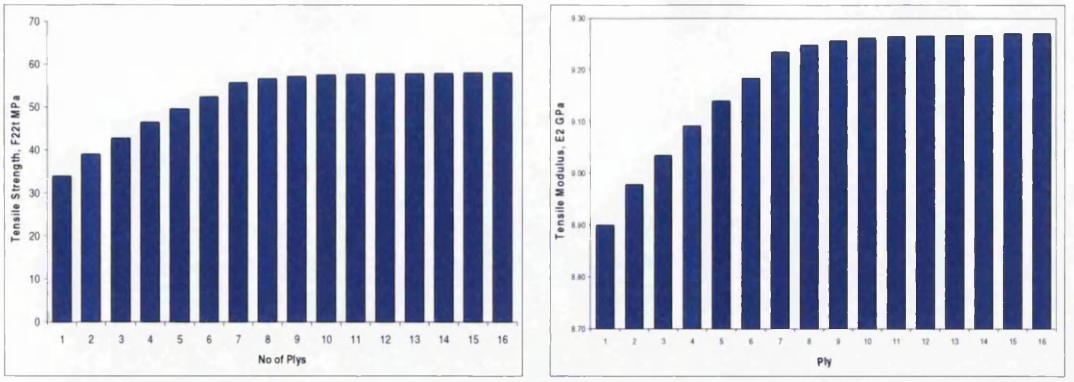

Figure 6-9: 90° tension 8mm (240 hours conditioning)

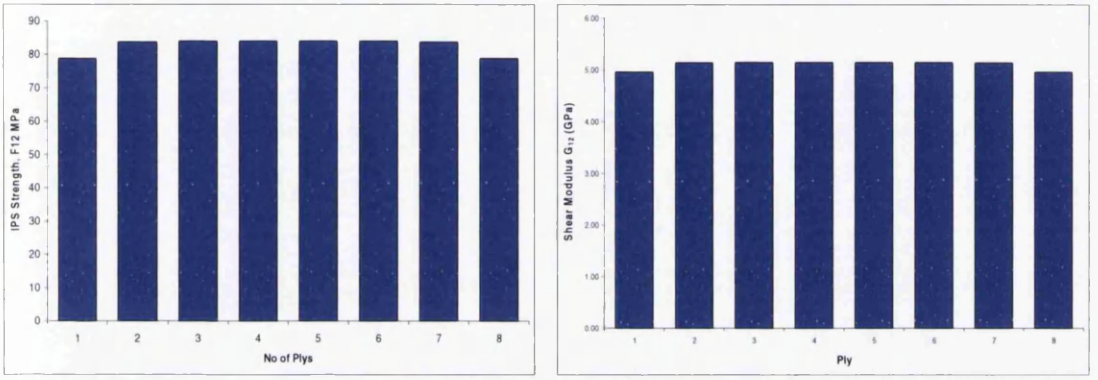

Figure 6-10: IPS – (conditioned for 4 hours).

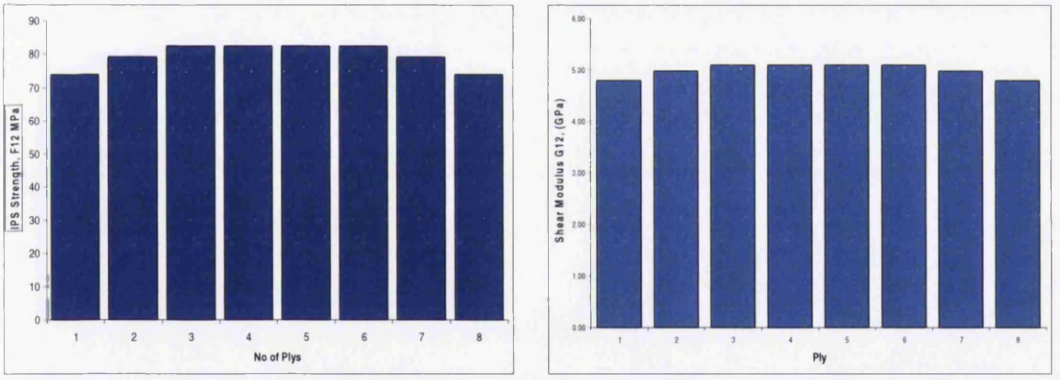

Figure 6-11: IPS (conditioned for 9 hours).

This method incorporates the effect of different moisture contents and thus different mechanical properties for each ply. There is both a moisture and mechanical property profile across the laminate. As can be seen from figure 6-5 to figure 6-11 that plies at the exposed surfaces will have higher moisture contents and hence lower strength and stiffness properties. The predicted properties of the laminate will now be different from those where the conventional assumption of a uniform moisture level across all plies has been assumed.

6.3 Classical Laminate Theory

Composite structural components are most often based on plies bonded together with the fibres at arbitrary orientations. Classical laminate Analysis (CLA) relates the stress-strain relations of a laminate to the properties of its constituent lamina. The properties required for this analysis are for a single ply (lamina) of the composite, which were obtained from mechanical testing of the UD material. CLA is based on the Kirchhoff hypothesis, following these assumptions[30]:

- A section perpendicular to the middle plane of the laminate remains perpendicular under loading.
- For 2D plane stress analysis, the strain is a constant through-the-thickness.
- For bending the strain varies linearly through-the-thickness.
- The laminate is thin compared with its in-plane dimensions.
- Displacements are small compared with the thickness.
- The behaviour remains linear.

With the assumptions satisfied, the laminate theory allows the response of a laminate to be calculated (by determining engineering constants and substituting them into standard formulas for stresses and deflections) and material properties of the laminate to be defined. Details of the CLA theory can be found in Analysis and Performance of Fibre Composites by Broutman and Argarwal[39]. An overview of the principles are outlined here:

For each layer, the stress-strain relations in the axis defined by the fibre direction are:

$$\begin{bmatrix}\sigma_1\\ \sigma_2\\ \tau_{12}\end{bmatrix}=\begin{bmatrix}Q_{11} & Q_{12} & 0\\ Q_{12} & Q_{22} & 0\\ 0 & 0 & Q_{66}\end{bmatrix}\begin{bmatrix}\varepsilon_1\\ \varepsilon_2\\ \gamma_{12}\end{bmatrix} \qquad 6\text{-}1$$

Where the Q_{ij} terms, known as the reduced stiffness coefficients, are given by;

$$Q_{11} = E_1/(1-\nu_{12}\nu_{21})$$

$$Q_{22} = E_2/(1-\nu_{12}\nu_{21})$$

$$Q_{12} = \nu_{21} E_1 / (1 - \nu_{12}\nu_{21})$$
$$Q_{66} = G_{12}$$
$$\nu_{21} = \nu_{12} E_2 / E_1 \qquad 6\text{-}2$$

where E_1 is the longitudinal modulus, E_2 the transverse modulus, G_{12} the shear modulus, ν_{12} the major Poisson's ratio and ν_{21} the minor Poisson's ratio.

In the axis system defined by the principal laminate directions this becomes;

$$\begin{bmatrix} \sigma_x \\ \sigma_y \\ \tau_{xy} \end{bmatrix} = \begin{bmatrix} \overline{Q}_{11} & \overline{Q}_{12} & \overline{Q}_{16} \\ \overline{Q}_{12} & \overline{Q}_{22} & \overline{Q}_{26} \\ \overline{Q}_{16} & \overline{Q}_{26} & \overline{Q}_{66} \end{bmatrix} \cdot \begin{bmatrix} \varepsilon_x \\ \varepsilon_y \\ \gamma_{xy} \end{bmatrix} \qquad 6\text{-}3$$

Where

$$\begin{aligned}
\overline{Q}_{11} &= Q_{11}\cos^4 + \theta + 2(Q_{12} + Q_{66})\sin^2\theta\cos^2\theta + Q_{22}\sin^4\theta \\
\overline{Q}_{12} &= (Q_{11} + Q_{22} - 4Q_{66})\sin^2\theta\cos^2\theta + Q_{12}(\sin^4\theta + \cos^4\theta) \\
\overline{Q}_{16} &= (Q_{11} + Q_{12} - 2Q_{66})\sin\theta\cos^3\theta + (Q_{12} - Q_{22} + 2Q_{66})\sin^3\theta\cos\theta \\
\overline{Q}_{22} &= Q_{11}\sin^4\theta + 2(Q_{12} + 2Q_{66})\sin^2\theta\cos^2\theta + Q_{22}\cos^4\theta \\
\overline{Q}_{26} &= (Q_{11} - Q_{12} - 2Q_{66})\sin^3\theta\cos\theta + (Q_{12} - Q_{22} + 2Q_{66})\sin\theta\cos^3\theta \\
Q_{66} &= (Q_{11} + Q_{22} - 2Q_{12} - 2Q_{66})\sin^2\theta\cos^2\theta + Q_{66}(\sin^4\theta\cos^4\theta)
\end{aligned} \qquad 6\text{-}4$$

And

$$\begin{bmatrix} \varepsilon_x \\ \varepsilon_y \\ \gamma_{xy} \end{bmatrix} = \begin{bmatrix} \varepsilon_x^{\,0} \\ \varepsilon_y^{\,0} \\ \gamma_{xy}^{\,0} \end{bmatrix} + z \begin{bmatrix} \kappa_x \\ \kappa_y \\ \kappa_{xy} \end{bmatrix} \qquad 6\text{-}5$$

Where ε^0 and κ are the mid plane strains and curvatures respectively, z is measured from the mid-plane.

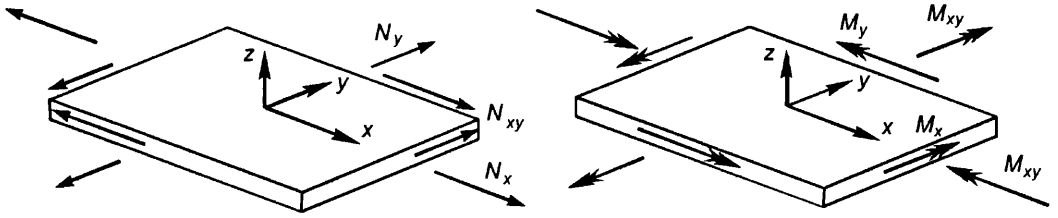

Figure 6-12: Load conventions for in-plane and out-of-plane loadings.

The resultant forces, N_i, and moments, M_i, in a laminate (figure 6-12) can be derived from integrating through the laminate thickness, h;

$$N_i = \int_{-h/2}^{h/2} \sigma_i \, dz$$

$$M_i = \int_{-h/2}^{h/2} \sigma_i \, z \, dz \qquad 6\text{-}6$$

Substituting for the stress terms, we get;

$$\begin{bmatrix} N_x \\ N_y \\ N_{xy} \\ M_x \\ M_y \\ M_{xy} \end{bmatrix} = \begin{bmatrix} A_{11} & A_{12} & A_{13} & B_{11} & B_{12} & B_{13} \\ A_{12} & A_{22} & A_{23} & B_{12} & B_{22} & B_{23} \\ A_{13} & A_{23} & A_{33} & B_{13} & B_{23} & B_{33} \\ B_{11} & B_{12} & B_{13} & D_{11} & D_{12} & D_{13} \\ B_{12} & B_{22} & B_{23} & D_{12} & D_{22} & D_{23} \\ B_{13} & B_{23} & B_{33} & D_{13} & D_{23} & D_{33} \end{bmatrix} \begin{bmatrix} \varepsilon_x \\ \varepsilon_y \\ \varepsilon_{xy} \\ \kappa_x \\ \kappa_y \\ \kappa_{xy} \end{bmatrix} \qquad 6\text{-}7$$

Where the membrane stiffness matrix **A**, the coupling stiffness matrix **B** and the bending stiffness matrix **D** are defined as:

$$A_{ij} = \sum_{k=1}^{NL} (\overline{Q}_{ij})_k (z_k - z_{k-1})$$

$$B_{ij} = \frac{1}{2} \sum_{k=1}^{NL} (\overline{Q}_{ij})_k (z_k^2 - z_{k-1}^2) \qquad 6\text{-}8$$

$$D_{ij} = \frac{1}{3} \sum_{k=1}^{NL} (\overline{Q}_{ij})_k (z_k^3 - z_{k-1}^3)$$

NL=number of layers in the laminate,

z_k, z_{k-1}= z co-ordinates at layer boundaries, $z_k > z_{k-1}$

Equations *6-8* are called the stiffness equations because of their analogy with Hooke's law $\sigma = E\varepsilon$. The compliance equations of the laminate are obtained by inverting the matrices in *6-8*.

So the general constitutive equations 6-8 for a laminate can be written:

$$\begin{Bmatrix} N \\ M \end{Bmatrix} = \begin{bmatrix} A & B \\ B & D \end{bmatrix} \begin{Bmatrix} \varepsilon^o \\ K \end{Bmatrix} \qquad 6\text{-}9$$

In symmetric laminates the coupling stiffness matrix B is zero. For laminates with asymmetric stacking sequence there are non-zero B_{ij} terms. In that case coupling between bending and extension in the laminate occurs. The inverted form of the constitutive equations for laminates is:

$$\begin{Bmatrix} \varepsilon^o \\ K \end{Bmatrix} = \begin{bmatrix} A' & B' \\ B' & D' \end{bmatrix} \begin{Bmatrix} N \\ M \end{Bmatrix} \qquad 6\text{-}10$$

By the constitutive equations for laminates (equation *6-9*) or by its inverted form (equation *6-10*) the lamina stresses and strains can be calculated on the basis of their elastic properties (i.e. Q_{ij} values) and the stacking sequence.

6.4 Failure Criteria

Strength analysis of a laminate requires that the stresses in each layer (ply/lamina) of the laminate are determined and used to establish a factor of safety (RF) of each layer. As the layers are anisotropic, an appropriate failure theory is required. The success of CLA depends on the appropriateness of the failure criterion. Many different failure criterion exist which may give different results and different degrees of agreement with the experimental test data. Correlation with experimental results is notoriously difficult especially when a laminate is loaded in compression.

Numerous failure theories have been proposed, they are classified into three groups;

- Independent criteria (maximum stress, maximum strain): no interaction between different stress components.
- Fully interactive criteria (Tsai-Hill, Tsai-Wu); all the different stresses are combined in a single equation.
- Partly interactive criteria (Hashin-Rotem, Puck): these criteria allow a distinction between the different failure modes (fibre or matrix failure). A combination of different stresses is possible.

The first ply failure (FPF) criteria are based on the assumption that laminate failure occurs when the first ply fails (by matrix or fibre failure). Ultimate failure (ULF) is calculated by reducing the stiffness components of the failed ply to zero (except E_1, unless σ_1 exceeds F_1^t) and re-analyzing the laminate, to see whether the remaining plies can carry the load. This process is repeated until fibre failure or all plies have failed. Iterative criteria have a good correlation with test results. The philosophy of these criteria is consistent with the failure behaviour of a laminate: the laminate failure occurs when fibre failure occurs. Moreover, iterative criteria take into account the fact that matrix cracking reduce the stiffness of the laminate.

The validity and applicability of a given theory depends on the convenience of application and agreement with experimental results. The overabundance of theories is accompanied by a lack of suitable and reliable experimental data, which makes the selection of one theory over another rather difficult. Considerable effort has been devoted recently to alleviate this difficulty.

A 'Worldwide Failure Exercise' was organised and conducted by Hinton, Soden and Kaddour[126] over a 12-year period for the purpose of assessing the predictive capabilities of current failure theories. The results of this exercise encompass 19 failure theories. One observation of this exercise was that, even for the unidirectional lamina, predictions of the various theories differed by up to 200–300% from each other.

In general, a wide variation has been observed in the prediction of laminate failures by the various theories. The variance in the predictions is greater for FPF than for ULF; it is also greater for matrix-dominated failures than for fibre-dominated ones. In general, it is difficult to reach definitive conclusions on the applicability of the various theories based on comparison with the limited experimental data available,

especially in the cases of FPF and under biaxial compression or compression and shear. Some of the different failure criteria's are discussed below.

6.4.1 Independent Criteria

a) Maximum stress criterion

The maximum stress is an independent criterion. Failure occurs as soon as one of the stresses (σ_1, σ_2, τ_{12}) is larger than the allowable failure stress.

$$F = \max\left(\frac{\sigma_1}{F_1^t}, \left|\frac{\sigma_1}{F_1^c}\right|, \frac{\sigma_2}{F_2^t}, \left|\frac{\sigma_2}{F_2^c}\right|, \left|\frac{\tau_{12}}{F_{12}}\right|\right) \qquad 6\text{-}11$$

There is no interaction between the different stress components. Here F_1^t is the tensile strength in the fibre direction, F_1^c is the compressive strength in the fibre direction, F_2^t is the tensile strength perpendicular to the fibre direction, F_2^C is the compressive strength perpendicular to the fibre direction and F_{12} is the in-plane shear strength.

All stresses are independent. If the lamina experiences biaxial stresses, the *failure envelope* is a rectangle (see figure 6-13) - the existence of stresses in one direction doesn't make the lamina weaker when stresses are added in the other.

b) Maximum strain criterion

The principle of the maximum strain criterion is similar to the maximum stress criterion except that failure occurs as soon as one of the strains (ε_1, ε_2 , γ_{12}) is larger than the allowable failure strain.

$$F = \max\left(\left|\frac{\varepsilon_1}{F_1^{\varepsilon}}\right|, \left|\frac{\varepsilon_2}{F_2^{\varepsilon}}\right|, \left|\frac{\gamma_{12}}{F_{12}^{\gamma}}\right|\right) \qquad 6\text{-}12$$

There is no interaction between the different strain components. For biaxial stresses (τ_{12} = 0), the failure envelope is a parallelogram (see figure 6-13). In the positive quadrant, the maximum stress criterion is more conservative than maximum strain.

6.4.2 Fully Interactive Criteria

In fully interactive criteria all stress components can be combined into one equation. Commonly only quadratic terms are used. The general form of the second order polynomial is given by

$$F = F_{11}.\sigma_1^2 + F_{22}.\sigma_2^2 + F_{66}.\tau_{12}^2 + 2F_{12}.\sigma_1.\sigma_2 + F_1.\sigma_1 + F_2.\sigma_2 + F_6.\tau_{12} \qquad 6\text{-}13$$

The coefficients F_{ij} and F_i are functions of the UD strengths f_{1c}, ... f_{12} and are varied in the different failure criteria.

a) Tsai-Hill criterion

This is one example of many criteria which attempt to take account of interactions in a multi-axial stress state. Based on von Mises yield criterion, 'failure' occurs if:

$$\left(\frac{\sigma_1}{F_1}\right)^2 - \frac{\sigma_1\sigma_2}{F_1^{\ 2}} + \left(\frac{\sigma_2}{F_2}\right)^2 + \left(\frac{\tau_{12}}{F_{12}}\right)^2 \geq 1 \qquad 6\text{-}14$$

A single calculation is required to determine failure. The appropriate failure stress is used, depending on whether σ is positive or negative. For all 'quadratic' failure criteria, the biaxial envelope is elliptical (figure 6-13). The size of the ellipse depends on the value of the shear stress

Different theories are reasonably close under positive stresses. Big differences occur when compressive stresses are present.

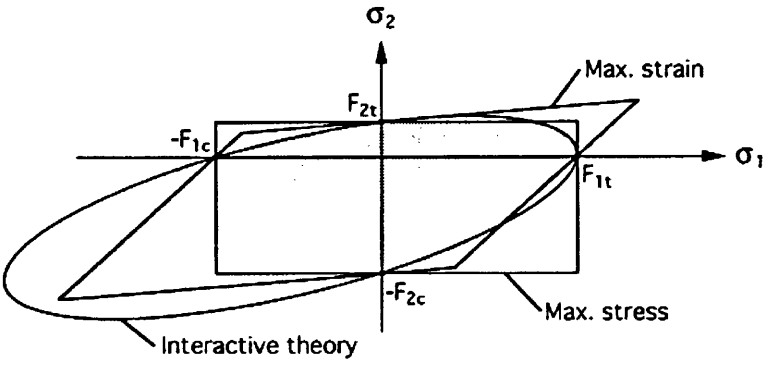

Figure 6-13: Failure envelopes for non-interactive and interactive failure criteria.

6.4.3 Classical Laminate Analysis Predictions

The unidirectional test coupon data generated in the first phase of this test campaign resulted in a set of UD lamina properties, listed in table a-2 in Appendix F. From the lamina properties derived (F_1^t, F_2^t, F_1^c, F_2^c, F_{12}, E_1, E_2 and G_{12}) and their consequential relationship due to moisture content (table 6-2), Classical Laminate Analysis[39,127] was performed. Laminate analysis allows a prediction of the overall performance characteristics for a laminate to be calculated by using the combination of properties and the orientation of each ply in a known stacking sequence.

The CLA theory provides the in-plane stresses and strains for each lamina of the laminate and is combined with a failure criterion to give a first-ply failure (FPF). Ultimate failure (ULF) is then derived by reducing the related stiffness of the failed ply and reanalysing, to see whether the plies can still carry the load.

During this work Maximum Stress failure criteria[39] was employed in the CLA predictions. The maximum stress theory simply compares the maximum stress experienced by the material with its strength across a number of failure modes.
To predict the mechanical properties of laminates with a distribution of moisture TTT using CLA, steps 1-3 were followed:

Steps 1 & 2

For CLA property predictions, Step 1 and Step 2 were followed as in section 6.2, in order to derive a unique set of mechanical properties for each ply containing a pre-defined moisture content.

Step 3

The unique set of properties for each individual ply in the laminate (defined in step 1 and 2) were inputted to a computer program called LAP 3.0F[127] (Laminate Analysis Program). LAP is a commercially available Windows software tool for the analysis and design of composite material laminates. Airbus use LAP 3.0F as their standard in-house composite laminate analysis tool. The solution algorithms employed in LAP are based on the Classical Laminate Theory, which was discussed previously in this chapter. The program requires the definition of basic material engineering properties at the lamina level. To account for the property degradations due to the moisture distribution, mechanical properties were defined for each ply according to the amount of moisture content (from Step 1 & 2 using the relationships defined in table

6-2). The stacking sequences are also user defined. Thus meaning LAP was able to predict the mechanical properties for any laminate lay-up with a given distribution of moisture TTT for the defined material system.

Figure 6-14 shows a flow diagram detailing each step of the process for predicting the mechanical properties of a composite with a moisture distribution, using the environmental CLA approach.

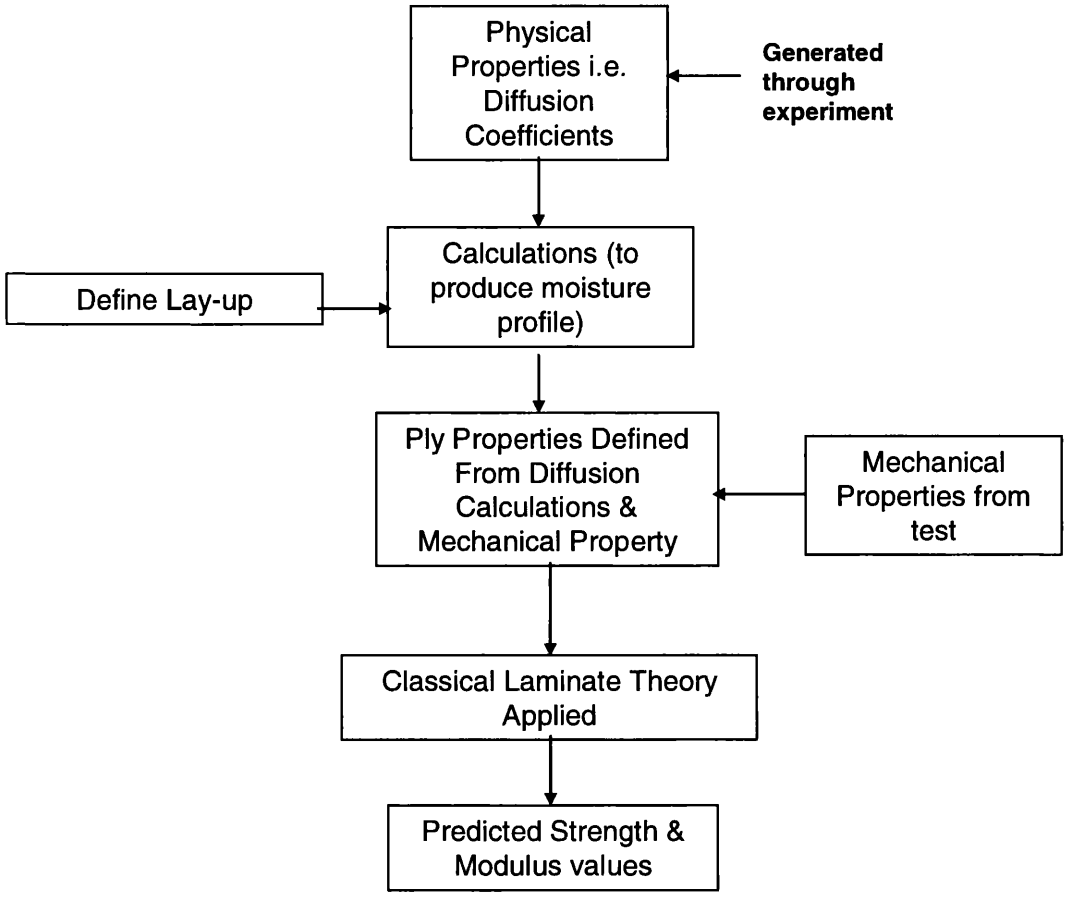

Figure 6-14: Workflow of property predictions.

Table 6-3 lists macro-mechanical and the CLA predictions, along with the experimentally measured properties for validation.

Appendix G shows screen-shots of each step of the procedure for creating the environmental profile models in LAP 3.0F[127]. First, each ply is defined (Figure A-23) as a separate material, having a unique set of material properties depending on its moisture content (defined in Step 1 & 2). Secondly, the laminate lay-up, ply property and ply thickness (shown in Figure A-24) are defined. A sample output is shown in Figure A-25.

6.4.4 Predicting Open Hole Properties

To perform CLA predictions for the quasi-isotropic (QI) open hole tension and compression coupons (Material B), the lamina properties relationships derived from the UD tape (Material A) were employed. Table 6-2 shows the relationships for E_1, E_2, G_{12}, F_1^t, F_2^t, F_2^C and F_{12} for lamina properties that were used to predict the properties for the quasi-isotropic laminate.

Firstly a classical laminate analysis prediction was performed for an oven dry un-notched QI lay-up laminate.

Using the experimental test results of the oven dry QI laminates with holes, a notch knockdown factor, K_t was calculated (ratio of the notched strength to the un-notched strength) using the following equation:

$$K_t = \frac{\sigma_{notched}}{\sigma_{un-notched}} \qquad 6\text{-}15$$

where $\sigma_{notched}$ is the strength of the laminate with a hole and $\sigma_{un\text{-}notched}$ is the strength with no hole present. Using this approach K_t factors of 0.43 and 0.38 for open hole tension and compression coupons respectively, were calculated

Table 6-3: Model predictions and validation test data.

Test Type	Material Type	Material Thickness (mm)	Dry-core [%]	Experimental Moisture Content, M (wt%)	Strength (MPa)				Modulus (GPa)	
					Validation Test Data	Macro-Mechanical Predictions[1]	CLA Predictions[2]		Validation Test Data	Macro-Mechanical Predictions[1]
							FPF	ULF		
90° Tension	A	2	100	0.00	55.1±7.4	57.8	55.9	55.9	9.3±0.1	9.3
	A	2	50	0.050	70.7 ±4.5	51.8	42	42	9.4 ±0.1	9.2
	A	2	25	0.080	60.4 ±6.5	50	39.1	39.1	9.1 ±0.1	9.2
	C	8	75	0.075	73.3 ±5.7	52.8	38.5	38.5	8.9 ±0.2	9.2
	C	8	50	0.131	71.4 ±5.4	51.1	35.9	35.9	8.9 ±0.4	9.2
	C	8	25	0.198	65.6 ±5.3	49.2	34.8	34.8	8.5 ±0.3	9.1
90° Compression	A	2	100	0.00	232 ± 5	235	232	232	-	-
	A	2	50	0.057	241 ±22	235	233.8	233.8	-	-
In-Plane Shear	A	1.5	100	0.00	85.3± 1.1	83.9	83.3	83.3	5.2 ±0.1	5.2
	A	1.5	50	0.042	83.7 ±1.8	81.9	78.5	78.5	5.1 ±0.2	5.1
	A	1.5	25	0.069	83.7 ±1.6	80.6	77.5	77.5	4.8 ±0.2	5.1
Open Hole Compression,	B	4.4	100	0.00	317±16	314	141	298	-	-
	B	4.4	50	0.060	312 ±8	311	107	294	-	-
	B	4.4	25	0.090	304 ±3	308	95	290	-	-
Open Hole Tension	B	4.4	100	0.00	336±8	332	149	336	-	-
	B	4.4	50	0.08	335 ±13	342	129	331	-	-
	B	4.4	25	0.130	329 ±12	340	99	329	-	-

(1) Calculated following section 6.2.1

(2) Calculated following section 6.4.3

6.5 Validation of Property Predictions

To validate the mechanical property predictions performed (sections 6.2 and 6.3), a second phase of testing was performed, termed "validation testing". To carry out the validation tests, the mechanical test coupons were first oven dried and then conditioned, following the procedures outlined in sections 3.4 to 3.5. The validation test coupons were conditioned to the times specified by the predictions performed in section 6.1 and listed in table 6-4. These conditioning times produced the simulated moisture distributions through-the-thickness of the test coupons and provided a route to validate the mechanical property predictions performed previously. All conditioning was performed at 70°C/85%RH, which are the typical "HOT/WET" conditions employed for environmental conditioning at Airbus.

Coupons with a moisture profile through-the-thickness with a region of "dry-core" (assumed to be full strength unaffected by the moisture) at the centre, were conditioned and mechanically tested. Dry-core was defined when the moisture content calculated per ply was less than 0.001wt%.

As-well as the material and coupon configuration utilised for the equilibrium saturation tests (section 3.1), further testing was carried-out utilising Material C, with 8mm thick UD coupons produced for 90° tension tests, as this was the property most affected by moisture ingress. Thicker coupons were used, to allow a greater resolution between the moisture distribution levels and to be less sensitive to short conditioning times. The material utilised for these extra tests coupons was effectively the same as Material A (i.e. same resin type, fibre type and V_f). The difference was an increase in fibre areal weight (FAW), (268g/m^2 compared to 196g/m^2 for Material A). This resulted in a larger cure ply thickness (0.25mm compared to 0.184mm for Material A) meaning fewer plies were required for a thicker laminate.

Table 6-4 shows the test matrix used for the validation testing. For each test type performed, the laminate thickness and the number of coupons tested are shown. Also listed are the conditioning times required to produce the predicted moisture profiles of each coupon, leaving a percentage width of the coupon dry (<0.001wt% moisture) in the centre of the coupon (shown in figure 6-1 to figure 6-4).

Table 6-5 lists the experimentally measured moisture content, M, of the validation test coupons, including calculated standard deviations of the data set. Also shown for comparison are the predicted moisture contents, calculated in table 6-1.

Table 6-4: Validation test matrix.

				Time to condition (hrs)		
Test	**Lay-up**	**Thickness (mm)**	**No. Coupons**	**75% dry core**	**50% dry core**	**25% dry core**
90° Tension	$[90]_{11}$	2	12	-	6	15
	$[90]_{16}$	8	18	36	120	240
IPS	$[0/90]_{2S}$	1.5	12	-	4	9
90° Compression	$[90]_{11}$	2	12	-	6	15
OHT	$[+45/0/-45/90]_{2S}$	4.4	12	-	20	50
OHC	$[+45/0/-45/90]_{2S}$	4.4	12	-	20	50

Table 6-5: Validation testing moisture uptake results.

Test Type	**Material Type**	**Moisture Profile (%-dry-core, <0.001wt% moisture)**	**Experimental Moisture Content, M (wt%)**	**Predicted Moisture Content, M (wt%)**
90° Tension	Material A	50	0.050 ±0.004	0.062
		25	0.080 ±0.008	0.117
	Material C	75	0.075 ±0.006	0.030
		50	0.131 ±0.007	0.072
		25	0.198 ±0.002	0.117
90° Compression	Material A	50	0.057 ±0.008	0.062
In-plane shear	Material A	50	0.042 ±0.003	0.046
		25	0.069 ±0.002	0.082
OHT	Material B	25	0.130 ±0.003	0.142
OHC		25	0.090 ±0.002	0.144

6.5.1 Mechanical Testing Results

Table 6-6 to table 6-8 list the mechanical testing results for each validation test type. The mean strength and modulus from six coupons are shown, along with the calculated standard deviation (±SD in MPa) of each data-set. The experimentally measured oven dry test results (from section 5.4) are also shown, for a baseline comparison.

Table 6-6: 90° tension validation test results.

Material	Thickness (mm)	Dry-core (%)	Moisture Content, M (wt%)	Tensile strength, F_2^t (MPa)	Modulus, E_2 (GPa)
A	2	100	0.00	55.1 ± 7.4	9.3±0.1
A	2	50	0.05	70.7 ± 4.5	9.4±0.1
A	2	25	0.08	60.4 ± 6.5	9.1±0.2
C	8	75	0.08	73.3 ± 5.7	8.9±0.2
C	8	50	0.13	71.4 ± 5.4	8.9±0.4
C	8	25	0.2	65.6 ± 5.3	8.5±0.3

Table 6-7: In-plane shear validation test results.

Material	Thickness (mm)	Dry-core (%)	Moisture Content, M (wt%)	In-Plane Shear Strength, F_{12} (MPa)	Shear Modulus, G_{12} (GPa)
A	1.5	100	0.00	85.3±1.1	5.2±0.1
A	1.5	50	0.04	83.7±1.8	5.1±0.2
A	1.5	25	0.07	83.7±1.6	4.8±0.2

Table 6-8: Open hole validation test results.

Test Type	Material	Thickness (mm)	Dry-core (%)	Moisture Content (wt %)	Strength, (MPa)
Open Hole Compression	B	4.4	100	0.00	317±16
	B	4.4	50	0.06	312±8
	B	4.4	25	0.09	304±3
Open Hole Tension	B	4.4	100	0.00	336±8
	B	4.4	50	0.08	335±13
	B	4.4	25	0.13	329±12

7 Discussion

The following chapter discusses the results obtained from the initial diffusion constants experiment in section 5.2, as well as issues that affected the equilibrium moisture uptake results, shown in section 5.3. These include residual moisture content in the AR material, individual constituents of the material and the consequences of the end tabs.

Results of neat epoxy resin moisture absorption tests are also discussed and relate the Rule of Mixtures approach for predicting moisture content in composites to the CFRP material system studied.

The equilibrium-saturated mechanical test results in section 5.4 are discussed in detail and the effect of moisture on each material property investigated is reviewed.

The new approach to predicting properties for a composite laminate with a moisture distribution through-the-thickness (shown in Chapter 5) is discussed in relation to the macro-mechanical ply-by-ply approach and predictions performed using Classical Laminate Analysis. The mechanical testing that was carried out to validate the property predictions is also reviewed.

A case study is performed at the end of this chapter to quantify the benefits of the proposed new method (i.e. using a moisture profile) in terms of weight savings that could potentially be achieved in aircraft structures.

7.1 Diffusion Constants

Section 5.2 gives the results of the diffusion constants determination experiments. Materials were exposed to 85%RH at 70°C until equilibrium saturation was achieved, table 5-3 lists the measured maximum moisture content and calculated diffusion coefficients for the two materials tested.

Material A, (a UD tape) contained 0.606wt% equilibrium moisture content, M_{max}, which was lower than the measured M_{max} of Material B of 0.708wt%. This was mainly attributed to the higher resin content of the woven material as compared to the UD material, verifying that moisture absorption in the materials being studied is a resin dominated process. From figure 5-4 it was evident that the moisture absorption rates of the composite materials being studied were linear at the beginning of the process and plateaued to asymptotic values after long periods of time, in a manner consistent with the Fickian diffusion process[19]. Close Fickian numerical fits (shown in figure 5-5 and figure 5-6) of the mass uptake versus square root of time, for both materials, suggested that diffusion that could be modelled using Fick's Second Law.

The rate of water absorption (measured from the initial slopes in figure 5-4) for the woven Material B (4.05×10^{-4}wt%/s), was lower than that for the UD Material A (5.53×10^{-4}wt%/s). This could be due to the nature of woven material, which may be making the diffusion path for the water molecules more complex than that of the UD tape and hence moisture traverses at a slower rate. Choi et al[49] showed that the water absorption rate was fastest in laminates with 0° fibre angle. Comparing the calculated diffusion coefficients, D_x (which is a factor of proportionality, representing the amount of substance diffusing across a unit area, through a unit concentration gradient, in unit time) from table 5-3 shows the woven material B has the greater calculated D_x of 10.51×10^{-7}mm^2/s, compared to 6.67×10^{-7}mm^2/s for Material A. This may be because the higher resin content in Material B (V_f of 0.58%) compared to Material A (V_f of 0.68%) makes it easier for moisture to diffuse into the resin.

The maximum moisture contents, M_{max}, for Materials A and B (given in table 5-3) confirm that moisture content is a function of the resin content. The higher resin value results in an increased M_{max}. Material A has approximately 32% resin by volume and the measured M_{max} was 0.607wt%, compared to Material B with approximately 42% resin content by volume and a measured M_{max} of 0.708wt%.

Material A and B were dried prior to any conditioning being performed to ensure an accurate M_{max} value. This drying data was used to calculate the desorption coefficients in the same way as the absorption coefficients. Table 5-2 lists the calculated diffusion coefficients for drying of both materials. The Material A showed an increased rate of moisture desorption (slope of the curve) $2.14x10^{-4}$wt%/√s compared to material B $1.47\ x10^{-4}$wt%/√s. This is in agreement with the absorption characteristics of the materials; however for both materials desorption rates are lower than the absorption rates.

The desorption diffusion coefficients were calculated using equation *2-20*. Material A had a lower calculated drying D_x than Material A; 3.74 and 11.87 $(x10^{-7})mm^2/s$ for material A and B respectively. This is in agreement with the absorption characteristics of the materials. The diffusion coefficients for drying and conditioning ranged between 3.74 and $6.67(x10^{-7})mm^2/s$ respectively for Material A and 10.51 and 11.87 $(x10^{-7})mm^2/s$ respectively for Material B, indicating a negligible effect between drying and conditioning on this diffusion parameter.

7.2 Equilibrium Saturation Conditioning

Section 5.3 details the conditioning results obtained for the mechanical test coupons that were used in the equilibrium saturation testing program to derive moisture/mechanical property relationships.

This section discusses issues that affected the environmental conditioning and the results gained. It is very important in composite testing to assess results and learn from any errors made, so that any future programmes can be carried out more effectively. This was an important aspect of this work for Airbus, as it assisted in implementation of lean specimen handling procedures that will minimise errors when running such testing programmes in the future. The new procedure[128] details specimen monitoring, cutting and the oven drying process, along with recommendations for storage and conditioning prior to test. The new process allows better control of the environmental history of specimens/components, thus reducing any potential inaccuracies during the manufacturing and handling processes, which have been proven to impart significant uncertainty about the final equilibrium moisture content, M_{max} of the specimens. This new procedure is discussed in detail in section 7.3.

The comparison of the diffusion properties of Material A and B suggested that M_{max} is a function of the relative humidity the material is exposed to, i.e. the greater the %RH the greater the M_{max}; this trend is shown in table 5-4. The results are in accordance with diffusion theory, in that the maximum moisture content M_{max} is a function of the relative humidity and increased with increasing %RH level. Figure 5-7 shows the moisture content as a function of %RH, which follows the power relationship given in equation *2-22*. Table 5-5 shows that predictions of M_{max} using this relationship are reasonably accurate (within 10% of the experimentally measured value).

It was observed that the M_{max} values measured for the 90° tension coupons were consistently lower when compared to the other specimen types (see table 5-4). Possible factors that may have affected M_{max} values are:

- Presence of residual moisture
- End tab absorption

- Resin effects
- Void content
- Fibre volume fraction, V_f

These issues are discussed with reference to measured M_{max} values in the following sections.

7.2.1 Residual Moisture

When performing experiments that involves the exposure of test coupons to conditions other than ambient, strict procedures should be followed. If not, significant errors can be introduced during the manufacturing and handling processes, potentially leading to inaccuracies in the data analysis and the final model predictions. Due to some discrepancies in material handling, some errors were introduced (highlighted in section 5.2). This will now be discussed in greater detail.

Airbus standard procedure is to utilize material from its AR condition. As moisture absorption is a relatively slow process, Airbus considers these coupons to be effectively dry. Thus, no environmental control of the coupons was deemed necessary and the AR approach was employed for coupons utilised for the equilibrium saturation testing (i.e. coupons were not oven dried prior to conditioning). Due to this coupon handling procedure the coupons were left in an ambient environment (approximately 23°C and 50%RH) for up to 18 months and were deemed to be in the as-received (AR) state, prior to conditioning.

These equilibrium saturation coupons were tested over a long timescale, therefore the amount of AR moisture present, prior to conditioning may have varied with no way of quantifying the amounts. Therefore, following this testing, a study was performed to measure the residual moisture in the AR coupons, with the aim of estimating their initial moisture content. Between 0.1-0.26wt% moisture was measured in the coupons that had been stored in the ambient environment prior to conditioning (values are listed in table 3-5). These corrections were then applied to those coupons that had not been dried prior to conditioning. All results discussed in this report have been corrected to include the approximated, as-received residual moisture.

All coupons utilised in the initial moisture constant determination tests (section 5.2) and the validation testing experiments (section 6.5), were oven dried at 80°C until a "dry" state was achieved i.e. the moisture desorption reached equilibrium.

When carrying out any environmental test campaign, all coupons should begin in a dry condition. Therefore a key lesson learnt is to either test manufactured coupons over a short timescale, thus limiting the amount of moisture absorption in the AR state, or strictly monitor material and coupon movement and store coupons in desiccators once manufactured and prior to testing/conditioning, in order to prevent further moisture ingress. These approaches will be implemented at Airbus in the future during all environmentally critical testing[128].

This error in coupon storage has had a discernible effect on all equilibrium saturation test coupons that underwent conditioning. It was not possible to have absolute confidence in the maximum moisture level, M_{max} measured from each batch of equilibrium saturation coupons. Knowing the maximum moisture content at full saturation is critical to the success of an accurate model, as it is essential when assigning material properties based on moisture content in each ply. Drying is a critical step in such work in order to provide a zero reference point for moisture uptake calculations.

7.2.2 End Tab Moisture Absorption

The use of Tufnol 10G/40 bonded end tabs, added further errors to the recorded moisture content in the equilibrium saturation coupons. Tabs can and often do affect tests results and complicate modelling, because exact details on tab material and bonding adhesive are not known.

Within the test methods followed[110], there is a defined procedure to monitor the moisture absorption in specimens. In this case the procedure was not followed because it involves the manufacture of separate traveller specimens, which are then used to monitor moisture concentration for a batch of coupons. This method was deliberately ignored because it was felt that monitoring the individual moisture uptake of each coupon would provide better fidelity. This decision was made without considering end tab diffusion properties. In hindsight, if these procedures had been followed, many of the issues relating to the measurement of moisture during conditioning would have been negated.

In this work the end tabs and coupon edges were insulated with aluminium tape to ensure moisture absorption through the thickness of the test coupons only. With this method there are risks of an imperfect seal and moisture penetrating through the edges of the coupon. When calculating the M_{max} values in the CFR composite specimens, the mass of the Tufnol end tabs were subtracted from the specimen mass in-order to calculate the weight increase of the composite due to moisture absorption.

For interest, a study was carried out using Tufnol end-tab material to determine the diffusion constants. Coupons of Tufnol (100x100x2mm) were conditioned (as described in section 3.4) and the equilibrium moisture constants of the Tufnol were calculated using equations shown in section 3.4.1. These values are displayed in table 7-1.

Table 7-1: Diffusion constants for Tufnol end tab material at 70°C.

Condition @ 70°C	Maximum Content M_{ma} (wt%)	Diffusion Coefficient, D (x10^{-7}) mm^2/s
75%RH	0.5	2.47
85%RH	0.7	4.60
95%RH	1.0	4.12

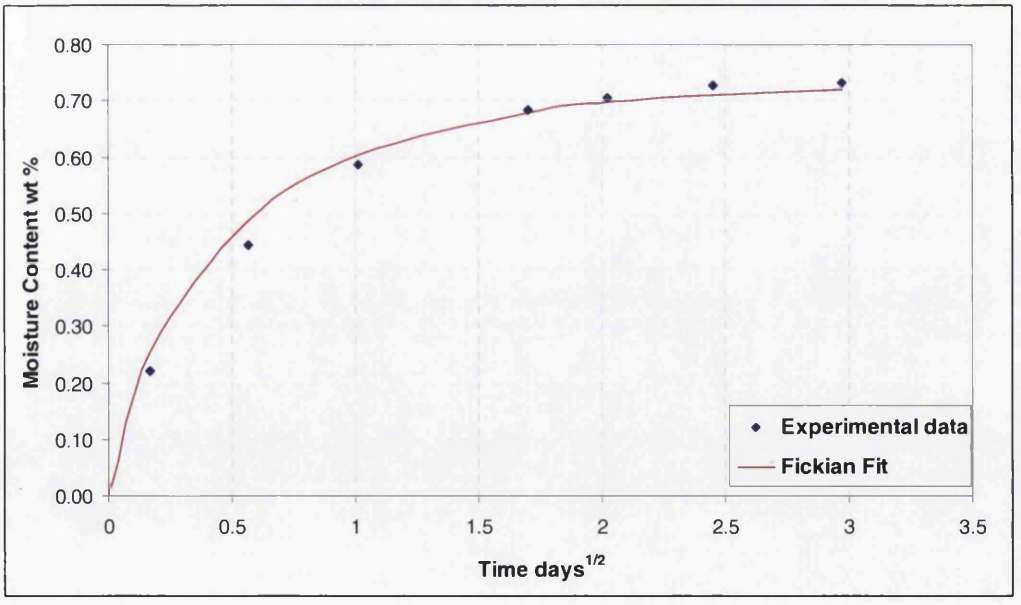

Figure 7-1: Tufnol end tab material moisture uptake at 70°C & 85%RH, with Fickian plot.

Figure 7-1 shows an uptake curve for the Tufnol material (conditioned at 70°C and 85%RH) and a Fickian fit to the data, plotted using equation 5-1. A comparison of the diffusion constants of the Tufnol end tab material and the CFRP laminate (see table 5-2) show that the maximum moisture content M_{max} for UD CFRP (70°C and 85%RH) is 0.6wt% and Tufnol© is 0.7wt%. Also, the diffusion coefficient under the same conditions is of the same magnitude, being $6.67 \times 10^{-7} mm^2/s$ for the CFRP laminate and $4.6 \times 10^{-7} mm^2/s$ for the Tufnol end tab material. For future testing it is recommended that tabs are applied post conditioning to negate any effects on M_{max} measurements

7.2.3 Void Content V_v

From the C-scans (Appendix B) it was deemed that the quality of the composites was acceptable. It was shown in table 5-1 that the void contents of the composite laminates were low (between 0.4 and 1.8%). The higher void contents were observed in Material B, which is a woven material. Airbus accepts a void content of less than 2% as indication of an adequately fabricated composite laminate, therefore from the calculated void contents the laminates used were of satisfactory quality.

Voids/porosity present in the material can increase the equilibrium amount of moisture that can be absorbed, hence the larger the void content, the greater the moisture content[84,129,130]. Table 5-1 lists the calculated void contents for each different coupon type. The IPS coupons had a V_v of 1.57%, which was more than double that of the 90° tension coupon (V_v=0.40%), potentially contributing to the difference in measured moisture contents.

This procedure for calculating void volume is sensitive to variations in densities and constituent weight percents. The coefficient of variation for the V_v calculations was very high (between 10-95%), confirming that measuring void content in composites is very difficult. The measurement of composite void content (V_v) by this technique requires the determination of the fibre density ρ_f, the composite density ρ_c, the resin density ρ_r, the weight of the sample W_c and the weight of fibres in the sample W_f. It is common practice not to measure the fibre density but to use the value quoted by the manufacturer .However, on calculating composite void contents using this value for the density high values of scatter were obtained.

7.2.4 Fibre Volume Fraction, V_f

Fibre volume fraction results for each composite panel manufactured can be found in chapter 5.1. The fraction of fibres and matrix that make up the laminate can have a marked effect on the maximum moisture content. As it is assumed that the absorbed moisture affects only the epoxy matrix material, it follows that as the fibre volume fraction increases the value of maximum moisture content, M_{max}, will decrease. Two factors can cause laminate fibre volume fraction to vary: (1) the amount of matrix resin present relative to the amount of fibre (resin content), and (2) the amount of porosity (void volume). These factors give rise to changes in fibre volume fraction from material to material, batch to batch, panel to panel, and even specimen to specimen within a panel. Because of the high standard of specimen material preparation within Airbus it can be stated with some certainty that void fraction within test coupons is minimal, this was further verified by the C-scans in Appendix B. In addition, the fibre volume fraction of each test panel used has been determined (see chapter 5.1).

Table 5-1 lists the experimental results of the tests conducted to determine the constituents of the materials used. As the coupons were manufactured from different panels of material, a section from each panel was utilised in the acid digestion test, described in section 3.3.

The V_f of Material A (which is a UD tape) varies between 66.25 and 69.58%. The highest V_f of 69.58% was measured for the panel used to manufacture the 90° tension coupons and the lowest V_f of 66.25% was calculated for the panel used to manufacture the ILS coupons. The V_f measurements for Material B (the woven fabric) were significantly lower. The calculated V_f for the panels used to manufacture OHC and OHT coupons was 57.81% and the 56.29% respectively, meaning there was a higher resin content for this material. It would be expected that the Material B with the lower V_f would have a higher measured M_{max}. However, at 70°C and 95%RH, for both OHC and OHT coupons, a M_{max} of 0.61 and 0.65wt% was measured respectively. These results must be attributed to the errors described earlier (sections 7.2.1, 7.2.2 and 7.2.3) and it was determined that these tests would need to be repeated.

7.2.4.1 Normalised Composite Weight Gain

As carbon fibre absorbs little moisture, the moisture uptake of a composite can be normalised to the resin weight gain according to

$$(M_{max})_r = \frac{M_{max}}{W_r} \qquad 7\text{-}1$$

$(M_{max})_r$ and M_{max} are the moisture uptakes of the matrix and composite respectively, while W_r is the resin weight fraction.

Table 5-4 lists the moisture content values, M_{max} for the equilibrium saturation test coupons. The measured M_{max} for the 90° tension coupons were consistently lower (30-45%) than the M_{max} measured for the other UD material coupons. To assess if the V_f variation was contributing to this difference, equation 7-1 was used to normalise the M_{max} values in table 5-4, the results of which are given in table 7-2.

Table 7-2: Normalised composite weight gain.

%RH	Normalised M_{max} in wt%			
	90° Tension	90° Compression	IPS	ILS
60	0.91	1.56	1.51	-
75	1.49	2.22	2.12	1.92
85	1.82	2.61	2.42	2.69
95	2.35	3.00	3.25	3.31

Table 7-3: Coefficient of Variation of M_{max} for UD equilibrium saturation test coupons.

%RH	CV of M_{max} from Table 5-4 (%)	CV of normalised M_{max} from Table 7-2 (%)	Difference (%)
60	30.6	27.4	10
75	19.4	16.8	14
85	19.2	16.6	14
95	17.9	14.7	18

As can be seen, the 90° tension M_{max} normalised weights are still somewhat lower than the other test coupons, however by assessing the coefficient of variations from

the M_{max} values and the normalised M_{max} values (shown in table 7-3), it can be seen that there was between 10-18% contribution in wt% measured, due to the difference in fibre volume fraction. The remaining difference in measured M_{max} may be attributed to some of the other factors that have been discussed in this section.

From the perspective of aircraft certification, the testing performed here would not be acceptable and as a result, a procedure was created at Airbus to allow strict control of material for future testing. This future test work would conform to fully traceable documentation suitable for audit and will provide highly accurate material property data for use by the developed model. Furthermore, any uncontrolled moisture ingress leads to specimens requiring oven drying prior to test, typically increasing timescales and costs.

7.3 Recommended New Specimen Handling Procedure

The overriding driver behind the recommended new specimen handling process is to limit the exposure to and monitor undefined environmental conditions, thus removing the possibility of any conditioning of the coupon occurring, other than that specified for the test. This removes any ambiguity in the level of moisture contained within a specimen, allowing confidence in the results. Appendix H shows a flowchart detailing the new specimen handling procedure that was introduced in Airbus as a direct result of the work performed here. Each step of the new procedure is detailed in sections 7.3.1 to 7.3.6.

7.3.1 Specimen Manufacturing

Seven days is considered the maximum time allowed between removal from the autoclave and specimen cutting. This timeframe is considered the shortest amount of time that is acceptable with current working processes. During this time, material should be stored in a controlled environment, such as a sealed bag containing desiccant and data loggers to record environmental history. A data logger monitoring temperature and humidity should accompany the panel from when it leaves the autoclave up until it returns from specimen cutting and is placed into the oven (which will have independent environmental monitoring) for drying. Environmental data loggers should be calibrated before use and logging should take place at 1 minute intervals.

Tight control of the manufacturing process must be maintained, so that the panels are manufactured and delivered for coupon machining on time in order to minimise environmental exposure and subsequent moisture ingress via diffusion. It then becomes the responsibility of those cutting the specimens, to cut and return the specimen within the allowed seven days (5 working days). Suppliers should be held to strict timescales and should be responsible for the environmental control of material. The requirement of environmental control and logging after cure should be stated within the appropriate manufacturing instruction sheet (MIS).

7.3.2 Specimen Cutting

Seven days is considered a maximum turn-around of specimen machining for each panel delivered. This is derived from previous experience and is considered reasonable for batches of around 300 specimens. Larger batches may be permitted, upon agreement with the contractor responsible for machining. Specimens should be returned in a controlled environment, such as a sealed container containing desiccant. An environmental data logger should also accompany the specimens. This gives a potential maximum of two weeks exposure to the ambient environment between leaving the autoclave and receiving the specimens back from cutting. Specimens should be weighed within one day after being received back from the contractor.

7.3.3 Oven Drying

Upon receiving the specimens after machining they should be weighed, then placed straight into an oven to remove any moisture absorbed during the NDT and cutting processes. Humidity in the oven should be continually monitored. The specimens should then be weighed weekly or twice weekly until there is no further decrease in weight, indicating that all absorbed moisture has been lost. The samples are then ready to be placed into a desiccator so that they remain dry.

7.3.4 Storage

Once the specimens are dry they should be placed in a desiccator, where humidity and temperature should be logged. Once the specimens have been placed in the desiccators, care should be taken to minimise the disruption to the desiccator environment.

7.3.5 Conditioning

Specimens should be weighed prior to the start of conditioning and compared against the weight taken prior to storage and drying. During the conditioning process, specimens should be weighed weekly and the results recorded. Specimens have reached equilibrium when their weight remains constant for a period of three weeks.

It is important to check the functionality of the conditioning chambers regularly. Chamber breakdown can lead to unwanted drying, which increases the time required for conditioning and may also cause unwanted cyclic conditioning of the specimen. Thus it is important to ensure that the environmental history of the chambers is recorded independently.

If the specimens are to be tested at equilibrium, then time spent in the chamber after equilibrium is reached can be allowed. If the specimens are being only partially saturated then it is important that they are removed and tested as soon as the desired moisture content is reached. Any further exposure will lead to an undesired increase in moisture content. The effect of any excess exposure will be dependent on the temperature and humidity levels; i.e. the higher the temperature or humidity, the faster the rate of diffusion, or the higher the level of moisture that will be driven into the specimen.

7.3.6 Testing

The testing of specimens exposed to environmental conditions requires careful control. Specimens should be weighed as they are removed from the chamber. Ideally, specimens should be tested as soon as possible after removal from the chamber, spending no longer than 30 minutes out of the chamber before testing. For tests carried out at ambient conditions, a quick turnaround is the only addition to the normal test procedures. When testing specimens that are partially saturated, it is important to be aware that these specimens are particularly sensitive to time spent in environments other than that which they were conditioned.

7.4 Neat Resin Moisture Absorption

The moisture absorption in the composite materials studied here is mainly a function of the resin, so in order to better understand the composite materials, the diffusion characteristics of the neat 977-2 epoxy resin were investigated.

7.4.1 Neat Resin Moisture Constants

Coupons of neat resin were conditioned at 70°C/85%RH to measure the moisture constants; the same procedures were followed as in section 3.4.1. The experimentally measured moisture uptake is plotted in figure 7-2, which also shows a Fickian fit to the data using equation 5-1.

Table 7-4 lists the calculated moisture constants for the neat 977-2 resin. It is evident from the shape of the moisture absorption curve of the neat epoxy resin, that the diffusion characteristics of the material are Fickian in nature.

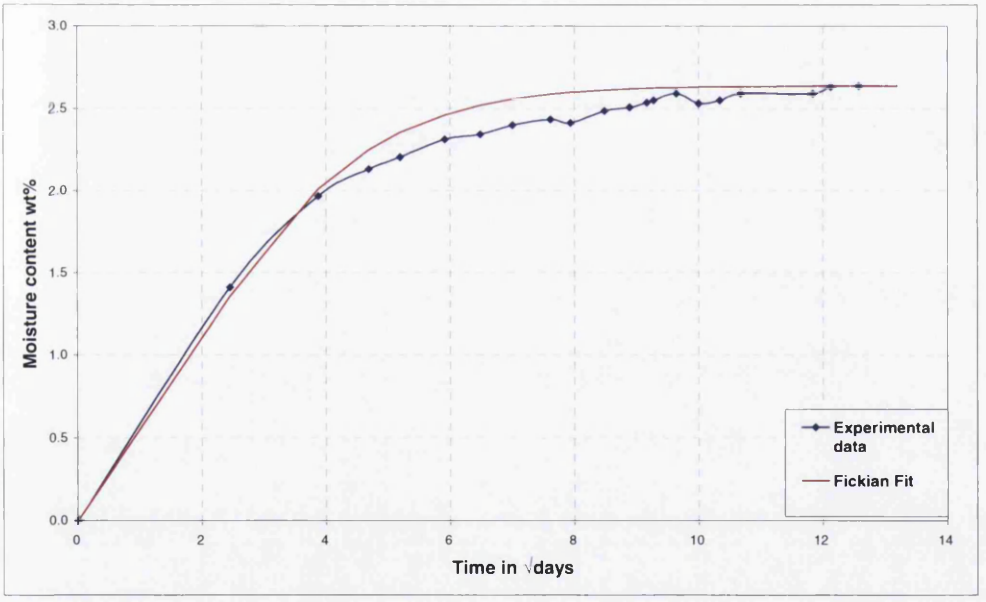

Figure 7-2: Uptake data for plain epoxy resin at 70°C and 85%RH.

Table 7-4: Neat epoxy resin moisture constants at 70°C and 85%RH.

Material	Environment	Maximum Moisture Content, $(M_{max})_r$ (wt%)	Diffusion Coefficient, D_r (mm^2/s)
Neat Epoxy Resin	70°C/ 85%RH	2.6wt%	4.8×10^{-5}

A comparison the diffusion coefficients calculated for the composites and for the matrix (see table 5-3 and table 7-4) indicates the diffusion coefficients are smaller for the composites than for the matrices. This may be attributed to the presence of the fibres, which can act as a barrier to moisture absorption and inhibit transport through the resin[86]. The equilibrium moisture contents for both materials A and B (UD and woven) were approximately 25% of the observed equilibrium moisture content of the cured neat resin samples; this is typical for CFRP[97,98,99].

The maximum moisture content in neat resin $(M_{max})_r$ can be estimated from the maximum moisture content in the composite, M_{max}. By assuming fibre absorbs no moisture, M_{max} and $(M_{max})_r$ are related by the expression given in equation *7-1*. For an ideal composite with no interface effect on the moisture uptake, the normalised weight gain of the composite should be the same as that of the neat resin. Equation 7-1 was used to predict the neat resin moisture content, the results of which are shown in table 7-5.

Table 7-5: Prediction of $(M_{max})_r$ values.

Test	Enviro-nment	Composite Moisture content M_{max} (wt%)	Resin weight Fraction (W_r)	Predicted Resin Moisture content $(M_{max})_r$ in wt%
90 Tension	70°C/85%RH	0.44	0.24	1.82
90 Compression		0.67	0.26	2.61
IPS		0.64	0.26	2.42
ILS		0.70	0.26	2.69

The predicted $(M_{max})_r$ values at 70°C/85%RH for the 90° compression, IPS and ILS coupon show good agreement with the experimentally measured value of resin (2.6wt%), thus validating equation 7-1. However, the predictions of $(M_{max})_r$ for the 90° tension coupon is 30% lower than the experimentally measured value of resin M_{max} (2.6wt%). This is probably due to the lower than average M_{max} value. This indicates that the Rule of Mixtures equation (7-1) can be used to accurately predict the amount of equilibrium moisture content in a composite, given the neat resin values.

The most widely applied theory of moisture diffusion in UD composites is that of Shen and Springer [19], which is based on a model of thermal conductivity proposed by Springer and Tsai[88]. In their models the flow of heat/water is assumed linear.

The expression for transverse (TTT) diffusivity for impermeable fibres is given in equation 2-26. Comparison of the experimentally measured diffusion coefficients for the composite and the resin were made using the Shen and Springer[19] model (equation *2-26*). Table 7-6 presents the experimentally measured and predicted diffusion coefficients for the matrix, D_r and the composite, D_c. The measured values, D_r and D_c differ by a factor of 5 and 20 respectively to the predicted values.

Table 7-6: Predicted D_c and D_r using equation by Springer[19].

Material	**Experimentally Measured D_x, mm²/s**	**Predicted by Springer[22] – (Eq. *2-26*), D_x mm²/s**
Neat Resin, D_r	4.8×10^{-5}	0.96×10^{-5}
Composite Material A, D_c	6.67×10^{-7}	0.33×10^{-7}

Shen and Springer [19] presented experimental data that agreed with their own model, but from the literature it seems composite diffusivity values obtained by most other authors are much higher than the theoretical predictions of equation *2-26.* This disagreement between theory and experiments is to be expected because of its simplified nature. The model assumes that water diffuses in straight lines, i.e. it cannot flow around fibres. Thus, equation *2-26* is an underestimation of the transverse diffusivity of a composite material. This disproves the validity of the rule of mixtures for this resin system and verifies that calculating composite properties from simple resin uptake and V_f measurements is not always possible, hence the need for the detailed moisture ingress studies for composite materials carried out in this work. The investigation into the neat resin properties has shown that neat resin absorption can be used to reliably predict equilibrium moisture content in composites, but is not dependable to predict the composite diffusion coefficient.

7.5 Mechanical Testing

In general it was observed that all tested coupons presented the same failure modes, regardless of moisture content. However it was seen from the fractographic investigations that the failure surfaces had a more ductile appearance in the conditioned coupons than the non-conditioned ones.

7.5.1 Effect of Moisture on Tensile Strength of CFRP

For coupons with a fibre orientation parallel to the load direction (i.e. $\theta=0^{o}$) the tensile strength was not affected by moisture. This can be seen in figure 5-8 and figure 5-9. The results support current knowledge[17,18,85], demonstrating that only the epoxy resin is affected by water ingress, which would have negligible effect on fibre-dominated properties in the 0^{o} direction.

For coupons with a fibre orientation transverse to the load direction (i.e. $\theta=90^{o}$) tensile strength was a very sensitive parameter to moisture ingress. Figure 5-12 illustrated that the greater the equilibrium moisture content, the more the fracture strength decreased. This is in contrast to the longitudinal tensile properties, as transverse strength is highly dependent on the resin properties, which is significantly affected by moisture ingress[85,94,97]. Experimentally measured data showed a reduction of 47% in strength for the coupons containing 0.57wt% moisture, as compared to the oven dry strengths. Figure 5-11 showed a decreased elongation with increasing M_{max}. This suggests a weakening of the fibre-matrix interface (if matrix softening only was occurring, an increase in elongation would be seen). Figure 7-3 shows clean fibres are more obvious in image (c) as compared to (a), indicating interface degradation.

For coupons of $\theta=90^{o}$ a large degree of scatter was observed in the data with low wt% moisture content. This scatter may be due to a loss of resin toughness associated with low moisture content, preventing localised yielding. If this stress redistribution process was retarded this would result in stress concentrations building up and eventually leading to a premature catastrophic failure. This test type is also very susceptible to coupon quality and any small edge delamination could be the cause of a premature failure, thus contributing to scatter in the data set. Other

factors such as specimen misalignment, grip pressure and end tab stress distribution may all be contributing to the scatter measured in the test data.

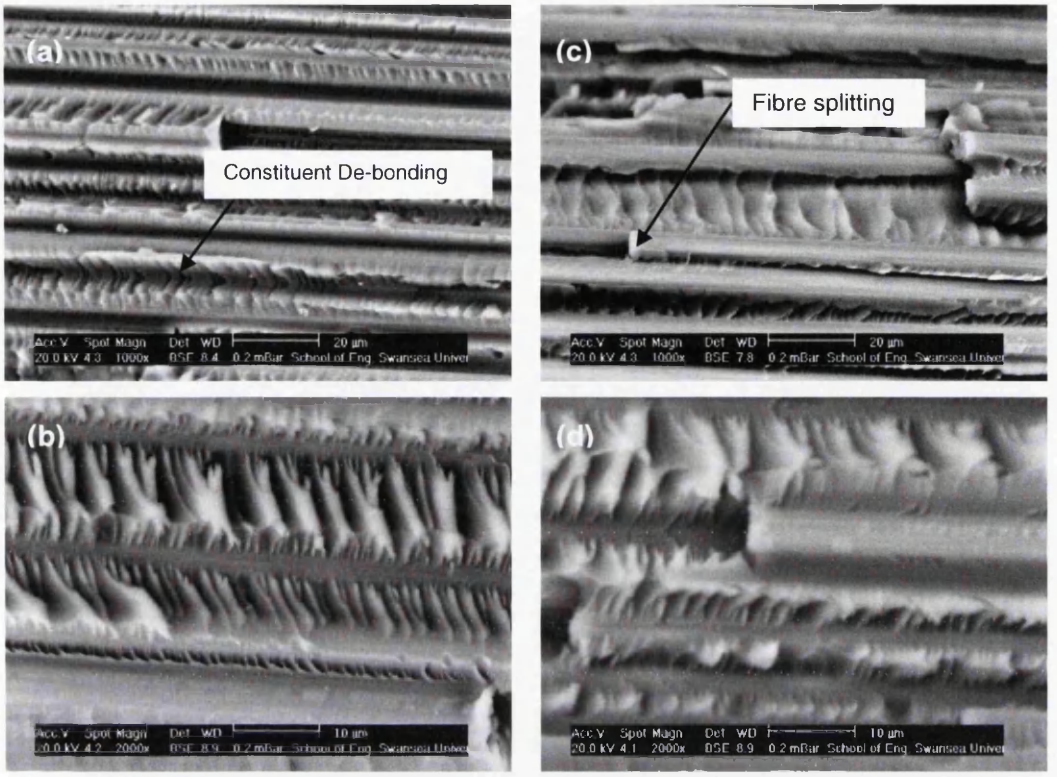

Figure 7-3: Micrographs of a 90° tension coupon; AR (a,b), & 70°C/ 95%RH (c,d).

Figure 7-3 shows SEM micrographs of 90° tension coupons, with figure 7-3 (a) and (b) showing as-received coupons and (c) and (d) showing those conditioned to equilibrium at 95%RH/70°C. Failure in transverse tension occurs on a plane perpendicular to the direction of the applied load. Therefore failure in the transverse tension coupons occurred at the fibre/matrix interface, or in the matrix itself with some additional fracture in the fibres. This is because fibres perpendicular to the loading direction act to produce stress concentrations at the interface and in the matrix. They fail because of matrix/interface tensile failure; although in some cases they fail by fibre transverse tensile failure, if the fibres are highly oriented and weak in the transverse direction. Thus the composite's failure modes under transverse tensile loads may be described as (1) matrix tensile failure and (2) constituent debonding and/or fibre splitting[39]. Constituent debonding means that some portions of the failure surface are formed because of failure of interfacial bonds between fibres and the matrix. Figure 7-3 (a) and (c) indicates that constituent debonding and fibre splitting have both taken place during failure.

Figure 7-3 shows the SEM images at a magnification (x1000). The fracture surface appears flat and the orientations of the fibres are well defined. The fracture surface consists mostly of fibres that are free of all matrix material, with a few visible fractured fibres. The influence of the matrix and fibre-matrix interface becomes evident at high magnifications. At x2000 magnification, the micrographs show the "hackles" formed by debonding of the fibre-matrix interface. These markings are normal to the direction of the fibres. A comparison of the two sets of micrographs shows that in the coupon with the higher moisture content, the fracture surface has a more ductile appearance. This is because the water has plasticized the matrix material, leading to the softer/less defined fracture surface features. In conclusion both matrix softening and fibre-matrix interface weakening has occurred in the 90° tension test coupons due to the presence of moisture.

7.5.2 Effect of Moisture on Tensile Modulus of CFRP

In this study it was found that moisture absorption can lead to a decrease in transverse and longitudinal modulus (shown in figure 5-10 and figure 5-13) of the composite laminates, owing to irreversible plasticisation of the epoxy matrix. This was also observed by Singh[98] and his co-workers. The wet composites exhibit lower moduli than the dry epoxies at room temperature. Plasticisation of the epoxy matrix causes deterioration in the mechanical properties[132]. Lekatou et al[131] suggested that water penetration into polymer matrix composites involves three mechanisms: (1) direct diffusion of water molecules into matrix and to a lesser extent, into filler material; (2) flow of water molecules along the fibre-matrix interface, followed by diffusion into the bulk resin; and (3) transport of water by microcracks or other forms of microdamage. They concluded that water has the tendency to migrate to the fibre-matrix interface.

The amount of moisture absorbed by the epoxy matrix is significantly greater than that absorbed by the carbon fibres. This results in a significant mismatch in the moisture induced volumetric expansion between the matrix and the fibres and can lead to the evolution of localised stress and strain fields in the composite. In addition, stresses are also induced in composites, due to a mismatch in coefficients of thermal expansion.

When compared to oven dried values, Young's modulus E_1 and E_2 are reduced by approximately 5-6% when conditioned to equilibrium moisture content at 70°C and

95%RH. Chou et al[123] reported similar reductions of E_1 and E_2 for carbon fibre reinforced epoxy material exposed to 85°C and 100%RH. In theory, E_1 is dictated by the fibres, which are insensitive to moisture. Nevertheless, coupons may swell slightly when absorbing moisture, thus enlarging the cross-sectional area and reducing all moduli. Measurements of the 0° tension coupons could not be made after testing to confirm any swelling effects, as the coupons fractured catastrophically on failure. Along with dimensional changes, internal stresses can also arise, since the fibres are constrained by the matrix, the fibre matrix interface is subjected to tensile stresses which can encourage de-bonding of the fibres. A microscopic investigation could confirm this, but due to the explosive failure of this coupon type no fracture surface survived for investigation. This is certainly an area that requires further investigation in order to fully understand the mechanisms and influence of moisture absorption on the mechanical properties of composite structure.

7.5.3 Effect of Moisture on the Shear Properties of CFRP

In-plane shear (IPS) is a sensitive parameter to moisture ingress. During testing an average 22% reduction in IPS strength, τ_{12}, was measured when conditioning to equilibrium at 95%RH and 70°C to give 0.86wt% moisture content. A reduction of more than 10% was measured for the IPS modulus, G_{12} for the same environmental conditions. The moisture in the polymer disrupts the initial inter-chain Van-der-Waals forces and hydrogen bonds, resulting in increased segment mobility, acting to plasticize the matrix and deteriorate the strength, lowering the T_g[133]. The shear stress acts in the plane of the laminate. Failure of the laminate occurs by delamination between the +45° and -45° layers and due to cracks across the width of each layer. A typical shear failure can be seen in figure 5-25.

The interlaminar shear strength (ILSS) was strongly affected by the presence of moisture in the composite material. This was attributed to the fact that wet conditioning induces strong matrix plasticisation[97] and ILSS is a matrix dominated property. Figure 5-27 shows that with an equilibrium moisture content of 0.86wt%, (achieved by conditioning at 70°C and 95%RH) a 24% decrease in ILSS was measured compared to the oven dried material. Botelho et al[85] saw similar reductions in interlaminar shear strength for carbon fibre epoxy composites with conditioning regimes of 80°C and 90%RH. He reported strength decreases of 21%

in UD CFR epoxy composites. This result is expected, as the interlaminar shear strength is a property that is driven by the matrix properties.

An interesting phenomenon occurs with the absorption of a low (0.26wt%) amount of moisture into the test coupon. It appears that the presence of the small amount of moisture within the matrix provides an increase in ILSS, since there was a measured increase in ILSS strength of around 8% compared to the 0wt% (oven dried) coupons. It is feasible that moisture in the matrix provides an element of fracture toughness[135] to the matrix that delays the initiation and propagation of inter-laminar cracks. So in the 0wt% moisture samples the matrix resin has a low toughness and this could lower the ILSS. A brittle resin means that there is limited resin yielding, which is an important stress redistribution mechanism. But with increasing moisture the T_g lowers, resulting in matrix plasticisation and leading to further degradation of the ILSS. Similar behaviour has also been noted by Joshi et al[16] with the testing of graphite/epoxy composites. They also observed an increase in ILSS when a small amount of moisture was absorbed. Joshi attributed the increase of strength to the moisture providing a release of residual strains, induced by differential thermal contraction during cooling (during the cure cycle). For a 0.2wt % increase in moisture from the dry state, Joshi observed an increase in the ILSS values of around 10%. On further absorption he recorded a decrease in strength of 25% for 2.0wt% moisture content and more ductile failures were noted.

Composites' shear properties are mainly governed by the epoxy matrix and possible mechanisms of failure include cracking and debonding[39,92]. The plasticization, swelling stresses and any epoxy degradation due to moisture absorption, will contribute to the matrix failure mechanisms. This increase in the mechanical strength of carbon–epoxy laminate may be related to the mechanism of water sorption by the composite and how the water molecules were bonded to the polymeric chain

Zhou and Lucas[89] affirmed that water molecules bond to the thermoset resin network through hydrogen bonding; they classified the bonding into two types: Type I – water molecules form one hydrogen bond with the resin network and have lower activation energy and Type II – water molecules form more than one hydrogen bond with the resin network and have higher activation energy. Type I bound water diffuses into the thermoset network and breaks the initial interchain van-der-Waals' forces resulting in the increase of chain segment mobility and swelling. As the

amount of Type I bound water is dominant in the water sorption process, primarily when the polymer is not so polar, it readily plasticizes the thermoset resin. Water molecules which form multisite interconnective bond complexes (Type II) do not contribute significantly to the plasticization of the resin. Moreover, these complex bonds create bridging between chain segments resulting in secondary cross-linking (pseudo crosslinking). Thus, the environmentally conditioned resin becomes plasticized and an initial increase in interlaminar shear strength was observed. However increasing the relative humidity which in turn increases the maximum moisture content in the coupon leads to steady decreases the ILS strength.

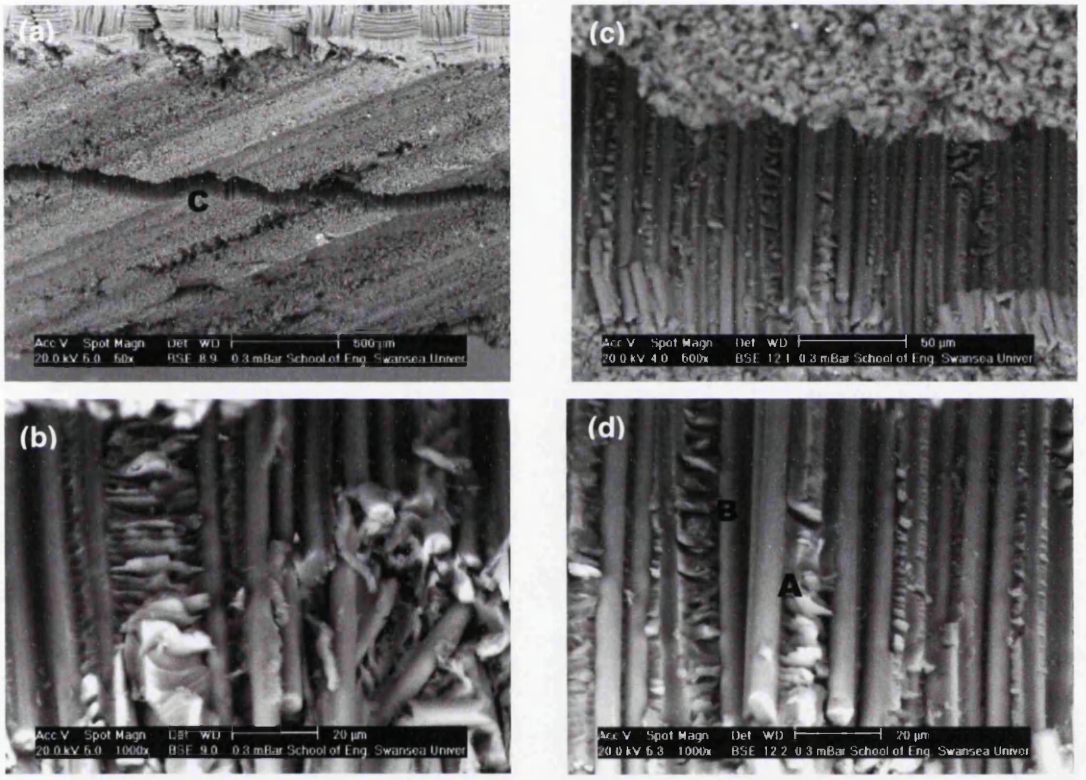

Figure 7-4: Micrographs of ILSS coupon. OD (a,b), 95%RH/70°C (c,d).

Figure 7-4 shows SEM images of an ILSS coupon. Images (a) and (b) are of a coupon that has been oven dried (0wt% moisture content), while images (c) and (d) show the coupon that has been conditioned to equilibrium moisture content at 70°C/95%RH. The failure of an interlaminar shear coupon is by multiple cracking of the matrix between the layers of fibres. The cracks are formed opposite the central roller or at the edge of the coupon, usually they tend to develop and propagate between the plies as a delamination crack. Figure 7-4(a) shows a test coupon with 0wt% moisture at a low magnification (x50), illustrating a typical interlaminar shear failure mode, with a single interlaminar shear crack between the layers of the

coupon (marked **C)**. The fracture energy for cracking through a resin rich layer between plies is orders of magnitude lower than cracking through the fibres[39]. Similar failure modes are observed for coupons submitted to environmental conditioning.

Figure 7-4(d) is an ILSS coupon conditioned at 95%RH/70°C. The image of the fracture surface shows that the clean fibres where the matrix has delaminated (indicated by **A)** can be clearly seen, along with some fractured fibres. The SEM micrographs presented in figure 7-4 (b) and (d) are at higher magnifications and show the most distinguishable features of the failure surface are the hackle (serration or tear) markings (indicated by **B)**. The hackles are seen in the matrix between the fibres and are broken resin layers amid the fibres. From a comparison of figure 7-4 (b) and (d), it can be seen that the coupons conditioned at 95%RH, in order to achieve high moisture content, have cleaner fibres i.e. more of the matrix has de-bonded, this can be attributed to the weakening of the fibre-matrix interface by the absorbed moisture.

7.6 Mechanical Property Predictions and Validation

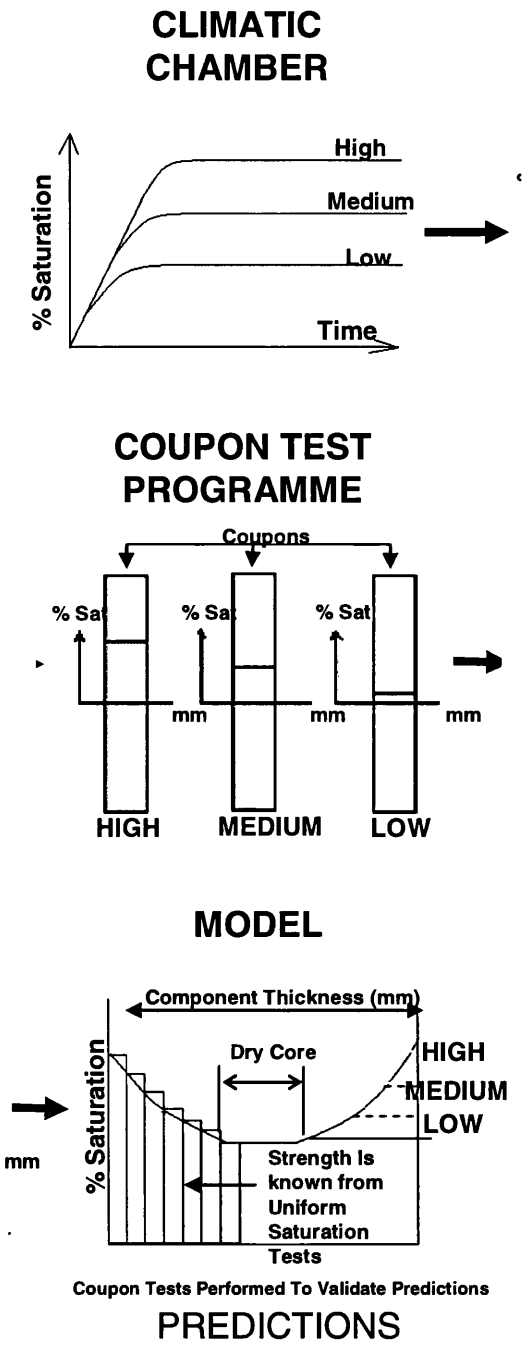

Figure 7-5: Schematic representation of property prediction and validation.

Figure 7-5 shows a schematic representation of what was to be achieved during this PhD research programme. The first phase of the programme generated mechanical property data for different levels of equilibrium moisture content, (see Chapter 5). From these results relationships for strength/stiffness as a function of moisture were derived (presented in table 6-2). These relationships were employed to perform mechanical property predictions for coupons with a distribution of moisture through

the thickness, a simple gauge section averaging approach and also by using a CLA approach, the results of which can be found in table 6-3. Finally, mechanical testing was performed to simulate the predictions and validate the approach. These results can be found in Chapter 6.5.

7.6.1 Prediction of Moisture Profiles

The ability to predict the moisture content and its distribution within a laminate throughout its lifetime, when exposed to steady state or changeable environments, is important for determining safe allowables on structural strengths for CFRP primary aircraft structures. Moisture prediction for the laminates studied here can be based on the classical theory of diffusion, described by Fick's Second Law (equation 2-8).

With knowledge of materials diffusion constants (i.e. D_x and M_{max}) and that the moisture uptake within the material could be modeled by Fick's Second Law (figure 5-5 and figure 5-6), it was possible to predict though-the-thickness moisture content using an error function analytical solution to Fick's Second Law. The derived curves provide the basis for predicting mechanical properties of composite laminates that have a distribution of moisture though-the-thickness.

7.6.2 Mechanical Properties Predictions

Mathematical relationships were derived from equilibrium saturation testing (see table 6-2). These relationships formed the basis of the mechanical property predictions. Variability in composite mechanical property data may result from a number of sources including variability in fabrication, batch-to-batch variability of raw materials, testing variability and variability intrinsic to the material. It is important to acknowledge this variability when designing with composites and to incorporate possible variability in design values of material properties. For these reasons, statistical analyses are often used in conjunction with test data acquisition. Airbus typically uses B-basis values in the derivation of design values. Procedures for calculating statistically based material properties are well-established[47] and with an appropriately designed test program, statistical procedures can account for some of these sources of variability. For more robust predictions, it would be recommended that multiple batches of coupons be tested to reduce scatter, produce B-basis values and increase data dependability.

Validation of predictions were carried out by performing mechanical testing on coupons that had been conditioned at 70°C and 85%RH for the times specified in table 6-4, in order to simulate the modelled moisture distributions in Chapter 6.1. From the initial mechanical property predictions performed in Chapter 6.2, it can be seen that a profile of properties may exist through the thickness of the material due to the distribution of moisture (see figure 6-5 to figure 6-11). Therefore, if a part is never going to reach equilibrium saturation, the HOT/WET K_{EKDF} factors applied may be considered over conservative. Therefore, the alternative approach suggested here may provide a possibility to reduce conservatism and save weight. The following sections (7.6.2.1 to 7.6.2.3) discuss the predictions performed for each coupon type.

7.6.2.1 90° Tensile Strength Predictions

As stated in section 6.5, additional 8mm thick test coupons (manufactured from Material C) were employed in addition to the coupon types used in the initial set of tests. The thicker coupons were used to observe greater resolution between the different moisture profiles. Material C is identical in terms of mechanical properties and fibre volume fraction to Material A and was utilized because it has a greater cpt (0.25mm). Thus, thicker laminates could be manufactured with less plies. The material has the same mechanical properties/resin system and V_f so the data set was analysed as one.

Table 6-6 lists the validation experimental testing results for the 2mm and 8mm thick 90° tension coupons, showing measured mean strength and modulus along with the measured standard deviations of the data sets. The 2mm coupons absorbed 0.05 and 0.08wt% moisture for 50% and 25% dry-core respectively. The 8mm thick coupons absorbed 0.08, 0.13 and 0.2wt% moisture for 75%, 50% and 25% dry-core respectively. This property is very sensitive to moisture content, as can be seen from the equilibrium saturated results listed in table 5-8. This sensitivity is also seen in the moisture profile cases, as the coupons conditioned with a 25% dry-core show a reduction of around 15% in strength compared to the 50% dry-core coupons.

Table 6-3 shows the mechanical property predictions for the 90° tension tests. The mean experimental values for the 2mm thick 90° tension tests were 70.7±4.5 and 60.4±6.5MPa for 50 and 25% dry-core respectively. For the 8mm thick coupons,

mean strengths of 73.3±5.7, 71.4±5.4 and 65.6±5.3MPa were measured for 75, 50 and 25% dry-core respectively. Both macro-mechanical and CLA predictions show a very clear trend of decreasing strength with increasing moisture content, in a similar manner to the experimental data. It is worth noting that the experimental oven dry strength of 55.1±7.4MPa is lower than the strengths of the laminates containing moisture profiles. This may be attributed to better quality laminates, as the OD test coupons were cut with a diamond saw and the coupons used for the validation testing were cut via water-jet cutting; a process giving a superior edge finish. This test type is susceptible to coupon quality and any small edge delamination could be the cause of a premature failure, thus contributing to scatter in the data set. It can be seen that the scatter in the test results for the diamond cut specimens is quite large: up to 13% for the OD case. This has been observed throughout the test programme when analysing 90° tension test results, therefore the scatter has to be attributed to the test type or the material quality. Due to this, the observations made here do not comment on the absolute accuracy of the model predictions for this coupon type; they refer only to the reliability of the model validations using the available experimental data and the observed and predicted trends.

Table 6-3 shows the range of macro-mechanical predictions to be 8.6MPa and the standard deviations of the experimental datasets are between 4.5 and 7MPa. Therefore it is difficult to unequivocally validate any individual prediction for the specified moisture profiles, since the range of predicted data is slightly greater than the scatter of the experimental data. However, it allows for general trends to be compared. The range of the predictions made using the CLA approach is 21MPa; this is greater than the experimental standard deviation (of 4.5-7MPa), which should allow a more confident validation of the CLA model using the available experimental data. It was observed that the CLA predictions are consistently more conservative when compared to the macro-mechanical predictions. This is due to CLA employing a first ply failure (FPF) criterion and thus, once the weakest (in this case the outermost saturated) ply has failed, final failure is assumed, in the case of a UD laminate.

When a 90° tension coupon has a profile of moisture TTT there is a near 40% reduction in strength from the saturated outer ply, as compared to the dry plies in the core of the laminate (see figure 6-5 to 6-9). CLA predicts failure to occur at the outer most ply by applying a first ply failure (FPF) criterion, after which no further

load can be maintained. The analysis therefore reports failure strength based on the weakest ply (in the case of the UD lay-ups, the ply with the most moisture content being the outer most ply). This strength is considerably lower than the one predicted by the macro-mechanical approach and much lower than the experimentally measured value. This FPF criterion does not account for any material still being able to carry load in the structure, but for UD laminates in this situation, the inner plies are "dry/full strength" and may be capable of doing so.

Confidence in model validation depends on having low scatter in experimental data and a higher range of predicted values. Due to the high scatter and variation in cutting processes between the coupons types, it is concluded that further, more robust testing would be required to validate the accuracy of the predictions.

7.6.2.2 In-Plane Shear Strength Predictions

Table 6-7 lists the validation testing results for the in-plane shear (IPS) tests; these include mean strength and modulus results, the calculated standard deviations for the data sets and the measured moisture contents of the coupons. It should be noted that the amount of moisture absorbed by the validation test coupons was relatively small, being 0.04 and 0.07wt% for a 50 and 25% dry-core (DC) respectively. The mean experimental values for in-plane shear strength (given in table 6-3) were 85.3±1.1, 83.7±1.8 and 83.7±1.6MPa for OD, 50% and 25% dry-core respectively. A comparison with the macro-mechanical predicted values of 83.9MPa (OD), 81.9MPa (50%DC) and 80.6MPa (25%DC) shows a similar decrease in strength for a given profile of saturation. It is also worth noting that the standard deviations of the experimental results are close to encompassing these predicted values. The CLA predicted values of 83.3MPa (OD), 78.5MPa (50%DC) and 77.5MPa (25%DC) are consistently lower than the previous predictions, due to the FPF criteria that classical laminate theory applies. These predictions are outside the standard deviations of the experimental data, but show a decrease with increasing wt% moisture. IPS is quite a sensitive parameter to moisture absorption; from table 5-10 it can be seen that when conditioned to equilibrium saturation at 85%RH a 17% reduction in IPS strength is observed.

Table 6-3 shows the range of the macro-mechanical strength predictions is 3.3MPa and the range of the predictions made using the CLA approach is 5.8MPa. Both are

greater than the standard deviation of the experimental data (1.1-1.8MPa). For in plane shear strength the macro-mechanical predictions give a reasonable match to the experimental test data, but the CLA model overestimates the reduction in strength. Since the range using CLA is greater, this allows for a more confident validation of the CLA model using the experimental data, but due to the small range in experimental data, (1.6MPa) it is difficult to robustly validate the predictions. In order to attempt to improve the range of the experimental data, the thickness of the coupon could be increased from the standard 1.5mm. This may increase the resolution of the experimental data set, as was done for the 90° tension tests where 8mm test coupons were used. Also the duration of the conditioning could be extended to give a shallower moisture profile (i.e. less dry-core). This would provide a greater range of properties with which to compare the predicted values. Figure 7-6 shows predictions of IPS strength and moisture content for a range of conditioning times (up to 60 hours) and the associated relationship.

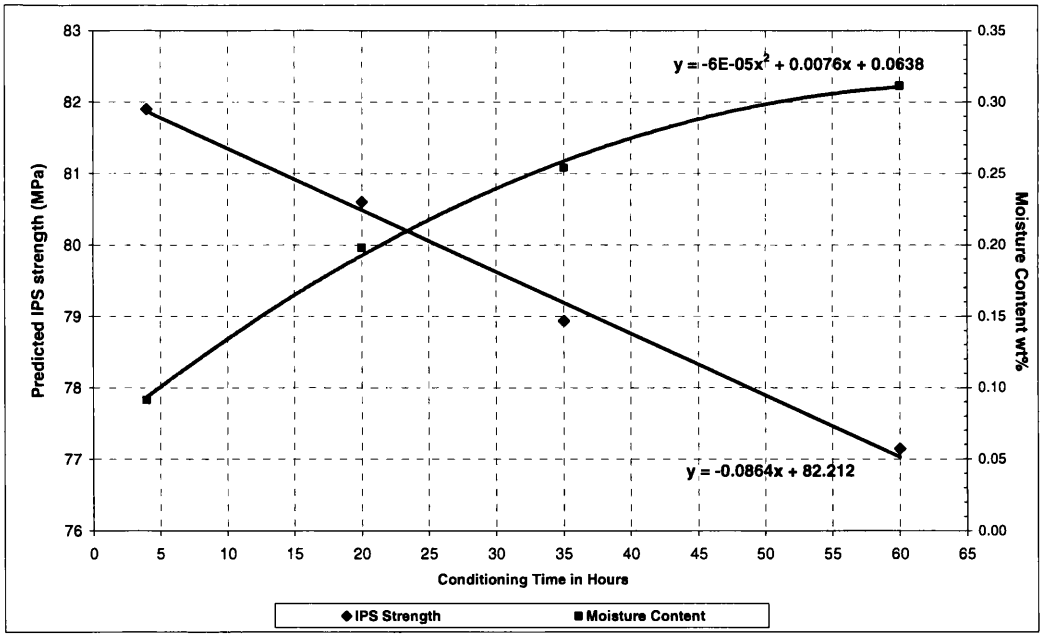

Figure 7-6: Effect of conditioning time on IPS strength predictions.

7.6.2.3 Multi-directional Laminate Strength Predictions

The macro-mechanical predictions for multidirectional lay-up coupons rely on F_{xx}^{oht} and F_{xx}^{ohc} equations given in table 6-2. These equations are only applicable for the geometric features (i.e. lay-up and hole radius) of the test coupons used in this work. Since failure in composite materials is lay-up dependent, the macro-mechanical approach cannot be used for any multi-directional laminate, without

producing a set of equilibrium saturation curves for the coupon geometry, in order to generate the moisture relationship equation. However by employing the CLA approach, any change in lay-up can be accounted for as only UD (lamina) coupon data is required, which has been generated in this work (although for open hole coupons a new factor would need to be calculated to account for any change in hole diameter). Results show that using the Material A lamina property relationships to predict values for the multi-directional properties (even though these coupons were made from material B – which is a woven fabric) in conjunction with CLA predictions provides a good approximation to the experimental results when compared to the predicted final failure values.

A knockdown factor K_t, derived from the dry laminate prediction was applied to the CLA predicted results, in order to account for the presence of the hole. The knockdown factor is partially calculated from a laminate analysis result and to improve accuracy and reliability of the predictions it is recommended by the author that further experimental work be performed using un-notched coupons. This would provide a better understanding of the strength reduction resulting from the presence of a hole. Also, for more robust validation, it would be beneficial to perform further un-notched multidirectional testing on coupons manufactured from Material A, as this material was used to experimentally measure the lamina properties and derive the relationships listed in table 6-2.

A) Open Hole Tension

Table 6-8 lists the validation testing experimental results for the OHT tests, showing mean strength results with standard deviations of the data sets and the measured moisture content of the coupons. It should be noted that the amount of moisture absorbed is 0.08 and 0.13wt% for a 50 and 25% dry-core respectively.

Table 6-3 shows the predicted open-hole tension strength using the macro-mechanical and the CLA approach. The main observations from table 6-3 are the mean experimentally measured values for open hole tensile strength; 336±8, 335±13 and 329±12MPa (for OD, 50% and 25%DC respectively). These compare well to the macro-mechanical predictions of 332, 342 and 340MPa (for OD, 50% and 25%DC respectively) and the CLA predicted values of 336, 331 and 329MPa (for OD, 50% and 25%DC respectively). The OHT CLA predictions show a trend of decreasing strength with increasing wt% moisture content, whereas the macro-

mechanical predictions show an increase in strength with a moisture profile. Another key observation is that the experimental standard deviations measured, encompass all the corresponding predicted values for both methods of calculation.

However, the standard deviations measured are greater than the variation in the means, thus making it difficult to truly validate these property predictions. Table 6-3 shows the range of the macro-mechanical predictions is 10MPa and 7MPa for the predictions using the CLA approach. As the standard deviations of the experimental datasets are between 8 and 13MPa it is difficult to validate any individual prediction for the specified moisture profiles, since the range of predicted data is less than the scatter of the experimental data. Also, this property did not see any significant decrease in strength due to moisture content, i.e. because the OHT strength is fairly insensitive to moisture content, as can be seen from table 5-12.

B) Open Hole Compression

Table 6-8 lists the validation experimental results for the OHC tests, showing the mean strength results with standard deviations of the data sets and also the measured moisture content of the coupons. It should be noted that the amount of moisture absorbed was 0.06 and 0.08wt% for a 50 and 25% dry-core respectively.

Table 6-3 shows the predicted open hole compression strengths using the macro-mechanical and the CLA approach. The mean experimentally measured values for open hole compression strength are 317±16, 312±8 and 304±3MPa (for OD, 50% and 25%DC) and these compare well to the macro-mechanical predicted values of 314, 311 and 308MPa (for OD, 50% and 25%DC respectively) and also to the CLA predicted values of 298, 294 and 290MPa (for OD, 50% and 25%DC respectively). The OHC predictions show a trend of decreasing strength with increasing wt% moisture content. It can be seen that the macro-mechanical predictions fall within the standard deviation of the experimental data; however the CLA predictions consistently fall outside the standard deviations, being lower than the actual experimental values.

It is shown in table 6-3 that the range of the macro-mechanical predictions is 6MPa and 8MPa for the predictions using the CLA approach. Since the standard deviation of the experimental dataset is between 3-16MPa it is difficult to validate any

individual prediction for the specified moisture profiles, since the standard deviation of the experimental data set is generally larger than the range of the predicted data.

7.6.3 Failure Criteria Comparison

As out lined in section 6.4 a wide range of failure criteria is available for the analysis of composite materials. For this work the Maximum Stress Criteria was chosen for the CLA predictions. The success of CLA depends on the appropriateness of the selected failure criterion. A comparison of different failure criteria is shown in table 7-7; two independent criteria (Max stress and Max strain) and a fully interactive failure criterion (Tsai-Hill). Predictions were performed using a 4mm thick quasi-isotropic laminate (using the RT/dry lamina properties measured via mechanical testing in section 5). Predictions of the ultimate failure (ULF) strength were performed for uniaxial normal and shear loading.

Table 7-7: Comparison of failure criterions.

Uniaxial Loading	Max Stress		Max Strain		Tsai Hill	
	ULF (MPa)	$\sigma_{theo}/\sigma_{exp}$	ULF (MPa)	$\sigma_{theo}/\sigma_{exp}$	ULF (MPa)	$\sigma_{theo}/\sigma_{exp}$
Tension	336	1.00	336	1.00	336	1.00
Compression	298	0.94	298	0.94	336	1.06
Shear	229	-	226	-	213	-

A ratio of theoretical stress, σ_{theo}, to experimental stress, σ_{exp}, was calculated (using the RT/dry open hole tension and compression experimental test results).

The results show for the tension case all failure criteria are in agreement with each other and with experimental data. For the compression case the Max stress and Max strain are in agreement and both predict lower failure strength than the experimentally measured results, whereas the Tsai-Hill criteria is unconservative and over estimates the ultimate failure strength. For the shear case all criteria give different results, the two independent criteria are quite similar within 3MPa of each other but the interactive Tsai-Hill criteria gives a much more conservative prediction for ultimate failure.

All three failure theories tested are in reasonable agreement. In general, it is difficult to reach definitive conclusions on the applicability of the various theories based on comparison with the limited experimental data available.

7.6.4 Comparison of Models

Both the macro-mechanical and CLA models give reasonable agreement with experimental data and show similar trends in strength reduction. However the CLA predictions are consistently more conservative due to the first ply failure criterion (which is usually a matrix dominated failure mode and therefore more sensitive to moisture) that is applied during calculation. Thus, the predictions given are always slightly lower that the predictions made using the simplified averaging technique applied in the macro-mechanical approach. But as the macro-mechanical model does not take into account changes in coupon lay-up, it is not practical for application to multi-directional laminates, whereas the CLA model uses UD lamina properties to predict laminate strength for any laminate lay-up.

The mechanical property predictions performed in this work have shown a good comparability to the experimental data, with similar reductions in strength observed for a given profile of moisture. The predicted strengths also fall within the measured standard deviation of the experimental data in a significant proportion of the results. The reliability of the model validations can only be assessed using the available experimental data and the greater the range of the experimental results the more reliable the model validation. Since the variation in predicted values for each material were so small in some cases (i.e. less than the scatter of the measured strengths) the predicted values cannot be fully validated.

To provide unequivocal validation of the predicted results, further work is recommended, in which one should attempt to reduce the scatter of the measured experimental data and thus reduce the standard deviations and/or study samples over a wider range of TTT moisture contents, for which there would be a much greater variation in the predicted strengths. However, the approach/model used in this programme of work for performing the predictions has provided promising initial results.

7.7 Case Study

Airbus state that a worst case aircraft lifecycle is 20 years at 20°C and 85%RH (which represents an average of Tropical and European climates – considered to be the worst average climate condition). This worst case lifecycle can be simulated by accelerated conditioning for 1000 hours at 70°C and 85%RH[11]. As a thick composite structure will not reach saturation in its lifetime, case studies were performed to compare predicted properties, using the new proposed moisture profile approach and the current approach (which is to apply an equilibrium HOT/WET knockdown factor to all properties). These case studies were performed using 1000 hours at 70°C and 85%RH conditioning regime to produce a moisture profile through the laminates.

7.7.1 Case Study 1 - 8mm Thick Laminate

To show the potential benefits of using the proposed new method, a case study was performed for 8mm thick laminates with unidirectional and quasi-isotropic lay-up. Specifications of the laminates can be found in table 7-8. Predictions were performed using environmental conditions 70°C/85%RH and the associated diffusion constants calculated in section 5.2, which are as follows:

M_{max} = 0.606 wt%
D_x = 6.67 x 10^{-7} mm^2/s

Table 7-8: Laminate specifications used for predictions.

Lay-up	Symbol	Stacking sequence	No. Plies	Thickness mm	Cure Ply Thickness (cpt) mm
Unidirectional	UD	$[90]_{32}$	32	8	0.25
Quasi-isotropic	QI	$[45/0/-45/90]_{4S}$	32	8	0.25

Predictions were performed using the CLA model (using the process defined in section 6.4.3). The three following cases were considered:

a) Dry; M_{max}=0wt%.
b) Equilibrium saturated at 70°C/85%RH; M_{max} =0.606wt%.
c) Moisture profile of 1000 hours at 70°C/85%RH (which is equivalent to 20 years at 20°C/85%RH, which simulates an aircraft lifecycle[11]).

Case (a) is the dry/baseline properties, case (b) is the current methodology employed at Airbus and case (c) the new proposed way of working.

The moisture profile (case c) through an 8mm laminate was predicted using the error function solution to Fick's Second Law (equation *2-11*) and is shown in figure 7-7. The laminate was then discretized by the cure ply thickness and the amount of moisture present in each ply was calculated (figure 7-7). This individual ply moisture content was then used in the derived property/moisture relationships (see table 6-2) in order to calculate a unique set of mechanical properties for each ply. Classical Laminate Analysis was then performed, using the unique set of properties calculated for each ply. The results of the CLA predictions are shown in table 7-9. Tensile and shear strengths and moduli are shown for comparison. The first ply (FPF) and ultimate ply (ULF) failure strengths are listed.

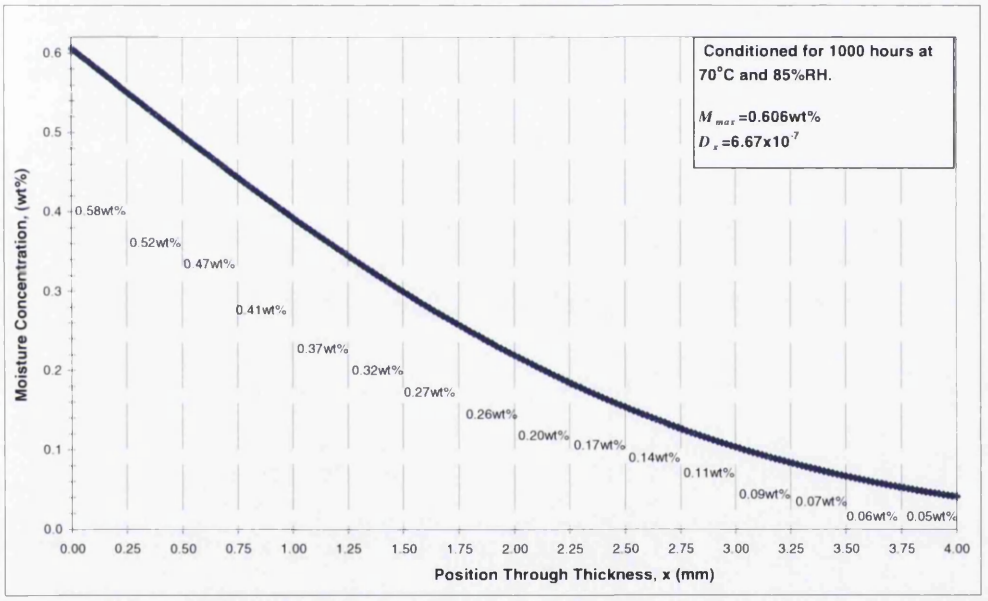

Figure 7-7: Moisture distribution in an 8mm thick laminate (1000hrs at 70°C and 85%RH).

Table 7-9: CLA model predictions for 8mm laminate.

Lay-up	Environmental Condition	Strength				Stiffness		
		Tensile		Shear		E_2	E_1	G_{12}
		FPF	ULF	FPF	ULF			
		MPa	MPa	MPa	MPa	GPa	GPa	GPa
UD	a) DRY	58.0	58.0	84.0	84.0	9.3	151.0	5.1
	b) SAT	31.0	31.0	70.0	70.0	8.9	143.0	4.7
	c) 1000hrs	32.8	33.5	73.2	73.2	9.1	146.4	4.9
QI	a) DRY	399.0	792.1	358.5	358.5	57.6	57.6	22.0
	b) SAT	211.0	792.1	214.9	326.1	54.5	54.5	20.7
	c) 1000hrs	275.2	792.1	259.3	326.3	55.9	55.9	21.2

For an 8mm thick UD laminate, table 7-9 shows the dry (case a) predicted ULF tensile strength was 58MPa and the saturated (case b) ULF was 31MPa; all plies in these laminates failed simultaneously. For the UD laminate with a moisture profile of 1000 hours (case c), an ULF of 33.5MPa was predicted (only plies 1 and 32 failed first), giving an 8% strength improvement compared to the conservative equilibrium saturated case. A similar improvement is seen for the UD shear strengths. The UD laminate moduli E_2, E_1, and G_{12} were predicted as 9.3, 151 and 5.1GPa for the dry case and 8.9, 143 and 4.7GPa for the saturated case. For the moisture profile case, the moduli E_2, E_1, and G_{12} were all slightly stiffer (up to 5%) than the saturated case.

For the QI lay-up laminate, the tensile strength FPF for was predicted as 399.5, 211.1 and 275.2MPa for the dry, saturated and moisture profile cases respectively; providing a 23% increase in tensile strength, if designing to the worst case environmental profile instead of applying the conservative saturated HOT/WET knockdown. The QI laminate shear strength FPF for dry, saturated and moisture profile cases was predicted as 358.5, 214.9 and 259.3MPa respectively. This is a 17% improvement in strength for an 8mm laminate with a moisture profile compared to the saturated strength. As ultimate failure strength in this laminate lay-up is driven by the 0° plies (which were not affected by moisture, see figure 5-9), no difference is noticed for ULF in both tensile and shear strength. The moduli E_2, E_1 and G_{12} all see a 2-3% increase when comparing the 1000 hour profile case to an equilibrium saturated case.

7.7.1.1 Potential Weight Savings

As the results in table 7-9 show, a benefit can be obtained from applying a moisture profile approach to design. This benefit can be quantified in terms of a weight saving, described here.

For an initial estimate of the reduced thickness (t_2) capable of carrying the original loads (of the saturated material), the following ratio was used:

$$t_2 = \frac{\sigma_{SAT}}{\sigma_{1000hrs}} \times t_1 \qquad 7\text{-}2$$

t_1 is the original coupon thickness, mm

t_2 is the optimised coupon thickness, mm

σ_{SAT} is the strength of the equilibrium saturated material, MPa

$\sigma_{1000hrs}$ is the strength of the material that has been exposed to 85%RH/70°C for 1000 hours, MPa.

Table 7-10 list the values of t_2. However, Airbus stacking sequence rules state laminates have to be balanced and symmetrical, so optimisation must be performed to within two plies (0.5mm). Values t_3 in table 7-10 are the optimised coupon thicknesses obeying the stacking sequence rules.

A second iteration of CLA predictions were performed using the new material thickness t_3, subjected to a 1000 hour moisture profile, as a thinner part will contain a higher wt% moisture content than a thicker part, making the previous strength calculations (table 7-9) slightly optimistic. These optimised coupon strength predictions are listed in table 7-10.

Table 7-10: Possible weight savings in an 8mm thick laminate.

Property	Lay-up	Failure Type	Optimised coupon thickness, t_2 (mm)	Optimised coupon thickness, t_3 (mm)	Optimised coupon strength (MPa)	Weight saving (%)
Tensile Strength	UD	FPF	7.52	7.5	32.8	6
		ULF	7.29	7.5	33.4	6
	QI	FPF	6.14	6.5	264.2	19
		ULF	8.00	-	-	0
Shear Strength	UD	FPF	7.67	7.5	73.1	6
		ULF	7.67	7.5	73.1	6
	QI	FPF	6.64	7.0	240.0	13
		ULF	8.00	-	-	0

A comparison of the optimised coupon strengths in table 7-10 to the first iteration of moisture profile strengths (table 7-9) shows that equation 7-2 gives a reasonable approximation to the strengths calculated using the CLA approach.

For a coupon with dimensions of 300 x 25 x 8mm (length x width x thickness) the coupon mass can be calculated using:

$$Mass = Volume \times density \qquad 7\text{-}3$$

The material density is 1590Kg/m^3, giving an original coupon weight of 95.4g. The mass of the optimised coupons were calculated and compared to that of the original coupon mass to determine a percentage weight saving, shown in table 7-10. The thinner optimised coupon strengths are still greater than that of the saturated coupon, showing that a weight saving of between 6 and 20% is achievable using the moisture profile approach, even for relatively thin 8mm laminates.

If designing a coupon to fail due to 90° tension loads, the UD coupon could be optimised when designing to ULF, by reducing the thickness to 7.29mm. The cure-ply-thickness (cpt) of the lamina is 0.25mm, meaning two plies could be removed and a weight saving of around 6% could be realised whilst still being able to carry the same load. If designing to FPF for a QI coupon failing due to 90° tension, the laminate thickness could be reduced to 6.14mm when using a 1000 hour moisture profile. This could potentially offer savings of 23% compared to the 8mm fully saturated coupon. Obeying laminate stacking sequence rules six plies could be removed, offering a 19% weight saving.

If designing the laminate to account for shear loading, the UD laminate designed with a moisture profile could offer a 6% weight reduction, as compared to the equilibrium saturated laminate. If the QI laminate were designed for shear loading, using the FPF criterion, the laminate thickness could be optimised to 6.64mm if designed to a 1000 hour moisture profile. This could potentially offer weight savings of 17% compared to an 8mm laminate. Obeying laminate stacking sequence rules four plies could be removed, offering a 13% weight saving.

7.7.2 Case Study 2 - 70mm Thick Laminate

To quantify the possible weight savings for typical in-service components, the predictions performed in section 7.7.1 were repeated for a 70mm thick laminate (which is the typical thickness of a composite wing-box structure). Details of the laminates used in the prediction are shown in table 7-11.

Table 7-11: Details of laminates used for predictions.

Lay-up	Symbol	Stacking sequence	No. Plies	Thickness mm	cpt mm
Unidirectional	UD	$[90]_{280}$	280	70	0.25
Quasi-isotropic	QI	$[45/0/-45/90]_{35S}$	280	70	0.25

If a 70mm thick laminate was subjected to the worst case aircraft lifecycle conditioning time (1000 hours at 70°C/85%RH), the moisture profile would be as shown in figure 7-8 (predicted using equation *2-11*). At a distance of 10mm in from the laminate edge a 0.25mm thick ply would contain less than $2x10^{-6}$wt% moisture, while at 18.5mm from the laminate edge there was no measurable moisture.

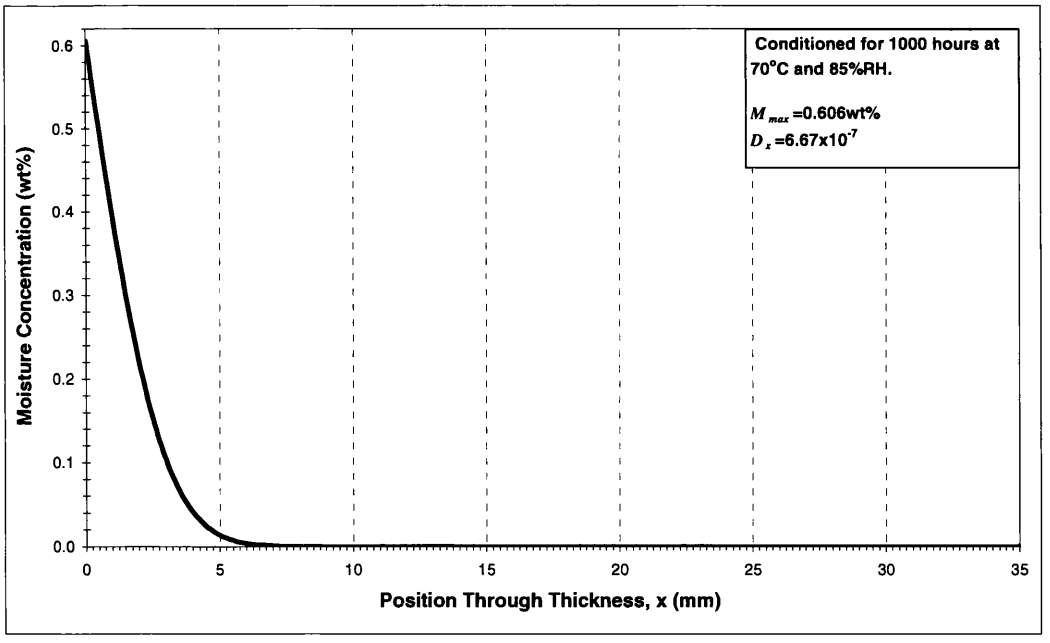

Figure 7-8: Moisture distribution in a 70mm thick laminate (1000 hrs at 70°C & 85%RH).

The predicted dry, equilibrium saturated and 1000 hour moisture profile tension and shear properties for UD and QI lay-up 70mm thick laminates are listed in table 7-12. Similar trends to the 8mm thick laminate are observed, however the 1000 hour

profile case for the 70mm predictions shows a greater strength benefit over the saturated case than the 8mm predictions. Also, the stiffnesses predicted for the moisture profile case in the 70mm laminate are approaching that of a dry laminate.

Using the procedure described in section 7.7.1.1, the laminate thickness was optimised and the potential weight savings were calculated (shown in table 7-13). Similar results to the 8mm thick coupons are observed; however greater weight savings are achievable for the thicker laminate, due to the larger volume of full strength material about the mid-plane of the laminate.

Table 7-12: CLA predictions for a 70mm thick laminate.

LAY-UP	ENVIRONMENTAL CONDITION	STRENGTH				STIFFNESS		
		Tensile		Shear		E_2	E_1	G_{12}
		FPF	ULF	FPF	ULF			
		MPa	MPa	MPa	MPa	GPa	GPa	GPa
UD	DRY	58.0	58.0	84.0	84.0	9.3	151.0	5.1
	SAT	31.0	31.0	70.0	70.0	8.9	143.0	4.7
	1000hrs	32.4	50.2	76.4	76.9	9.2	150.5	5.1
QI	DRY	399.0	792.1	358.5	358.5	57.6	57.6	22.0
	SAT	211.0	792.1	214.9	326.1	54.5	54.5	20.7
	1000hrs	287.7	792.1	268.3	350.5	57.6	57.6	22.0

Table 7-13: Possible weight savings in a 70mm thick laminate.

Property	Lay-up	Failure Type	Optimised coupon thickness, t_2 (mm)	Optimised coupon thickness, t_3 (mm)	Optimised coupon strength (MPa)	Weight saving (%)
Tensile Strength	UD	FPF	67.07	67.0	32.6	4
		ULF	43.22	43.5	46.9	38
	QI	FPF	51.34	51.5	290.1	26
		ULF	70.00	-	-	-
Shear Strength	UD	FPF	64.12	64.5	76.4	8
		ULF	63.73	64.0	76.8	9
	QI	FPF	56.08	56.5	266.2	19
		ULF	65.12	65.5	347.8	6

Using the conservative design approach, a long range airliner wing would have a wing set weight of approximately 8000kg. Assuming that the maximum weight saving outlined above will not be achieved for all components (due to thickness dependence), let us assume an average weight saving of 14% using the proposed new design approach. This would result in a new weight of 6600kg, giving a saving of 1400kg per aircraft. Assuming a short range mission, a tonne of weight will

produce around 6300 tonnes of CO_2 over an aircraft life. Therefore each aircraft would save around 8820 tonnes of CO_2 over its lifetime, making a significant contribution to current air quality targets. The ACARE[134] industry goal for 2020 is 50% reduction in CO_2 emissions per passenger-kilometre (which means a 50% cut in fuel consumption in the new aircraft of 2020).

These weight savings show an improvement over the HOT/WET equilibrium saturated design approach, however in practice other design drivers would need to be considered for composites, which may mean that the full potential demonstrated here could not be capitalised upon. Furthermore, the failure mode and subsequent critical design drivers for a component may change when applying these principles to a failure that is unaffected by environmental degradation, such as a 0^{o} fibre orientated failure, where the fibres maintain a relatively unchanged strength and stiffness.

7.7.3 Effect of Thickness on Strength and Stiffness

From the case studies performed in sections 7.7.1 and 7.7.2 it was observed that for the 70mm thick laminate, some properties saw a significant improvement compared to 8mm thick coupons. Figure 7-9 plots the percentage strength increase calculated using a moisture profile approach compared to a saturated case, for each of the predicted properties.

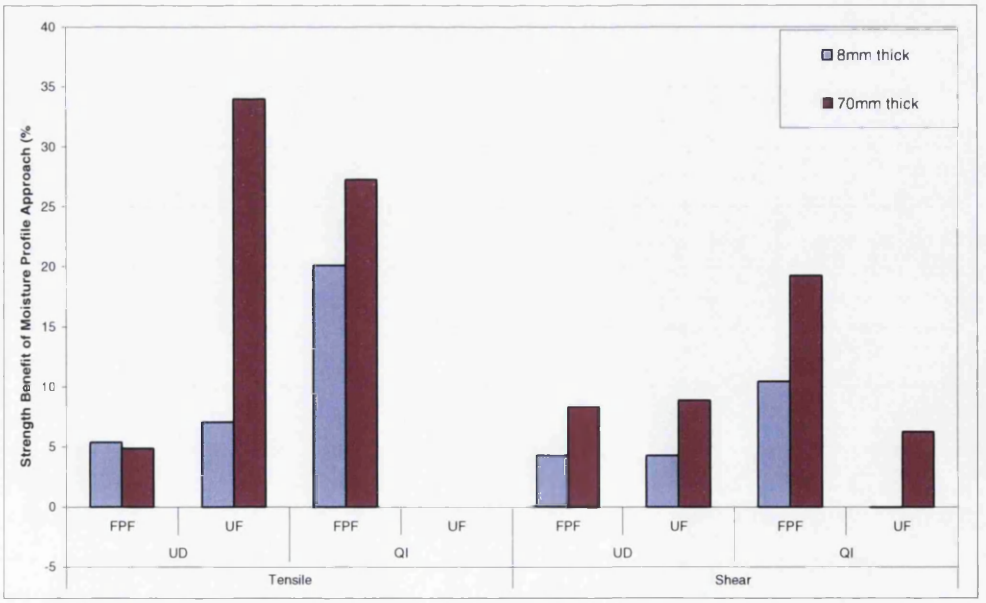

Figure 7-9: Strength benefit of a moisture profile (% improvement from saturated condition)

Figure 7-10 shows the tensile ultimate failure as a function of thickness for a UD laminate. For the material properties used in this investigation, there is 47% difference between the saturated and dry (0wt% moisture) tensile strength for a UD lay-up. For thick laminates, over 85% of the dry material strength can be utilised, by using a moisture profile approximation (1000 hours 70°C/85%RH) for 70mm thick laminate. The predicted properties (with a moisture profile) increase gradually with increasing thickness and approach the dry strengths for thick laminates. This is due to this property being matrix dominated and very sensitive to moisture; even with less than 0.1wt% moisture content a reduction in strength is observed.

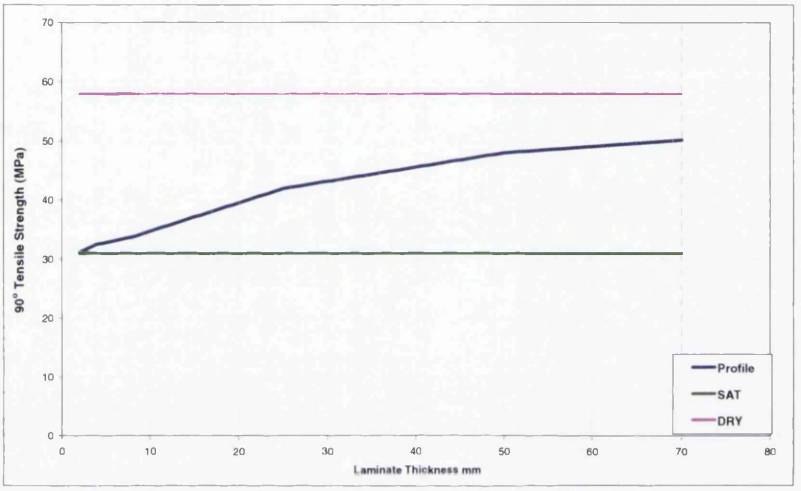

Figure 7-10: UD tensile ULF strength as a function of laminate thickness.

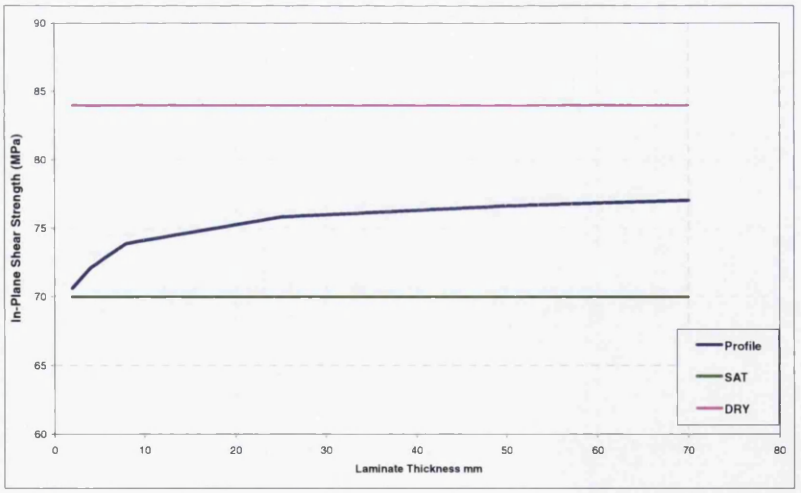

Figure 7-11: UD In-plane shear ULF strength as a function of laminate thickness.

Figure 7-11 and figure 7-12 shows ULF in-plane shear strength as a function of thickness for UD and QI lay-up laminates respectively. The UD in-plane shear has a 17% difference between saturated and dry properties. With a moisture profile

approach, 50% of the Dry strength can be utilised for thicker laminates. However, for UD in-plane shear, the predicted moisture profile properties approach that of the predicted dry laminate properties more quickly; at 30mm thick most of the 50% benefit is re-established. For the QI shear strength there is a 10% difference between saturated and dry properties and employing a moisture profile approach to design can utilise 80% of the strength of predicted dry properties for thicker laminates. The benefit increases gradually with increasing laminate thickness.

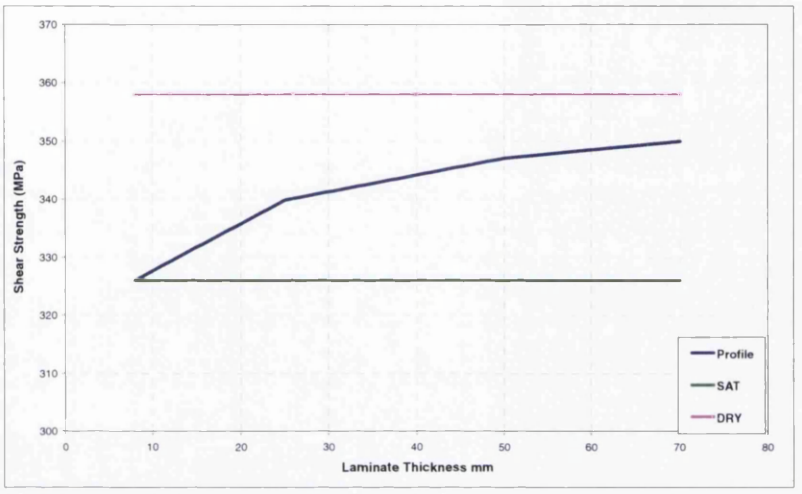

Figure 7-12: Shear ULF strength for a QI lay-up as a function of laminate thickness.

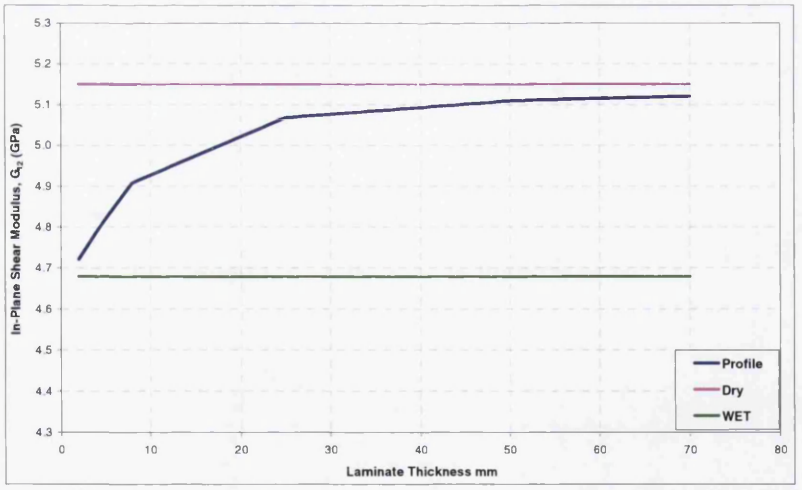

Figure 7-13: In-plane shear modulus as a function of laminate thickness.

Figure 7-13 shows the effect of thickness on the in-plane shear stiffness of UD laminates. For the properties used in this case, there is a 9% difference in G_{12} between the saturated and dry laminates. Again the moisture profile technique can utilise 90% of the stiffness predicted for dry, thick laminates. A similar plot is shown for the shear modulus of a quasi-isotropic laminate, where a 6% difference is

measured between wet and dry moduli, meaning for thick laminate 90% of the dry stiffness can be utilised if a moisture profile approach is used. The tensile moduli, as a function of laminate thickness for UD and QI laminates show similar trends.

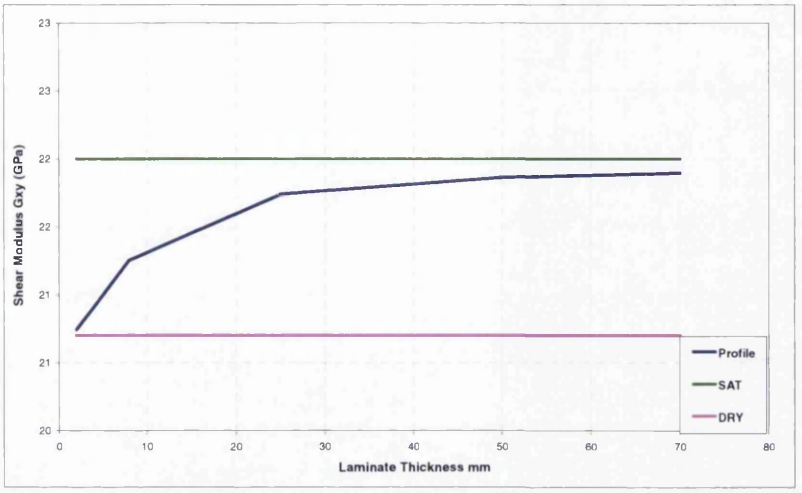

Figure 7-14: Shear modulus of a quasi-isotropic as a function of laminate thickness.

7.8 Thickness Sensitivity Study

To assess the effect laminate thickness has on the potential benefit of using a moisture profile approach in design, simulations were performed at 1000 hours and 70°C/85%RH for laminate thicknesses ranging from 2mm to 70mm. Figure 7-15 shows the plot of moisture content in laminates, as a function of laminate thickness (predicted using the diffusion constants specified in section 7.7). As can be seen the wt% moisture content in a laminate decreases as the thickness increases and can be modelled well using a power relationship of the form:

$$M = 1.0628(h)^{-0.8} \qquad 7\text{-}4$$

Where M is the moisture content and h is the laminate thickness.

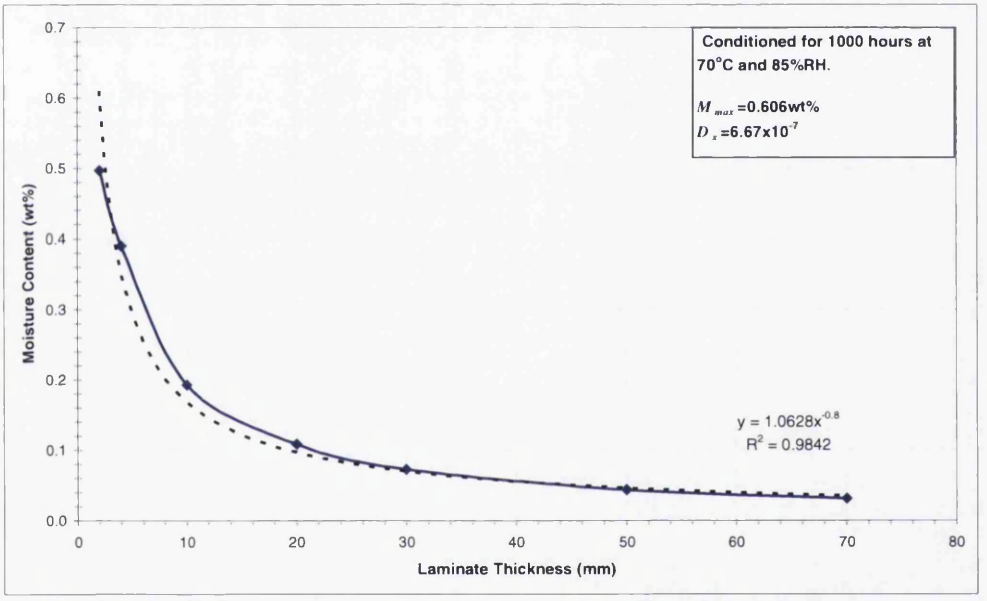

Figure 7-15: Moisture content as a function of laminate thickness.

Figure 7-16 shows the moisture distribution profiles for different laminate thicknesses (x / h) ranging from 0.5mm to 70mm. It can be seen that the moisture distribution curve steadily becomes flatter as the thickness of the laminate decreases. For a 0.5mm thick laminate after 1000 hours conditioning (at 70°C and 85%RH) the distribution is approaching equilibrium. However a 70mm thick laminate only has moisture present at the outer most plies leaving a dry, full strength laminate about the mid-plane. This reinforces the conservatism that is applied when

designing all parts to an equilibrium saturated condition. Laminate moisture content is a function of its thickness and should be taken account of during design.

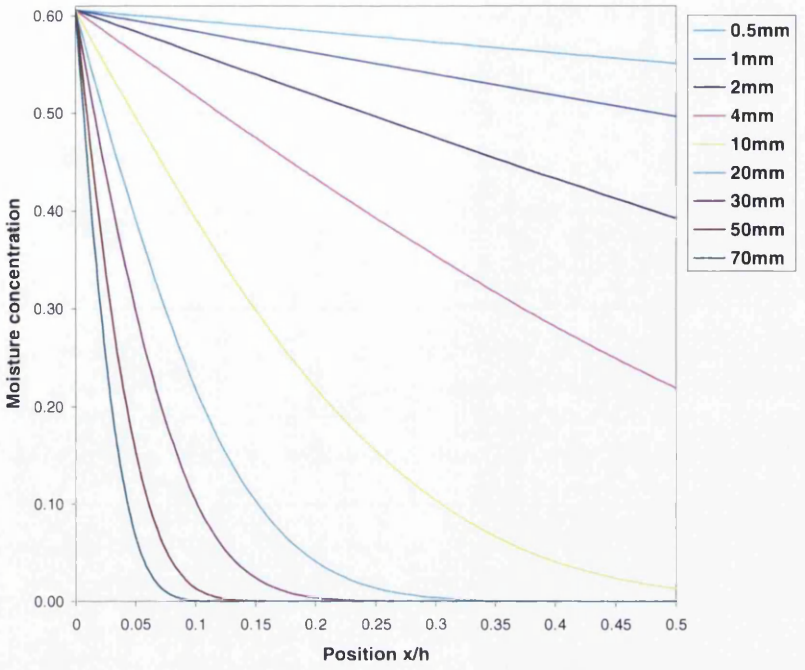

Figure 7-16: Moisture distribution profiles for different thickness laminates (exposure time of 1000hrs at 70°C/85%RH).

This work challenges conventional equilibrium saturated HOT/WET knockdown factors being applied to thick airframe structures. Airbus state that a worst case aircraft lifecycle is 20 years at 85%RH which can be simulated by 1000 hours at 70°C and 85RH[11]. It has been shown that with a moisture profile that simulates this worst case exposure, thick CFRP parts are not nearing saturation within their lifetime. Thus, applying equilibrium saturated HOT/WET knockdowns (which is the current methodology employed at Airbus) is introducing an unnecessary level of conservatism. If the approach proposed here were to be introduced, it has been shown that a definite weight saving could be realised. The aim of this work was to develop the ability to predict failure in a composite laminate with a moisture profile through-the-thickness. The methodology has proven promising, but for full model validation further studies and testing is recommended.

8 Conclusions

The research described in this thesis has provided new understanding in the following areas:

1. With respect to mechanical testing procedures, this work showed that the details of coupon/material handling prior to testing may have a significant influence on measured mechanical properties, due to moisture absorption from the atmosphere occurring during material storage and/or transit. This resulted in a new control procedure for all materials being implemented within Airbus prior to testing; a procedure that is currently in force for new testing campaigns.

2. In terms of the data generated, for the first time, a comprehensive database of environmentally degraded properties for carbon fibre reinforced epoxy now exists. As expected this data showed that the uptake of moisture in the materials studied was described well by Fick's Second Law and the properties most affected by moisture ingress were matrix-dominated properties.

3. In terms of property prediction, a novel enhancement of conventional approaches was used and the prediction of failure for a composite laminate with a distribution of moisture through-the-thickness was demonstrated, by extending classical laminate analysis techniques using experimentally derived moisture/properties relationships. This new approach has proved promising and further, more comprehensive experimental data would provide additional validation. This opens up a range of significant potential benefits for the use of such materials in airframe applications, particularly if the 'hot-wet' design criterion can be safely replaced by a less conservative technique.

Some of the key conclusions established during this programme are:

- The results for the diffusion constants are in accordance with diffusion theory, in that the maximum moisture content M_{max} is a direct function of the relative humidity and increased with increasing %RH.

- The transverse tensile strength, F_{2t} was most affected by the ingress of moisture, with a near 50% reduction in strength with a fully saturated moisture

content of 0.6wt%. This was attributed to interface degradation and plasticisation of the matrix due to moisture ingress.

- Another key result showed an initial increase of 10% in the σ_{ILSS} with ~0.2wt% absorbed moisture, with further moisture ingress (M_{max}=0.8wt %) the σ_{ILSS} decreased by 25% compared to the oven dried strength. Such information is a necessary prerequisite if improved design procedures are going to be developed in the future.

- It was found that moisture absorption led to a decrease of up to 5% in transverse and longitudinal modulus of the composite, owing to hydrolysis and plastizisation of the epoxy matrix.

- Stiffness and strength performance profiles, as a function of moisture content, were generated for a range of different levels of saturation; something that is rarely found in the literature. This is needed to fundamentally understand the effect on material performance, as well as providing mechanical data that can be used to model/predict the mechanical properties of a laminate.

- Limiting exposure to an uncontrolled environment (in terms of humidity and temperature) and monitoring environmental conditions prior to carrying out this type of test programme removes the possibility of any conditioning of the specimens occurring, other than that specified for the test. This removes any ambiguity in the level of moisture contained within a specimen, allowing confidence in the results.

- The mechanical property predictions performed in this work compared well with the experimental data, with similar reductions in strength observed for a given profile of moisture. The predicted strengths also fall within the measured standard deviation of the experimental data in a significant proportion of the results.

- The mechanical property predictions show promising results, however due to the scatter and variability in the test results, further more extensive experimentation is recommended to fully validate the approach for composite material mechanical property prediction.

9 Future Work

Further testing is currently being performed at Swansea University, in conjunction with Airbus and is focussing on material properties for varying temperatures and saturation levels.

9.1 Moisture Distribution Validation

To verify the moisture distribution through the thickness of the coupon the following approach could be used in future:

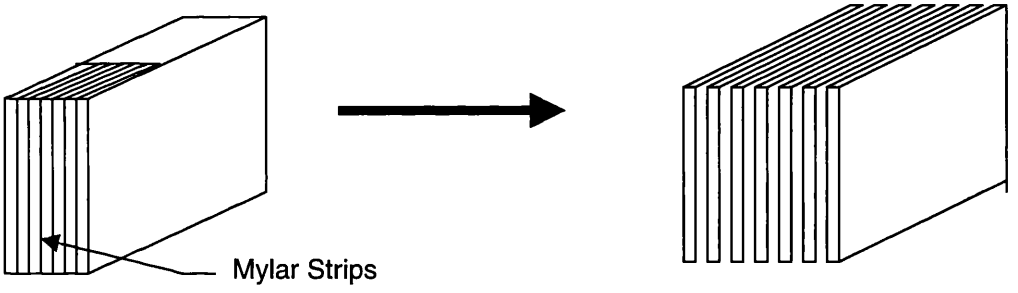

Figure 9-1: Moisture distribution verification

- Small coupons of thickness around 10mm.
- Mylar strips placed through the thickness of the laminate on lay-up – to aid splitting (shown in Figure 9-1).
- Coupons conditioned in atmospheric chamber
- Coupons removed from chamber and split along Mylar strips (shown in Figure 9-1).
- Individual plates then weighed.
- Individual plates dried and re-weighed
- Moisture distribution can be plotted from results.

9.2 Further Property Prediction Validation Studies

In order to fully validate the predictions performed here, more mechanical testing of laminates with moisture profiles would be required. In order to carry out validation of the model, it is recommended that one should concentrate on 90° tensile tests (since these are the ones giving the greatest variations in mechanical properties) and use %RH conditions that give a wide range of strength prediction levels.

In this work, the moisture profile coupons tested here did not show a wide enough range of results as to account for the scatter. For future testing it is recommended to allow a smaller dry core about the mid-plane of the laminate to give greater variation in test results, so models can be more robustly validated. It is recommended that batches of coupons for all property types be increased, in order to reduce scatter and provide a more robust means of validation.

Airbus standard design is 20 years at 20°C and 85%RH, which Airbus state can be simulated by conditioning at 70°C and 85%RH for 1000 hours. An idea for future validation testing would be to perform verification testing based on the prediction performed in 7.7; using this conditioning criterion to validate the approach here for actual in-service aircraft parts.

9.3 Other Studies

- Temperature effects: as the combined effect of temperature and moisture aggressively degrades the resin dominated properties of composite materials, the property/moisture relationships will need to be performed for a range of aircraft operating temperatures.

- Swelling effects: swelling causes residual stresses, this could be investigated by performing further tests and measuring the thickness pre and post conditioning to see if any swelling has occurred.

- Cyclic effects: exploring the effects of cycling moisture levels, as would be experienced in a real aircraft lifecycle. First saturate, then dry to give a saturated inner core and dry edges to see what effect this has.

References

1. Plastics; Determination of tensile properties, Part 1 - General Principle, BS EN ISO 527-1:1996.

2. Plastics; Determination of tensile properties, Part 4 - Test conditions for isotropic and orthotropic fibre-reinforced plastic composites, BS EN ISO 527-4:1997.

3. Plastics; Determination of tensile properties, Part 5 - Test conditions for unidirectional fibre-reinforced plastic composites, BS EN ISO 527-5:1997.

4. Carbon fibre reinforced plastics; Unidirectional laminate - Tensile test parallel to the fibre direction, BS EN 2561:1998.

5. Carbon fibre reinforced plastic; Unidirectional laminate - Tensile test perpendicular to the fibre direction, BS EN 2597:1998.

6. Fibre-reinforced plastic; Determination of compressive properties in the in-plane direction, BS EN ISO 14126:1999.

7. Fibre-reinforced plastics; Determination of the apparent interlaminar shear strength by short beam method, BS EN ISO 14130:1998.

8. Fibre-reinforced plastic; Determination of the in-plane shear stress/shear strain response, including the in-plane shear modulus and strength by the ±45° tension test method, BS EN ISO 14129:1998.

9. AITM 1-0007; Airbus Test Method, Fibre Reinforced Plastics - Determination of plain, open hole and filled hole tensile strength, Issue 3, (2004).

10. AITM 1-0008; Airbus Test Method, Fibre Reinforced Plastics - Determination of plain, open hole and filled hole compression strength, Issue 3, (2004).

11.Airbus UK Internal Document; Justification of the thickness limit for humidity saturation, technical report, RP050898 (2005).

12. C Parkin, Finite element approach for relating moisture ingress to strength in composite materials, PhD Thesis, Department of Engineering,, Swansea University, (2009).

13. J Crank, The mathematics of diffusion, Oxford University Press, (1979).

14. G.S. Springer, Environmental effects on glass fibre reinforced polyester and vinylester composites, Journal of Composite Materials, 14 (1980) 213-232.

15. C Shen & G.S Springer, Environmental effects on the elastic moduli of composite materials, Journal of Composite Materials, 11 (1977) 250-264.

16. O.M.K. Joshi, The effect of moisture on the shear properties of carbon fibre composites, Composites, 14, (1983) 196-200.

17. R. Vodica, Accelerated Environmental Testing of Composite Materials, Department of Defense, Defense Science & Technology, DSTO-TR-0657, (1998).

18. K Ogi, H.S. Kim, T. Maruyama, Y. Takao, The influence of Hygrothermal conditions on the damage processes in quasi-isotropic carbon/epoxy laminates, Composites Science and Technology, 59 (1999) 2375-2382.

19. C Shen, G.S. Springer, Moisture absorption and desorption of composite materials, Journal of Composite Materials, 10 (1976) 2-20.

20. J.P. Komorowski., Hygrothermal effects in continuous fibre reinforced composites, Part I: Thermal and moisture diffusion in composite materials, National Research Council Canada, Aeronautical note; NAE-AN-4, NRC No. 20974 (1993).

21. J.J. Imaz, J.L. Rodriguez, A. Rubio, I. Mondragon, Hydrothermal environment influence on water diffusion and mechanical behavior of carbon fibre/epoxy laminates, Journal Material Science Letters, 10 (1991) 662-665.

22.A.A.Baker, P J. Callus, S Georgiadis, P.J. Falzon, S.E. Dutton, K.H. Leong, An affordable methodology for replacing metallic aircraft panels with advanced composites, Composites Part A, 33 (2002) 687-696.

23. S Nilsson, Manufacturing Control - Certification and standards for composite materials, Masters Thesis, Luleä University of Technology (2005).

24. Y.Q. Ding, Y Yan, R McIlhagge, Effect of impact and fatigue loads on the strength of plain weave carbon-epoxy composites, Journal of Materials Processing Technology, 55 (1995) 58-62.

25. The research requirements of the transport sectors to facilitate an increased usage of composite materials - Part I: The composite material research requirements of the aerospace industry, EADS Deutschland Corporate Research Centre (2004).

26. H.M. Flower, High performance materials in aerospace, Chapman & Hall, London, (1995).

27. A Quilter, Composites in Aerospace Applications, IHS, Inc. (2008) http://engineers.ihs.com/NR/rdonlyres/AEF9A38E-56C3-4264-980C-D8D6980A4C84/0/444.pdf

28. Airbus's A350 vision takes shape, Flight International Magazine, December 2006.

29. Why new wing is key A350 XWB, Flight International Magazine, December 2006.

30. E. J. Barbero, Introduction to composite materials design, 2nd Edition, Taylor & Francis (2010).

31. Composite awareness (course notes), run at Swansea University, by Prof. W.J. Evans (2003).

32. Composite conversion course (course notes), run at Airbus UK (2006).

33. J.M.Hodgkinson, Mechanical Testing of Advanced Fibre Composites, Woodhead Publishing, Ltd, Cambridge, (2000).

34. R.J. Young, P.A. Lovell, Introduction to polymers, 2nd ed., Chapman & Hall, London, (1991)

35. H Marsh, Introduction to carbon science, Butterworths, Boston, (1989).

36. J Comyn, Polymer permeability, Chapman & Hall, London, (1985).

37. Carbon fibre reinforced plastics; Unidirectional laminates - Flexural test parallel to the fibre direction, BS EN 2562:1997.

38. Fibre reinforced plastic composites - Determination of flexural properties, BS EN ISO 14125:1998.

39. L.J. Broutman, B.D. Argarwal, Analysis and performance of fibre composites, John Wiley and Sons Inc, USA, (1990), 339-351.

40. M Bykowski, A Hudgins, R..M. Deacon, A.R. Marder, Failure analysis of the space shuttle columbia RCC leading edge, Journal of Failure Analysis & Prevention, 6, (2006) 39-45.

41. W.D. Bascom, S.Y. Gweon, Fractography and failure mechanisms of carbon-fibre-reinforced composite materials, Elsevier Applied Science, London, (1989).

42. Carbon fibre reinorced plastics; Unidirectional laminates - Determination of apparent interlaminar shear strength, BS EN 2563:1997.

43. J Summerscales, Shear modulus testing of composites, Proceedings 4th International Conference on Composite Structures, Elsevier Applied Science, 2 (1987) 305-316.

44. S Chatterjee, D.F Adams, D.W. Oplinger, Test methods for composite – A status report, Vol. II Compression test methods, DOT/FAA/CT-93/17-II, FAA Technical Centre, Atlantic City International Airport, NJ 08405 (1993).

45. A Lowe, Transverse compressive testing of T300/914, Journal of Material Science 31(4): (1996) 1005-1011.

46. S.L. Bazhenov, V Kozey, Transversal compression fracture of unidirectional fibre-reinforced plastics, Journal of Material Science, 26(10), (1991), 2677-2684,.

47. MIL-HDBK-17-1E, Polymer Matrix Composites; Volume 1 - Guidelines for characterization of structural materials, Chapter 8, Statistical Methods, (1997).

48. H Ishida, J.L. Koenig., The reinforcement mechanism of fibre-glass reinforced plastics under wet conditions: A Review, Polymer Engineering Science, 18(2), (1978) 128–45.

49. H.S. Choi, K.J. Ahn, J.D. Nam, H.J. Chun, Hydroscopic aspects of epoxy/carbon fibre composites laminates in aircraft environments, Composites: Part A, 32 (2001) 709-720.

50. E.R. Long., Moisture Diffusion Parameter Characteristics for epoxy composites and neat resins, NASA Technical Paper 1474, Langley Research Centre, Virginia (1979).

51. E. G. Wolff, Introduction to dimensional stability of composite materials, DEStech Publications, Inc, (2004).

52. D.F. Adams, Properties characterization — Mechanical/physical/hygrothermal properties test methods, in Reference Book for Composite Technology, S.M. Lee, (ed), 2nd edition, Technomic Publishing Co, USA(1989), 49-81.

53. L.C. Bank, T.R.. Gentry, A Barkatt, Accelerated test methods to determine the long term behaviour of FRP composite structures, Journal Reinforced Plastics and Composites, 14, (1995) 559-587.

54. F.U. Buehler, J.C. Seferis, Effect of reinforcement and solvent content on moisture absorption in epoxy composite materials. Composites Part , 31 (2000) 741-748.

55. G Marom, The role of water transport in composite materials, in Polymer Permeability, J. Comyn, (ed), Elsevier Applied Science, UK, Chapter 9 (1985), 341-374.

56. M.R. Vanlandingham, R.F. Eduljee, J.W. Gillespie, Jr., Moisture Diffusion in Epoxy Systems, Journal Applied Polymer Science, 71, (1999) 787-798.

57. G.J. Fleming, T Rose, Graphite composites for ocean ordinances, US Department of Commerce, National Technical Information Service, Report AD-770-407, (1973).

58. C Maggana, P Pissis, Water sorption and diffusion studies in an epoxy resin system, Journal Applied Polymer Science Part B, 37, (1999) 1165-1185.

59. C.E. Browning, G.E. Husman, J.M Whitney, Moisture effects in epoxy matrix composites, STI 617, ASTM (1977), 481-96.

60. A Lekatou, S.E. Faidi ,D Dhidaoui, S.B. Lyon, R..C. Newman, Composites Part A, 28, (1997), 223–36.

61. V.F. Janas, R.L. McCullough, Moisture absorption in unfilled and glass-filled, cross-linked polyester, Composites Science and Technology, 29 (1987) 293–315.

62. K Komai, K Minoshima, S Shiroshita, Hygrothermal degradation and fracture process of advanced fibre-reinforced plastics, Materials Science and Engineering , (1991) 155-127.

63. S.P. Jackson, Y Weitsman, Moisture effects and moisture induced damage in composites, In: W.C. Harrigan Editor, Fifth International Conference on Composite Materials ICCM-V Metallurgical Society, Warrendale (1985), 1435–1452.

64. C Tsenoglou, C Pavlidou, C Papaspyrides, Evaluation of interfacial relaxation due to water absorption in fibre-polymer composites, Composites Science and Technology, 66, (2006) 2855-2864.

65. A Fick, On liquid diffusion, Philosophical Magazine Series 4, Taylor & Francis, 10, (1855) 30-39.

66. H.S. Carslaw, J.C. Jaeger, Conduction of heat in solids, Oxford Science Publications, (1959).

67 W Jost, Diffusion in Solids, Liquids, Gases, 3rd Edition, New York: Academic Press, (1960).

68. W.R. Broughton, F Lordeiro, Techniques for monitoring water absorption in fibre-reinforced polymer composite, NPL Measurement Note, CMMT (MN) 064, (2000).

69 J Weistman.,A method to determine moisture profiles from total moisture weight-gain data in polymeric composites, Office of Naval Research, Arlington, Virginia, Report ESM91-1.0-MECH, (1991).

70. Y.J. Weitsman., Effect of fluids on polymeric composites - A Review, Contractural Technical Report MAES 95-10, Office of Naval Research Arlington, Virginia, USA.

71. A.O. Kays, Determination of moisture content in composites by dielectric measurements, Lockheed-Georgia Company, Technical Report, AFDL-TR-79-3086, (1979).

72.KDC Technology Corporation, 2011 Research Drive, Livermore, CA 94550 USA.

73. M Werner, R King, Microwave sensors for imaging moisture and flaws in composite materials, Review of Progress in Quantitative Non-Destructive Evaluation, 15, (1995).

74. R.J. Dalasi, R.L. Schulte, Moisture detection in composites using nuclear reaction analysis, Journal of Composite Materials, 13, (1979).

75. P Siva, A Novel accelerated moisture absorption test and characterization, Composites Part A, 40, (2009), 1501-1505.

76. T.A. Collings, S.M. Copley, On the accelerated aging of CFRP, Composites, 14 (1983) 180-188.

77. L Cai, Y Weitsman, Non-Fickian moisture diffusion in polymeric composites, Journal of Composite Materials, 28(2), (1994) 130-154.

78. A Revathi, Moisture Distribution profiles in RT-cured glass/epoxy laminates of different thickness, Journal of Reinforced Plastic and Composites, 23(10), (2004) 1075-1093.

79. J.B Whiteside, R.J. Delasi, R.L. Schulte, Distrubution of absorbed moisture in graphite/epoxy laminates after real-time environmental cycling, ASTM STP,(1984) 192-205.

80. G.S Springer, Environmental effects on composite materials, Volumes 1 and 2, Technomic Publishing Company, USA (1984).

81. F.R. Jones, Durability of polymer composites in liquid environments, in Reinforced plastics durability, G. Pritchard (ed), 2nd edition, Woodhouse Publishing, Cambridge, Chapter 3, (1998).

82. G.S. Springer, Environmental effects of composite materials – Volume 3, Technomic Publishing Co.USA (1988).

83. G.C. Papanicolaou, A. Pappa, Water sorption and temperature effects on the dynamic mechanical behaviour of epoxy-matrix particulates, Journal of Material Science, 27, (1992), 3889-3896.

84. B.D. Harper, G.H. Staab, R.S. Chen, A note on the effects of voids upon the hygral and mechanical properties of AS4/3502 graphite/epoxy, Journal of Composite Materials ,21, (1987), 280-289.

85. E Botelho, L Pardini and M Rezende, Hygrothermal effects on the shear properties of carbon fibre/epoxy composites, Journal of Material Science, 41, (2006) 7111-7118.

86. B.F. Boukholda, E Adda-Bedia, K .Madani, The effect of fibre orientation angle in composite materials on moisture absorption and material degradation after hygrothermal aging, Composite Structures, 74, (2005), 406-418.

87. Q Zhen, R.J. Morgan, Synergistic thermal-moisture damage mechanisms of epoxies and their carbon fiber composites, Journal of Composite Materials, 27 (1993), 1465-1478.

88. G.S. Springer., S.W. Tsai., Thermal conductivities of unidirectional material, Journal of Composite Materials, 1(2), (1967) 166-173.

89. J Zhou, J.P. Lucas, The Effects of a water environment on anomalous absorption behaviour in graphite/epoxy, Composites Science and Technology, 53 (1995) 57-64.

90. C Shen, G.S. Springer, Effects of moisture and temperature on the tensile strength of composite materials, in Environmental Effects on Composite Materials, Westport, CT: Technomic Publishing Company, Inc. (1981) 79-93.

91. M Zhang, S.E. Mason, The effects of contamination on the mechanical properties of carbon fibre reinforced epoxy composite materials, Journal of Composite Materials, 33 (14), (1999) 1363-1374.

92. S.B. Kumar, I Sridhar, S Sivashanker, Influence of humid environment on the performance of high strength structural carbon fibre composites, Materials Science and Engineering A, 498, (2008), 174-178

93. W.L. Bradley, T.S. Grant, The effect of moisture absorption on the interfacial strength of polymeric matrix composites, Journal of Materials Science, 30 (21), (1995) 5537-5542.

94. R. Selzer, K Friedrich, Mechanical properties and failure behaviour of carbon fibre-reinforced polymer composites under the influence of moisture, Composites Part A, 28 (1997), 595-604.

95. T.A. Collins, Transverse compressive behaviour of unidirectional carbon fibre reinforced plastics, Composites, 5 (3), (1974) 108-116.

96. R.A. Weinberger, A.R. Somoroff, US navy certification of composite wings for the F-18 and the advanced harrier aircraft, AGARD-R-660, (1977).

97. G Sala, Composite degradation due to fluid absorption, Composites Part B: Engineering, 31(5), (2000) 357-373.

98. G.K. Bhavesh, R.P. Singh,T Nakamura, Degradation of carbon fiber-reinforced epoxy composites by ultraviolet radiation and condensation, Journal of Composite Materials, 36, (2001), 271-2733.

99. B.C. Hoskins, A.A. Baker, Composite materials for aircraft structures, New York: American Institute of Aeronautics and Astronautics, Inc., (1984).

100. H.B. Dexter and D.J. Baker, Flight service environmental effects on composite Materials and structures, Advanced Performance Materials, 1, (1994) 51-85.

101. J Daniel et al, Environmental exposure effects on composite materials for commercial aircraft, NASA CR-187478 National Aeronautics and Space Administration Langley Research Center Hampton, USA, (1991).

102. R. Vodicka, B Nelson, J. Van Den Berg, R. Chester, Long-term environmental durability of F/A-18 composite material, DSTO-TR-0826, (1999).

103. S.L. Gao, J.K. Kim, Cooling rate influences in carbon fibre/PEEK composites. Part III: Impact damage performance, Composites Part A, 32 (2001) 775-785.

104. Polymeric Composites, A division of Ipeco Holdings Ltd, Unit 15, Windmill Business Park, Windmill Road, CLEVEDON, BS21 6SR..

105. Aerospace Series; Carbon Fibre Laminates - Determination of the fibre, resin and void contents, BS EN 2564:1998.

106. Carbon Fibre - Determination of Density, BS ISO 10119:2002.

107. JTS Environmental Test Chambers; Unit 3, Talgarth Business Park, Talgarth, Brecon, Powys, LD3 0PQ.

108. Plastics; Standard atmospheres for conditioning and testing, BS EN ISO 291:1997.

109. Gemini data loggers http://www.geminidataloggers.com/, July 2007.

110. ASTM D5229/D5229M-92, Standard test method for moisture absorption properties and equilibrium conditioning of polymer matrix composite materials, (1992).

111. S.J. Thompson, R.T. Hartshorn, J Summerscales, Strain gauges on glass fibre reinforced polyester laminates, Ed. IH Marshall, Composite Structures 3, Elsevier, London, (1985), 748-759.

112. Instruction Bulletin B-127-14, Strain Gauge Installations with M-Bond 200 Adhesive, Vishay Micro-Measurements, Document No. 11127, Revision Jan 2005.

113. Vishay Measurements Group - http://www.vishay.com/, August 2008.

114. Aerospace series; Fibre-Reinforced Plastics - Standard procedures for conditioning prior to testing un-aged material, BS EN 2743:2002.

115. Carbon Fibre Laminates; Determination of the fibre, resin and void contents, BS EN 2564:1998.

116. AECMA; Aerospace Series Carbon Fibre Thermosetting Resin; Unidirectional Laminates - Compression test parallel to fibre direction, prEN 2850-1997.

117. Wyoming Test Fixtures Inc. 2960 E. Millcreek Canyon Rd. Salt Lake City, UT 84109 (www.wyomingtestfixtures.com).

118 J.M. Whitney, Moisture diffusion in fibre reinforced composites, ICCM 2: proceedings of the 1978 International Conference on Composite Materials, Toronto, Canada, (1978).

119. O Gillat, L.J. Broutman, Effect of an external stress on moisture diffusion and degradation in a graphite reinforced epoxy laminate, Advanced Composite Materials Environmental Effects, ASTM STP 658:61 (1978).

120. S.W Tsai, H.T Hahn,, Introduction to Composite Materials, Technomic Publishing Co, Westport, CT, Chapter 8 (1980).

121. M.C. Lee, N.A. Peppas, Water transport in graphite/epoxy composites, Journal of Applied Polymer Science, 47, (1993) 1349-1359

122. G.A. Schoeppner and D.B. Curliss, Model-based design for composite materials life management, Proceedings of the 9th AIAA/ISSMO Symposium on Multidisciplinary Analysis and Optimization Conference, 4-6 September 2002, Atlanta, GA, Paper number AIAA-2002-5516.

123. P.J.C. Chou, D Ding, Characterization of moisture absorption and its influence on composite structures, Journal of Thermoplastic Composite Materials; 13, (2000) 207-225.

124. L.A. Carlsson, R.B. Pipes (eds), Experimental characterization of advanced composite materials, 2nd.edition, USA, Lancaster, Technomic Publishing, USA, (1997) 81-91.

125. J.E. Master, Basic failure modes of continuous fiber composites, In: Engineered Materials Handbook, Volume 1, Metals Park, OH, USA, (1987) 781-785.

126. M.J. Hinton, P.D. Soden, A.S. Kaddour, Failure criteria in fibre reinforced polymer composites: the world-wide failure exercise, .Elsevier, Oxford. (2004).

127. Laminate Analysis Program (LAP, version 3.0F, Anglyph Ltd UK. © 1995-2001.

128. R Older, The preparation and handling of FRP specimens subjected to environmental conditioning and testing, Airbus internal document, Issue 1.0, (2008).

129. J.M. Tang, W Lee, G.S Sprnger, Effects of cure pressure on resin flow, voids, and mechanical properties Journal of Composite Materials, 21, (1987) 421-440.

130. J.L. Kardos, R Dave, M.P. Dudukovic, Voids in composites, Proceeding of Manufacturing International, 41 (1988).

131. A Lekatou, SE Faidi, D Ghidoui, SB Lyon, RC Newman, Effect of water and its activity on transport properties of glass/epoxy particulate composites, Composites Part A, 28, (1997), 223-236.

132. R.J. Morgan, J.E. O'Neal, D.L. Fanter, The effect of moisture on the physical and mechanical integrity of epoxies Journal of Materials Science, 15, (1980), 751-767.

133. J Zhou, J.P. Lucas, Hygrothermal effects of epoxy resin, Part I: The nature of water in epoxy, Polymer, 40(20), (1999), 5505-5512.

134. European Aeronautics: A Vision for 2020, Meeting society's needs and winning global leadership, Report of the group of personalites, Office for Offical Publications of the European Communities,L-2985 Luxembourg (2001).

135. S Ravi, N.G.R. Iyengar, B.D. Agarwal, Influence of Moisture Absorption on Fracture Toughness of Kevlar Fabric/Epoxy Composite, Journal of the Institution of Engineers (India), 76, (1995) 23-28.

APPENDIX

APPENDIX A: Autoclave Cure-cycle

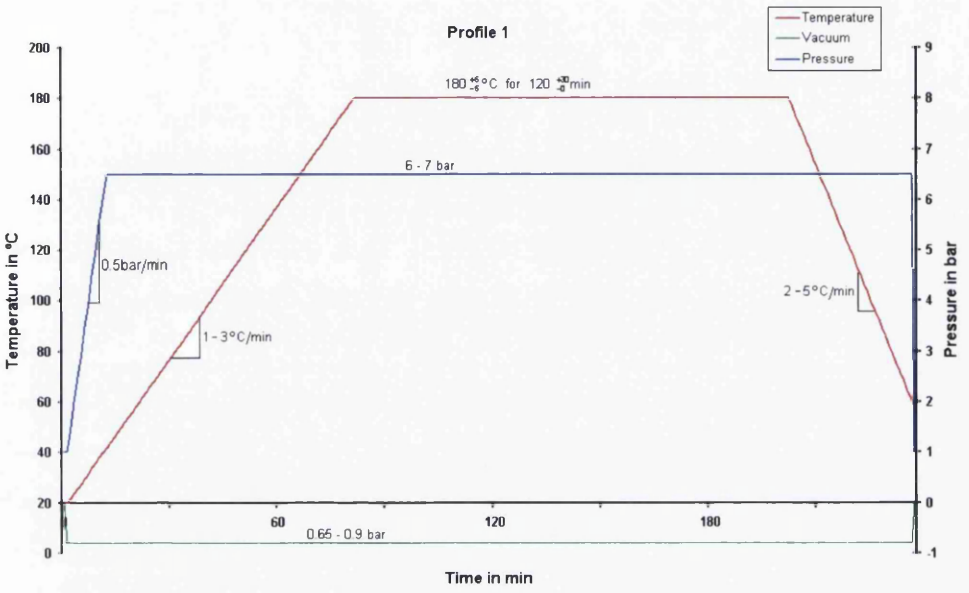

Figure A-1:Autoclave cure cycle

APPENDIX B: C-Scans Results and Comments

Note: - All laminate scans have a small white circle in the top left hand corner of the scan. This is to identify orientation of the panel. The position of this is marked on each panel by a white circle.

Panel number CDC/05/5287

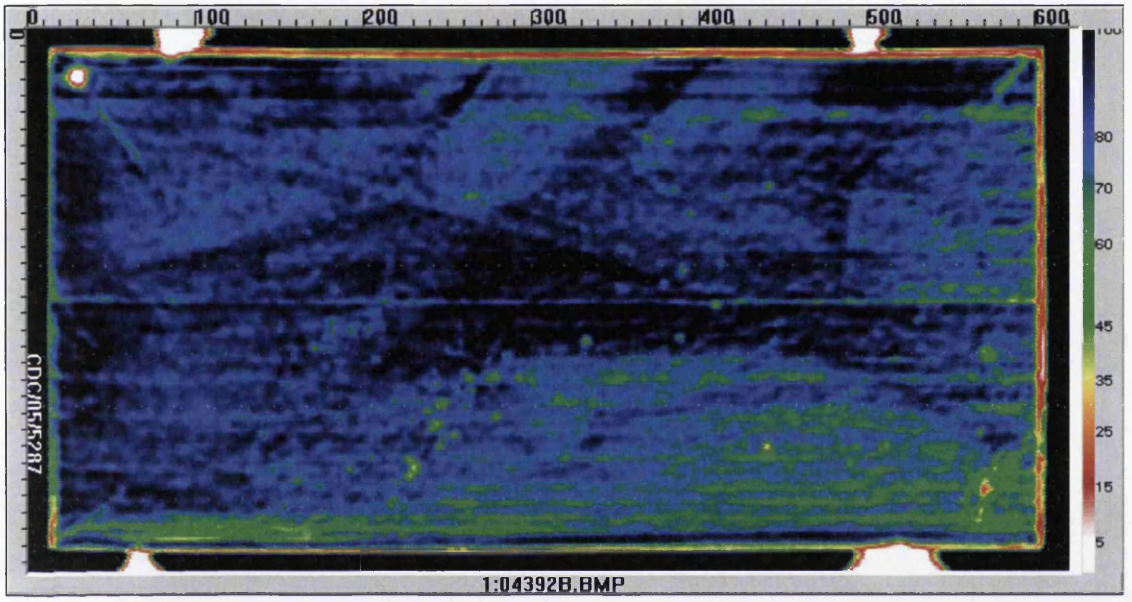

Figure A-2: CDC/05/5287 90° Compression coupons panel.

This is the panel that was used to manufacture 90° Compression coupons. This panel shows generally uniform levels of ultrasound attenuation, with a maximum variation of approximately 2dB.

Panels CDC/05/5288 and CDC/05/5289

These two panels were used to manufacture In-Plane Shear test coupons. CDC/05/5288 shows generally uniform levels of ultrasound attenuation, with a maximum variation of approximately 2-3dB. CDC/05/5289 shows generally uniform levels of ultrasound attenuation, with a maximum variation of approximately 2dB.

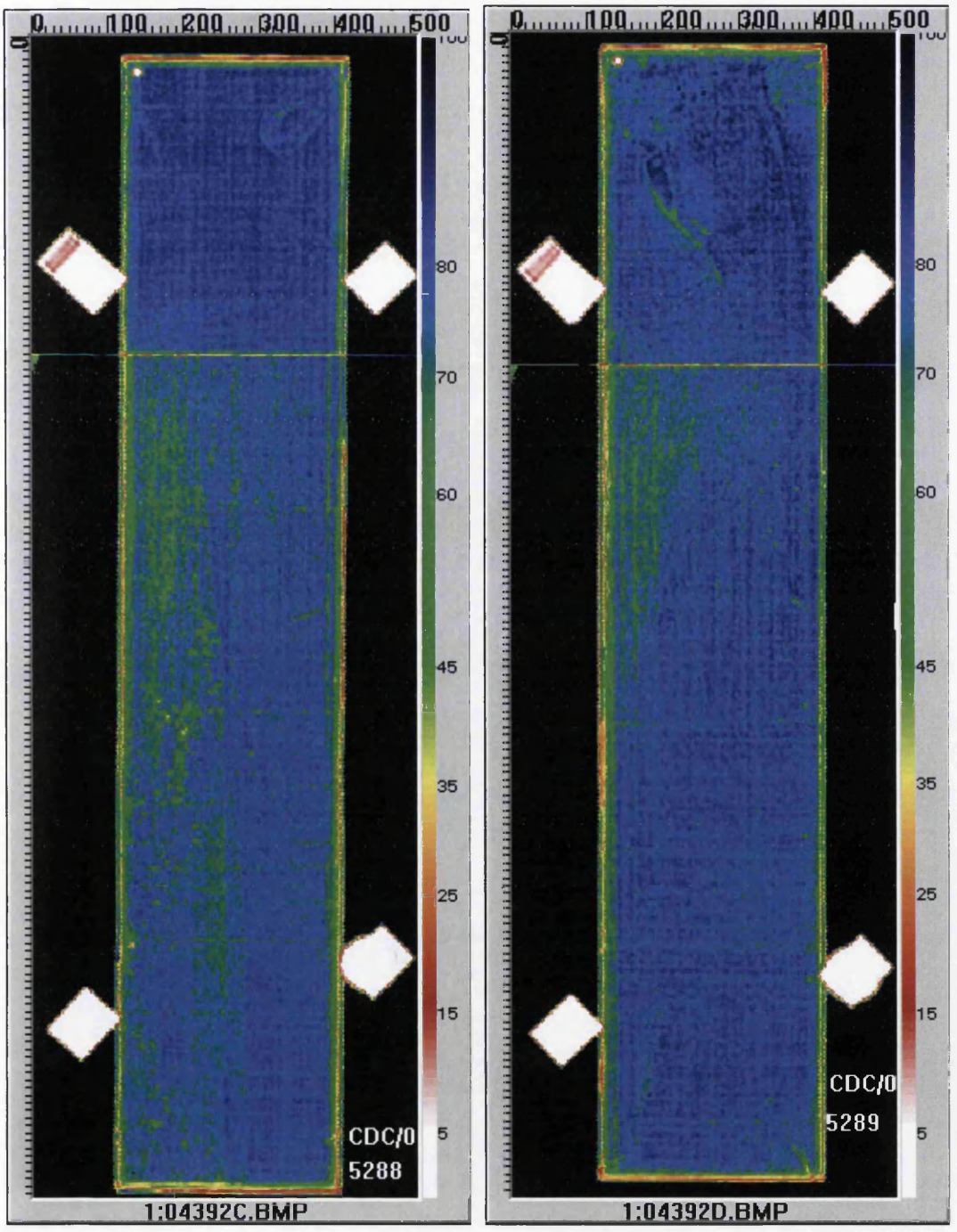

Figure A-3: CDC/05/5288 and 5299 in-plane shear coupons panel.

Panels CDC/05/5285 and CDC/05/5286

Panel CDC/05/5285 was used to manufacture 0° tension test coupons. This panel shows generally uniform levels of ultrasound attenuation, with a maximum variation of approximately 2dB.

Panel CDC/05/5286 was used to manufacture 90° tension test coupons. This panel shows generally uniform levels of ultrasound attenuation, with a maximum variation of approximately 2-3dB.

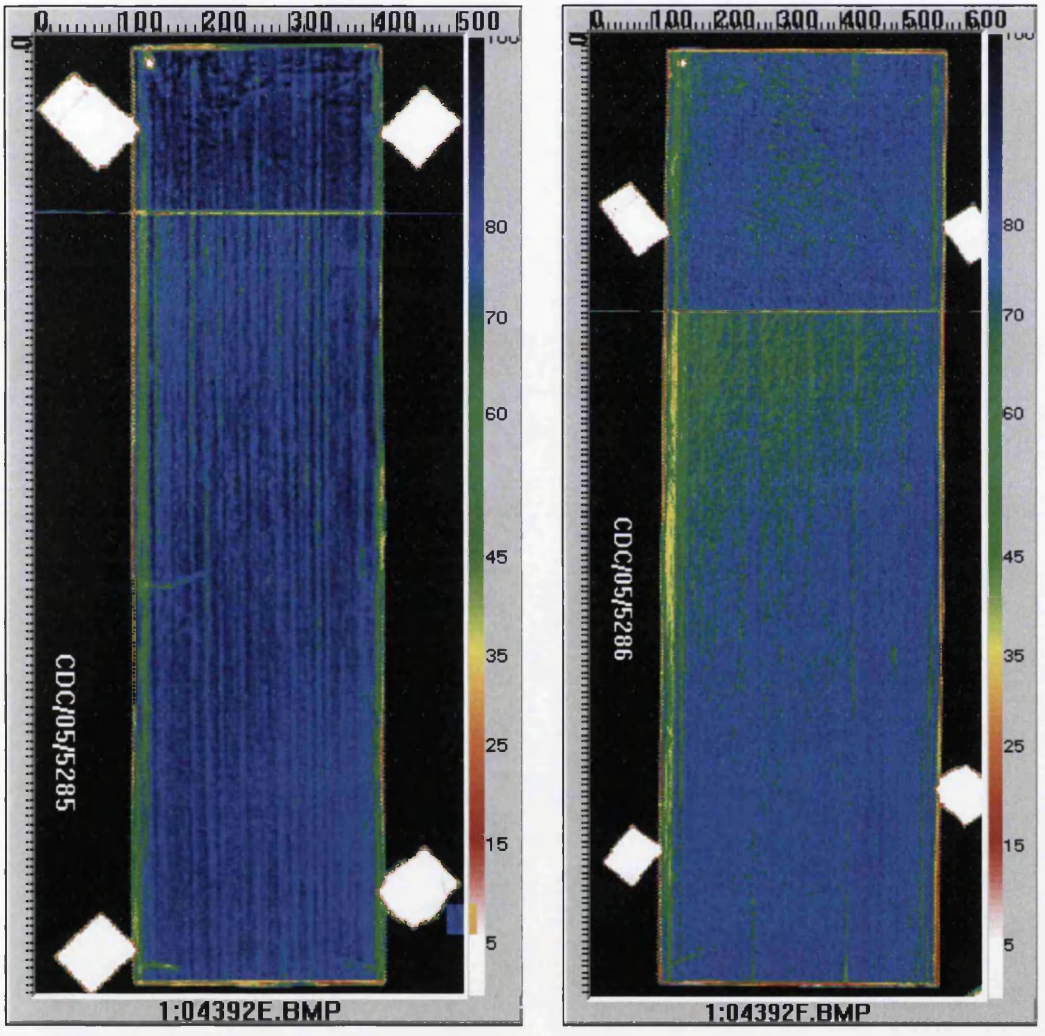

Figure A-4: CDC/05/6388 moisture coefficient determination panel.

Panels CDC/05/6388 and CDC/05/5318

Panel CDC/05/6388 was used to manufacture moisture coefficient determination test coupons. The C-Scan image of this laminate shows a variation in ultrasound attenuation levels of approximately 5dB. This is ACCEPTABLE to ABP 6-5233 Cat 2. Panel CDC/05/5318 was also used to manufacture moisture coefficient determination test coupons. The image above shows generally uniform levels of ultrasound attenuation (approximately 3-4dB variation maximum).

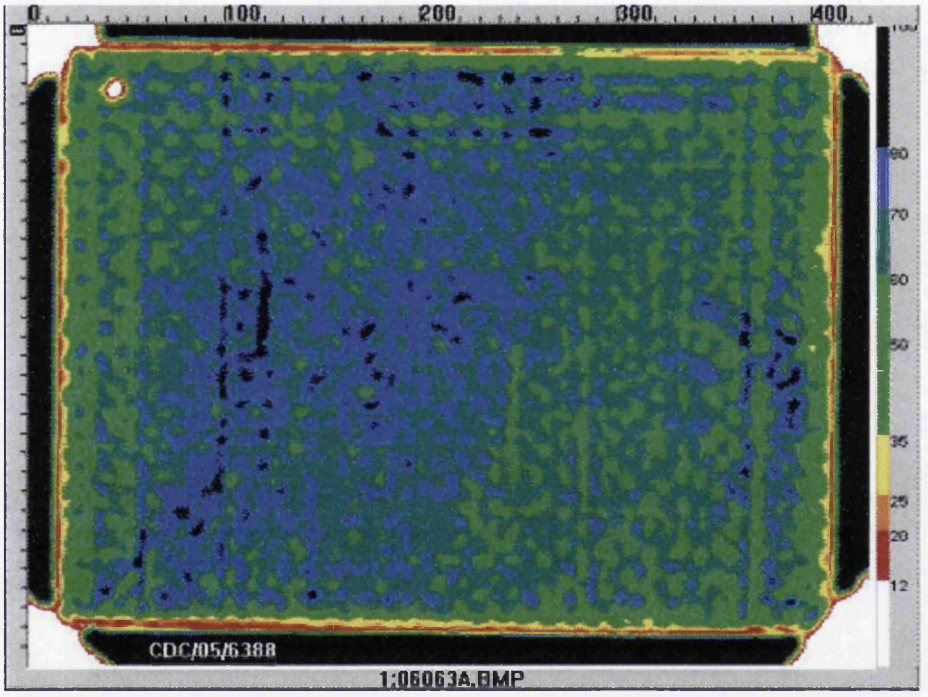

Figure A-5: CDC/05/6388 moisture coefficient determination panel.

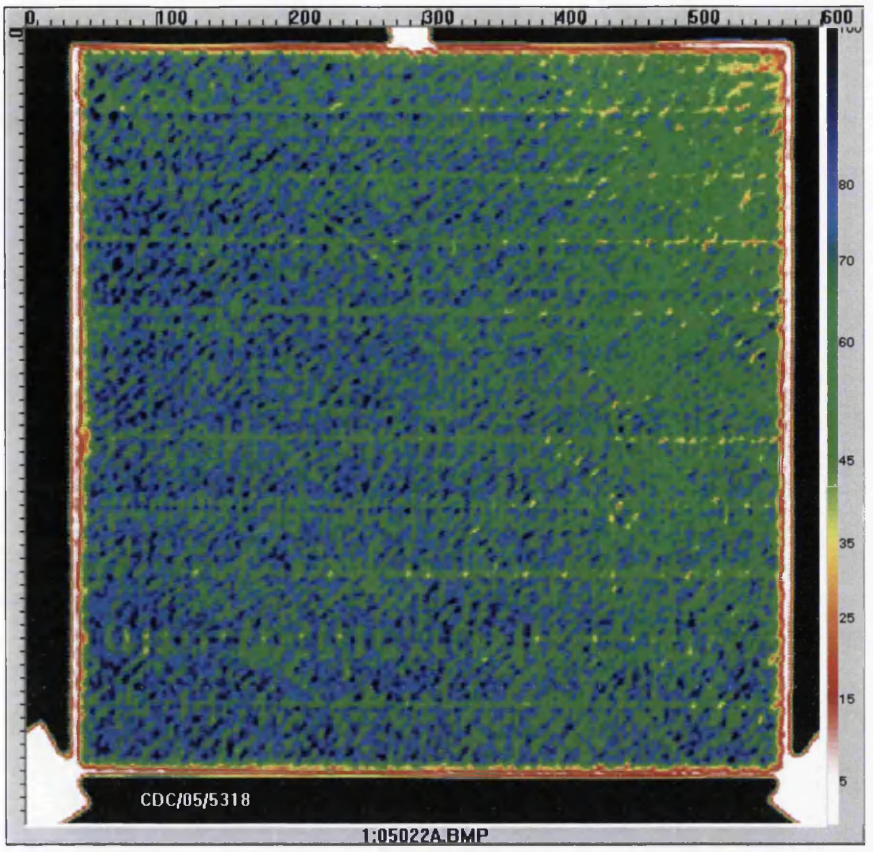

Figure A-6: CDC/05/5318 moisture coeffiecient determination.

Panels CDC/05/5316 & CDC/05/5317

Panel CDC/05/5316 and CDC/05/5317 were used to manufacture interlaminar shear coupons. The image above shows generally uniform levels of ultrasound attenuation for both panels (approximately 3dB variation maximum), except for a yellow line down the right side of CDC/05/5317. This could be caused by porosity, dry area or some other anomaly in the lay-up, this area was removed prior to any coupon manufacture.

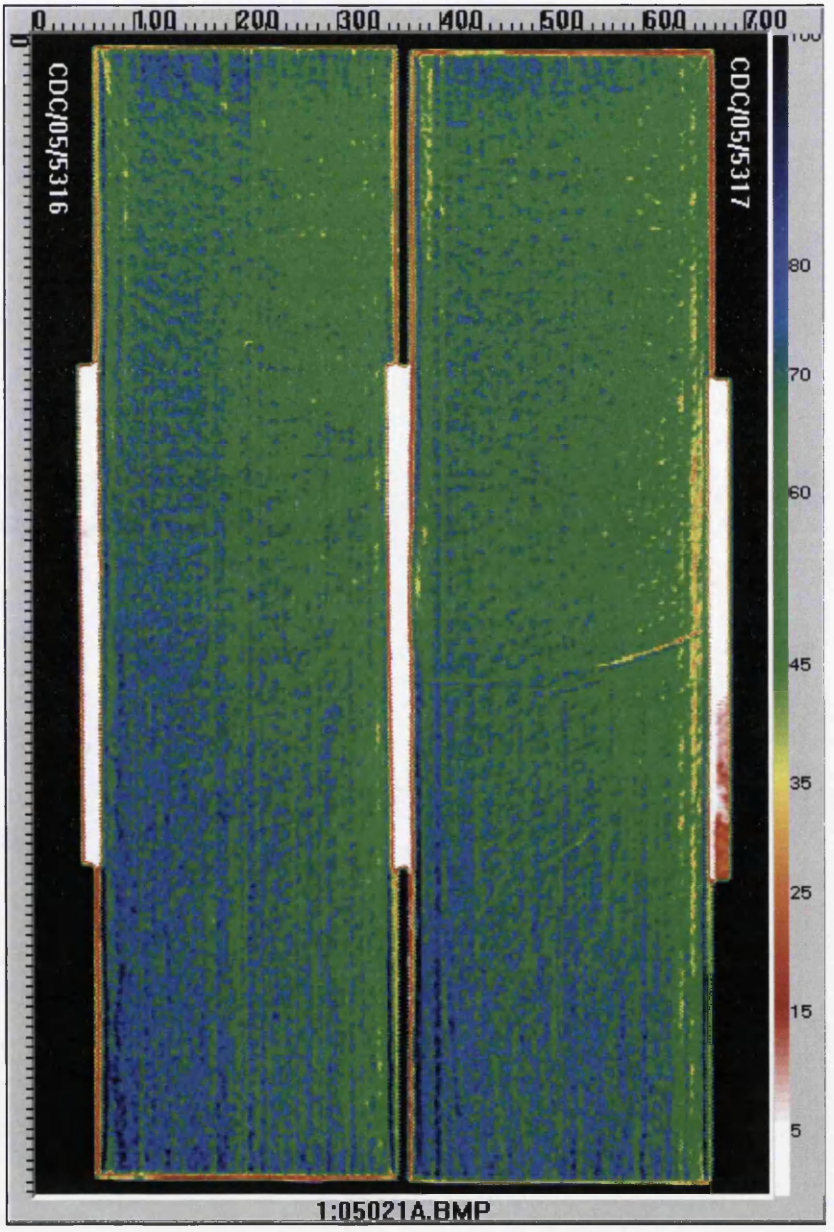

Figure A-7: CDC/05/5316 was used to manufacture interlaminar shear coupons.

Panels CDC/05/5293 and CDC/05/5295

Panel CDC/05/5293 was used to manufacture quasi-isotropic open hole tension coupons. This panel shows generally uniform levels of ultrasound attenuation, maximum variation approximately 2-3dB.Panel CDC/05/5295 was used to manufacture quasi-isotropic open hole tension coupons. This panel shows generally uniform levels of ultrasound attenuation, maximum variation approximately 2-3dB. Note: - the small red dots are caused by air bubbles trapped under the coupon.

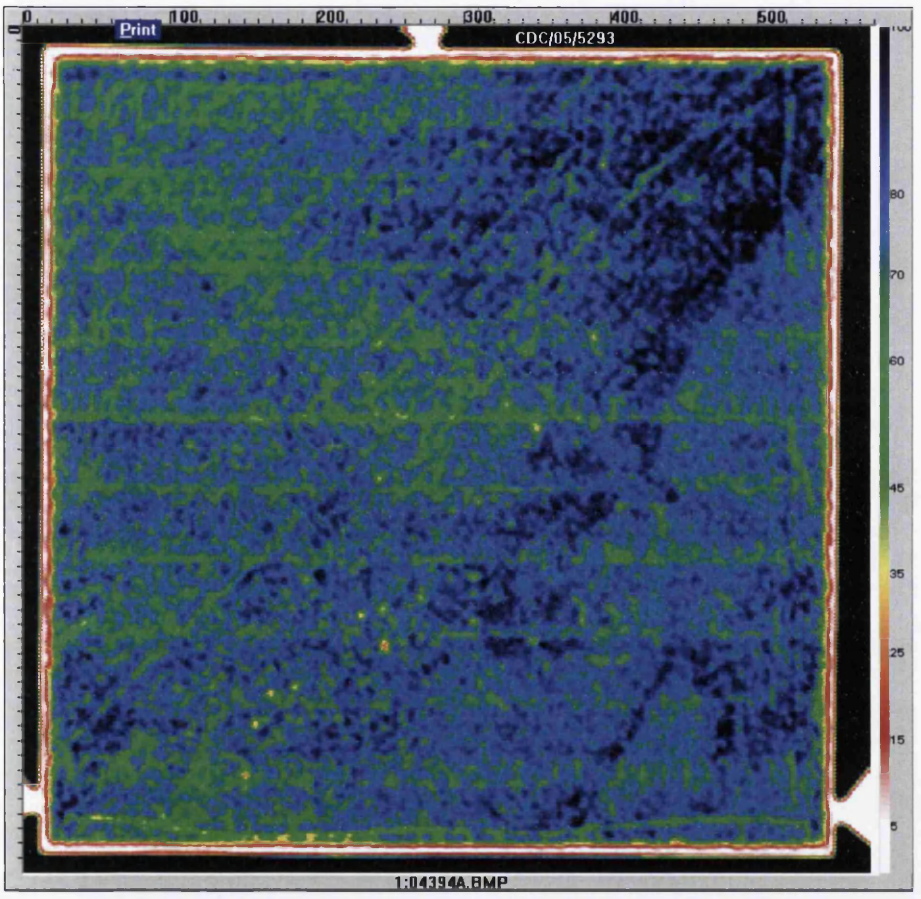

Figure A-8: CDC/05/5293 was used to manufacture quasi-isotropic open hole tension coupons.

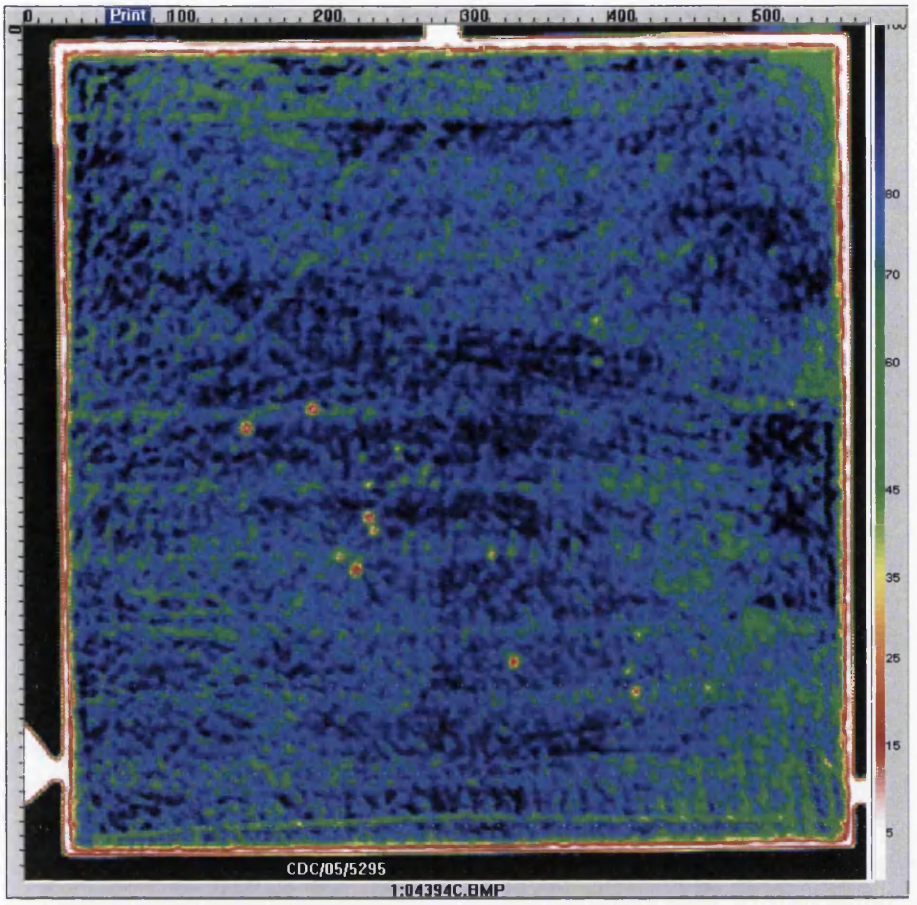

Figure A-9: CDC/05/5295 was used to manufacture quasi-isotropic open hole tension coupons.

Panel Number CDC/05/5294

This panel was used to manufacture quasi-isotropic open hole compression coupons. This panel shows generally uniform levels of ultrasound attenuation, maximum variation approximately 2-3dB. Note: - the small red dots are caused by air bubbles trapped under the coupon.

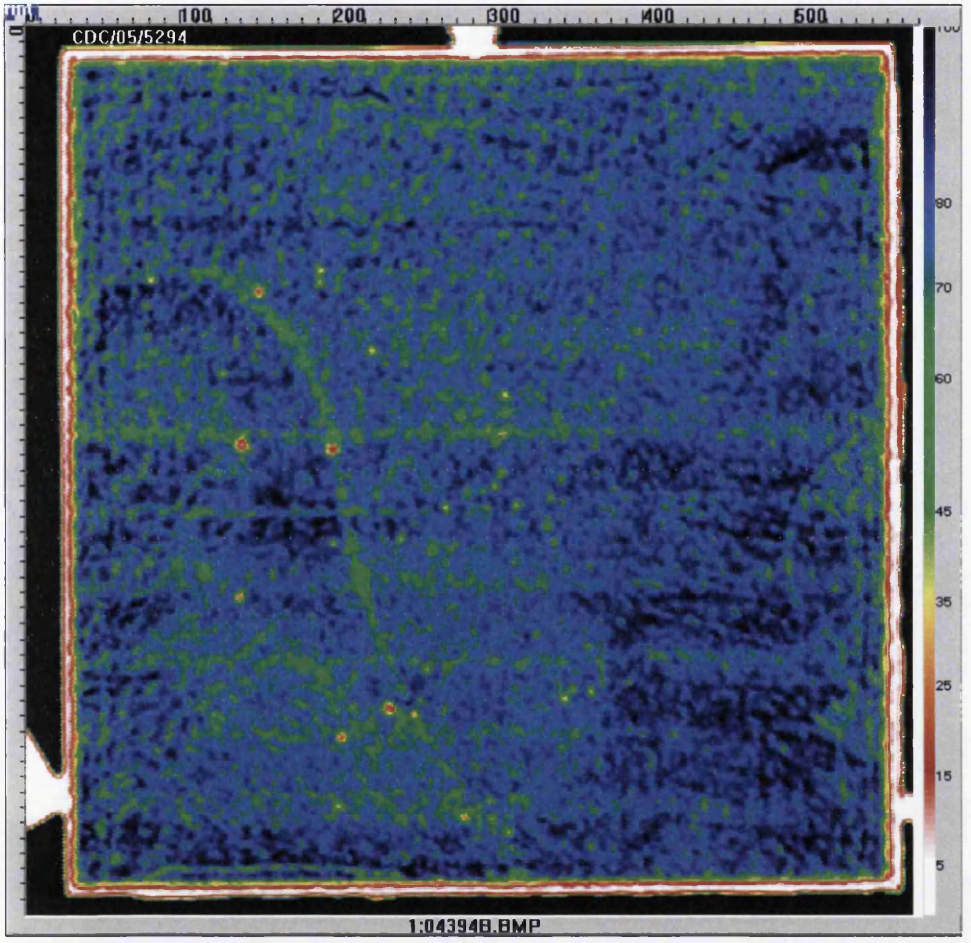

Figure A-10: CDC/05/5294 panel was used to manufacture quasi-isotropic open hole compression coupons.

APPENDIX C: Coupon Extraction Diagrams

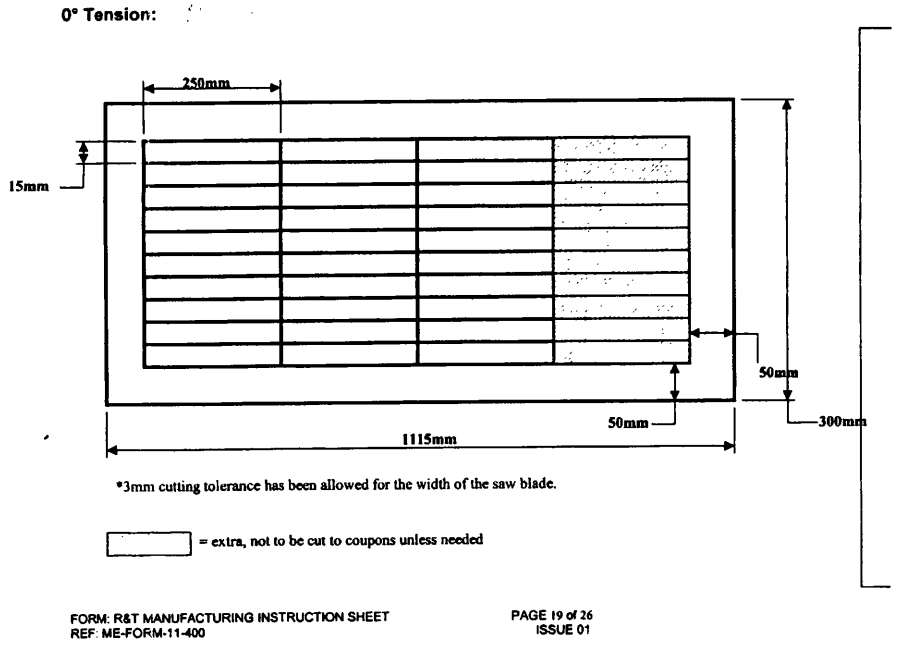

Figure A-11: 0° tension coupon extraction diagram.

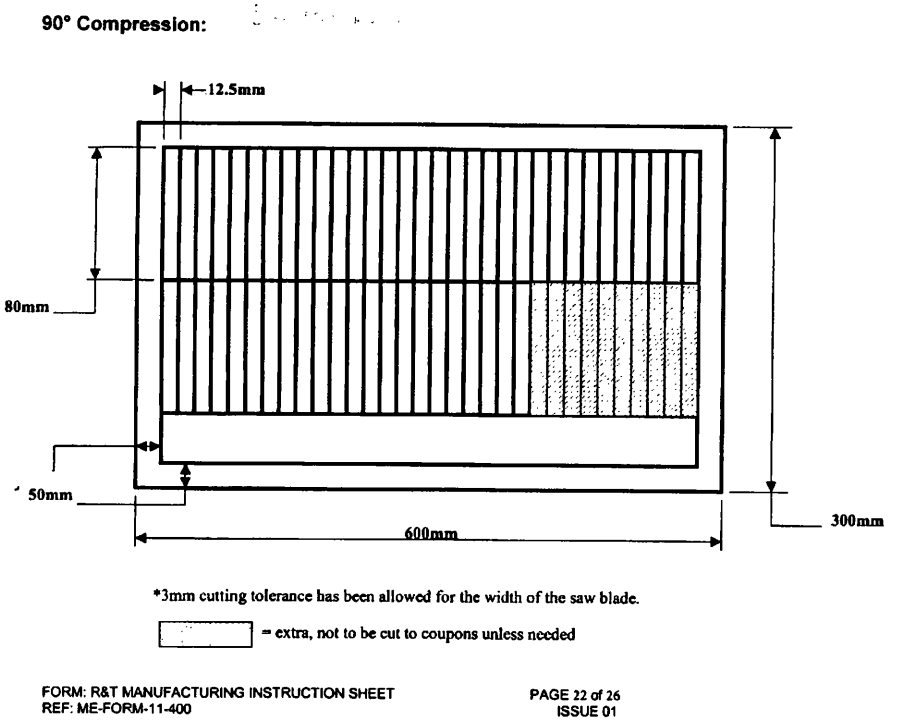

Figure A-12: 90° compression coupon extraction diagram.

90° Tension:

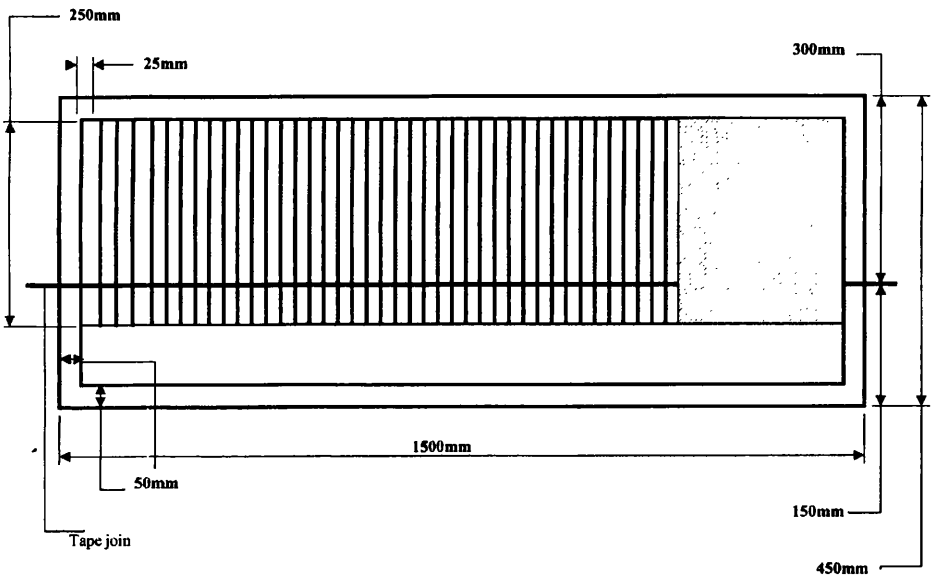

*3mm cutting tolerance has been allowed for the width of the saw blade.

= extra, not to be cut to coupons unless needed

FORM: R&T MANUFACTURING INSTRUCTION SHEET
REF: ME-FORM-11-400

PAGE 20 of 26
ISSUE 01

Figure A-13: 90° tension coupon extraction diagram.

In-Plane Shear:

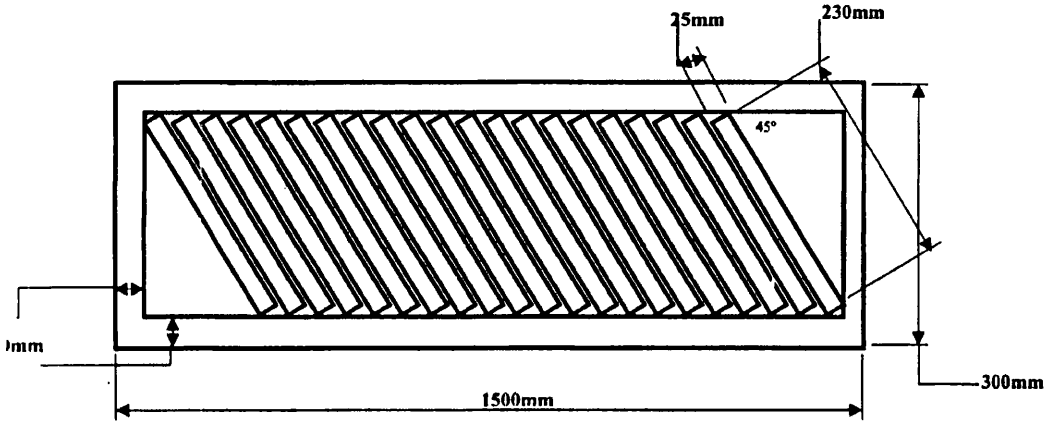

*3mm cutting tolerance has been allowed for the width of the saw blade.

**2 panels will need to be produced to to provide the amount of coupons required

Figure A-14: In-plane shear coupon extraction diagram.

QI Compression:

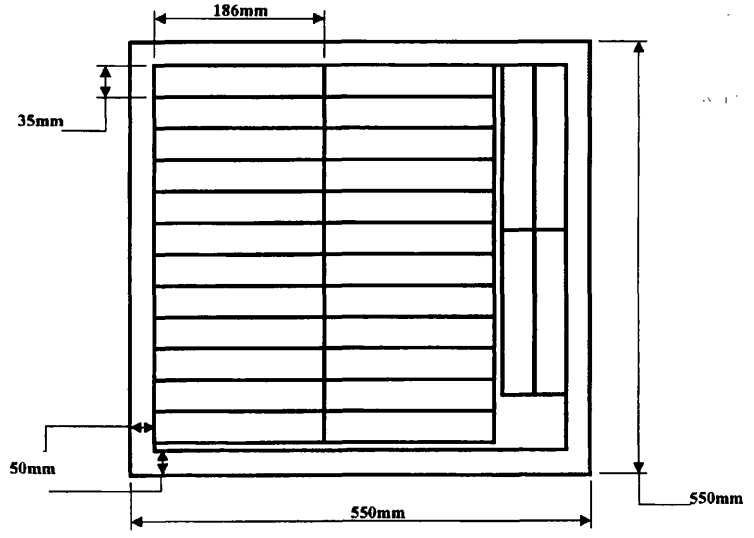

*3mm cutting tolerance has been allowed for the width of the saw blade.

FORM: R&T MANUFACTURING INSTRUCTION SHEET
REF: ME-FORM-11-400
PAGE 19 of 25
ISSUE 01

Figure A-15: Open hole compression coupon extraction diagram.

QI Tension:

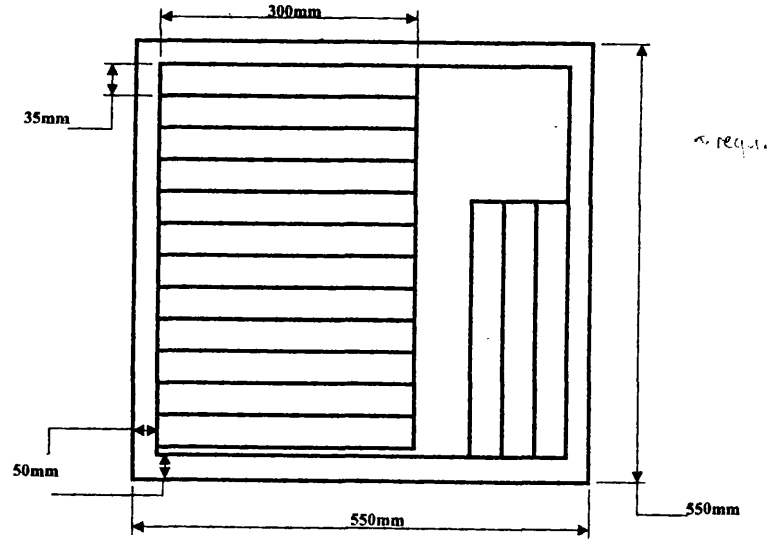

*3mm cutting tolerance has been allowed for the width of the saw blade.

**2 panels will have to be produced to achieve the needed amount of coupons.

FORM: R&T MANUFACTURING INSTRUCTION SHEET
REF: ME-FORM-11-400
PAGE 20 of 25
ISSUE 01

Figure A-16: Open hole tension coupon extraction diagram.

APPENDIX D: EQUILIBRIUM MOISTURE UPTAKE CURVES

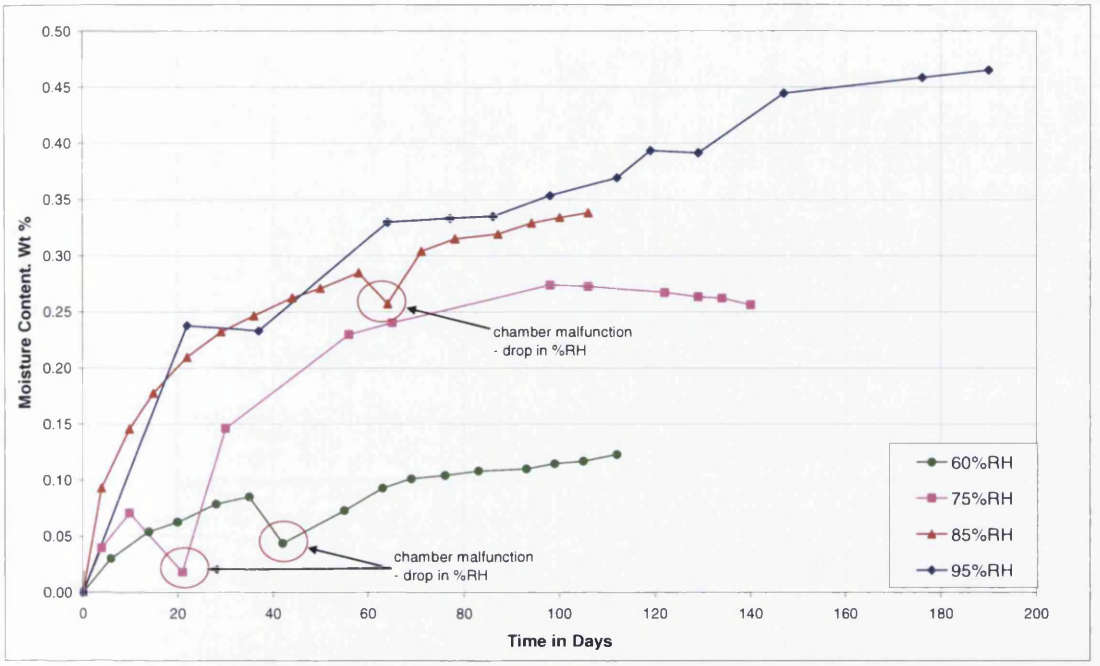

Figure A-17: Moisture uptake in 90° Tension coupons.

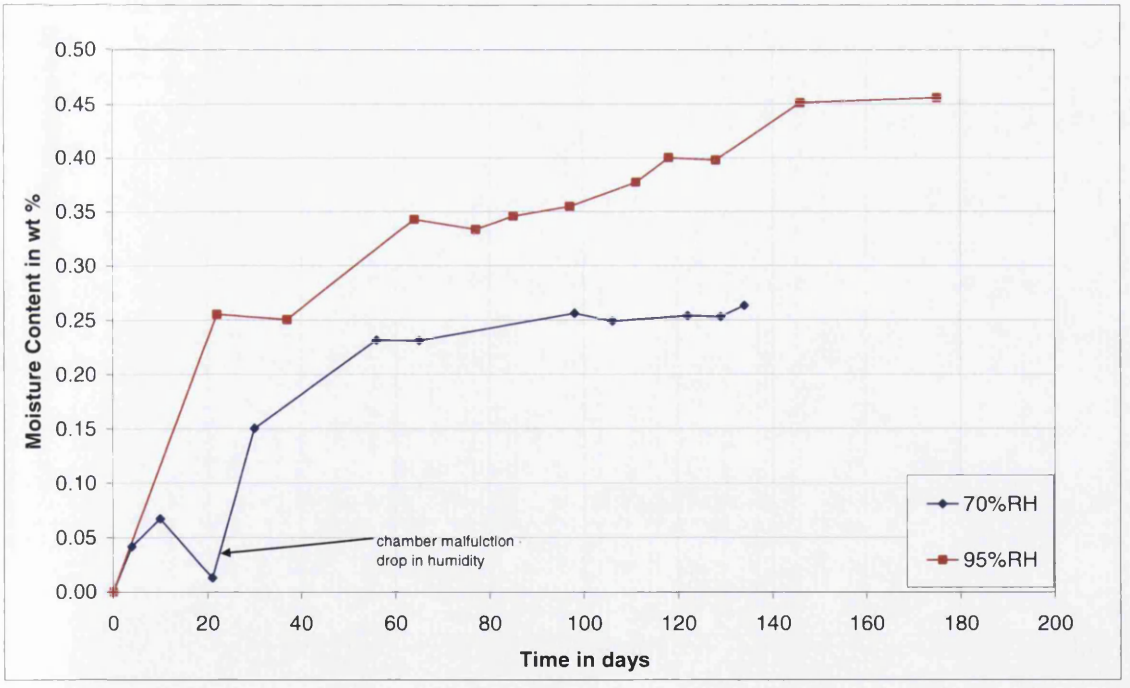

Figure A-18: Moisture uptake in 0° Tension coupon.

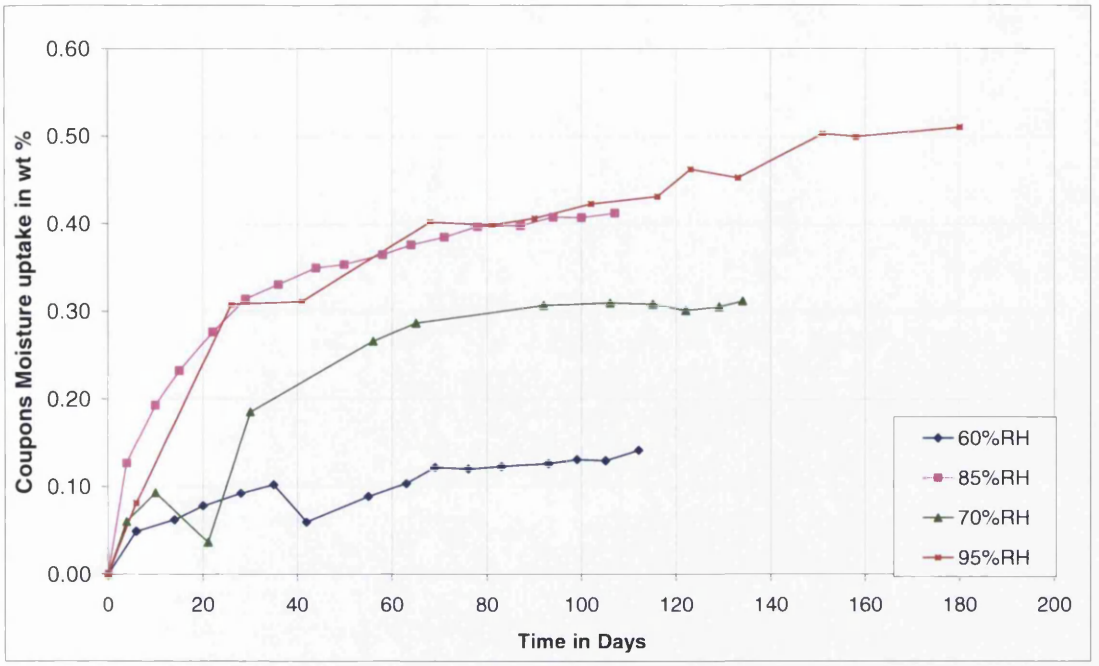

Figure A-19: Moisture uptake in 90° Compression coupon.

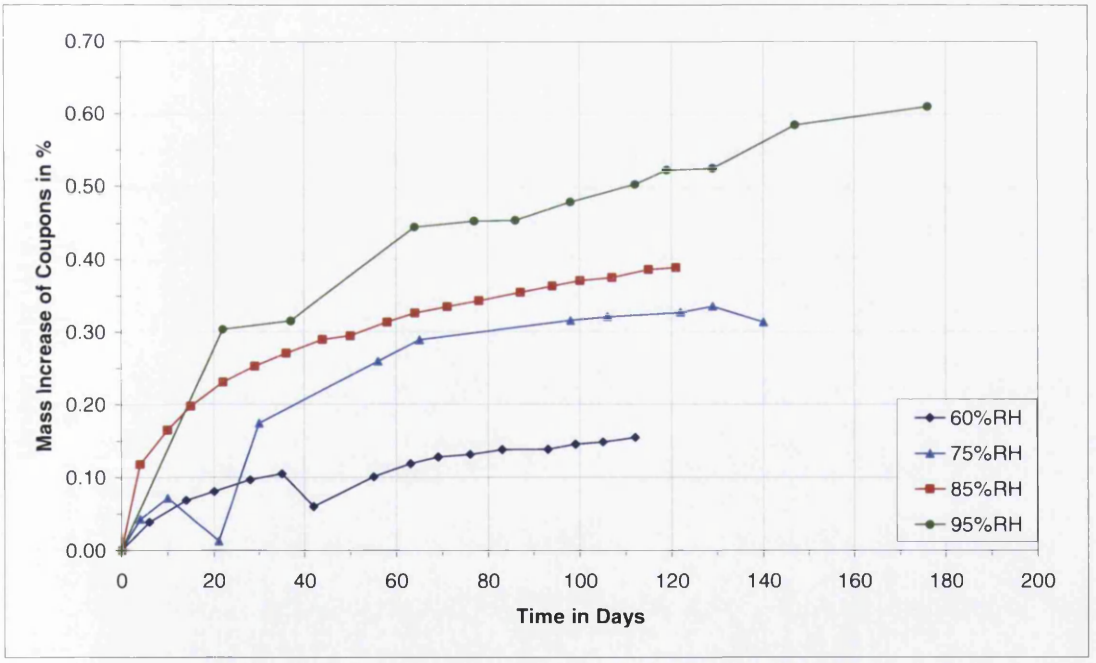

Figure A-20: Moisture uptake in ±45° Tension coupons.

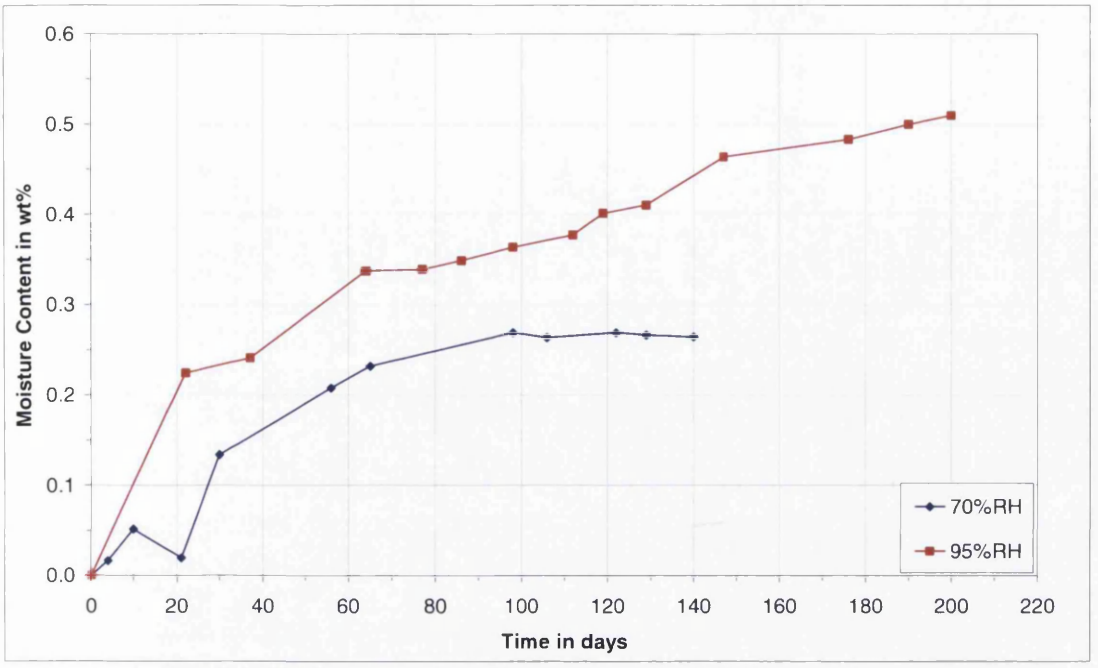

Figure A-21: Moisture uptake in open hole tension coupons

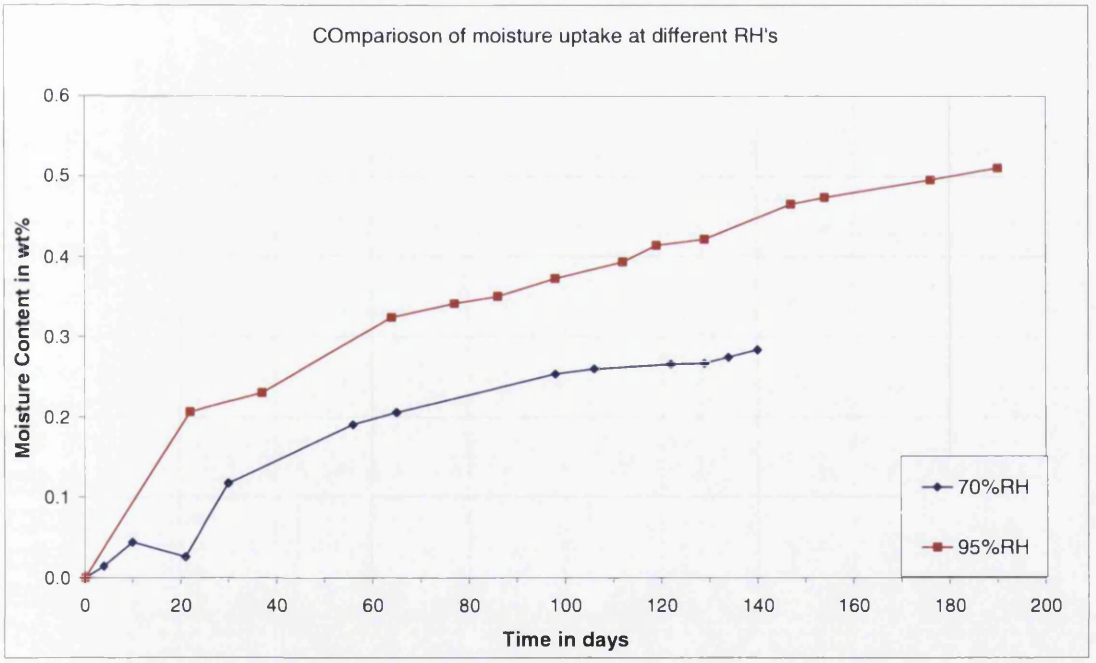

Figure A-22: Moisture uptake in open hole compression coupons.

APPENDIX E: Experimental Test Data

*Table A-1: Table of raw experimental data; see * at end of table.*

Coupon ID	Test Type	Material Type	Condition (%RH)	w	t	F_x MPa	E_x GPa
CDC/05/5285/19	0° Tension	Material A	OD	15.26	1.02	2471.4	152.0
CDC/05/5285/20	0° Tension	Material A	OD	15.12	1.06	2261.4	151.0
CDC/05/5285/21	0° Tension	Material A	OD	15.23	1.04	2531.9	151.0
CDC/05/5285/27	0° Tension	Material A	OD	15.14	1.01	2382.7	153.0
CDC/05/5285/30	0° Tension	Material A	OD	15.77	1.02	2136.1	155.0
CDC/05/5285/2	0° Tension	Material A	AR	15.15	1.01	2306.0	-
CDC/05/5285/3	0° Tension	Material A	AR	15.14	1.03	2525.0	145.0
CDC/05/5285/4	0° Tension	Material A	AR	15.14	1.04	2447.0	147.0
CDC/05/5285/5	0° Tension	Material A	AR	15.08	1.03	2342.0	145.0
CDC/05/5285/6	0° Tension	Material A	AR	15.20	1.04	2360.0	141.0
CDC/05/5285/7	0° Tension	Material A	75	15.18	1.04	2288.0	146.0
CDC/05/5285/8	0° Tension	Material A	75	15.14	1.04	2501.0	150.0
CDC/05/5285/9	0° Tension	Material A	75	15.47	1.04	2375.0	147.0
CDC/05/5285/10	0° Tension	Material A	75	15.42	1.03	2323.0	145.0
CDC/05/5285/11	0° Tension	Material A	75	15.15	1.04	2498.0	147.0
CDC/05/5285/12	0° Tension	Material A	75	15.18	1.04	2387.0	138.0
CDC/05/5285/13	0° Tension	Material A	95	15.18	1.04	2565.0	145.0
CDC/05/5285/14	0° Tension	Material A	95	15.14	1.04	2312.0	-
CDC/05/5285/15	0° Tension	Material A	95	15.47	1.04	2192.0	139.0
CDC/05/5285/16	0° Tension	Material A	95	15.42	1.03	2274.0	141.0
CDC/05/5285/17	0° Tension	Material A	95	15.15	1.04	2453.0	143.0
CDC/05/5285/18	0° Tension	Material A	95	15.18	1.04	2295.0	145.0
CDC/05/5286/31	90° Tension	Material A	OD	25.12	1.96	48.0	9.3
CDC/05/5286/32	90° Tension	Material A	OD	25.08	2.01	51.0	-
CDC/05/5286/33	90° Tension	Material A	OD	25.11	1.99	65.0	9.4
CDC/05/5286/21	90° Tension	Material A	AR	25.73	1.92	59.0	9.2
CDC/05/5286/22	90° Tension	Material A	AR	25.73	1.92	57.0	9.3
CDC/05/5286/24	90° Tension	Material A	AR	25.73	1.92	62.0	9.2
CDC/05/5286/25	90° Tension	Material A	AR	25.73	1.92	45.0	9.0
CDC/05/5286/26	90° Tension	Material A	AR	25.73	1.92	62.0	9.2
CDC/05/5286/1	90° Tension	Material A	60	25.19	1.91	46.0	9.0
CDC/05/5286/2	90° Tension	Material A	60	25.43	1.94	46.0	9.1
CDC/05/5286/3	90° Tension	Material A	60	25.22	1.91	48.0	9.0
CDC/05/5286/4	90° Tension	Material A	60	25.45	1.91	55.0	9.1
CDC/05/5286/5	90° Tension	Material A	60	25.46	1.93	55.0	9.3
CDC/05/5286/6	90° Tension	Material A	60	25.20	1.94	56.0	9.1
CDC/05/5286/13	90° Tension	Material A	75	25.09	1.97	41.0	9.1
CDC/05/5286/14	90° Tension	Material A	75	25.04	1.95	-	-
CDC/05/5286/15	90° Tension	Material A	75	25.21	1.94	-	-
CDC/05/5286/16	90° Tension	Material A	75	25.18	1.93	45.0	9.5
CDC/05/5286/17	90° Tension	Material A	75	25.02	1.95	42.0	10.8

Coupon ID	Test Type	Material Type	Condition (%RH)	w	t	F_x MPa	E_x GPa
CDC/05/5286/18	90° Tension	Material A	75	25.16	1.99	38.0	8.9
CDC/05/5286/7	90° Tension	Material A	85	25.28	1.92	51.0	9.1
CDC/05/5286/8	90° Tension	Material A	85	25.37	1.93	45.0	8.9
CDC/05/5286/9	90° Tension	Material A	85	25.35	1.94	44.0	8.9
CDC/05/5286/10	90° Tension	Material A	85	35.33	1.92	40.0	9.4
CDC/05/5286/11	90° Tension	Material A	85	25.40	1.91	39.0	9.2
CDC/05/5286/12	90° Tension	Material A	85	25.13	1.95	47.0	9.3
CDC/05/5286/19	90° Tension	Material A	95	25.24	1.96	31.0	9.0
CDC/05/5286/20	90° Tension	Material A	95	25.07	1.96	34.0	8.9
CDC/05/5286/23	90° Tension	Material A	95	25.62	1.96	24.0	8.8
CDC/05/5286/27	90° Tension	Material A	95	25.66	1.94	31.0	8.9
CDC/05/5286/28	90° Tension	Material A	95	25.25	1.98	33.0	8.9
CDC/05/5286/30	90° Tension	Material A	95	25.25	1.96	23.0	8.9
CDC/05/8911-17	90° Tension	Material C	25%drycore	25.22	8.26	64.3	8.6
CDC/05/8911-18	90° Tension	Material C	25%drycore	25.26	8.27	74.4	8.5
CDC/05/8911-19	90° Tension	Material C	25%drycore	25.30	8.34	58.9	8.5
CDC/05/8911-20	90° Tension	Material C	25%drycore	25.15	8.23	71.3	8.4
CDC/05/8911-22	90° Tension	Material C	25%drycore	25.22	8.24	68.2	8.5
CDC/05/8911-14	90° Tension	Material C	50%drycore	25.04	8.15	65.2	9.0
CDC/05/8911-26	90° Tension	Material C	50%drycore	25.04	8.24	68.9	8.6
CDC/05/8911-28	90° Tension	Material C	50%drycore	25.12	8.20	75.7	-
CDC/05/8911-29	90° Tension	Material C	50%drycore	25.03	8.25	72.1	8.9
CDC/05/8911-31	90° Tension	Material C	50%drycore	25.11	8.25	75.4	9.2
CDC/05/8911-1	90° Tension	Material C	75%drycore	25.13	8.23	76.4	9.6
CDC/05/8911-2	90° Tension	Material C	75%drycore	25.03	8.28	78.6	n/a
CDC/05/8911-4	90° Tension	Material C	75%drycore	25.14	8.34	77.0	8.8
CDC/05/8911-7	90° Tension	Material C	75%drycore	25.10	8.22	74.9	8.7
CDC/05/8911-10	90° Tension	Material C	75%drycore	25.38	8.20	68.1	8.7
CDC/05/8911-11	90° Tension	Material C	75%drycore	25.11	8.28	64.2	-
CDC/05/5286-37	90° Tension	Material A	25%drycore	25.05	1.92	69.2	9.1
CDC/05/5286-40	90° Tension	Material A	25%drycore	25.05	1.92	-	-
CDC/05/5286-41	90° Tension	Material A	25%drycore	24.88	1.99	68.0	9.1
CDC/05/5286-30	90° Tension	Material A	25%drycore	25.00	2.00	67.4	9.0
CDC/05/5286-31	90° Tension	Material A	25%drycore	25.00	2.00	59.3	9.3
CDC/05/5286-32	90° Tension	Material A	25%drycore	25.00	2.00	52.6	9.1
CDC/05/5286-33	90° Tension	Material A	25%drycore	25.00	2.00	31.1	
CDC/05/5286-34	90° Tension	Material A	25%drycore	25.00	2.00	69.3	9.3
CDC/05/5286-35	90° Tension	Material A	25%drycore	25.00	2.00	66.3	9.1
CDC/05/5286-38	90° Tension	Material A	50%drycore	25.00	2.00	68.2	9.8
CDC/05/5286-39	90° Tension	Material A	50%drycore	25.00	2.00	35.6	9.2
CDC/05/5286-42	90° Tension	Material A	50%drycore	25.00	2.00	27.8	
CDC/05/5286-43	90° Tension	Material A	50%drycore	24.98	1.98	76.2	9.3
CDC/05/5286-44	90° Tension	Material A	50%drycore	24.94	1.94	71.7	9.5

Coupon ID	Test Type	Material Type	Condition (%RH)	w	t	F_x MPa	E_x GPa
CDC/05/5286-45	90° Tension	Material A	50%drycore	24.95	1.94	48.6	9.1
CDC/05/5286-46	90° Tension	Material A	50%drycore	24.88	1.93	72.8	9.4
CDC/05/5286-47	90° Tension	Material A	50%drycore	24.91	1.99	64.4	9.3
CDC/05/5286-48	90° Tension	Material A	50%drycore	24.90	1.99	51.6	9.9
CDC/05/5287/31	90° Compression	Material A	OD	13.07	1.94	268.8	n/a
CDC/05/5287/32	90° Compression	Material A	OD	13.09	1.93	323.5	n/a
CDC/05/5287/33	90° Compression	Material A	OD	13.14	1.96	358.9	n/a
CDC/05/5287/34	90° Compression	Material A	OD	13.03	2.00	389.6	n/a
CDC/05/5287/35	90° Compression	Material A	OD	13.12	1.99	323.9	n/a
CDC/05/5287/36	90° Compression	Material A	OD	13.09	2.00	384.9	n/a
CDC/05/5287/13	90° Compression	Material A	AR	13.17	2.00	234.6	n/a
CDC/05/5287/14	90° Compression	Material A	AR	13.12	2.00	221.3	n/a
CDC/05/5287/15	90° Compression	Material A	AR	13.15	2.00	216.7	n/a
CDC/05/5287/16	90° Compression	Material A	AR	13.24	1.97	227.5	n/a
CDC/05/5287/17	90° Compression	Material A	AR	13.20	2.00	237.4	n/a
CDC/05/5287/18	90° Compression	Material A	AR	12.62	1.97	266.9	n/a
CDC/05/5287/1	90° Compression	Material A	60	12.56	1.89	237.8	n/a
CDC/05/5287/2	90° Compression	Material A	60	12.51	1.93	234.6	n/a
CDC/05/5287/3	90° Compression	Material A	60	12.44	1.90	223.9	n/a
CDC/05/5287/4	90° Compression	Material A	60	12.50	1.94	239.9	n/a
CDC/05/5287/5	90° Compression	Material A	60	12.49	1.89	236.7	n/a
CDC/05/5287/6	90° Compression	Material A	60	12.53	1.90	247.4	n/a
CDC/05/5287/19	90° Compression	Material A	75	12.47	2.03	232.0	n/a
CDC/05/5287/20	90° Compression	Material A	75	12.39	2.02	229.2	n/a
CDC/05/5287/21	90° Compression	Material A	75	12.54	2.00	254.1	n/a
CDC/05/5287/22	90° Compression	Material A	75	12.48	1.96	261.0	n/a
CDC/05/5287/23	90° Compression	Material A	75	12.47	1.99	259.8	n/a
CDC/05/5287/24	90° Compression	Material A	75	12.53	1.95	244.5	n/a
CDC/05/5287/7	90° Compression	Material A	85	12.46	2.00	246.0	n/a
CDC/05/5287/8	90° Compression	Material A	85	12.52	2.05	215.7	n/a
CDC/05/5287/9	90° Compression	Material A	85	12.49	1.96	223.0	n/a
CDC/05/5287/10	90° Compression	Material A	85	12.47	1.94	210.2	n/a
CDC/05/5287/11	90° Compression	Material A	85	12.51	2.00	226.9	n/a
CDC/05/5287/12	90° Compression	Material A	85	12.48	1.94	228.8	n/a
CDC/05/5287/25	90° Compression	Material A	95	12.54	1.92	248.8	n/a
CDC/05/5287/26	90° Compression	Material A	95	12.53	1.97	241.3	n/a
CDC/05/5287/27	90° Compression	Material A	95	12.54	1.98	254.4	n/a
CDC/05/5287/28	90° Compression	Material A	95	12.56	1.99	220.3	n/a
CDC/05/5287/29	90° Compression	Material A	95	12.56	1.93	242.6	n/a
CDC/05/5287/30	90° Compression	Material A	95	12.56	2.00	-	n/a
CDC/05/5288/31	IPS	Material A	OD	24.98	1.42	86.0	5.2
CDC/05/5288/32	IPS	Material A	OD	25.02	1.42	84.4	5.1
CDC/05/5288/33	IPS	Material A	OD	25.03	1.40	86.6	5.2
CDC/05/5288/34	IPS	Material A	OD	25.01	1.38	86.6	5.3
CDC/05/5288/35	IPS	Material A	OD	24.98	1.5	83.8	5.0

Coupon ID	Test Type	Material Type	Condition (%RH)	w	t	F_x MPa	E_x GPa
CDC/05/5288/36	IPS	Material A	OD	25.02	1.41	84.5	5.2
CDC/05/5288/8	IPS	Material A	AR	25.02	1.42	71.9	-
CDC/05/5288/9	IPS	Material A	AR	25.00	1.41	71.6	-
CDC/05/5288/10	IPS	Material A	AR	25.01	1.47	77.6	3.2
CDC/05/5288/11	IPS	Material A	AR	25.02	1.39	70.5	4.9
CDC/05/5288/12	IPS	Material A	AR	24.83	1.41	73.3	4.8
CDC/05/5288/13	IPS	Material A	AR	24.77	1.38	76.8	3.2
CDC/05/5288/18	IPS	Material A	60	25.02	1.42	72.5	4.8
CDC/05/5288/19	IPS	Material A	60	25.00	1.41	74.3	4.8
CDC/05/5288/20	IPS	Material A	60	25.01	1.47	72.3	4.6
CDC/05/5288/21	IPS	Material A	60	25.02	1.39	73.7	4.8
CDC/05/5288/22	IPS	Material A	60	24.83	1.41	73.0	4.8
CDC/05/5288/24	IPS	Material A	60	24.77	1.38	73.2	4.9
CDC/05/5288/13	IPS	Material A	75	25.02	1.48	74.9	4.7
CDC/05/5288/14	IPS	Material A	75	25.02	1.48	73.2	-
CDC/05/5288/15	IPS	Material A	75	24.98	1.44	74.9	4.8
CDC/05/5288/16	IPS	Material A	75	25.00	1.40	72.9	4.8
CDC/05/5288/17	IPS	Material A	75	24.93	1.44	72.3	4.8
CDC/05/5288/23	IPS	Material A	75	24.99	1.45	72.6	4.6
CDC/05/5288/1	IPS	Material A	85	24.98	1.43	69.9	4.7
CDC/05/5288/2	IPS	Material A	85	24.98	1.41	72.5	4.9
CDC/05/5288/3	IPS	Material A	85	24.92	1.37	71.3	4.6
CDC/05/5288/4	IPS	Material A	85	24.96	1.46	69.3	4.5
CDC/05/5288/5	IPS	Material A	85	24.97	1.42	69.2	4.6
CDC/05/5288/6	IPS	Material A	85	24.98	1.40	71.1	4.7
CDC/05/5288/25	IPS	Material A	95	24.65	1.43	67.7	4.8
CDC/05/5288/26	IPS	Material A	95	24.87	1.49	67.5	4.7
CDC/05/5288/27	IPS	Material A	95	24.91	1.50	67.4	4.6
CDC/05/5288/28	IPS	Material A	95	24.73	1.47	66.5	4.6
CDC/05/5288/29	IPS	Material A	95	24.82	1.46	65.9	4.6
CDC/05/5288/30	IPS	Material A	95	24.85	1.45	65.9	4.6
CDC/05/5288/37	IPS	Material A	50%drycore	24.85	1.44	82.9	5.5
CDC/05/5288/38	IPS	Material A	50%drycore	24.77	1.43	84.9	5.0
CDC/05/5288/39	IPS	Material A	50%drycore	24.89	1.44	80.9	4.9
CDC/05/5288/40	IPS	Material A	50%drycore	24.77	1.45	84.4	5.1
CDC/05/5288/41	IPS	Material A	50%drycore	24.68	1.44	85.2	5.0
CDC/05/5288/42	IPS	Material A	50%drycore	24.68	1.46	-	-
CDC/05/5288/47	IPS	Material A	25% drycore	24.70	1.44	82.1	4.7
CDC/05/5288/48	IPS	Material A	25% drycore	24.65	1.43	83.7	4.6
CDC/05/5288/55	IPS	Material A	25% drycore	24.84	1.45	85.4	5.0
CDC/05/5316/20	ILS	Material A	OD	10.31	2.00	83.2	n/a
CDC/05/5316/21	ILS	Material A	OD	10.31	2.03	86.1	n/a
CDC/05/5316/22	ILS	Material A	OD	10.39	2.03	81.7	n/a
CDC/05/5316/23	ILS	Material A	OD	10.37	2.00	80.9	n/a
CDC/05/5316/24	ILS	Material A	OD	9.84	2.00	92.0	n/a

Coupon ID	Test Type	Material Type	Condition (%RH)	w	t	F_x MPa	E_x GPa
CDC/05/5316/25	ILS	Material A	OD	10.40	2.01	88.9	n/a
CDC/05/5316/1	ILS	Material A	AR	10.02	2.01	87.9	n/a
CDC/05/5316/2	ILS	Material A	AR	10.01	2.01	92.3	n/a
CDC/05/5316/3	ILS	Material A	AR	10.00	2.01	87.2	n/a
CDC/05/5316/4	ILS	Material A	AR	9.96	2.00	96.6	n/a
CDC/05/5316/5	ILS	Material A	AR	10.02	2.01	88.4	n/a
CDC/05/5316/6	ILS	Material A	AR	9.92	2.03	99.0	n/a
CDC/05/5316/7	ILS	Material A	75	9.97	2.03	73.6	n/a
CDC/05/5316/8	ILS	Material A	75	10.01	2.03	67.8	n/a
CDC/05/5316/9	ILS	Material A	75	10.00	2.05	77.1	n/a
CDC/05/5316/10	ILS	Material A	75	10.00	2.03	71.5	n/a
CDC/05/5316/11	ILS	Material A	75	9.91	2.00	71.7	n/a
CDC/05/5316/13	ILS	Material A	95	10.02	2.01	69.6	n/a
CDC/05/5316/15	ILS	Material A	95	10.00	2.01	59.5	n/a
CDC/05/5316/16	ILS	Material A	95	9.96	2.00	67.0	n/a
CDC/05/8910-26	ILS	Material C	25%drycore	40.22	8.25	61.6	n/a
CDC/05/8910-25	ILS	Material C	25%drycore	40.24	7.91	87.9	n/a
CDC/05/8910-24	ILS	Material C	25%drycore	40.25	8.34	84.8	n/a
CDC/05/8910-33	ILS	Material C	25%drycore	40.23	8.36	84.0	n/a
CDC/05/8910-35	ILS	Material C	25%drycore	40.13	8.29	85.2	n/a
CDC/05/8910-36	ILS	Material C	25%drycore	40.16	7.98	87.1	n/a
cdc/05/0910-2	ILS	Material C	50%drycore	40.25	8.61	84.5	n/a
cdc/05/0910-16	ILS	Material C	50%drycore	40.21	8.50	83.8	n/a
cdc/05/0910-18	ILS	Material C	50%drycore	40.23	8.56	82.8	n/a
cdc/05/0910-19	ILS	Material C	50%drycore	40.22	8.53	85.4	n/a
cdc/05/0910-21	ILS	Material C	50%drycore	40.23	8.54	84.9	n/a
cdc/05/0910-23	ILS	Material C	50%drycore	40.22	8.53	84.0	n/a
cdc/05/0910-9	ILS	Material C	75%drycore	39.91	8.21	89.7	n/a
cdc/05/0910-22	ILS	Material C	75%drycore	39.93	8.21	88.1	n/a
cdc/05/0910-17	ILS	Material C	75%drycore	39.88	8.24	90.1	n/a
cdc/05/0910-27	ILS	Material C	75%drycore	40.00	8.20	87.0	n/a
cdc/05/0910-28	ILS	Material C	75%drycore	39.97	8.19	89.6	n/a
cdc/05/0910-30	ILS	Material C	75%drycore	40.10	8.20	84.8	n/a
CDC/05/5289-28	ILS	Material A	25%drycore	9.96	2.00	76.8	n/a
CDC/05/5289-48	ILS	Material A	25%drycore	9.92	2.00	69.0	n/a
CDC/05/5289-49	ILS	Material A	25%drycore	9.85	2.02	75.3	n/a
CDC/05/5289-50	ILS	Material A	25%drycore	10.04	2.05	77.6	n/a
CDC/05/5289-52	ILS	Material A	25%drycore	9.94	2.01	82.0	n/a
CDC/05/5289-53	ILS	Material A	25%drycore	9.96	1.99	73.0	n/a
	ILS	Material A	50%drycore	9.87	1.97	80.8	n/a
CDC/05/5289-26	ILS	Material A	50%drycore	9.90	1.98		n/a
CDC/05/5289-27	ILS	Material A	50%drycore	9.84	1.98	87.6	n/a
CDC/05/5289-29	ILS	Material A	50%drycore	9.98	1.94	83.0	n/a
CDC/05/5289-30	ILS	Material A	50%drycore	9.87	2.01	80.7	n/a
CDC/05/5289-31	ILS	Material A	50%drycore	10.06	2.03	84.7	n/a

Coupon ID	Test Type	Material Type	Condition (%RH)	w	t	F_x MPa	E_x GPa
CDC/05/5293/19	OHT	Material B	OD	32.80	4.44	323.0	n/a
CDC/05/5293/20	OHT	Material B	OD	32.83	4.42	-	n/a
CDC/05/5293/21	OHT	Material B	OD	32.76	4.43	343.0	n/a
CDC/05/5293/22	OHT	Material B	OD	32.87	4.38	346.0	n/a
CDC/05/5293/23	OHT	Material B	OD	32.88	4.39	333.0	n/a
CDC/05/5293/24	OHT	Material B	OD	32.80	4.48	335.0	n/a
CDC/05/5293/1	OHT	Material B	AR	32.04	4.41	338.0	n/a
CDC/05/5293/2	OHT	Material B	AR			342.0	n/a
CDC/05/5293/3	OHT	Material B	AR	32.85	4.46	338.0	n/a
CDC/05/5293/4	OHT	Material B	AR			360.0	n/a
CDC/05/5293/5	OHT	Material B	AR			325.0	n/a
CDC/05/5293/6	OHT	Material B	AR			341.0	n/a
CDC/05/5293/7	OHT	Material B	75	32.04	4.47	363.0	n/a
CDC/05/5293/8	OHT	Material B	75	32.15	4.45	355.0	n/a
CDC/05/5293/9	OHT	Material B	75	32.02	4.44	374.0	n/a
CDC/05/5293/10	OHT	Material B	75	32.05	4.43	366.0	n/a
CDC/05/5293/11	OHT	Material B	75	32.00	4.35	378.0	n/a
CDC/05/5293/12	OHT	Material B	75	32.03	4.31	363.0	n/a
CDC/05/5293/13	OHT	Material B	95	32.10	4.49	335.0	n/a
CDC/05/5293/14	OHT	Material B	95	32.04	4.45	340.0	n/a
CDC/05/5293/15	OHT	Material B	95	32.04	4.45	343.0	n/a
CDC/05/5293/16	OHT	Material B	95	32.06	4.33	382.0	n/a
CDC/05/5293/17	OHT	Material B	95	32.05	4.34	367.0	n/a
CDC/05/5293/18	OHT	Material B	95	32.05	4.42	386.0	n/a
CDC/05/5293/28	OHT	Material B	25% drycore	31.00	4.40	338.1	n/a
CDC/05/5293/09	OHT	Material B	25% drycore	31.92	4.27	320.8	n/a
CDC/05/5293/30	OHT	Material B	25% drycore	31.93	4.40	-	n/a
CDC/05/5293/26	OHT	Material B	50% drycore	32.00	4.40	325.9	n/a
CDC/05/5293/27	OHT	Material B	50% drycore	31.92	4.34	344.1	n/a
CDC/05/5294/19	OHC	Material B	OD	31.90	4.48	312.0	n/a
CDC/05/5294/20	OHC	Material B	OD	32.19	4.46	314.0	n/a
CDC/05/5294/21	OHC	Material B	OD	31.73	4.52	332.0	n/a
CDC/05/5294/22	OHC	Material B	OD	32.02	4.46	302.0	n/a
CDC/05/5294/23	OHC	Material B	OD	31.02	4.47	343.0	n/a
CDC/05/5294/24	OHC	Material B	OD	31.97	4.43	300.0	n/a
CDC/05/5294/1	OHC	Material B	AR	32.84	4.26	306.0	n/a
CDC/05/5294/2	OHC	Material B	AR	32.84	4.26	301.0	n/a
CDC/05/5294/3	OHC	Material B	AR	32.84	4.26	294.0	n/a
CDC/05/5294/4	OHC	Material B	AR	32.84	4.26	326.0	n/a
CDC/05/5294/6	OHC	Material B	AR	32.84	4.26	286.0	n/a
CDC/05/5294/7	OHC	Material B	AR	32.84	4.26	280.0	n/a
CDC/05/5294/5	OHC	Material B	75	32.10	4.43	275.0	n/a
CDC/05/5294/8	OHC	Material B	75	31.90	4.43	302.0	n/a
CDC/05/5294/9	OHC	Material B	75	32.02	4.45	287.0	n/a
CDC/05/5294/10	OHC	Material B	75	32.02	4.45	288.0	n/a

Coupon ID	Test Type	Material Type	Condition (%RH)	w	t	F_x MPa	E_x GPa
CDC/05/5294/11	OHC	Material B	75	31.95	4.39	306.0	n/a
CDC/05/5294/12	OHC	Material B	75	31.98	4.38	308.0	n/a
CDC/05/5294/13	OHC	Material B	95	32.02	4.38	298.0	n/a
CDC/05/5294/14	OHC	Material B	95	32.06	4.27	296.0	n/a
CDC/05/5294/15	OHC	Material B	95	31.84	4.34	297.0	n/a
CDC/05/5294/16	OHC	Material B	95	32.73	4.45	291.0	n/a
CDC/05/5294/17	OHC	Material B	95	32.02	4.44	302.0	n/a
CDC/05/5294/18	OHC	Material B	95	32.74	4.48	281.0	n/a
CDC/05/5294/28	OHC	Material B	25% drycore	31.95	4.34	310.9	n/a
CDC/05/5294/29	OHC	Material B	25% drycore	31.77	4.35	299.4	n/a
CDC/05/5294/30	OHC	Material B	25% drycore	31.84	4.33	302.5	n/a
CDC/05/5294/25	OHC	Material B	50% drycore	31.83	4.34	318.4	n/a
CDC/05/5294/26	OHC	Material B	50% drycore	31.78	4.32	315.2	n/a
CDC/05/5294/27	OHC	Material B	50% drycore	32.17	4.34	303.5	n/a

** OD=oven dried, AR=as-received, all tests conditioned at 70°C, %dry-core test conditioned at 70°C and 85%RH, w=width in mm, t=thickness in mm, F_x= maximum strength, E_x= maximum modulus.*

APPENDIX F : STATISTICAL ANALYSIS

A) COEFFICIENT OF VARIATION

The coefficient of variation, CV describes the magnitude sample values and the variation within them.

This is the ratio of the standard deviation (SD) to the mean, $\bar{x}$:

$$CV = \frac{SD}{\bar{X}} \times 100 \qquad A\text{-}1$$

B) STANDARD DEVIATION

The standard deviation is a measure of how widely values are dispersed from the average/mean value. The Standard deviation (SD) estimates the standard deviation based on a sample.

$$SD = \sqrt{\frac{\sum (x - \bar{x})^2}{(n-1)}} \qquad A\text{-}2$$

where x is the sample mean and n is the sample size.

Table A-2:Equilibrium saturation test data

Property	Test Condition (°C/%RH)	M_{max} (wt%)	V_f (%)	Mean Strength (MPa)	Mean Modulus (GPa)	Strength Knock down %	Modulus Knock down %
0° Tension	OD	0.00	-	2357	152	-	-
	AR	0.26		2396	144	+1.7	0.0
	70 / 75	0.53		2395	145	+1.6	+0.7
	70 / 95	0.73		2349	142	-0.3	-1.3
90° Tension	OD	0.00	69.57	55	9.3	-	-
	AR	0.1		54	9.2	-1.8	-0.9
	70 / 60	0.22		51	9.1	-7.3	-1.7
	70 / 75	0.36		41	-	-25.1	3.5
	70 / 85	0.44		43	9.0	-19.4	-1.4
	70 / 95	0.57		29	8.9	-47	-4
90° Compression	OD	0.00	67.42	232	-	-	-
	AR	0.26		40	-	+3.4	-
	70 / 60	0.40		240	-	+3.6	-
	70 / 75	0.57		247	-	+6.7	-
	70 / 85	0.67		228	-	-1.9	-
	70/95	0.77		245	-	+5.6	-
IPS	OD	0.00	66.26	85.3	5.2	-	-
	AR	0.25		73.6	4.9	-13.7	-6.1
	70 / 60	0.40		73.2	4.8	-14.3	-7.3
	70 / 75	0.56		73.5	4.7	-13.9	-8.3
	70 / 85	0.64		70.6	4.7	-17.3	-9.7
	70 / 95	0.86		66.8	4.6	-21.7	-10.2
ILS	OD	0.00	66.25	8	-	-	-
	AR	0.26		92	-	+7.5	-
	70 / 85	0.60		74	-	-15.3	-
	70 / 95	0.86		65	-	-23.5	-
Open hole Tension	OD	0.00	57.81	336	-	-	-
	AR	0.15		341	-	+1.4	-
	70 / 75	0.40		366	-	+9.1	-
	70 / 95	0.65		359	-	+6.9	-
Open Hole Compression	OD	0.00	56.29	317	-	-	-
	AR	0.11		299	-	-5.8	-
	70 / 75	0.38		294	-	-7.1	-
	70 / 95	0.61		294	-	-7.2	-

Table A-3: Equilibrium testing Statistical data.

Test	Environment (°C/%RH)	Mean Strength (MPa)	SD (MPa)	CV (%)	No. of coupons, n.
0° Tension	OD	2357	143	6.1	5
	AR	2396	79	3.3	5
	70 / 75	2395	80	3.3	6
	70 / 95	2349	123	5.2	6
90° Tension	OD	55	7	12.7	6
	AR	54	6	11.1	6
	70 / 60	51	5	9.8	6
	70 / 75	41	3	7.3	6
	70 / 85	43	3	7.0	6
	70 / 95	29	5	17.2	6
UD 90° Compression	OD	232	5	2.2	6
	AR	240	15	6.3	6
	70 / 60	240	7	2.9	6
	70 / 75	247	13	5.3	6
	70 / 85	228	12	5.3	6
	70 / 95	245	14	5.7	5
IPS	OD	85.3	1.1	1.3	6
	AR	73.6	2.7	3.7	6
	70 / 60	73.2	0.7	1.0	6
	70 / 75	73.5	1.1	1.5	6
	70 / 85	70.6	1.2	1.7	6
	70 / 95	66.8	0.8	1.2	6
ILLS	OD	85	4	4.7	6
	AR	92	4	4.3	6
	70 / 75	74	3	4.1	5
	70 / 95	65	4	6.2	4
Open Hole Tension	OD	336	8	2.4	5
	AR	341	10	2.9	6
	70 / 75	366	7	1.9	6
	70 / 95	359	21	5.8	6
Open Hole Compression	OD	317	15	4.7	6
	AR	299	15	5.0	6
	70 / 60	294	12	4.1	6
	70 / 75	294	7	2.4	6

Table A-4: Validation testing statistical data.

Property	Thickness mm	% dry-core	M_{max} wt%	Mean Strength (MPa)	Strength SD (MPa)	Strength CV (%)
90° Tension	2	50	0.05	70.7	4.5	0.9
	2	25	0.08	60.4	6.5	1.3
	8	75	0.08	73.3	5.7	7.8
	8	50	0.13	71.4	5.4	6.2
	8	25	0.20	65.6	5.3	8.1
90° Comp	2	50	0.05	241	22	9.3
IPS	2	50	0.04	83.7	1.8	2.1
	2	25	0.07	83.7	1.6	1.9
Open Hole Compression	4	50	0.06	312	8	2.5
	4	25	0.09	304	3	4.0
Open Hole Tension	4	50	0.08	335	13	3.8
	4	25	0.13	329	12	0.8

APPENDIX G : Laminate Analysis Program

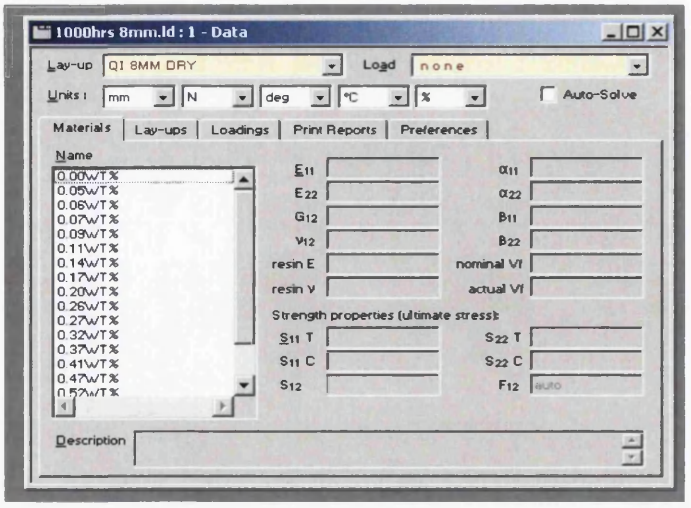

Figure A-23: Defining each ply properties in LAP.

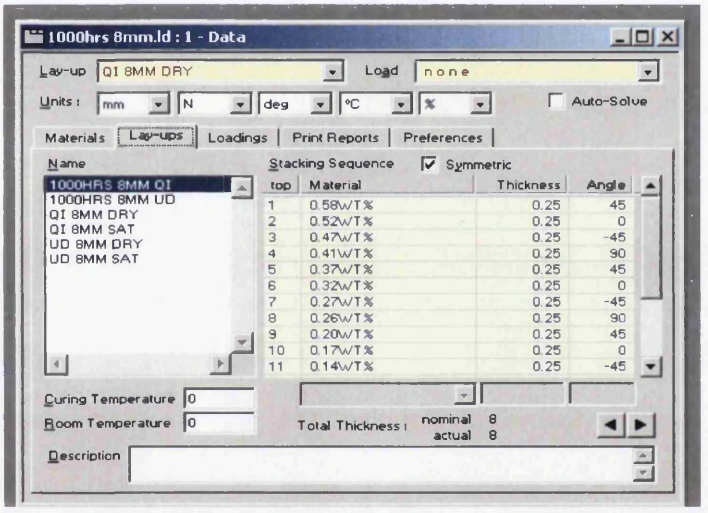

Figure A-24: Defining laminae lay-up, material and ply thickness.

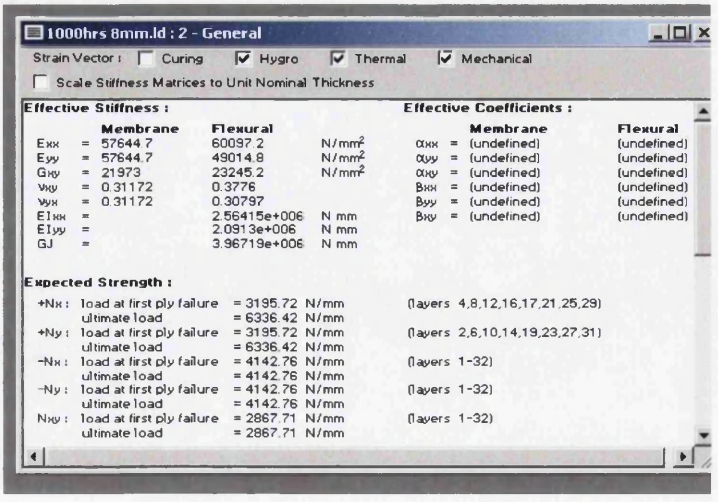

Figure A-25: Sample of results ouput in LAP.

APPENDIX H: Airbus New Specimen Handling Proceedure.

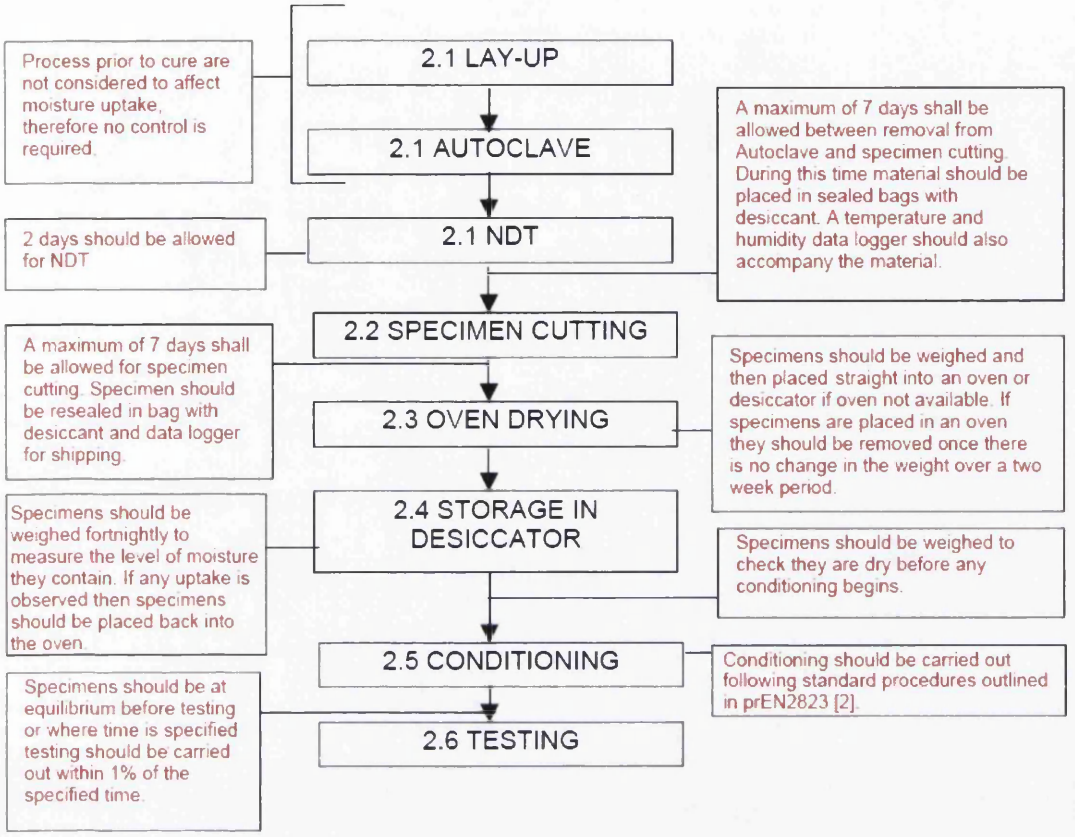

Figure A-26: Airbus new specimen handling procedure[128].